James N. Furze · Saeid Eslamian
Safanah M. Raafat · Kelly Swing *Editors*

Earth Systems Protection and Sustainability

Volume 2

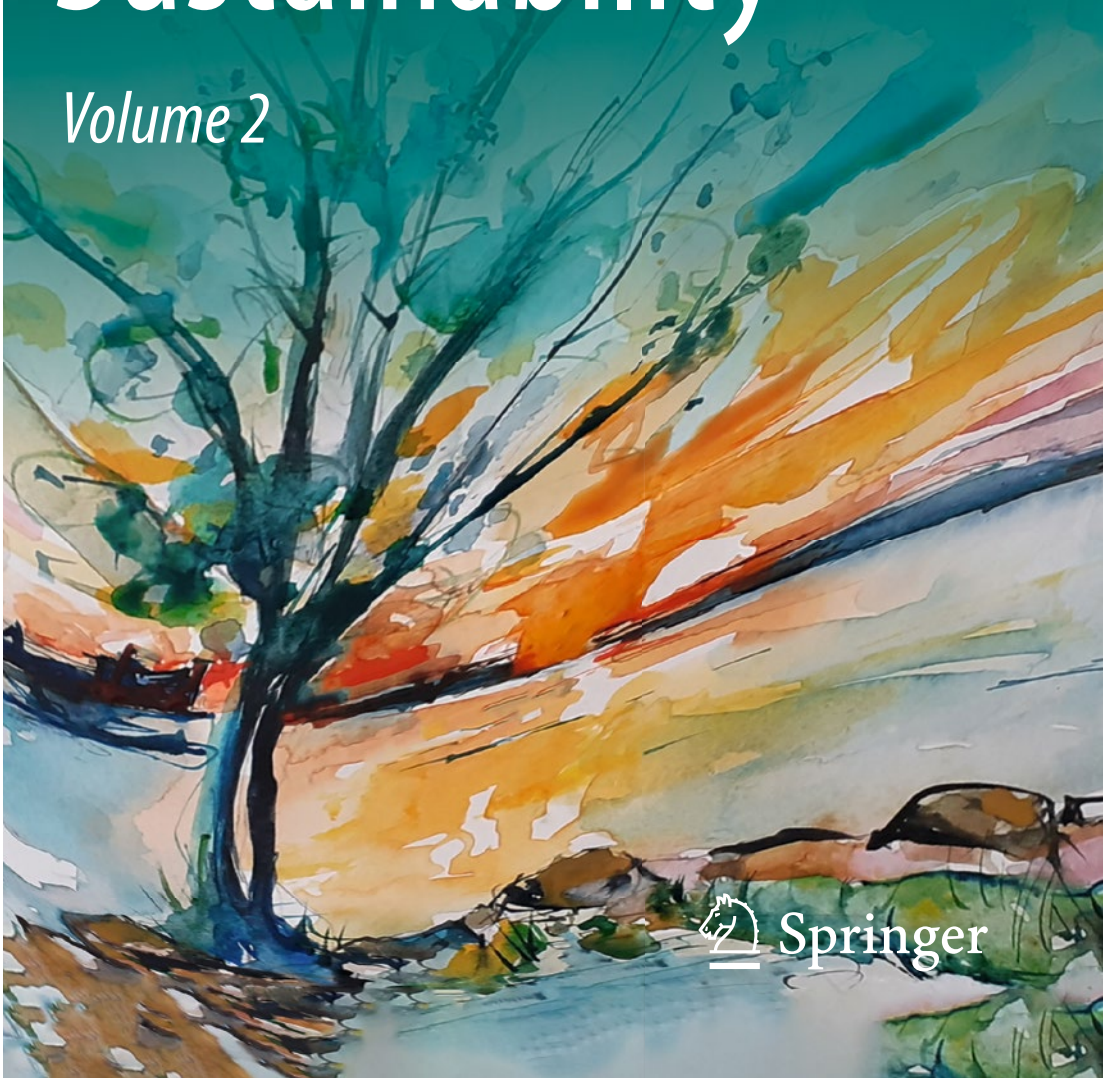

Springer

Earth Systems Protection and Sustainability

James N. Furze • Saeid Eslamian
Safanah M. Raafat • Kelly Swing
Editors

Earth Systems Protection and Sustainability

Volume 2

Springer

Editors
James N. Furze
Royal Geographical Society
(with the Institute of British Geographers)
London, UK

Saeid Eslamian
Department of Water Engineering
Isfahan University of Technology
Isfahan, Iran

Safanah M. Raafat
Control and Systems Engineering
Department
University of Technology-Iraq
Baghdad, Iraq

Kelly Swing
Tiputini Biodiversity Station
College of Biological
and Environmental Sciences
University of San Francisco de Quito
Quito, Ecuador

ISBN 978-3-030-98583-7 ISBN 978-3-030-98584-4 (eBook)
https://doi.org/10.1007/978-3-030-98584-4

Cover artwork: 'Resonating Horizons'. Semin Sinem Cacho Duran, Antalya, Turkey. E: semincacho@outlook.com

This Springer imprint is published by the registered company Springer Nature Switzerland AG
The registered company address is: Gewerbestrasse 11, 6330 Cham, Switzerland

This volume is dedicated...
To you with confident or meek nature, whose tears remain recognizing your humble ownership of the Earth

(James N. Furze)

To every person who kindly prefers the improvement of nature to its overuse

(Saeid Eslamian)

To all who are concerned for our beautiful planet Earth and seek to develop sustainable strategies that keep it safe and serve it well

(Safanah M. Raafat)

To the creativity and resilience of all those who contribute to overcoming the expansive challenges of the Anthropocene

(Kelly Swing)

Foreword

To understand the importance of Earth Systems Protection (ESP) and Sustainability, recall that upon the opening of our eyes we recognize the beauty of the Earth and the diversity of life. A single blade of grass for example, each day and each second changes in colour and shape; soon we associate this individual life form with another blade, flowers and insects that move around and interact. We see the changes in particles of soil or sand, sense the smell after rain or feel the baking sun. Recognize that every day is unique; every second there is a unique combination of light, water and gases surrounding those blades of grass or other species within terrestrial, aquatic or even atmospheric ecosystems. The smallest changes in conditions prevailing upon every habitat in fact determine its evolutionary proliferations. We realize that all forms of life are connected in terms of chemical, spatial and topographic variation. The acknowledgement of this premise comes as a wave of enlightenment, across the highest mountains and deepest valleys; the beauty and elegance of the Earth is beyond compare and brings tears of both joy and sadness.

Humans have developed their cultures and communities amidst an extraordinary pool of diversity, and are reliant on the seemingly insignificant changes in conditions prevailing upon the smallest components of life to support their needs. So we feed on animals and plants we can catch to eat, breed and grow for our needs, and use minerals and resources to develop our medicines and material requirements. Yet the demographics and concentration of each feeding level of an ecosystem must be respected in order that we do not do not surpass the thresholds or carrying capacity of the systems themselves. We must appreciate that as a highly competitive species with intelligent and adaptive behavioural and linguistic abilities, we are the guardians of the Earth and must protect it and ensure the beauty continues. This core responsibility feeds our cultural and dynamic behaviour, the root being essential for our continued presence on Earth, surpassing all other political and societal goals. Ownership of ESP and where we live represent a key for the sustainability of all species and resources upon which we rely.

In order to survive within prevailing climate change on Earth we must consider how sustainability of our and all other species may be accomplished resiliently;

holistic adaptation plans must be developed, updated and acted upon. The United Nations 2030 Agenda for sustainable development goals integrates economic, social and environmental dimensions within policy to guide our current and future governance. The Intergovernmental Panel on Climate Change heralds that vast land masses are prone to extreme events, including flooding and elevated temperature leading to increased aridity and desecration of diverse vegetation, all of which pose a high risk to our communities' stability. Sophisticated climate models are applied, though due to increased climatic instability, the projected dynamics they consider may give controversial outcomes. Coastal areas suffer in their limited freshwater resources and imbalances imposed through rising intrusion of salt water. Although we make use of optimisation techniques in order to counter water scarcity in these and other areas, these might be thought of as curative/reactive responses. Surely a more preventative approach is called for, entailing a reduction in our resource extraction and use in the first place.

Increased incidence of natural risks has led us to develop multicriteria decision-making processes of increased complexity. Ultimately, such tools are reduced to simple hierarchical consideration in order to achieve our development needs within frightening global risk indications, including volcanoes, fires, tsunamis and mass removal. It appears that we cannot have our cake and eat it after all. Might embracing the systems we rely on rather than destroying them result in less erratic risks ensuring the security and harmony of all species to a greater degree? Faced with an increasingly unstable Earth, we must consider methods of literally stabilizing the ground beneath our feet, lest we reap the consequences of our vandalistic tendencies. The diversity of bacteria and sensitive microorganisms may contribute additive solutions to our peril; however, our irresponsible activities risk even these. In the onslaught of climate change, the vulnerability not only of those species we mindlessly destroy but also of our own settlements and socioeconomic activity is increased. Assessments of risk become increasingly diverse in terms of the range of risks that we manifest and are projected to encounter in the coming decades. Environmental risks endanger and contaminate not only ourselves but additionally those supportive species we have abused to affect the risks in the first place, often disturbing entire webs across different levels of species diversity. We must resort to desperate measures to save the integrity of our systems and rescue our safety and security. The need for mitigation has never been more urgent.

The recent growth of green energy combined with increased public need for clean and low-cost energy has resulted in a global clean energy revolution. Increased power from sustainable energy sources such as wind at lower prices presents a promising solution for humans as well as the planet. As a result, extensive studies have been rapidly developed to further emphasise this vital field of knowledge.

Advanced mathematical approaches have proven to be an essential requirement for the accomplishment of sustainable engineering systems. Estimation methods such as Kalman filters (KF) and fault estimation (FE), for instance, can provide the most suitable estimates for unmeasured states of a system. These can effectively help in reducing the required efforts, cost and energy for precise measurements of each component of compound systems. The gained estimated states can later be used

to develop adaptive control or robust fault-tolerant control (FTC) that can ensure sustainable performance with complex constraints.

Deep learning algorithms enable the inclusion of large expert knowledge in building a sustainable environmental system. Recent development of these approaches has enriched some important applications in many effective areas such as control of quadrotors, wind-turbine energy management, earthquake prediction, weather forecasting, and environmental protection and sustainability.

Although multiple approaches have been employed in efforts to alter the trajectory of human impacts on our environment, indicators suggest that currently applied strategies are inadequate; we are not effecting improvements necessary for sustained positive conditions into the future. Good intentions, thrifty personal and local efforts and costly global campaigns have resulted in laudable advances in the human/nature interface (including the labor-intensive conservation of a miniscule fraction of biodiversity). Nevertheless, we must acknowledge that we remain on a path of destruction, of our world and of ourselves. We must appreciate that understanding the governing factors that act to represent the laws of nature does not represent immunity to natural change. Indeed, our claimed understanding binds us together as a unit and we should recognize both our individual and collective responsibility. The circumstances are indeed dire; however, we must try to have some hope. The world will keep on turning after all, with or without the presence of humans. We currently have the opportunity to demonstrate our choice.

Generations of concerned citizen-visionaries and legions of scientists have diligently made observations and collected reliable data on our surroundings and the species with which we inhabit the Earth. The resulting analyses make a few points abundantly clear:

1. Most humans are endlessly selfish in their disregard for anything and anyone outside their own limited life/work bubble. Given current circumstances, many people, if not most, feel there is no feasible alternative to their vainglorious, self-absorbed attitudes.
2. There are far too many of us already, but our numbers persistently increase. All that is known about resource use and carrying capacities tells us that we can only reasonably expect conditions to follow the same inexorably declining trends for the foreseeable future.
3. We have destroyed or degraded too much of the planet already. Certain anthropogenic impacts simply cannot be resolved altogether, in the short term or ever, through increasing expenditures.
4. Money and materialism cannot be seen as the only indicators of quality of life.
5. We cannot turn back the clock, but we can, and must, change minds as well as the course of our destiny.

Environmental responsibility and mitigating activities in all societies represent the urgent motivations which we and great figures over history bare witness to; reinforcing our need to change to ensure that which supports us does not become extinct in its sensitive dynamic on this ‘small’ rocky planet. Simply put, ‘where there

is action, there is hope'. Although our actions thus far appear to reflect that we are ignorant of the consequences of our activity, finite beacons of hope are better than none and collectively allow us to demonstrate whether we wish to stay or not.

London, UK — James N. Furze
Isfahan, Iran — Saeid Eslamian
Baghdad, Iraq — Safanah M. Raafat
Quito, Ecuador — Kelly Swing
28 June 2022

Preface

We are honoured to provide the preface for the third book of the Mathematical Advances Towards Sustainable Environmental Systems (MATSES) series. The series commenced in 2017. The first book recognized the need to understand our planet and learn to manage its resources. Dr. James Furze and the editorial collective met the requirement achieving an arena of rigourous instruction pertaining to MATSES, consequently contributing functional and sustainable environmental systems.

Acquiring the key subjective nodes of environmental specialties requires a working knowledge of mathematical developments effective in sustainable systems. The refined chapters of MATSES covered a range of specific subjective areas; highlighting the importance of sustainable mathematical or engineering complexes, which when confronted together allow balanced progress.

The first volume of *Earth Systems Protection and Sustainability* represented new ideas of science and technology, from the core perspectives of scientific, policy relations and imperatives, community implementations, and mathematic systems learning and intuition. Contributions were felt recalling fundamental and emergent areas with timely wisdom for development into the future. The second volume of *Earth Systems Protection and Sustainability* includes the four perspectives again being complemented by community priorities requiring safeguarding, with documented progress enabling restoration of ecosystems. Thorough disciplined consideration, innovative analysis and empathetic consideration of community needs and issues are reinforced to expand our capacity to mitigate risks to Earth systems; providing keys to the central themes of protection of structural integrity and renewing life systems, which are essential facets of Earth systems and resource dynamics in variable scenarios.

It is our intention that this book will provide an exhilarating experience for those who have interest in learning, working or enjoying the essential facets which support our existence on Earth into the indefinite future.

Unique points include:

- Imperative frontier research for environmental sustainability
- Management and directions for resource usage and cooperation in both human and naturalized ecosystems
- A collection of leading authors augmenting qualitative and quantitative chapters across refined sections
- Community and subject driven 'problems' and 'solutions' which reward ownership for sustainability directly to those the volume is designed to assist

In addition to the 12 author teams with global scope, reviewers located between the authors, communities, governmental members and organizational unit representatives (from many of our 'United' core bodies), the editorial collective consists of 4 members spanning the subjective fields of study and disciplines of the volume, across Earth's geographical spread. We extend our sincere gratitude to the authors, publishers and community members who generously gave their time and support in preparation of this book, and to whom we share and direct our efforts. *Earth Systems Protection and Sustainability* is addressed to a global audience (academic/research, professional, classroom, governmental, unit and community members) in both descriptive and illustrative sections including all sectors, thus advising management of every resource type and use, to ensure ongoing Earth systems protection.

London, UK — James N. Furze
Isfahan, Iran — Saeid Eslamian
Baghdad, Iraq — Safanah M. Raafat
Quito, Ecuador — Kelly Swing
30 June 2022

Introduction

This volume elucidates, refines and incorporates areas of Earth Systems Protection and Sustainability. To show effective integration and practical application of subjects, leading research from specialists in different disciplines as well as practically driven implementations of sustainable developments key to our equilibrated needs are included.

The four perspectives of the volume have been chosen to reflect distinct pillars of sustainability that have a reflective and balancing quality, within Earth Systems Protection (ESP). These perspectives are (i) biological/chemical/geographic; (ii) sustainability policy imperatives/social perspectives; (iii) mathematic and applied systems learning and (iv) pictorial – problems and solutions for special focus. With these aspects we balance qualitative/quantitative approaches and provide reflective ownership of ESP and sustainability to the communities and issues that the volume is designed to assist.

In the second of two volumes, the pillars of sustainability in ESP are represented across balanced chapters. Chapter 1 approaches bioaccumulation processes from a chemically competitive viewpoint, respecting a particular species' ability to quench polluting heavy metal elements produced by anthropic activities; offering a restorative potential to aquatic and terrestrial habitats. Chapter 2 covers climate change, sustainability and resilience, relating the need for effective policy formation to cooperatively manage ecosystem requirements and developmental stability with reference to the United Nations Sustainable Development Goals. The chapter details the application of global circulation models with corresponding socioeconomic scenarios at a regional scale affecting different sector developments. Imperatives in a water-stressed country are considered and climatic arguments between different models are settled. Chapters 3 and 4 discuss mathematical models which work towards provision of freshwater in coastal areas of arid and semi-arid regions, and multicriteria decision-making required in natural disaster situations for social project assessments respectively. Chapter 5 covers elemental details and models of chemical and biological reaction processes in peat solidification work for environmental sustainability, enabling geotechnical engineers to achieve terrestrial stability with

minimal environmental impact. Chapter 6 incorporates innovative green energy conversion systems which will augment mixed coalitions of energy and additionally benefit organic waste utilization and flow. Chapter 7 documents the present status and future challenges in increasingly required flood risk estimation and mapping, considering scientific, geographic, policy and community factors. Chapter 8 presents a trend analysis of rainfall for the high-risk area of western India, reflecting evidence of climate change. Chapter 9 discusses risk assessment in the context of exposure, safety and security, and considers environmental contamination whilst unsustainable use of natural resources continues to augment socioeconomic and ecological risk. Furthermore, a range of factors and approaches determining such instability are covered and the chapter projects five key steps in risk assessment processes. Chapter 10 considers the control aspects of quadrotors and gives applications including journalistic reporting, disaster management, health care, mapping, monitoring, law enforcement and other underlying resource efficiencies of robotic tools with sophisticated mathematic modelling implementation. Chapter 11 relays fault-tolerant control and 'online' fault estimation of sustainable wind turbines, helping to robustly optimise energy production systems. Chapter 12 discusses deep learning with respect to environmental systems, giving examples of predictive approaches which could lead to many thousands of lives being saved amidst the increasing risks and erratic conditions of planet Earth. This final chapter holds keys for both mitigation and responses to problematic scenarios that we face with increasing frequency.

The chapters covering the first three perspectives are evenly spaced by pictorial contributions made from across the world, highlighting that which we must safeguard and value. The pictorial sections refine particularly urgent problems which require attention, or additionally provide solutions through different methods of environmental sustainability operated constructively, in terms of ecology and communities. The pictorial sections consist of community-donated material and serve to complement the descriptive chapter sections, enabling combined ownership of the volume and synergistic learning to take place between approaches of countering protection and provision of sustainable systems. Part I takes us to Indonesia, illustrating traditional local villages, islands, waterfalls and birds; endemic and rare species requiring collaborative protection lest they are lost forever. Part II returns us to Indonesia and shows international and local conservation implementation and monitoring led by key community members and initiatives. Unique and perilously vulnerable species are shown, some of which may be lost before extensive studies have been carried out due to the lack of global systematic programmes valuing our planet's diversity. Part III contains a contrast between Greece and the Philippines. Greek approaches to illustrate and counteract ecosystem desolation brought about through management processes, which led to loss of organic matter and land resources, are shown in plantation restoration efforts. Finally, proudly resilient communities of the Philippine Islands are shown instigating innovative methods, mixed management and natural complements to diversity. Coconut farming, small livestock and fishing provide community strength, whilst the islands are

devastated by the increasing frequency of extreme weather and sea level rise. Heartfelt thanks to those who contributed.

Mathematic rigour incorporates both Boolean/operational techniques and semantic, logic-based Bayesian methodologies and generative math pertinent to situation projection and progressive development. Mathematic techniques incorporating optimisation, functional expressions, linguistic categorization, and mention of critical areas for policy makers in their measurements of changing demographics amidst uncertain environments are given due attention. Considering a deep learning approach assists in moderating the effect of our activities and provides proactive response options to enrich our collective overview of Earth frameworks. We emphasize protective significance; supported naturalized variety is possible, given that we make full consideration of the consequences which our seemingly unbounded resource use cause.

Earth Systems Protection and Sustainability has refined focus and a combinatorial function for protection and insurance of sustainability amidst pressures projected to worsen, given our increasing demographics. Relevant chapters and synergistic parts are provided; key nodes inform centres of learning, governments, international units and local individuals of the undeniable threats to planet Earth and its diversity. Scientific and analytical chapters are mixed with qualitatively resilient approaches and socioeconomic development, framing sustainability in complexes of climatic forces and species relations.

Alternate reflective formats of enlightening chapters, and beautiful pictorial sections refine the descriptive parts for readers; giving ownership of 'ESP' and sustainability to the global community, and issues of most pressing concern. Hence 'problems' and 'solutions' are given across Earth and human influence, providing effective balance for our continued presence.

The relevance of this volume for development goes beyond current predicaments and aims to enhance the proliferation of life on Earth, through and beyond the current era. A final thanks to those who read the volume or express appreciation of ESP and sustainability; we hope you enjoy your adventures as much as the beauty around you benefits from your focus on the horizon.

London, UK — James N. Furze
Isfahan, Iran — Saeid Eslamian
Baghdad, Iraq — Safanah M. Raafat
Quito, Ecuador — Kelly Swing
14 July 2022

Contents

Contributors

Ismail Abd-Elaty Water & Water Structures Engineering Department, Faculty of Engineering, Zagazig University, Zagazig, Egypt

Ruaa H. Ahmed Electrical Engineering Department, University of Technology-Iraq, Baghdad, Iraq

Ahmed A. Alawsi College of Science, Physics Department, University of Wasit, Wasit, Iraq

Adel Ali Saeed Al-Gheethi Micropollutant Research Centre (MPRC), Department of Water and Environmental Engineering, Faculty of Civil and Environmental Engineering, Universiti Tun Hussein Onn Malaysia, Parit Raja, Batu Pahat, Johor, Malaysia

Carolina Cabezas Department of Physical Resources, Health Service of Talcahuano, Talcahuano, Chile

Alicia Cerda Department of Pre-inversion, Ministry of Health, Santiago, Chile

Mostafa Chorom Faculty of Agriculture, Department of Soil Science, Shahid Chamran University, Ahvaz, Iran

Nor Haakmal Ab Durahim Micropollutant Research Centre (MPRC), Department of Water and Environmental Engineering, Faculty of Civil and Environmental Engineering, Universiti Tun Hussein Onn Malaysia, Parit Raja, Batu Pahat, Johor, Malaysia

Semin Sinem Cacho Duran Artist, Antalya, Turkey

Saeid Eslamian Department of Water Engineering, College of Agriculture, Isfahan University of Technology, Isfahan, Iran

James N. Furze Royal Geographical Society (with the Institute of British Geographers), London, UK

Laboratory of Biotechnology and Valorization of Natural Resources, Faculty of Sciences-Agadir, Department of Biology, Ibn Zohr University, Agadir, Morocco

Control and Systems Engineering Department, University of Technology-Iraq, Baghdad, Iraq

Claudio Garuti Fulcrum Engineering, University of Chile, Santiago, Chile

Ali S. Hadi Electrical Engineering Department, University of Technology, Baghdad, Iraq

Mona G. Ibrahim Environmental Engineering Department, Egypt-Japan University of Science and Technology (E-JUST), New Borg El Arab City, Alexandria, Egypt

Environmental Health Department, High Institute of Public Health, Alexandria University, Alexandria, Egypt

Neemat Jaafarzadeh Environmental Technologies Research Center, Ahvaz Jundishahpur University of Medical Sciences, Ahvaz, Iran

Subhankar Karmakar Centre for Environmental Science and Engineering (CESE), Inter Disciplinary Program in Climate Studies, Centre for Urban Science & Engineering (C-USE), Indian Institute of Technology Bombay, Powai, Mumbai, India

Asaad A. Kraidi Electrical Engineering Department, University of Technology-Iraq, Baghdad, Iraq

Anand Kumar Department of Electrical Engineering, Indian Institute of Technology Banaras Hindu University, Varanasi, Uttar Pradesh, India

Electrical Division, CSIR-National Aerospace Laboratories, Bangalore, Karnataka, India

Sachin Kumar Department of Electrical Engineering, Indian Institute of Technology, Banaras Hindu University, Varanasi, Uttar Pradesh, India

Dipa Lalwani Department of Environmental Science and Technology, Institute of Science and Technology for Advance Studies and Research (ISTAR), Vallabh Vidhyanagar, India

Zalak Lukhi Faculty of Civil Engineering, Dr. S. & S. S. Ghandhy Government Engineering College, Surat, India

Ali M. Mahmood Control and Systems Engineering Department, University of Technology-Iraq, Baghdad, Iraq

Zainab S. Mahmood Control and Systems Engineering Department, University of Technology-Iraq, Baghdad, Iraq

Darshan Mehta Faculty of Civil Engineering, Dr. S. & S. S. Ghandhy Government, Engineering College, Surat, India

Radin Maya Saphira Radin Mohamed Micropollutant Research Centre (MPRC), Department of Water and Environmental Engineering, Faculty of Civil and Environmental Engineering, Universiti Tun Hussein Onn Malaysia, Parit Raja, Batu Pahat, Johor, Malaysia

Mohit Prakash Mohanty Centre for Environmental Science and Engineering, Indian Institute of Technology Bombay, Mumbai, India

Ahmed R. Nasser Control and Systems Engineering Department, University of Technology-Iraq, Baghdad, Iraq

Amir Parnian National Salinity Research Center (NSRC), Agricultural Research Education and Extension Organization (AREEO), Yazd, Iran

Gautam V. Priyadarshi Department of Earth and Environmental Science, Krantiguru Shyamji Krishna Verma (KSKV) Kachchh University, Bhuj, Kachchh, India

Safanah M. Raafat Automation and Robotics Research Unit, Control and Systems Engineering Department, University of Technology-Iraq, Baghdad, Iraq

Firas A. Raheem Automation and Robotics Research Unit, Control and Systems Engineering Department, University of Technology-Iraq, Baghdad, Iraq

Junita Abd Rahman Micropollutant Research Centre (MPRC), Department of Water and Environmental Engineering, Faculty of Civil and Environmental Engineering, Universiti Tun Hussein Onn Malaysia, Parit Raja, Batu Pahat, Johor, Malaysia

Raghavan Rajendran Propulsion Division, CSIR-National Aerospace Laboratories, Bangalore, Karnataka, India

R. K. Saket Department of Electrical Engineering, Indian Institute of Technology, Banaras Hindu University, Varanasi, Uttar Pradesh, India

Mahmoud Samy Environmental Engineering Department, Egypt-Japan University of Science and Technology (E-JUST), New Borg El Arab City, Alexandria, Egypt

Department of Public Works Engineering, Faculty of Engineering, Mansoura University, Mansoura, Egypt

Montadher S. Shaker Electrical Engineering Department, University of Technology-Iraq, Baghdad, Iraq

Salvatore Straface Department of Environmental Engineering, University of Calabria, Rende, Italy

Kelly Swing Tiputini Biodiversity Station, College of Biological and Environmental Sciences, University of San Francisco de Quito, Quito, Ecuador

Tropical Ecology Program, Boston University, Boston, MA, USA

Syafik Akmal Tajuddin Micropollutant Research Centre (MPRC), Department of Water and Environmental Engineering, Faculty of Civil and Environmental Engineering, Universiti Tun Hussein Onn Malaysia, Parit Raja, Batu Pahat, Johor, Malaysia

Mrugesh H. Trivedi Department of Earth and Environmental Science, KSKV Kachchh University, Bhuj, Kachchh, India

Sahita Waikhom Faculty of Civil Engineering, Dr. S. & S. S. Ghandhy Government Engineering College, Surat, India

Vipin Yadav Faculty of Civil Engineering, Dr. S. & S. S. Ghandhy Government Engineering College, Surat, India

About the Editors

Dr. James N. Furze is a member and Fellow of the Laboratory of Biotechnology and Valorization of Natural Resources at Ibn Zohr University, Morocco; Control and Systems Engineering Department at the University of Technology-Iraq, Iraq; and an elected Fellow of the Royal Geographical Society (with the Institute of British Geographers), England.

Dr. Saeid Eslamian is a Professor of Hydrology and Water Resources Sustainability in the Department of Water Engineering and Director of the Centre of Excellence for Risk Analysis and Natural Hazards at Isfahan University of Technology, Iran.

Dr. Safanah M. Raafat is a Professor in the Control and Systems Engineering Department at the University of Technology-Iraq, Iraq.

Dr. Kelly Swing is a Professor of Tropical Ecology and Environmental Science and Director Emeritus of the Tiputini Biodiversity Station, at the University of San Francisco de Quito, Ecuador.

Part I
Indonesia – Local People and Reasons to Conserve

Indonesia is home to an array of biodiversity, for example a collection of local villages, islands, waterfalls, birds, endemic dwarf water buffalo and an indigenous breed of cow. The islands of Indonesia show unique beauty, endemic species and culture requiring essential protection. Photographic figures feature images between 2016 and 2020 and were provided in 2021 by resident conservation leader Hally Day.

Fig. 1 The Bajo people are an Indonesian ethnic tribe who live nomadically across Indonesia, Malaysia and the Philippines. A house of the 'Sea Gypsy' in a Bajo village, Buton Island, July 2017
Fig. 2 Bajo 'floating' village, Buton Island, July 2017
Fig. 3 Local traditionally built Bajo villagers house, Manui Island, July 2016
Fig. 4 'Coconut Island', Manui Island, July 2016
Fig. 5 Manui Island, July 2016
Fig. 6 Lesan Dayak, Kalimantan Timur, May 2017
Fig. 7 Palm tree, Lambusango Forest, Buton Island, February 2018
Fig. 8 Water-fall, Kusambi, Buton Island, June 2018
Fig. 9 Tarsier (*Tarsius* sp.) of Lambusango Forest, Buton Island, January 2019
Fig. 10 Malay Civet (*Viverra tangalunga*), Lapago Forest, Buton Island, June 2019
Fig. 11 Endemic Dwarf Buffalo (*Bubalus* sp.) and indigenous bred Banteng (*Bos javanicus*) of Kakenauwe Forest, Buton Island, May 2018
Fig. 12 Yellow-sided Flowerpeckers (*Dicaeum aureolimbatum*) of Kakenauwe Forest, Buton Island, March 2019
Fig. 13 Owl (*Ninox* sp.) present on farmland of Labundo-Bundo, Buton Island, December 2018
Fig. 14 Sulawesi Dwarf Kingfisher (*Ceyx fallax*) of Lapago (Lambusango Forest), Buton Island, July 2019
Fig. 15 Black-headed Kingfisher (*Actenoides monachus capucinus*) present in farmland of Labundo-Bundo, Buton Island, May 2017

Beautiful conservation work in this mega-diverse hotspot is shown in part II.

Fig. 1

Fig. 2

Fig. 3

Fig. 4

Fig. 5

Fig. 6

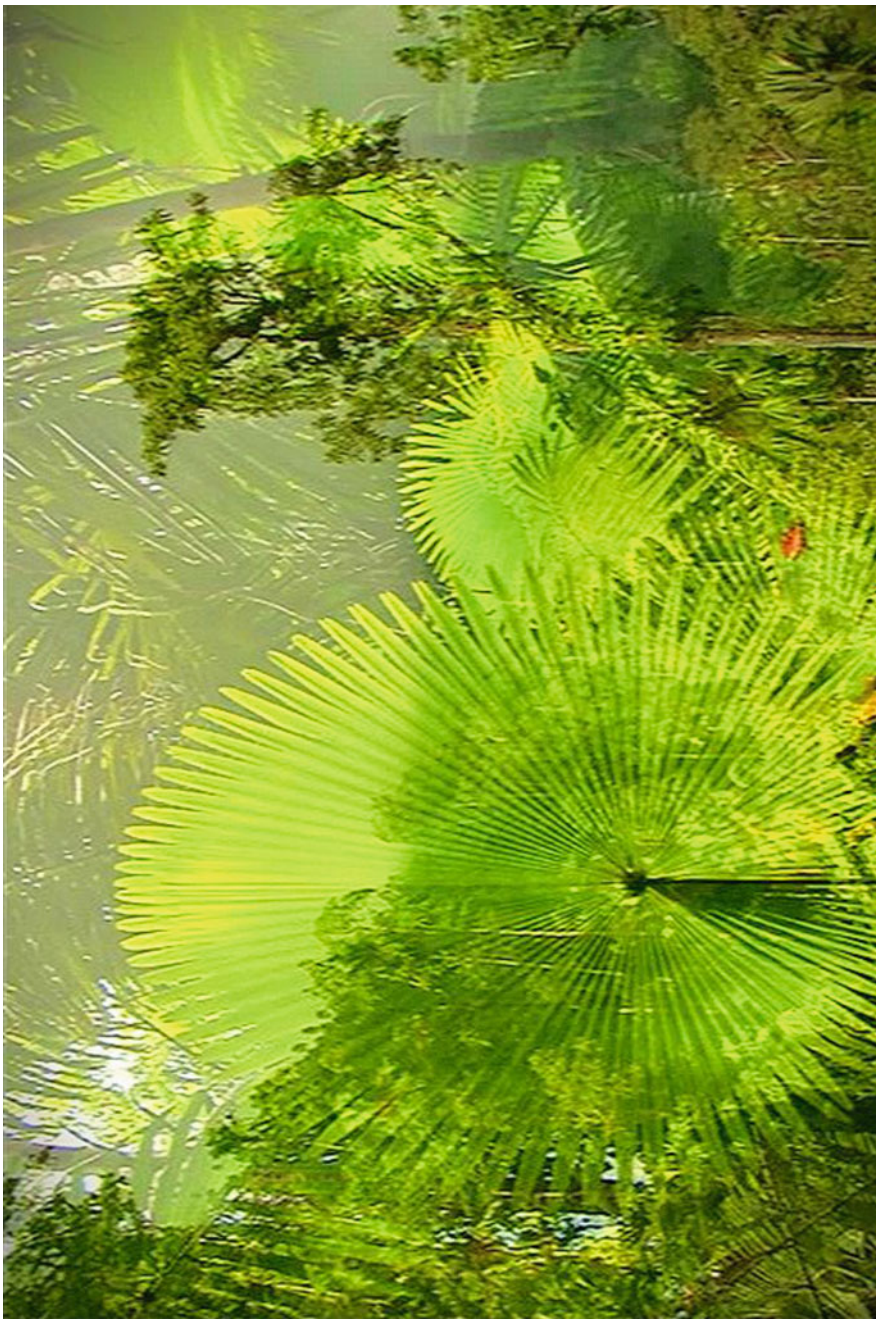

Fig. 7

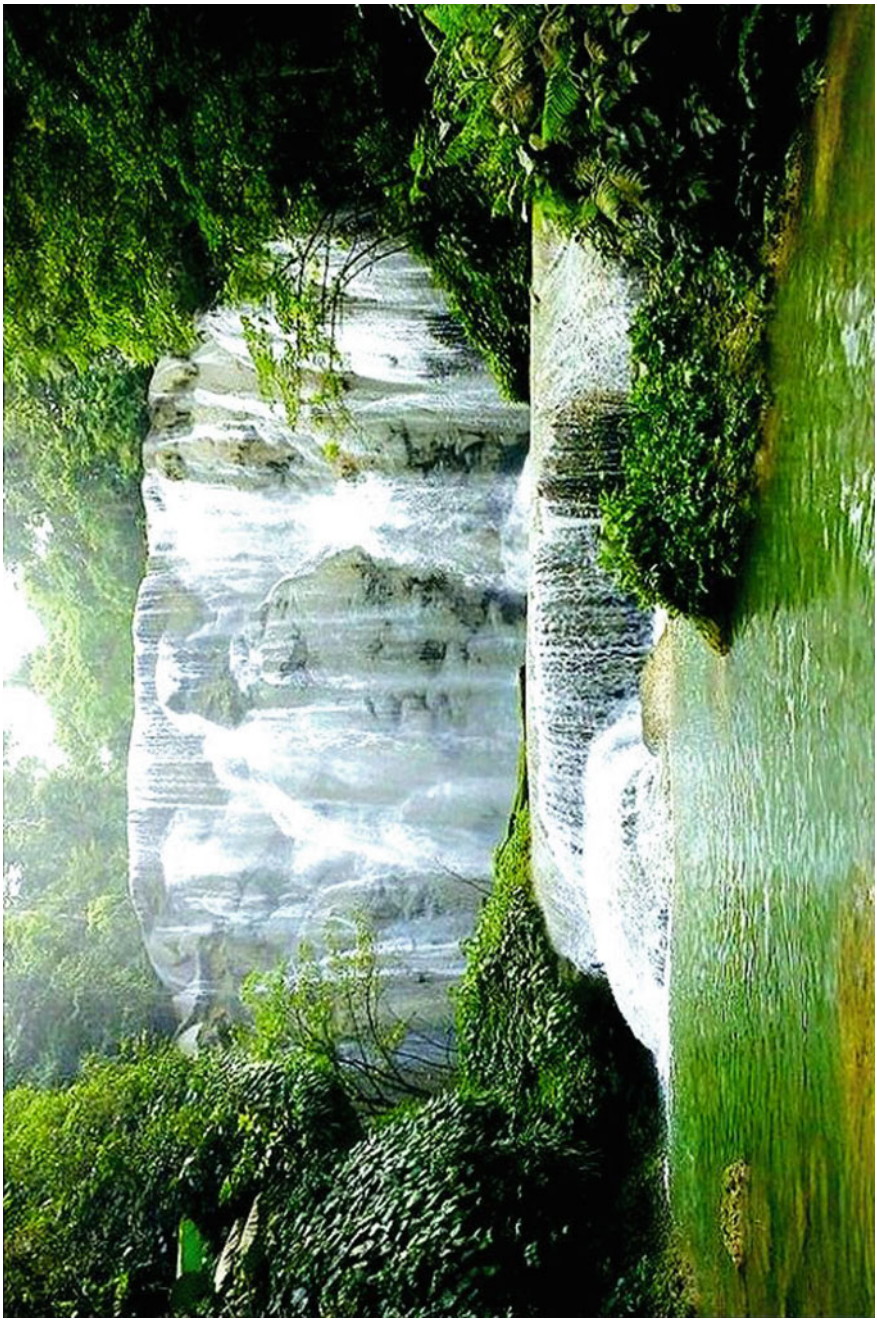

Fig. 8

Fig. 9

Fig. 10

Fig. 11

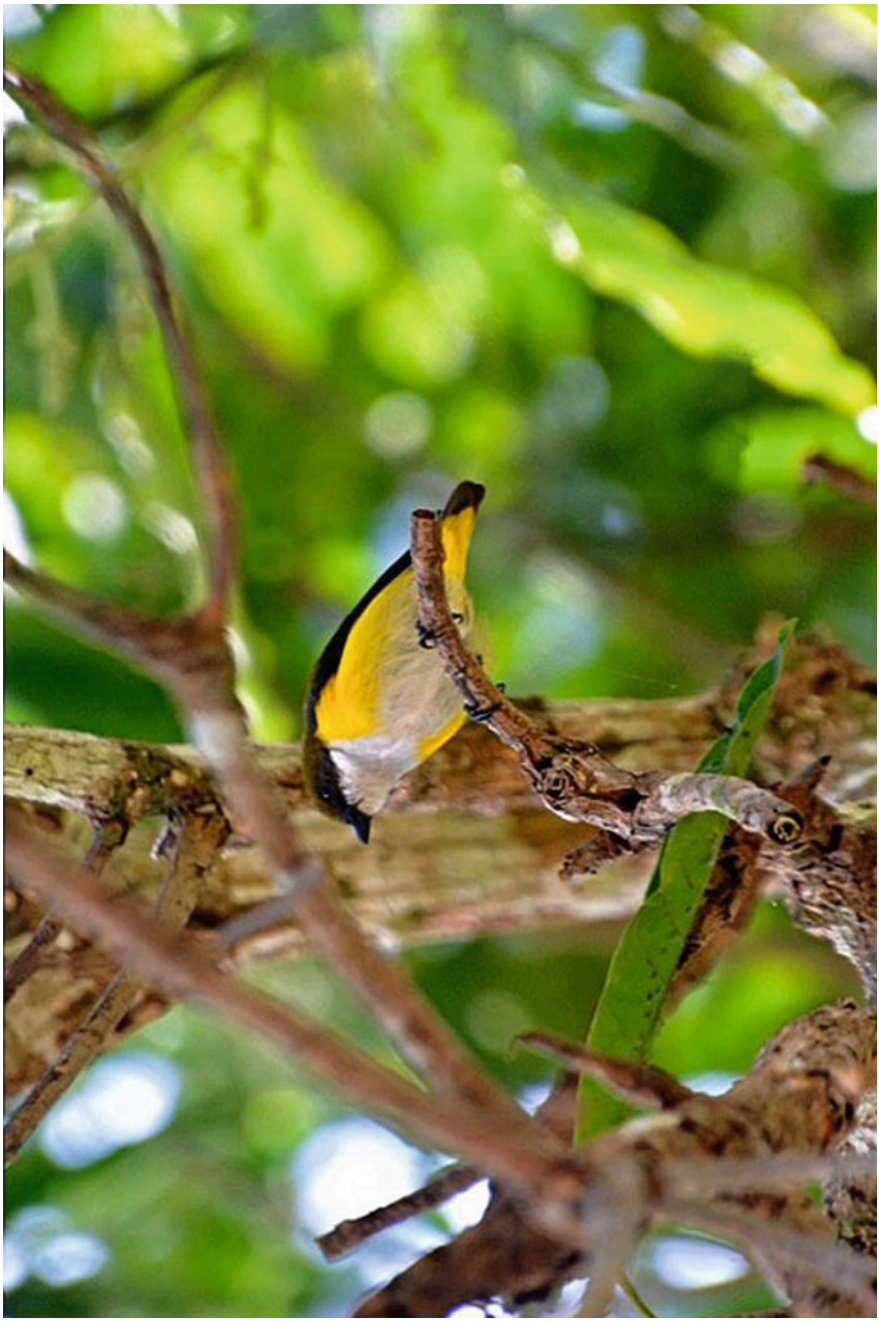

Fig. 12

Fig. 13

Fig. 14

Fig. 15

Chapter 1
Competitive Bioaccumulation by *Ceratophyllum demersum* L.

Amir Parnian, James N. Furze, Mostafa Chorom, and Neemat Jaafarzadeh

Abstract Heavy metals produced during anthropic activities and as a consequence of geological processes affect biological systems via bioaccumulation. Bioaccumulation is a process within phytoremediation. Specific classes of elements are bioaccumulated relative to other element classes and their concentrations. The aim of this chapter is to detail an investigation of the interaction and simultaneous absorption of two heavy metals by the aquatic plant *Ceratophyllum demersum* L.

Plants were cultivated for 8 days in nutrient solutions enriched with incrementally increasing concentrations of cadmium (Cd) and nickel (Ni). To examine the preferred/competitive absorption of these metals by plants, Ni and Cd concentrations were measured in initial, final growth solutions and in the plant matter. The highest absorption percentages were observed in treatments containing Cd 4 mg l^{-1} and Ni 1 mg l^{-1}, being 86.5% and 79.0%, respectively.

Increase of the heavy metals concentration correlates with plant absorption of the pollutants but was limited by toxicity effects. The performance of *C. demersum* was sufficient for simultaneous removal of Cd and Ni. Competitive bioaccumulation via

A. Parnian (✉)
National Salinity Research Center (NSRC), Agricultural Research Education and Extension Organization (AREEO), Yazd, Iran
e-mail: amir.parnian86@gmail.com

J. N. Furze
Royal Geographical Society (with the Institute of British Geographers), London, UK

Laboratory of Biotechnology and Valorization of Natural Resources, Faculty of Sciences-Agadir, Department of Biology, Ibn Zohr University, Agadir, Morocco

Control and Systems Engineering Department, University of Technology-Iraq, Baghdad, Iraq
e-mail: james.n.furze@gmail.com; jamesfurze@hotmail.com

M. Chorom
Faculty of Agriculture, Department of Soil Science, Shahid Chamran University, Ahvaz, Iran
e-mail: m.chorom@scu.ac.ir

N. Jaafarzadeh
Environmental Technologies Research Center, Ahvaz Jundishapur University of Medical Sciences, Ahvaz, Iran
e-mail: jaafarzadeh-n@ajums.ac.ir

J. N. Furze et al. (eds.), *Earth Systems Protection and Sustainability*,
https://doi.org/10.1007/978-3-030-98584-4_1

phytoremediation and its effective absorption dynamic offers great hope for remediation of aquatic and semi-aquatic ecosystems as well as restorative potential for land subjected to industrial activity or intensive agriculture.

Keywords *Ceratophyllum demersum* L. · Competitive bioaccumulation · Phytoremediation · Cadmium (Cd) · Nickel (Ni)

1.1 Introduction

Heavy metals are elements with a specific gravity of 5.0 $g.cm^{-3}$ or more and an atomic weight ranging from 63.5 to 200.6 $g.g^{-1}.mol^{-1}$ (Srivastava and Majumder 2008). Among these metals nickel (Ni) and cadmium (Cd) are released as divalent cations into the environment through human activities including metal finishing, automotive, electroplating, battery production, tannery, electric cable production, mining, steel, and textile industries. Different concentrations of metals consequently accumulate in wastewaters through runoff. Unless constrained by high pH values, these cations are highly mobile and bioavailable (Bonfranceschi et al. 2009). Heavy metals are toxic to the aquatic ecosystem and flow freely to water bodies, providing direct risks and danger to human and ecosystem health. In water bodies, several metals exist at toxic levels, resulting in undesirable living conditions and severe trophic consequences (Saygıdeğer and Doğan 2004). Heavy metals accumulate in organisms in tolerance levels (Sawidis et al. 2001; Demirezen et al. 2007).

The residual and persistent presence of Cd poses great environmental concerns due to its high toxicity to animals and humans. Cd is readily bioaccumulated by plants in levels that are not harmful to them though are toxic to the animals consuming those plants. In turn, humans are more sensitive to Cd toxicity, due to the metals' cumulative concentration and concentrated accumulation in internal organs following consumption of Cd-contaminated foods (Tudoreanu and Phillips 2004; Kirkham 2006). Toxic levels of Cd decrease water uptake, photosynthetic processes, and nutrient uptake in plants (Wojcik and Tukiendorf 2004; Mohanpuria et al. 2007).

Ni is essential for plant and ecosystem survival (Chorom et al. 2012). In plants it is required in small but critical concentrations. However, Ni causes serious kidney, lung, stomach, and skin problems in humans and animals and is a known carcinogen (Fu and Wang 2011). Ni toxicity in plants disrupts membrane functionality, effects ionic imbalance (of K^+) in the cytoplasm, and alters internal water relations (Pandey and Sharma 2002).

Phytoremediation is the use of plants to remediate contaminated environments. The biological method remediates air, soil, and aquatic environments (Pivetz 2001). Phytoremediation is promising, low cost, and environmentally sustainable and may be used in the remediation of contaminated water containing trace elements (Chorom et al. 2012; Parnian et al. 2016).

Plants have two physically differentiated means by which they remediate contaminants, foliar surfaces and root systems, enabling versatility depending on which

area has contact with the contamination (Demirezen et al. 2007; Sawidis et al. 2001). The phytoremediation active surface area is the plant's organ/part that is in direct contact with pollutants and plays a major role in the remediation process (Dhir 2013). In aquatic medium phytoremediation primary interfaces are commonly the roots or shoots (Parnian and Furze 2021; Thomas et al. 2016; Upadhyay et al. 2014). The higher active surface area of a plant effects the remediation performance of it, and is further supported by additional absorption uptake interfaces; accompanied by activities of suitable microorganisms (Pivetz 2001). Phytoremediation encompasses various mechanisms, the most successful being phytostabilization, rhizodegradation, rhizofiltration, phytodegradation, phytoextraction, phytoaccumulation, and phytovolatilization (Jeevantham et al. 2019).

Phytoremediation technology has been applied in the cleanup of aquatic environments including groundwater (Martino et al. 2019), seawater (Bastos et al. 2019), drainage (Parnian et al. 2017), and wastewater (Panja et al. 2020). There are numerous (originally aquatic) plants with a capacity for aquatic environment remediation (Ansari et al. 2020), some of which have migrated to terrestrial areas (Darajeh et al. 2019). All plants have restorative functions in ecosystems. Furthermore, phytoremediation approaches seek to make use of the most effective plants as candidates for different settings of environmental cleanup. The choice of species used in phytoremediation of contaminated environments is dependent on the following criteria: a high ability to absorb contaminants, a high biomass production, and a high ability of transferring contaminants from absorbing surfaces to "removable" parts. Optimistically, endemic or noninvasive plant species should be used, having a capacity for rapid adaptation to local climatic conditions, thus reducing economical costs and environmental impacts of the remediation.

Ceratophyllum demersum L. normally grows with its stem buried in sandy or silty substrates and is prone to dislodgement (Global Invasive Species Database 2022). It is a submerged, rootless, free-floating plant which achieves stable, cosmopolitan distribution (Szabó et al. 2022). It belongs to the order Nymphaeales, family Ceratophyllaceae (hornworts). Its growth proliferates in shallow, muddy, and quiescent water bodies at low light intensities (Aravind and Prasad 2005). *C. demersum* is known for its use in heavy metal remediation, including that of Cd (Polechońska and Klink 2021), Pb (Mahmoud et al. 2018), and Ni (Polechońska et al. 2018).

C. demersum remediates aquatic mediums through the following mechanisms:

(i) Phytoextraction: The uptake of a contaminant from contaminated environments by an absorbing organ/part of a plant and its translocation into harvestable/removable organs/parts. *C. demersum* does not possess a relatively large active root, though uptakes elements with its entire body. The physiology of the species enables its use in highly effective bioaccumulation of contaminants, and may be removed using biological control and mechanical methods following remediation (Jacobs and Best 1990; Engel 1990; Verma and Charudattan 1993; Wells et al. 2003). Further, although *C. demersum* is considered highly invasive, invasion of ecosystems can be moderated ecologically; complementary, selection effects amongst biodiversity and similar functional groups being

present where it is introduced have been seen to be effective (Petruzella et al. 2018). *C. demersum* is effective in heavy metal removal (Parnian et al. 2016).

(ii) Rhizodegradation: A special kind of surface degradation, contaminant degradation occurs in the contaminated environment, commonly in the rhizospheric areas. In most submerged aquatic plants, the entire surface of the plant's body is considered as a special surface; microorganisms are also involved in the degradation process. *C. demersum* effectively reduces chemical oxygen demand (COD) of water bodies (Luo et al. 2019).

(iii) Rhizofiltration or phytofiltration: Contaminant absorption from polluted environments. In the process contaminants are adhered onto the plant active area and then filtered through the plant. The technique is used in hydroponic growth of plants, though *C. demersum* commonly remediates waters of suspended solids, thereby reducing water turbidity (Beheary et al. 2019).

(iv) Phytodegradation: The process of contaminant degradation by plants as a result of the plant metabolism. Nitrate removal and remediation of contaminated water bodies using *C. demersum* exemplify the degradation process (Xu et al. 2019).

Hydrophyte uptake and accumulation of elements occur through the foliar surface and/or the root system (Shi et al. 2021). Moreover, hydrophytes' uptake of metals is dependent on biotic and abiotic factors such as temperature, pH, salinity, and the presence of dissolved ions in water (Ebrahimbabaie et al. 2020). In many regions, metals appear in combination together. It has become clear that toxic trace elements affect seed germination and plant growth, though the relationships affecting heavy metal accumulation in plants remain poorly understood. In this study, *C. demersum* is the chosen species as it accumulates high concentrations of trace elements (Khan et al. 2009). *C. demersum* has a high capacity for vegetative propagation and biomass production even under modest nutritional conditions. It is useful as an oxygenator and has found use in closed equilibrated biological aquatic systems (CEBAS). *C. demersum* can be a biofilter for heavy metals.

The objective of this chapter is to show the competitive bioaccumulation of heavy metals (Cd and Ni) by the free-floating hydrophyte *C. demersum* L.

1.2 Climatic Conditions of the Competitive Bioaccumulation Experimental Site

The experimental study was conducted between November 2009 and February 2010 at the College of Agriculture, Shahid Chamran University (SCU), in the city of Ahvaz in Iran (31° 18′ 12.2″ N, 48° 39′ 29.6″ E). Climatic conditions incuded a mean daily temperature of 24 ± 5 ° C, mean daily relative humidity of 55 ± 25%, daily maximum global radiation between 650 and 1100 Wm^{-2}, and direct radiation between 400 and 1050 Wm^{-2}, according to the university meteorological center (SCU Meteorological Data Collection Center 2010).

1.3 Maintenance of Stock Cultures of *Ceratophyllum demersum* L.

Hornwort cedar moss (*C. demersum* L.) is commonly available in Ahvaz County, Iran. Cultures of *C. demersum* L. were obtained from an irrigation dyke of Shahid Chamran University shown in Fig. 1.1. Five kilograms of plants were collected by hand during an irrigation cycle as shown in Fig. 1.2. Irrigation water properties are given in Table 1.1. Plants were placed outdoors in 30 L plastic containers shown in Fig. 1.3, filled with half-strength Hoagland-Arnon nutrient solution (Marin and Oron 2007); the composition used is given in Table 1.2.

Plants were cultivated for 4 weeks prior to the beginning of the experiment. The nutrient solution was stabilized at a pH equal to 7.0 and was replenished every 3 days. Preliminary tests for pH were performed to determine the optimum pH range for plant growth and metal accumulation.

1.4 Experimental Setup and Heavy Metal Analysis

Eight-day batch experiments were conducted to evaluate Cd and Ni removal by *C. demersum*. In this study, nickel nitrate ($Ni(NO_3)2{\cdot}6H_2O$) and cadmium chloride ($CdCl_2.4H_2O$) (Merck) were used in treatments. The experiments were performed

Fig. 1.1 *C. demersum* L. collection from irrigation dyke of Shahid Chamran University, Ahvaz, Khuzestan Province, Iran, 2010

Fig. 1.2 Dry irrigation dyke, Shahid Chamran University, Ahvaz, Khuzestan Province, Iran, 2010

Table 1.1 Irrigation water properties, Shahid Chamran University, Ahvaz, Khuzestan Province, Iran, 2010

Water properties	Turbidity	EC	pH	HCO_3^-	TDS	NO_3^-	COD	BOD	DO	TSS
Unit	NTU	dSm^{-1}	–	$mEql^{-1}$	$mg\ l^{-1}$					
Concentration	5	2.69	7.7	3.12	1722	7.58	13.2	3.58	6.4	60

EC electrical conductivity, HCO_3^- bicarbonate, *TDS* total dissolvable solids, NO_3^- nitrate, *COD* chemical oxygen demand, *BOD* biological oxygen demand, *DO* dissolved oxygen, *TSS* total suspended solids, *NTU* nephelometric turbidity units, dSm^{-1} deciSiemens per meter, $mEql^{-1}$ milliequivalents of solute per liter of solution, $mg\ l^{-1}$ milligrams per liter

outdoors in 3 L plastic receptacles with a surface area of 432 cm^2. A total of 16 different treatments were tested in half-strength Hoagland-Arnon nutrient solution. The selected Cd and Ni concentrations are shown in Table 1.3.

Table 1.3 shows the increasing concentrations of heavy metals investigated in the batch experiments.

Three replicates were made for each treatment; three receptacles without *C. demersum* were set as controls. Each replicate was filled with 2.5 L of half-strength Hoagland-Arnon hydroponic nutrient solution contaminated with a combination of Cd and Ni as shown in Fig. 1.4.

The solutions were adjusted to pH 7.0 with 0.01 M NaOH and 0.01 M HCl (Parneyan et al. 2011). Every day during cultivation, the solution volume was maintained with deionized water. Preliminary tests for Ni and Cd concentrations

Fig. 1.3 *C. demersum* L. collected and cultivated outdoors in half-strength modified Hoagland-Arnon nutrient solution, Shahid Chamran University, Ahvaz, Khuzestan Province, Iran, 2010

Table 1.2 The composition of half-strength modified Hoagland-Arnon nutrient solution

Chemical name	Chemical formula	Concentration	Unit
Potassium nitrate	KNO_3	3	mM
Calcium nitrate	$Ca(NO_3)_2$	2	mM
Ammonium dihydrogen phosphate	$NH_4H_2PO_4$	0.5	mM
Magnesium sulfate	$MgSO_4$	1	mM
Ferric EDTA	Fe–EDTA	10	μM
Boric acid	H_3BO_3	1.5	μM
Manganese(II) sulfate	$MnSO_4$	0.25	μM
Copper(II) sulfate	$CuSO_4$	0.1	μM
Zinc sulfate	$ZnSO_4$	0.2	μM
Molybdic acid	H_2MoO_4	0.025	μM

Table 1.3 Cd and Ni concentrations in treatments

Ni:Cd (mg l^{-1})			
0.00:0.00	0.00:1.00	0.00:2.00	0.00:4.00
1.00:0.00	1.00:1.00	1.00:2.00	1.00:4.00
2.00:0.00	2.00:1.00	2.00:2.00	2.00:4.00
4.00:0.00	4.00:1.00	4.00:2.00	4.00:4.00

were performed to determine the appropriate sensitivity range of *C. demersum* (Parnian et al. 2016; Chorom et al. 2012). Twenty grams fresh weight (FW) of plants were added to each treatment replicate set. Treatment and control vessels were randomly arranged.

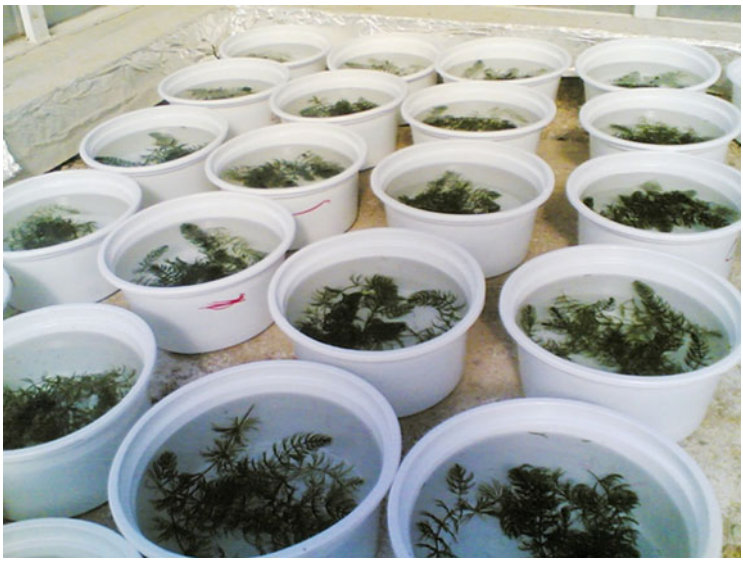

Fig. 1.4 *C. demersum* cultivated in contaminated hydroponic nutrient solution, Shahid Chamran University, Ahvaz, Khuzestan Province, Iran

1.5 Biomass Production Measurements

Plant biomass production, Pr (g FW day^{-1}), was calculated as follows:

$$\mathrm{Pr} = (\mathrm{FW2} - \mathrm{FW1})/\Delta t \tag{1.1}$$

where FW_1 and FW_2 were plant fresh weight (g) at time 1 and time 2, respectively, and Δt is the difference between time 1 and time 2 (Parnian et al. 2016).

1.6 Quantification of Metals Removed from Nutrient Solutions by Plants Active Uptake

Removal of the metals from the nutrient solutions was determined by measuring the concentration of metal left in the medium. The water sampling period commenced at day 0, with 2 ml samples being taken daily to ascertain the heavy metal concentration. Heavy metal presence and concentrations in water samples were determined by atomic absorption spectrophotometry according to standard methods for examination of water and wastewater (APHA 2005). Removal of metals was calculated using the following equation:

$$R(\%) = [(C_0 - C_t)/C_0] \times 100 \quad (1.2)$$

where C_0 and C_t represent the residual concentration of metal at the beginning of the experiment and at time t, respectively (Khellaf and Zerdaoui 2009).

1.7 Statistical Analysis

One-way ANOVA was performed to identify significant differences in metal concentrations in the different treatments. Differences were considered as significant at $p < 0.05$. Statistical analyses were performed with SPSS 16 and Excel 2010.

1.8 Cd and Ni Removal from Water

Table 1.4 shows the percentage of Ni removal for different initial concentrations by *C. demersum* in competition with different initial concentrations of Cd.

Under the conditions of this study, the highest removal efficiencies of Ni by *C. demersum* occurred in all of the treatments with an initial concentration of Ni equal to 1 mg l^{-1} as shown in Table 1.4. Overall, the Ni removal values by *C. demersum* increased with an increase of Cd initial concentration with the following three exceptions of Ni initial concentration and Cd initial concentration: 2 mg l^{-1}, 4 mg l^{-1}; 4 mg l^{-1}, 2 mg l^{-1}; and 4 mg l^{-1}, 4 mg l^{-1}. In these three treatments, *C. demersum* showed a low capacity of Ni removal. *C. demersum* growth was slowed when heavy metal concentrations were high; the Ni removal was thus impaired by heavy metal toxicity (Parnian et al. 2016). The increasing effect of Cd on the Ni removal efficiency of *C. demersum* is caused by decreasing cellular membrane selective permeability, causing plants to lose their controlled uptake ability (Marschner and Marschner 2012; Chen et al. 2015). Previous studies have shown that the submerged aquatic plant *C. demersum* can be successfully used for heavy metal (Pb, Zn, and Cu) removal under dilute metal concentrations (Keskinkan et al. 2004). Other macrophytes (*Spirodela polyrhiza*, *Pistia stratiotes*, and *Eichhornia crassipes*) demonstrated Ni and Cd removal percentages over 45% and more than 50%, respectively, in a 15-day period (Mishra and Tripathi 2008).

Table 1.4 *C. demersum* Ni removal efficiency for different initial concentrations of Ni and Cd

	Cd = 0 mg l^{-1}	Cd = 1 mg l^{-1}	Cd = 2 mg l^{-1}	Cd = 4 mg l^{-1}
Ni = 0 mg l^{-1}	0%^{a}	0%^{a}	0%^{a}	0%^{a}
Ni = 1 mg l^{-1}	77%^{a}	67%^{c}	71%^{b}	79%^{a}
Ni = 2 mg l^{-1}	52%^{b}	60%^{a}	62%^{a}	32%^{c}
Ni = 4 mg l^{-1}	50%^{b}	58%^{a}	30%^{d}	35%^{c}

Different letters in the same row indicate a significant difference at $p < 0.05$, $n = 3$

Table 1.5 *C. demersum* Cd removal efficiency for different initial concentrations of Ni and Cd

	Ni = 0 mg l^{-1}	Ni = 1 mg l^{-1}	Ni = 2 mg l^{-1}	Ni = 4 mg l^{-1}
Cd = 0 mg l^{-1}	0%[a]	0%[a]	0%[a]	0%[a]
Cd = 1 mg l^{-1}	74%[b]	77%[a, b]	38%[c]	81%[a]
Cd = 2 mg l^{-1}	84%[a]	79%[b]	82%[a, b]	29%[c]
Cd = 4 mg l^{-1}	35%[c]	86%[a]	48%[b]	37%[c]

Different letters in the same row indicate a significant difference at $p < 0.05$, $n = 3$

Table 1.6 Heavy metal effect on *C. demersum* biomass production

	Ni = 0 mg l^{-1}	Ni = 1 mg l^{-1}	Ni = 2 mg l^{-1}	Ni = 4 mg l^{-1}
Cd = 0 mg l^{-1}	2.30 ± 0.13	1.63 ± 0.08	1.27 ± 0.14	1.02 ± 0.05
Cd = 1 mg l^{-1}	1.84 ± 0.06	1.62 ± 0.10	1.15 ± 0.12	1.03 ± 0.11
Cd = 2 mg l^{-1}	1.49 ± 0.19	1.45 ± 0.13	1.01 ± 0.14	0.80 ± 0.09
Cd = 4 mg l^{-1}	1.32 ± 0.22	1.29 ± 0.16	0.83 ± 0.19	0.78 ± 0.10

Table 1.5 shows *C. demersum* percentage of Cd removal for different initial concentrations in competition with different initial concentrations of Ni ions.

Results showed that the highest removal efficiency of Ni by *C. demersum* (86%) occurred in the treatment with initial concentration of Ni 1 mg l^{-1} and Cd 1 mg l^{-1}. Overall the Cd removal values by *C. demersum* increased with increasing of metals' initial concentration. It has been proven that heavy metals can cause dysfunctions in cell plasma membranes (Devi and Prasad 1999); the latter is caused by a nickel distraction effect in ion transfer, affecting the plasma membrane of cells. In higher concentrations of Cd, this phenomenon effectively demolishes cellular membrane selective permeability (Marschner and Marschner 2012). Decreased Cd removal efficiency in high concentrations of heavy metals especially in 2 mg l^{-1} Ni, 4 mg l^{-1} Cd; 4 mg l^{-1} Ni, 2 mg l^{-1} Cd; and 4 mg l^{-1} Ni, 4 mg l^{-1} Cd initial concentrations results due to the decrease in plant biomass production as seen in Tables 1.5 and 1.6. These results are consistent with trace element removal efficiencies in different plants (Parnian et al. 2016; Chorom et al. 2012; Marin and Oron 2007).

In general, the competitive bioaccumulation of heavy metals (Ni and Cd) by *C. demersum* seen in Tables 1.4 and 1.5 shows critical metal concentrations of Ni equal to 4 mg l^{-1} and Cd equal to 4 mg l^{-1}; these concentrations of the metals mutually increased the removal efficiency of plants. At high concentrations, plant growth is reduced by the toxicity of the metal, although the metal removal efficiency may increase in certain conditions (Marschner and Marschner 2012; Parnian et al. 2016).

In highly contaminated mediums, heavy metals have been seen to demolish the cell membrane with the consequence of the cytoplasm being freely exposed to the outside environment (Wang et al. 2010). Active sites for metal adsorption will increase in such circumstance by inner sites being engaged, including proteins and the inner sides of cell membranes in addition to the outer cell membranes (Ruta et al.

2017). It may be surmised that a higher metal adsorption occurs after cell membrane defection. Exposing both the inner and outer sides of cell membranes to contaminated aqueous medium results in the defected plants adsorbing more heavy metals. In the current study, this explains *C. demersum*'s higher Cd removal efficiency when compared to 1 mg l^{-1} Ni:4 mg l^{-1} Cd and 0 mg l^{-1} Ni:4 mg l^{-1} Cd and when compared to 4 mg l^{-1} Ni:1 mg l^{-1} Cd and 2 mg l^{-1} Ni:1 mg l^{-1} Cd.

1.9 Heavy Metal Effect on Plant Biomass Production

Accumulation of heavy metal in hydrophytes produces significant growth responses (Thomas et al. 2016). Nonessential and highly toxic heavy metal Cd causes serious defects in *C. demersum* (Parnian et al. 2016). Trace concentrations of Ni are essential for plants, whereas high doses of Ni effect significant damage in *C. demersum* (Chorom et al. 2012). The biomass production results of the current study are shown in Table 1.6. Mean biomass production for *C. demersum* in the cultivation period was between 2.30 ± 0.13 and 0.78 ± 0.10 g FW day^{-1} in contaminated aquatic mediums. The mean of all treatments biomass production was in the order of Cd treated > Ni treated mediums indicating that Ni was more toxic to *C. demersum* than Cd in the experimental conditions of the current study. The latter is in agreement with published data where the same effective Ni toxicity was shown (Parnian et al. 2016). The crucial concentration of an element is one that effects its maximum absorption; at higher levels, plants show obvious physiological or morphological defects including leaf/root irregularities and additional internal dysfunction, which disrupts uptake of water/elements. The crucial concentrations for both heavy metals were 4 mg l^{-1} or less; in lower concentrations of metals, plants showed greater removal efficiency seen in Tables 1.4 and 1.5 and biomass production as in Table 1.6.

The different concentrations measured in Table 1.6 are expressed as: average ± standard deviation, $n = 3$. *C. demersum* biomass production was calculated according to equation (1.1).

In the three treatments (2 mg l^{-1} Ni, 4 mg l^{-1} Cd), (4 mg l^{-1} Ni, 2 mg l^{-1} Cd), and (4 mg l^{-1} Ni, 4 mg l^{-1} Cd), *C. demersum* showed an extreme reduction in biomass production and plant growth among these initial concentrations of contamination; the resultant change in plant morphology is illustrated in Fig. 1.5. Plant biomass production affects metal removal by reducing metal absorbance mass (Parnian et al. 2017). Hydrophytes may be selected for aquatic medium restoration based on their toxicity characteristics and removal efficiencies (Rezania et al. 2016). The tolerance of *C. demersum* to Cd and Ni indicates that this plant is effective for Cd and Ni remediation from contaminated water.

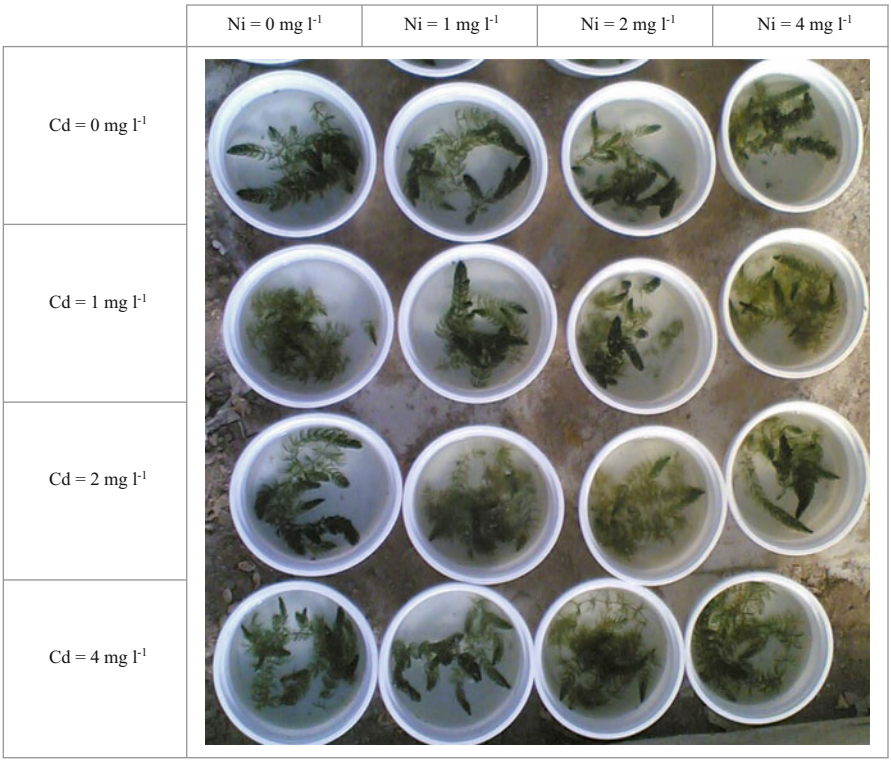

Fig. 1.5 Heavy metal effect on *C. demersum*. Day 5 of the experiment (Shahid Chamran University, Ahvaz, Khuzestan Province, Iran)

1.10 Conclusion

Heavy metal pollution poses a great risk to the environment. This pollution is present in aquatic areas including urban wastewater, drainage water, and industrial wastewater. The solution to this critical environmental problem is the use of phytotechniques.

In the current chapter, we demonstrated that the copious hydrophyte *C. demersum* of Khuzestan and Iran is very effective for phytoremediation of Ni and Cd from nutrient medium. Further the crucial metal concentration of both Ni and Cd was identified (4 mg l^{-1}) for each metal. *C. demersum* effectively mutually removed both heavy metal elements before this concentration. Concentrations greater than the crucial value impair removal efficiency.

C. demersum can be utilized for the large-scale treatment of heavy metals from contaminated effluent including steal industrial wastewater, mine and mine waste drainages, and battery factory wastewater. Further work is required with this plant in pilot studies ranging to full-scale constructed wetland with the recommended aim of

mixed-metal polluted water phytoremediation. *C. demersum* may upgrade waste stabilization lagoons in industrial zones. *C. demersum* is considered a cosmopolitan plant; integrating an ecological mosaic model involving additional species will assist in resolving complex chemical pollution, and with consideration of combinations of the correct species ultimately benefit biodiversity enrichment across the Earth.

Acknowledgments This chapter was a part of the research program "Phytoremediation of heavy metals (Ni and Cd) using two aquatic macrophytes (free-floating and floating-leaved) from steel industrial wastewater and synthetic medium", and was financially supported by the vice president for research and technology from Shahid Chamran University in Iran.

References

Ansari AA, Naeem M, Gill SS et al (2020) Phytoremediation of contaminated waters: an eco-friendly technology based on aquatic macrophytes application. Egypt J Aquat Res 46: 371–376. https://doi.org/10.1016/j.ejar.2020.03.002

APHA (2005) Standard methods for the examination of water and wastewater. American Public Health Association, Washington, DC

Aravind P, Prasad MNV (2005) Cadmium-Zinc interactions in a hydroponic system using *Ceratophyllum demersum* L.: adaptive ecophysiology, biochemistry and molecular toxicology. Braz J Plant Physiol 17:3–20. https://doi.org/10.1590/S1677-04202005000100002

Bastos E, Schneider M, Quadros DPCD et al (2019) Phytoremediation potential of *Ulva ohnoi* (Chlorophyta): influence of temperature and salinity on the uptake efficiency and toxicity of cadmium. Ecotoxicol Environ Saf 174:334–343. https://doi.org/10.1016/j.ecoenv.2019.01.130

Beheary M, Sheta BM, Hussein M et al (2019) Environmental remediation of tilapia aquaculture wastewater using *Ceratophyllum demersum* and *Lemna minor*. Egypt J Aquat Biol Fish 23:379–396. https://doi.org/10.21608/EJABF.2019.31974

Bonfranceschi BA, Flocco C, Donati ER (2009) Study of the heavy metal phytoextraction capacity of two forage species growing in an hydroponic environment. J Hazard Mater 165:366–371. https://doi.org/10.1016/j.jhazmat.2008.10.024

Chen M, Zhang LL, Li J et al (2015) Bioaccumulation and tolerance characteristics of a submerged plant (*Ceratophyllum demersum* L.) exposed to toxic metal lead. Ecotoxicol Environ Saf 122: 313–321. https://doi.org/10.1016/j.ecoenv.2015.08.007

Chorom M, Parnian A, Jaafarzadeh N (2012) Nickel removal by the aquatic plant (*Ceratopyllum demersum* L.). Int J Environ Sci Dev 3(4):372–375. https://doi.org/10.7763/IJESD.2012.V3.250

Darajeh N, Truong P, Rezania S et al (2019) Effectiveness of Vetiver grass versus other plants for phytoremediation of contaminated water. J Environ Treat Tech 7(3):485–500

Demirezen D, Aksoy A, Uruç K (2007) Effect of population density on growth, biomass and nickel accumulation capacity of *Lemna gibba* (Lemnaceae). Chemosphere 66:553–557. https://doi.org/10.1016/j.chemosphere.2006.05.045

Devi SR, Prasad M (1999) Membrane lipid alterations in heavy metal exposed plants. In: Heavy metal stress in plants. Springer, Berlin, Heidelberg, pp 99–116. https://doi.org/10.1007/978-3-662-07745-0_5

Dhir B (2013) Phytoremediation: role of aquatic plants in environmental clean-up. Springer, New Delhi

Ebrahimbabaie P, Meeinkuirt W, Pichtel J (2020) Phytoremediation of engineered nanoparticles using aquatic plants: mechanisms and practical feasibility. J Environ Sci 93:151–163. https://doi.org/10.1016/j.jes.2020.03.034

Engel S (1990) Ecological impacts of harvesting macrophytes in Halverson Lake, Wisconsin. J Aquat Plant Manage 28:41–45

Fu F, Wang Q (2011) Removal of heavy metal ions from wastewaters: a review. J Environ Manag 92:407–418. https://doi.org/10.1016/j.jenvman.2010.11.011

Global Invasive Species Database (2022) Species profile: *Ceratophyllum demersum*. http://www.iucngisd.org/gisd/species.php?sc=281. Accessed 12 July 2022

Jacobs FHH, Best EPH (1990) Effect of the time of cutting on regrowth of three species of submerged aquatic plants. Interim report on Project 717 Effects of type and frequency of mechanical management on the regrowth of submerged aquatic plants. Verslag - Centrum voor Agrobiologisch Onderzoek, No. 140. 51 pp. Available via CABI Invasive Species Compendium. https://www.cabi.org/isc/abstract/19922316717. Accessed 12 July 2022

Jeevantham S, Saravanan A, Hemavathy RV et al (2019) Removal of toxic pollutants from water environment by phytoremediation: a survey on application and future prospects. Environ Technol Innov 13:264–276. https://doi.org/10.1016/j.eti.2018.12.007

Keskinkan O, Goksu M, Basibuyuk M et al (2004) Heavy metal adsorption properties of a submerged aquatic plant (*Ceratophyllum demersum*). Bioresour Technol 92:197–200. https://doi.org/10.1016/j.biortech.2003.07.011

Khan S, Ahmad I, Shah MT et al (2009) Use of constructed wetland for the removal of heavy metals from industrial wastewater. J Environ Manag 90:3451–3457. https://doi.org/10.1016/j.jenvman.2009.05.026

Khellaf N, Zerdaoui M (2009) Phytoaccumulation of zinc by the aquatic plant, *Lemna gibba* L. Bioresour Technol 100:6137–6140. https://doi.org/10.1016/j.biortech.2009.06.043

Kirkham M (2006) Cadmium in plants on polluted soils: effects of soil factors, hyperaccumulation, and amendments. Geoderma 137:19–32. https://doi.org/10.1016/j.geoderma.2006.08.024

Luo Y, Sun S, Zhang H (2019) Effectiveness of various wetland vegetation species on mitigating water pollution from highway runoff. Water Environ Res 91:906–917. https://doi.org/10.1002/wer.1131

Mahmoud K, Mahmoud HA, Sayed SS (2018) Potential role of *Ceratophyllum demersum* in bioaccumulation and tolerance of some heavy metals. Egypt J Aquat Biol Fish 22:1–12. https://doi.org/10.21608/EJABF.2018.9738

Marin CMDC, Oron G (2007) Boron removal by the duckweed *Lemna gibba*: a potential method for the remediation of boron-polluted waters. Water Res 41:4579–4584. https://doi.org/10.1016/j.watres.2007.06.051

Marschner H, Marschner P (2012) Marschner's mineral nutrition of higher plants. Academic Press. https://doi.org/10.1016/C2009-0-63043-9

Martino L, Yan E, Lafreniere L (2019) A hybrid phytoremediation system for contaminants in groundwater. Environ Earth Sci 78:664. https://doi.org/10.1007/s12665-019-8675-4

Mishra VK, Tripathi B (2008) Concurrent removal and accumulation of heavy metals by the three aquatic macrophytes. Bioresour Technol 99(15):7091–7097. https://doi.org/10.1016/j.biortech.2008.01.002

Mohanpuria P, Rana NK, Yadav SK (2007) Cadmium induced oxidative stress influence on glutathione metabolic genes of *Camellia sinensis* (L.) O. Kuntze. Environ Toxicol 22:368–374. https://doi.org/10.1002/tox.20273

Pandey N, Sharma CP (2002) Effect of heavy metals Co^{2+}, Ni^{2+} and Cd^{2+} on growth and metabolism of cabbage. Plant Sci 163:753–758. https://doi.org/10.1016/S0168-9452(02)00210-8

Panja S, Sarkar D, Datta R (2020) Removal of antibiotics and nutrients by Vetiver grass (*Chrysopogon zizanioides*) from secondary wastewater effluent. Int J Phytoremediation 22:764–773. https://doi.org/10.1080/15226514.2019.1710813

Parneyan A, Chorom M, Haghighi-Fard NJ et al (2011) Phytoremediation of nickel from hydroponic system by hydrophyte coontail (*Ceratophyllum demersum* L.). J Sci Technol Greenh Cult 2:85

Parnian A, Furze JN (2021) Vertical phytoremediation of wastewater using *Vetiveria zizanioides* L. Environ Sci Pollut Res. https://doi.org/10.1007/s11356-020-11906-6

Parnian A, Chorom M, Jaafarzadeh N et al (2016) Use of two aquatic macrophytes for the removal of heavy metals from synthetic medium. Ecohydrol Hydrobiol 16(3):194–200. https://doi.org/10.1016/j.ecohyd.2016.07.001

Parnian A, Chorom M, Haghighi-Fard NJ (2017) Boron removal from contaminated water by two aquatic plants of *Zannichellia palustris* L. and *Ruppia maritima* L. J Environ Sci Technol 19: 439–450. https://doi.org/10.22034/JEST.2017.11347

Petruzella A, Manschot J, van Leeuwan CHA et al (2018) Mechanisms of invasion resistance of aquatic plant communities. Front Plant Sci. https://doi.org/10.3389/fpls.2018.00134

Pivetz BE (2001) Phytoremediation of contaminated soil and ground water at hazardous waste sites. United States Environmental Protection Agency, Office of Research and Development, Office of Solid Waste and Emergency Response: Superfund Technology Support Center for Ground Water, National Risk Management Research Laboratory, Subsurface Protection and Remediation Division, Robert S. Kerr Environmental Research Center. Available via United States Environmental Protection Agency. https://permanent.fdlp.gov/lps49242/epa_540_s01_500.pdf. Accessed 25 Feb 2021

Polechońska L, Klink A (2021) Validation of *Hydrocharis morsus-ranae* as a possible bioindicator of trace element pollution in freshwaters using *Ceratophyllum demersum* as a reference species. Environ Pollut. https://doi.org/10.1016/j.envpol.2020.116145

Polechońska L, Klink A, Dambiec M et al (2018) Evaluation of *Ceratophyllum demersum* as the accumulative bioindicator for trace metals. Ecol Indic 93:274–281. https://doi.org/10.1016/j.ecolind.2018.05.020

Rezania S, Taib SM, Din MFM et al (2016) Comprehensive review on phytotechnology: heavy metals removal by diverse aquatic plants species from wastewater. J Hazard Mater 318:587–599. https://doi.org/10.1016/j.jhazmat.2016.07.053

Ruta LL, Kissen R, Nicolau I et al (2017) Heavy metal accumulation by *Saccharomyces cerevisiae* cells armed with metal binding hexapeptides targeted to the inner face of the plasma membrane. Appl Microbiol Biotechnol 101:5749–5763. https://doi.org/10.1007/s00253-017-8335-0

Sawidis T, Brown M, Zachariadis G et al (2001) Trace metal concentrations in marine macroalgae from different biotopes in the Aegean Sea. Environ Int 27(1):43–47. https://doi.org/10.1016/S0160-4120(01)00052-6

Saygıdeğer S, Doğan M (2004) Lead and cadmium accumulation and toxicity in the presence of EDTA in *Lemna minor* L. and *Ceratophyllum demersum* L. Bull Environ Contam Toxicol 73: 182–189. https://doi.org/10.1007/s00128-004-0411-3

Shi D, Zhuang K, Chen Y et al (2021) Phytotoxicity and accumulation of Cu in mature and young leaves of submerged macrophyte *Hydrilla verticillata* (L.f.) Royle. Ecotoxicol Environ Saf. https://doi.org/10.1016/j.ecoenv.2020.111684

Srivastava N, Majumder C (2008) Novel biofiltration methods for the treatment of heavy metals from industrial wastewater. J Hazard Mater 151(1):1–8. https://doi.org/10.1016/j.jhazmat.2007.09.101

Szabó S, Koleszár G, Braun M et al (2022) Submerged rootless macrophytes sustain a stable state against free-floating plants. Ecosystems 25:17–29. https://doi.org/10.1007/s10021-021-00637-5

Thomas G, Andresen E, Mattusch J et al (2016) Deficiency and toxicity of nanomolar copper in low irradiance—a physiological and metalloproteomic study in the aquatic plant *Ceratophyllum demersum*. Aquat Toxicol 177:226–236. https://doi.org/10.1016/j.aquatox.2016.05.016

Tudoreanu L, Phillips CJC (2004) Empirical models of cadmium accumulation in maize, rye grass and soya bean plants. J Sci Food Agric 84(8):845–852. https://doi.org/10.1002/jsfa.1730

Upadhyay AK, Singh NK, Rai UN (2014) Comparative metal accumulation potential of *Potamogeton pectinatus* L. and *Potamogeton crispus* L.: role of enzymatic and non-enzymatic antioxidants in tolerance and detoxification of metals. Aquat Bot 117:27–32. https://doi.org/10.1016/j.aquabot.2014.04.003

Verma U, Charudattan R (1993) Host range of *Mycoleptodiscus terrestris*, a microbial herbicide candidate for eurasian watermilfoil, *Myriophyllum spicatum*. Biological Control 3(4):271–280

Wang L, Zhou Q, Zhao B et al (2010) Toxic effect of heavy metal terbium ion on cell membrane in horseradish. Chemosphere 80(1):28–34. https://doi.org/10.1016/j.chemosphere.2010.03.040

Wells RDS, Bannon HJ, Hicks BJ (2003) Control of macrophytes by grass carp (*Ctenopharyngodon idella*) in a Waikato drain, New Zealand. N Z J Mar Freshw Res, 37:85–93. https://doi.org/10.1080/00288330.2003.9517148

Wojcik M, Tukiendorf A (2004) Phytochelatin synthesis and cadmium localization in wild type of *Arabidopsis thaliana*. Plant Growth Regul 44:71–80. https://doi.org/10.1007/s10725-004-1592-9

Xu P, Xiao E, Wu J et al (2019) Enhanced nitrate reduction in water by a combined bio-electrochemical system of microbial fuel cells and submerged aquatic plant *Ceratophyllum demersum*. J Environ Sci 78:338–351. https://doi.org/10.1016/j.jes.2018.11.013

Chapter 2
Climate Change, Sustainability and Resilience in Egypt and Africa

Mona G. Ibrahim and Mahmoud Samy

Abstract As climate change has such a broad range of effects and impacts, successful adaptation plans must consider all areas lest they unbalance effects across the range and incur hazardous effects. The UN 2030 agenda targets achieve sustainable development goals (SDGs) through integration of economic, social and environmental dimensions of development policy.

Climate resilience entails the ability of a community or system to recover rather than a tool of measurement, it should be noted that we consider ecosystem capacity in dealing with any changes while trying to retain roles in development. To improve climate resilience, policies should be applied, which focus on climate impacts and adaptation strategies from a multi-scale point of view for entirely integrated ecosystem management with consideration of interactions between industry, agriculture, trade and health.

According to the Intergovernmental Panel on Climate Change (IPCC) reports, Africa is one of the most vulnerable areas to climate change. Africa faces climate change challenges of unpredicted floods, extreme heat events, increasing aridity, reduction of rain forests and frequent droughts, which threaten community stability through agriculture productivity, water and energy security. This chapter details the application of 17 global circulation models (GCMs) with corresponding socioeconomic scenarios at a regional scale. Egypt is a water-stressed country and is facing significant vulnerabilities from climate change. Respecting the flow of the Nile

M. G. Ibrahim (✉)
Environmental Engineering Department, Egypt-Japan University of Science and Technology (E-JUST), New Borg El Arab City, Alexandria, Egypt

Environmental Health Department, High Institute of Public Health, Alexandria University, Alexandria, Egypt
e-mail: mona.gamal@ejust.edu.eg

M. Samy
Environmental Engineering Department, Egypt-Japan University of Science and Technology (E-JUST), New Borg El Arab City, Alexandria, Egypt

Department of Public Works Engineering, Faculty of Engineering, Mansoura University, Mansoura, Egypt
e-mail: mahmoud.samy@ejust.edu.eg

J. N. Furze et al. (eds.), *Earth Systems Protection and Sustainability*,
https://doi.org/10.1007/978-3-030-98584-4_2

Basin, some models predict reductions of flow, others predict increase of flow, which affects available water resources and hence agricultural and ecological services. Climate models result in contradicted outcomes, revealing complexity in potential policy management and a need for learning operational detail.

Keywords Climate change · Resilience · Adaptation · Mitigation · SDGs

2.1 Introduction

According to the UN Framework, climate change is defined as the variability in climate due to direct or indirect human activity, resulting in variation of the global atmospheric composition (Sands 1992). Climate change effects occur over decadal and century scales. The UN 2030 agenda focuses on achieving 17 sustainable development goals (SDGs) (Willis 2018). Climate hazards obstruct the achievement of the SDGs. Climate change has various impacts on water resources, agriculture, health, tourism and energy sectors. Climate hazards lead to economic losses (Abel et al. 2016). Climate change resilience can be achieved through implementation of adaptation and mitigation measures. Africa and Egypt face severe climate change; several actions and policies need to be strictly applied. Furthermore, collaborations between different countries and organisations should be performed to overcome climate change. Biophysically, different models were developed to predict the change in flow of rivers. The prediction of flow in rivers helps to understand suitable measures, which must be taken to overcome the predicted deficit in case of flow decrease and stimulate ecosystem and social productivity.

The remainder of this chapter is structured as follows: Sect. 2.2 considers the relationship between climate change and sustainable development goals; Sect. 2.3 details the effects of climate change on different sectors in Egypt and Africa; Sect. 2.4 summarises climate change impacts in Egypt; Sect. 2.5 shows economic impacts of climate change in Egypt; Sect. 2.6 discusses the prediction of the Nile flow changes resulting from climate change; Sect. 2.7 covers resilience approaches; Sect. 2.8 covers mitigation measures in Egypt and Africa. Policies and collaborations overcoming climate change in the respective regions are covered in Sect. 2.9, and the chapter concludes in Sect. 2.10.

2.2 The Relationship Between Climate Change and Sustainable Development Goals

Addressing climate change is one of the core 17 SDGs issued by the UN 2030 agenda. Figure 2.1 shows the 17 SDGs and their order. The targets of 2030 agenda can be achieved through interactions between environmental, social and economic aspects (Halkos 2015). The aforementioned interactions are necessary to combat climate hazards. The control of climate change and the application of measures able

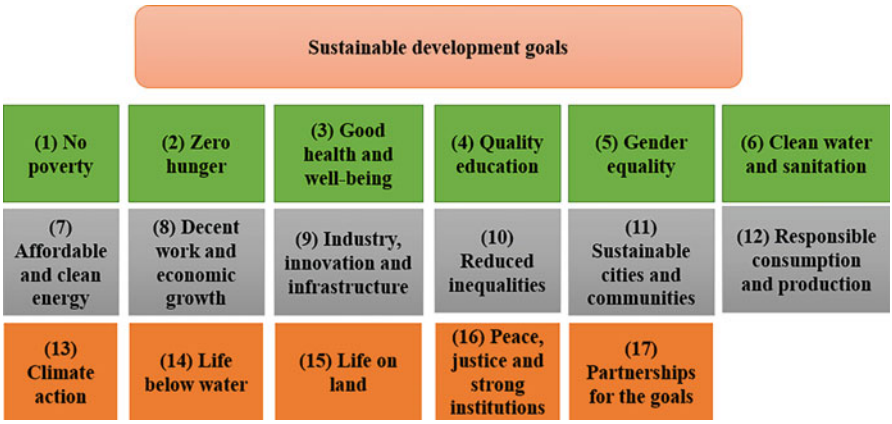

Fig. 2.1 Sustainable development goals and their order (Wilkinson et al. 2016)

to enhance resilience to climate hazards represent SDG 13 (Johnston 2016). Goal 13 also includes issuing new policies to overcome climate change and enhance awareness of mitigation measures for climate change hazards. Goal 13 has an overarching impact on the other goals. In particular, respecting goals 1–3, the increase of climate hazard frequency and intensity increases difficulties of overcoming poverty and hunger, accomplishing food security, enhancing nutrition, achieving sustainable agriculture and confirming healthy lives (SEI 2018). Climate hazards have an adverse impact on sustainability of water and energy systems (goals 6 and 7) and the safety and resilience of infrastructure, cities and human settlements (goals 9 and 11). Furthermore, continuous climate hazards prevent the sustained growth and development and increase the unemployment percentage (goal 8). All SDGs are affected by climate change.

The control of risks associated with climate change includes mitigation and adaptation measures. The effective way to face climate change hazards is via mitigation. However, several policies have responsive direction, concentrating on adaptation to overcome the detrimental consequences of climate hazards, to preserve resilience structures (IDSC 2011). Policies participate in the control of undesirable effects of climate hazards and also decrease the rate of climate change. Mitigation rather than adaptation is favoured due to the lack of available measurements of adaptation impacts compared to available metrics of mitigation measures.

2.3 Effects of Climate Change on Different Sectors

Continuous climate change leads to the rise of climate hazards through the increase of frequency, duration, extent and timing of severe weather (Lal et al. 2012). Climate change may result in human death and damage of infrastructure and resources. The damage caused by frequent climate change in countries may obstruct development

for several years. Climate hazards increase poverty and inequality levels through rising health problems, the decrease of economic growth rates and by threatening food security. Disasters related to climate change are constantly increasing around the world. It has been estimated that the number of disasters per year was 323 in the 1995–2015 period, total mortality apportioned was 600,000 and the overall number of people influenced by catastrophes was 4.2 billion during the same period (Halkos 2015). Floods are the main reason for death among various disasters resulting from climate change. Water-related hazards, storms and land-related hazards such as droughts and landslides are climate hazards that may result in disruption to people's lives. Climate change hazards are not equally distributed throughout the world. Climate change has an adverse impact on different sectors (water resources, agriculture, health, tourism and energy) in Egypt and Africa.

2.3.1 Water Resources

The Nile supplies 95% of the total fresh water needs of Egypt (IDSC 2011). Egypt is a hot, arid region with a scarcity of rainfall. The rise in temperature will increase evaporation rates in equatorial and great lakes of the Nile leading to water shortage. Climate change has an adverse impact on rivers due to the increase of evaporation rate (MacDonald et al. 2012). Variation of rainfall over different regions in Africa is high (Hulme 1992). Rise in evaporation rates will also increase precipitation in Ethiopian lands resulting in the rise of run-off in the Nile River flowing downstream to Sudan and Egypt. The rise of water demand in Africa threatens water security.

Sea level rise threatens Egyptian shores. Figure 2.2 shows the sea level rise problem in Egypt. Structures that can be used to overcome sea level rise hazards in Egypt include, for example, the stone structures of the Mohamed Ali seawall, Rosetta revetment, El Agami detached breakwaters and harbour breakwaters (Koraim et al. 2011).

Fig. 2.2 Sea level rise in Alexandria, Egypt (Magdy 2019)

Sahelian regions witnessed an increase in the stream flow of rivers due to high rainfall, while there was a decrease in the stream flow of rivers in Sudanian areas due to limited rains (Amogu et al. 2010).

Ground water is a major source of fresh water in sub-Saharan Africa (Calow and MacDonald 2009). Studies report that ground water has declined by 30–70% in western areas of southern Africa and increased by 30% in eastern areas of southern Africa (Döll 2009). Uncertainties related to ground water recharge rates are high due to the lack of knowledge of ground water aquifers, though attempts are being made to rectify the paucity of information.

2.3.2 Agriculture

In Egypt, it is predicted that crop production is generally decreasing and that water demand for irrigation will increase. The prices of crops will increase, and employment chances in agriculture will decline. All scenarios predict the decline of agricultural production (Asafu-Adjaye 2014).

The IPCC reports that Africa will be negatively affected by climate change. Crop yield loss has been reported as 24% and 71% for maize and beans, respectively, due to a temperature increase of 4 °C (Thornton et al. 2011). Further the decrease of crop yields reaches greater than 50% for maize in Sahelian regions and 10–20% for other regions in sub-Saharan Africa. High-temperature conditions are not suitable for many agricultural products. Further, high temperatures suit fungal growth leading to seedling damage (Serdeczny et al. 2017). The IPCC states that countries in Africa are highly subject to climate change hazards. By 2020, 75–250 million people in Africa will have been exposed to increased water stress imposed by climate change. The percentage of arid and semi-arid areas in Africa will increase from 5% to 8% by 2080. The adaptation cost due to this increase may be 5–10% of gross domestic product (GDP) (Halkos 2015).

2.3.3 Human Health

Just as climate change alters the quality of water, air, food, soil and agricultural products, extreme climate hazards such as floods, storms and hurricanes lead to increased mortality. Higher temperatures will result in an increased mortality in Cairo (IDSC 2011). Erratic water levels and sudden climate hazards such as floods, hurricanes and storms damage homes and medical facilities and lead to migration of large portions of the population. Climate affects water quality, further increased demand leads to impure lower-quality water being used, resulting in the spread of diseases such as cholera, typhoid fever, diarrhoeal diseases and paratyphoid fever (WHO 2015).

Malaria is one of the most dangerous diseases that result from climate change (Kalkstein and Smoyer 1993). The expected number of people that will be infected by malaria will be 260–320 million by 2080. However, Egypt has had zero cases of malaria in the past three years. Malaria transfers between African countries. Recently, malaria appeared in Ethiopia, Kenya, Rwanda and Burundi, although these countries did not report the disease in previous years. The spread of cholera in Mozambique in 2000 was due to extreme weather events such as floods polluting water and food (UNECS 2013).

In Africa, floods and landslides represent a major climate hazard that leads to high mortality (McMichael and Lindgren 2011). Exposure to high temperatures for long periods also leads to death, heat stroke, fainting and heat cramps. It has been reported that there is a relationship between death and increased temperature in African countries, Ghana and Kenya (Azongo et al. 2012; Egondi et al. 2012). Droughts are related to the spread of diseases such as diarrhoea, scabies, conjunctivitis and trachoma (Patz et al. 2008).

The decline of crop yields due to climate change also affects human health due to the lack of nutritious food. An increase of temperature by 1.2–1.7°C by 2050 will increase the percentage of undernourished people to 25–90% (Lloyd et al. 2011).

2.3.4 Energy

Energy from hydropower energy supply can be influenced by climate change, as climate change affects water availability. The continuous requirement of water to cool thermal plants is also adversely impacted by climate change due to predicted water shortages. The oil refining industry consumes large amounts of water and will be affected due to water shortage arising from climate change (IDSC 2011).

African countries depend on various types of energy. For instance, Zambia, Namibia and Mozambique rely on hydropower, while other regions produce electricity using thermoelectrical sources (World Bank 2010). The change of run-off and the existence of heat streams affect the hydroelectric dams and the cooling systems for thermoelectric power plants (Förster and Lilliestam 2009).

2.3.5 Tourism

The tourism sector requires water and agricultural products and increasing demand of water and food, amidst depletion of resources due to climate change. Tourism is also affected by sea level rise, as the rise of sea level destroys offshore protective sand belts, damaging recreational activities. The decline of tourism will affect country revenue (El-Din 2013).

The number of visitors is expected to decline due to climatic hazards effecting the spread of diseases, risks to food security, damage to natural ecosystem beauty and

hot conditions. The number of tourists has been seen to decrease in Morocco and Tunisia due to increased temperature. Declines in tourism activity may be due to high latitudes. The distribution of aquatic creatures is also negatively affected by climate change, and consequently tourism declines (UNEP 2012).

2.4 Summary of Climate Change Impacts in Egypt

It has been reported that climate change will have an adverse effect in Egypt by 2060. Table 2.1 summarises the predicted impacts of climate change on various sectors (Smith et al. 2013).

In Table 2.1 VSL is value of a statistical life (also in Fig. 2.3); GDP is gross domestic product; PM is particulate matter. CGCM63 is Canadian Global Climate Model, ECHAM is European Centre Hamburg Model and MIROC-M is Model for Interdisciplinary Research on Climate: three models that represent the highest increase and decrease in the Nile flow, where CGCM 63 represents the model of the highest decrease in the Nile flow, ECHAM is the model in which the variation in the Nile flow is near to the average flow in all models and MIROC-M represents the model of the highest increase in the Nile flow.

A majority of homes are considered unprotected from climate change hazards. It can be noted from Table 2.1 that precipitation will decrease due to high greenhouse gas emissions and aerosols. Moreover, the IPCC expects that Egypt will be drier and hotter.

The change in the Nile flow will be over 10% in the case of ECHAM, while the Nile flow will increase 30% in the case of MICRO-M by 2060. The Nile flow will decrease 37% in the case of CGCM63 in the same year (Smith et al. 2013).

According to Table 2.1, climate change will have a negative impact on agricultural production and employment changes. Agriculture product prices will be affected by climate change. By 2060, PM2.5 will increase, and this will lead to the death of 1000–2300 people, and the economic loss will be 0.74–2.11 billion US dollars per year. Furthermore, the rise of temperature will result in an economic loss of 5.59–6.38 billion US dollars per year in the case of tourism sector. The economic loss in housing sector in the Nile Delta region will be 0.16–0.99 billion US dollars per year by 2060 (Smith et al. 2013).

2.5 Economic Impacts of Climate Change in Egypt

Climate change has an adverse impact on different sectors in Egypt. Figure 2.3 shows the influence of climate change on the economy in 2030 and 2060. In African countries, climate change also has a severe impact on economic situations. For example, Table 2.2 shows the impacts of climate change on economic loss in Kenya.

Table 2.1 Summary of climate change impacts on different sectors in Egypt in 2060

Scenario	1	2	3	4
Socioeconomic scenario	High population; low GDP	High population; low GDP	High population; low GDP	Low population; high GDP
Nile flow scenario	Large	Small		Small
	Reduction (CGCM63)	Reduction (ECHAM)	Increase (MIROC-M)	Reduction (ECHAM)
Annual climate change in Cairo (temperature °C/% change in precipitation)	2/−10	1.9/0	2.2/−10	1.9/0
Sea level rise	High unprotected	High unprotected	High unprotected	High unprotected
Agricultural production reduction (%)	−47	−27	−8	−20
Food prices (% change)	68	41	16	32
Reduction in consumption of agriculture (%)	−30	−15	−5	−7
Welfare decline percentage (%)	−12	−6	−2	−2
Consumer surplus (% change)	−18	−11	−4	−7
Employment chances Reduction in agriculture (%)	−39	−20	3	−5
Coastal property losses (excluding agriculture; billion US $)[a]	0.45	0.45	0.45	1.01
Expected annual deaths due to air pollution (PM2.5)	1105–2308	1105–2308	1.105–2308	708–1610
Estimated economic loss due to air pollution (billion US $)	0.39–0.89	0.39–0.88	0.39–0.88	0.66–1.5
Expected annual deaths due to heat stress	2302	2187	2665	1579
Estimated economic loss due to heat stress (billion US $ using VSL)	0.88	0.84	1.02	1.47
Tourism revenues decline (billion US $)	5.25	5.25	5.25	6.38

[a]Values are estimated based on sea level rise (SLR) scenario. The annual economic losses are 0.12 and 0.15 billion US $ in the case of low- and middle-SLR scenarios depending on pessimistic socioeconomic scenario, while in the case of optimistic socioeconomic scenarios, the losses are 0.27 and 0.34 billion US $, respectively

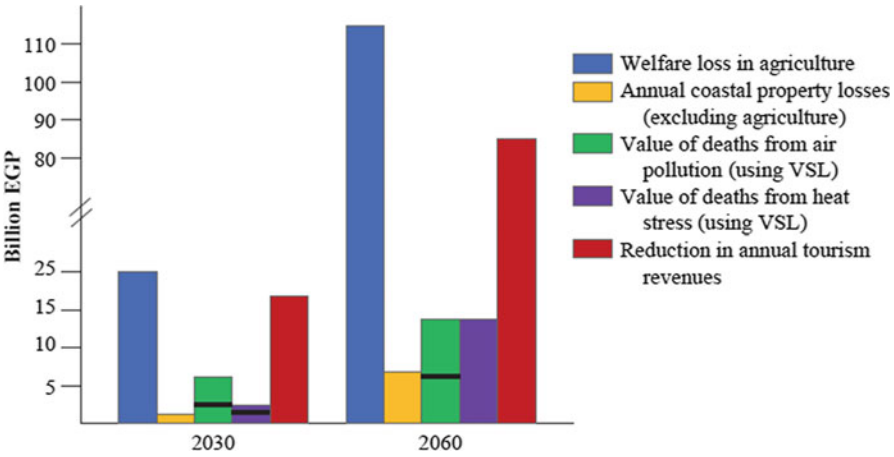

Fig. 2.3 The predicted economic loss (EGP - Egyptian Pounds) in different sectors in Egypt in 2030 and 2060 as a result of climate change (Smith et al. 2013)

Table 2.2 Impacts of climate change on economy loss in Kenya

	Import (million US $)			Needs (million US $)			
Sectors	Damage	Losses	Total	Recovery	Reconstruction	Total	DRR
Agriculture	Unknown	1191.09	1191.09	49.66	Unknown	49.66	135.11
Livestock	552.17	6326	6878.17	494.1	0.55	1046.27	837.01
Fisheries	4.94	36.01	40.95	4.0	7.41	11.41	29.42
Agro-industry	Unknown	70.42	70.42	Unknown	Unknown	Unknown	Unknown
Health	Unknown	46.68	46.68	50.15	Unknown	50.15	Unknown
Nutrition	Unknown	65.6	65.89	2.21	Unknown	2.21	1.29
Education	0.41	38.73	39.14	5.8	0.55	6.35	35.33
Energy	Unknown	318.59	318.59	127.86	Unknown	127.86	Unknown
Water and sanitation	76.09	791.42	867.5	48.82	121.01	169.84	773.32
Environment, tourism, forestry, wildlife	0.22	7.5	7.72	72.66	Unknown	72.66	6.37
Total	603.83	8892.32	9526.15	855.26	680.65	1536.41	1817.84

DRR disaster risk reduction

2.6 Prediction of Nile Flow Changes Resulting from Climate Change

Global circulation models (GCMs) were employed to investigate the influence of climate change on the flow generally in the Nile Basin and particularly in the Blue Nile sub-Basin. GCMs are global circulating models that provide 'pictures' for the

Nile Basin flow; consequently the flow of the river can be predicted. The study analysed data from 17 GCMs included in the 4th IPCC report. The modelling group of the 17 GCMs consisted of Bjerknes Centre for Climate Research, Norway (BCM); Canadian Centre for Climate Modeling and Analysis, Canada (CGCM); Canadian Centre for Climate Modeling and Analysis, Canada (CGCM63); Meteo-France/Centre National de Recherches Meteorologique, France (CNRM); CSIRO Atmospheric Research, Australia (CSIRO30); CSIRO Atmospheric Research, Australia (CSIRO35); NOAA/Geophysical Fluid Dynamics Laboratory, USA (CM20); NOAA/Geophysical Fluid Dynamics Laboratory, USA (CM21); NASA/Goddard Institute for Space Studies, USA; LASG/Institute of Atmospheric Physics, China (GOAL); Institute for Numerical Mathematics, Russia (INMCM); Center for Climate System Research, National Institute for Environmental Studies Frontier Research Center for Global Change, Japan (MIROCH); Center for Climate System Research, National Institute for Environmental Studies Frontier Research Center for Global Change, Japan (MIROCM); Max Planck Institute for Meteorology, Germany (ECHAM); Meteorological Research Institute, Japan (MRI); National Center for Atmospheric Research, USA (CCSM); and National Center for Atmospheric Research, USA (PCM). In the study, precipitation and potential evapotranspiration (PET) detailed scenarios were prepared over the Blue Nile Basin in the period 2081–2098. The Blue Nile Basin contributes 60% of the total annual flow of the Nile River. However, the uncertainties related to the climate change over the Nile Basin as well as the impacts of climate change on the Nile flow are very high.

In the period 2081–2098, Elshamy et al. (2009) reported that the sensitivity of the Blue Nile Basin to precipitation and evapotranspiration is high. Flow sensitivity resulting from potential evapotranspiration (PET) changes is mainly due to rainfall. The methods used corrected baseline climate data errors. A high reduction in rainfall may be accompanied with the increase of PET, especially during wet seasons due to the high reduction in cloud cover. Flow increases by 45% when rainfall is large enough to surpass the effect of PET rise. The majority of models showed that the flow tends to decrease. Simple relations between temperature, PET, precipitation and flow were developed. The relation between PET changes and temperature changes was linear. Flow changes can be determined using temperature and precipitation changes. All models demonstrated the rise of temperature from 2 to 5°C and stated that the rise of PET was from 2% to 14%.

A further study was made to investigate the changes in the Nile flow at Dongola (Sudan) depending on two scenarios (A2 and B2) using the data from three GCMs: CGCM2, ECHAM4 and HadCM3 (Elshamy and Sorteberg 2008). Potential evapotranspiration was estimated for the base period (1961–1990) and also for three periods in the future (2010–2039, 2040–2069 and 2070–2099); precipitation was measured for the period from 2010 to 2099. The results showed that ECHAM4 model predicted a uniform rise of the Nile flow, while CGCM2 underestimated the flow in the base period. A slight rise of flood season flow and limited increase of flow were observed in the case of HadCM3. The uncertainty of models was higher than the uncertainty imposed by the two scenarios. The uncertainty of downscaling was

high and depended on the flow. Increased intensity of flood seasons may lead to larger floods in the case of ECHAM4, while droughts were expected to take place in the case of CGCM2. In the case of HadCM3, the changes of water resources in Egypt were expected to be moderate.

2.7 Climate Resilience

Climate resilience is the ability to prepare a plan to overcome the events related to climate changes (Silva-Villanueva 2019). Climate resilience helps to face problems related to extreme climate change events such as hurricanes, floods and droughts. Urban green infrastructure is considered one of the ways which can achieve climate change resilience. Urban green infrastructure overcomes human and economic losses resulting from climate change hazards such as extreme rainfall and flooding (Ibrahim et al. 2019). Furthermore, urban green infrastructure solves the problems of water accumulation in the streets due to insufficient drainage capacity. The integration between flood modelling and land use classification facilitates the choice of suitable areas to implement urban green infrastructure to counter flood and rain accumulation. Urban green infrastructure options are bioretention systems, green roofs, permeable pavements and rain barrels. In bioretention systems, the enhancement of soil infiltration and the decline of rapid run-off can be achieved by adding soil filter media and native plants to small areas. In the case of green roofs, vegetated areas can be used to collect run-off. In permeable pavements, a porous material can be used to make rainfall infiltrate into the soils. Moreover, rainfall can be collected and stored through rain barrels.

Climate change resilience can be achieved through adaptation and mitigation measures. Adaptation is defined as a group of processes and actions that participate in the management of the impacts, while mitigation refers to the overcoming of the causes of the climate change (Yohe et al. 2007). Vulnerability to climate change measures the degree of impacts of climate change. Figure 2.4 shows a framework of climate change with adaptation and mitigation.

Climate resilience requires adaptations to be made in order to mitigate the effects of change; the current section details adaptations across the sectors of Sect. 2.3, while Sect. 2.8 mentions directive mitigations for both Egypt and Africa.

2.7.1 Water Resources

The adaptation techniques in this sector should focus on reductions in water demand (Smith et al. 2013). One of the actions to relieve water demand is to charge for water; this action requires measuring water quantity to determine fees. Water scarcity problems arising from climate change may be solved by desalination, water reuse

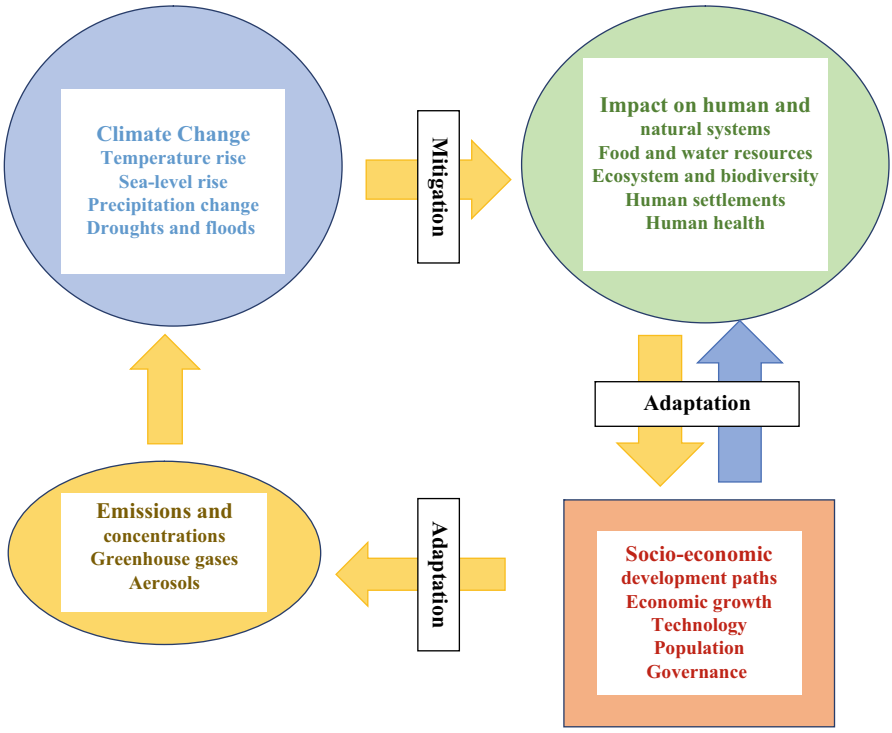

Fig. 2.4 The integrated evaluation framework of climate change with adaptation and mitigation (Vag 2009)

and ground water usage. In the case of desalination, the technology is already implemented in Egypt though needs to be expanded to deal with water shortage problems due to climate change. Conventional desalination practiced in the country requires high energy consumption, and the produced water still needs to be enhanced to be used for agriculture or drinking. Reuse is a further solution for water shortages in Egypt. The reuse of municipal and industrial wastewater reduces the demand for fresh water. Agricultural drainage water is reused at a wide scale to overcome water shortages.

In Africa, adaptation options to overcome climate change problems include increased availability of information and strict control measures on ground and surface water resources. Additionally, construction of water storage tanks can be an ideal solution to water shortage. For example, Sudan and Sierra Leone started a project to overcome climate change through rainfall catchment and storage tanks (Ministry of Environment [South Sudan] 2016).

2.7.2 Agriculture

In Egypt, modified crops and increase of agricultural imports provide major options of climate change adaptation (Attaher et al. 2009). The development of heat- and salinity-resistant crops can be achieved by genetic modification of crops, achieving growth in higher temperature and salinity conditions. Economic adaptation of a tenfold increase in agricultural imports will augment national agricultural production and additionally reduce costs.

The decrease of crop yields in Africa due to climate change will increase the number of undernourished people in Africa to 329 million in the period 2010–2100 (FAO 2014). Research in Africa focuses on the adaptation of agriculture against climate changes. For example, Chad and Cape Verde started projects for the enhancement of agricultural production, and this resulted in increased crop productivity (Ministry for Economy and Development 2010; Republic of Cape Verde – Ministry of Environment and Agriculture 2007).

2.7.3 Human Health

Air quality problems resulting from climate change should be controlled; the number of people that die due to air pollution is 20,000 per year (Sarraf 2002). Water problems arising from climate change lead to human health problems (Frumkin et al. 2011). To overcome heat stress problems, cooling centres can be an effective solution to overcome problems resulting from high temperatures (Ebi 2009).

To counter infectious diseases such as malaria resulting from climate change, surveillance systems and increased monitoring should be instigated to detect and deal with infectious disease. Health systems should be improved to overcome the outbreaks of diseases, saving costs associated with required medicines, training and communications (McMichael and Lindgren 2011). The development of regulations to overcome the spread of diseases can be a major option to overcome the problems related to climate change in African countries. For instance, Bog Togo and the Central African Republic initiated projects aimed at the prevention of diseases. These projects include the fight against malaria.

2.7.4 Energy

To overcome problems arising from climate change in the energy sector, the government in Egypt is inclined to increase the use of renewable energy such as solar/photovoltaic cells and wind power. Although targets have as yet been modestly approached, the contribution of renewable energy reached 20% by 2020 instead of 6% (Egyptian Environmental Affairs Agency 2016).

Hazards due to climate change are the increase of frequency and intensity of droughts; the increase of rainfall and extremes affects hydropower and thermoelectricity production (Förster and Lilliestam 2009). In addition to hydropower, successful application of solar and biogas projects has been made in Benin and Lesotho (UNEP 2012).

2.7.5 Tourism

To mitigate climate changes related to the tourism sector, sea level rise and variation should be considered as facilities are at risk in Egypt. Cooperation between the government and the tourism industry should be performed to overcome climate change (Egyptian Environmental Affairs Agency 2016).

Tourism creates job opportunities and increases the revenue of African countries. Due to limited information about adaptation measures in the tourism sector, a collaboration between the World Tourism Organization and UN Environment Program has been developed to check tourist destinations and evaluate tourism adaptation measures in relation to the impact of the industry and climatic change on biodiversity (UNEP 2012).

2.8 Mitigation Measures

Mitigation measures to counter climate hazards in Egypt and Africa are mentioned in the current section.

2.8.1 Mitigation Measures in Egypt

Mitigation measures that should be applied in Egypt have been proposed and documented for Egypt (Egyptian Environmental Affairs Agency 2016).

Mitigation measures include the conversion of wetlands to agricultural areas to increase the crop yield to face the rising food demand due to population increase; the development of a low-carbon strategy to mitigate greenhouse gases (GHGs); the availability of water to attract tourists, as the activities related to tourism consume considerable amounts of water with irrigation of green areas in hotels and resorts and washing of hotel towels and kitchen needs; coastal planning to protect tourism facilities from sea level rise; the increase of energy production from renewable sources especially solar energy; the promotion of sea water desalination relying on solar power using desalination technologies with high efficiency; the increased spread of natural gas use; the increased efficiency of energy delivery using new technologies; the use of efficient cars to generate fewer emissions; the

implementation of policies that encourage home builders to reduce energy consumption and increase the efficiency of energy delivery; the development of new technologies that produce low emissions such as nuclear power and clean coal technology; the improvement of irrigation management systems; the construction of integrated networks for evaluation of climatic and environmental hazards; the reduction of generated waste and the improvement of livestock production systems.

2.8.2 Mitigation Measures in Africa

Examples of directive mitigation measures in Africa are as follows: increase of renewable energy use; the use of efficient means of transportation such as electric public transport and bicycles; increase in planting of trees and plants to remove greenhouse gases from air; application of fees for greenhouse gas emission; application of efficiency standards for cars and trucks; the use of photovoltaic cells, wind power, solar and geothermal and compost/biofilm systems; preservation of natural ecosystems; the preparation of flexible cultivation to overcome catastrophe; restoration of degraded lands; management of nutrients in animal and human food production to reduce emissions and the improvement of productivity through rising nutrient quality (Tubiello 2012).

2.9 Policies and Collaborations Overcoming Climate Change in Egypt and Africa

Dealing with climate change hazards cannot be achieved individually and requires cooperation between countries. It is particularly useful to share information and experience of measures that should be followed to mitigate and adapt to climate hazards. Countries issue policies and measures to protect existing investment and achieve sustainable development.

2.9.1 Egyptian Policies, Success and Opportunities

Policies have been made to overcome problems resulting from climate change in Egypt. Focus is applied to actions that achieve resilience in water resources, agriculture and food security. Policies include the improvement of livestock productivity. Moreover, adaptation strategies overcome climate hazards in several sectors (Froehlich and Al-Saidi 2017a).

Cooperation between Egypt and regional and international organisations assists in the control of climate change collectively. The matter is not limited to shared experience and information but additionally to mitigation measures.

IDSC (2011) detailed some examples of working collaborations between Egypt and other agencies as shown in the remainder of this section.

In 2010, a project was initiated to mitigate the effects of climate changes on the Nile Delta. The project was established by the cooperation between the Egyptian Ministry of Water Resources and the UN Development Programme. The objective of this project was to increase the resistance of structures facing erosion and precipitation problems. The total cost of this project was US $ 16.2 million; the project lasted for 5 years.

To overcome disasters resulting from climate change in the coastal cities of North Africa, a project was developed to save the lives of 60–90 million people by 2030. This project focuses on the prevention of climatic disasters in four cities (Alexandria, Tunis, Casablanca and Morocco's Wadi Bour Greg). The situation of these regions has to be established, and then plans need to be developed to overcome disasters according to their conditions.

A project funded by the United Nations for Food and Agricultural Organization was initiated to control the risks arising from climate change and sea level rise in the Nile Delta. This project focused on the development of decisions to mitigate and predict the climate hazards in agriculture and environments along the Delta. The project costed US $ 337.2 million and lasted for 18–24 months.

To investigate the effect of sea level rise on human movement, a project was executed by the International Organization for Mitigation and the Ministry of Manpower and Migration. The group responsible for the study includes representatives from the International Organization for Mitigation, the Ministry of Manpower and Migration, the Ministry of Water Resources, the Environment Affairs Authority, Alexandria University, Friends of the Environment Society in Alexandria and the UN International Strategy for Disaster Reduction.

2.9.2 Policies and Cooperation in Africa

To reduce climate change impacts on livestock, resources and economy in Africa, climate change measures and actions should be integrated into national decision-making. In Africa, policies are developed with overcoming greenhouse gas emissions at their core. Cooperation between African countries and global institutions are ongoing to strengthen the response towards climate change. African countries issue their policies about climate change through the African Ministerial Conference on the Environment. Further policy directives are to reduce vulnerability and disasters resulting from climate change. Cooperation between the African Union Commission, the Economic Commission for Africa, the African Development Bank, the UN Environment Programme/Regional Office for Africa and other UN bodies and

development partners was developed to support the implementation of Africa's climate and development agenda.

Efforts exerted to overcome climate change in Africa are documented (Union 2010). A cooperation between African states, regional economic communities and private sector to involve climate change adaptation measures into development plans, strategies and programs at regional and national levels has to be conducted.

The construction of the African Climate Policy Centre has been achieved as a result of the decision of the African Union Conference of Ministers on the Economy and Finance and the Conference of African Ministers of Finance which provides countries' policy guidance to take required measures to overcome climate hazards. The cooperation between the African Union Commission, the African Development Bank and the Economic Commission for Africa also issued the implementation of the Climate for Development in Africa Programme depending on national, subregional and regional institutions. The objective of this programme was to promote the achievement of the Millennium Development Goals and overall sustainable development in Africa.

There are various projects initiated to overcome major climate hazards in different African countries. Table 2.3 includes projects in different African countries to combat climate hazards.

Table 2.3 Examples of projects initiated to overcome climate change in Africa (Troni et al. 2018)

Location	Project title	Project target	Average rainfall (mm/year)	Major climate hazards	Total cost (US $, in millions)
Burundi	Community risk management	Water	1700	Drought, floods	8.9
Comoros	Management of water resources	Health, food and water security, poverty reduction	7075	Droughts, floods, sea level rise and salt water intrusion, cyclones	2.85
Comoros	Improvement of the adaptive capacity and resilience in agriculture sector	Food security, poverty reduction	7075	Droughts, floods, sea level rise and salt water intrusion, cyclones	8.99
Democratic Republic of the Congo	The construction of women and children's capabilities to cope with climate change	Gender, food and water security, poverty reduction	1400	Drought, floods	4.7
Ghana	The integration of climate change into the management of priority health risks	Health	1600	Droughts, floods, heat	1.7

(continued)

Table 2.3 (continued)

Location	Project title	Project target	Average rainfall (mm/year)	Major climate hazards	Total cost (US $, in millions)
Guinea	Protection of coastal areas and communities against climate change	Food security, poverty reduction	4300	Droughts, floods, sea level rise and salt water intrusion	2.97
Eritrea	Adaptation of water and agriculture sectors towards climate change	Food and water security, poverty reduction	350	Drought, flash flooding	6.5
Ethiopia	Coping with drought and climate change	Food and water security, poverty reduction	1200	Drought	1
Kenya	Climate change adaptation in arid and semiarid lands	Food security, poverty reduction	550	Drought	1
Liberia	The improvement of resilience of vulnerable coastal areas	Coastal protection, human security	2391	Sea level rise, coastal erosion, flooding	2.9
Mali	Programme for climate change adaptation in the vulnerable regions of Mopti and Tombouctou (AF)	Food and water security, poverty reduction	1400	Drought	8.5
Malawi	Development plans for achieving adaptation to climate change	Food and water security, poverty reduction	1200	Drought, floods	4.5
Mauritius	The adaptation of coastal zone to climate change in Mauritius	Coastal protection, human security	2400	Droughts, sea level rise, coastal erosion, flooding, cyclones	8.4
Mozambique	Coping with drought and climate change	Food security, poverty reduction	800	Drought, floods	1
Namibia	Traditional crop improvement to face climate change	Food and water security, poverty reduction	450	Drought, floods	1
Niger	Scaling up community-based adaptation	Food and water security, poverty reduction	700	Drought	3.8

(continued)

Table 2.3 (continued)

Location	Project title	Project target	Average rainfall (mm/year)	Major climate hazards	Total cost (US $, in millions)
Rwanda	Construction of early warning systems to reduce vulnerability in flood-prone areas	Food and water security, poverty reduction	1400	Floods	3.84
Sao Tome and Principe	Construction of warning systems to overcome climate change	Food and water security, coastal protection	3200	Sea level rise and coastal erosion, drought, floods	3.6
Senegal	The improvement of land and ecosystem management	Gender, food and water security, poverty reduction	850	Drought	4.1
Zambia	Overcoming climate change impacts in agro-ecological zones	Food and water availability, overcoming poverty	648	Drought, pests	3.79
Zimbabwe	Coping with drought and climate change	Food and water availability, overcoming poverty	454	Drought	1
Egypt	Improvement of North Coast adaptation to climate hazards	Nile Delta low-lying land preservation	200	Sea level rise	31.4

2.10 Summary and Conclusions

In this chapter, the relation between climate change control and the achievement of SDGs was discussed. The effects of climate change on different sectors (water resources, agriculture, health, energy and tourism) were detailed in Africa and Egypt. The relationship between climate change and its force on economy was mentioned in order to show that predicted scenarios influence Egypt negatively in all sectors.

The construction of resilience stuctures is crucial to overcome climate change hazards. Climate change resilience can be achieved through the application of mitigation and adaptation measures. Moreover, urban green infrastructure can be applied to prevent floods and problems related to extreme rainfall.

The adaptation and mitigation measures were discussed for Egypt and Africa, and the framework for climate change control using adaptation and mitigation measures was explained. Examples of policies and cooperation between Egypt, African countries and regional and international organisations to overcome climate change were presented. A summary of ongoing projects initiated in different countries in Africa was shown in this chapter.

Seventeen global circulation models were used to predict the change in the Nile flow. The majority of models forecasted a decrease in the Nile flow. Three GCMs (CGCM2, ECHAM4 and HadCM3) were also used to investigate changes in the Nile flow. The results demonstrated that ECHAM4 model showed a uniform increase of the Nile flow, while CGCM2 underestimated the flow in the base period. A limited increase of seasonal flow and an overall small increase of flow were predicted in the case of HadCM3. The use of climate modelling requires the correct appreciation of the nature and weights of elements effecting change. Further research in climate mitigation should consider different metrics and structures which may be used to quantify impacts of both responsive and preventative approaches in order to stimulate populations to protect and sustain themselves into the future.

References

Abel GJ, Barakat B, Samir KC et al (2016) Meeting the sustainable development goals leads to lower world population growth. PNAS 113(50):14294–14299. https://doi.org/10.1073/pnas.1611386113

Amogu O, Descroix L, Yéro KS et al (2010) Increasing river flows in the Sahel? Water 2(2): 170–199. https://doi.org/10.3390/w2020170

Asafu-Adjaye J (2014) The economic impacts of climate change on agriculture in Africa. J Afr Econ 23(2). https://doi.org/10.1093/jae/eju011

Attaher SM, Medany MA, Abou-Hadid AF (2009) Possible adaptation measures of agriculture sector in the Nile Delta to climate change impacts. Adv Sci Res 3(1):123–126. https://doi.org/10.5194/asr-3-123-2009

Azongo DK, Awine T, Wak G et al (2012) A time series analysis of weather variability and all-cause mortality in the Kasena-Nankana districts of Northern Ghana 1995–2010. Glob Health Action 5:14–22. https://doi.org/10.3402/gha.v5i0.19073

Calow R, MacDonald A (2009) What will climate change mean for groundwater supply in Africa? Background Note Overseas Development Institute. Available via https://cdn.odi.org/media/documents/4120.pdf. Accessed 19 May 2021

Döll P (2009) Vulnerability to the impact of climate change on renewable groundwater resources: a global-scale assessment. Environ Res Lett 4(3). https://doi.org/10.1088/1748-9326/4/3/035006

Ebi KL (2009) Public health responses to the risks of climate variability and change in the United States. J Occup Environ Med 51(1):4–12. https://doi.org/10.1097/JOM.0b013e31816fd67b

Egondi T, Kyobutungi C, Kovats S et al (2012) Time-series analysis of weather and mortality patterns in Nairobi's informal settlements. Glob Health Action 5:23–32. https://doi.org/10.3402/gha.v5i0.19065

Egyptian Environmental Affairs Agency (2016) Egypt Third National Communication. https://unfccc.int/files/national_reports/non-annex_i_parties/biennial_update_reports/application/pdf/tnc_report.pdf. Accessed 19 May 2021

El-Din MM (2013) Proposed climate change adaptation strategy for the ministry of water resources & irrigation in Egypt. In: Climate change risk management in Egypt. UNESCO, Cairo Office, Cairo

Elshamy ME, Sorteberg A (2008) Impacts of climate change on Blue Nile flows using bias-corrected GCM scenarios. https://doi.org/10.5194/hessd-5-1407-2008

Elshamy ME, Seierstad IA, Sorteberg A (2009) Impacts of climate change on Blue Nile flows using bias-corrected GCM scenarios. Hydrol Earth Syst Sci 13(5):551–565. https://doi.org/10.5194/hess-13-551-2009

FAO (2014) The state of food insecurity in the world strengthening the enabling environment for food security and nutrition. Food and Agriculture Organisation. Available via FAO. http://www.fao.org/3/i4030e/i4030e.pdf. Accessed 19 May 2021

Förster H, Lilliestam J (2009) Modeling thermoelectric power generation in view of climate change. Reg Environ Chang 10(4):327–338. https://doi.org/10.1007/s10113-009-0104-x

Froehlich P, Al-Saidi M (2017a) Climate change research at universities, pp 235–250. https://doi.org/10.1007/978-3-319-58214-6

Froehlich P, Al-Saidi M (2017b) Community-based adaptation to climate change in Egypt—status quo and future policies. In: Filho WL (ed) Climate change research at universities. Springer, Cham. https://doi.org/10.1007/978-3-319-58214-6_14

Frumkin H, Hess J, Luber G et al (2011) Climate change: the public health response. Am J Public Health 98(3):435–445. https://doi.org/10.2105/AJPH.2007.119362

Halkos GE (2015) Climate change actions for sustainable development. Int J Innov Sustain Dev 9(2):118–136. https://doi.org/10.1504/IJISD.2015.068785

Hulme M (1992) Rainfall changes in Africa: 1931–1960 to 1961–1990. Int J Climatol 12(7):685–699. https://doi.org/10.1002/joc.3370120703

Ibrahim MG, Elboshy B, Mahmod WE (2019) Integrated approach to assess the urban green infrastructure priorities (Alexandria, Egypt). In: Chaminé H, Barbieri M et al (eds) Advances in sustainable and environmental hydrology, hydrogeology, hydrochemistry and water resources. CAJG 2018. Advances in science, technology & innovation (IEREK interdisciplinary series for sustainable development). Springer, Cham. https://doi.org/10.1007/978-3-030-01572-5_97

IDSC (2011) Egypt's national strategy for adaptation to climate change and disaster risk reduction. Available via The Egyptian Cabinet Information and Decision Support Centre. http://faolex.fao.org/docs/pdf/egy141200.pdf. Accessed 19 May 2021

Johnston RB (2016) Arsenic and the 2030 Agenda for sustainable development. Arsen Res Glob Sustain As 2016:12–14. https://doi.org/10.1201/b20466-7

Kalkstein LS, Smoyer KE (1993) The impact of climate change on human health: some international implications. Experientia 49(11):969–979. https://doi.org/10.1007/BF02125644

Koraim AS, Heikal EM, AboZaid AA (2011) Different methods used for protecting coasts from sea level rise caused by climate change. Curr Dev Oceanogr 3(1):33–66

Lal PN, Mitchell T, Aldunce P et al (2012) National systems for managing the risks from climate extremes and disasters. In: Field C, Barros V, Stocker T et al (eds) Managing the risks of extreme events and disasters to advance climate change adaptation: special report of the intergovernmental panel on climate change. Cambridge University Press. https://doi.org/10.1017/CBO9781139177245.009

Lloyd SJ, Sari Kovats R, Chalabi Z (2011) Climate change, crop yields, and undernutrition: development of a model to quantify the impact of climate scenarios on child undernutrition. Environ Health Perspect 119(12):1817–1823. https://doi.org/10.1289/ehp.1003311

MacDonald AM, Bonsor HC, Dochartaigh BÉÓ et al (2012) Quantitative maps of groundwater resources in Africa. Environ Res Lett. https://doi.org/10.1088/1748-9326/7/2/024009

Magdy S (2019) Egypt's historic Alexandria looks to fend off rising sea levels. Available via Independent. ie. https://www.independent.ie/world-news/egypts-historic-alexandria-looks-to-fend-off-rising-sea-levels-38450709.html. Accessed 19 May 2021

McMichael AJ, Lindgren E (2011) Climate change: present and future risks to health, and necessary responses. J Intern Med 270(5):401–413. https://doi.org/10.1111/j.1365-2796.2011.02415.x

Ministry for Economy and Development (2010) National Adaptation Programme of Action (NAPA) on climate change Democratic Republic of Timor-Leste: Timor-Leste National Adaptation Programme of Action to climate change. Available via UNFCC. https://unfccc.int/resource/docs/napa/tls01.pdf. Accessed 19 May 2021

Ministry of Environment [South Sudan] (2016) Republic of South Sudan's National Adaptation Programme of Actions (NAPA) to climate change. Available via UNFCC. https://unfccc.int/files/adaptation/workstreams/national_adaptation_programmes_of_action/application/pdf/south_sudan_final_napa_-_24th_nov-2016.pdf. Accessed 19 May 2021

Patz JA, Olson SH, Uejio CK et al (2008) Disease emergence from global climate and land use change. Med Clin N Am 92(6):1473–1491. https://doi.org/10.1016/j.mcna.2008.07.007

Republic of Cape Verde – Ministry of Environment and Agriculture (2007) National Adaptation Programme of Action on climate change 2008–2012. Available via UNFCC. https://unfccc.int/resource/docs/napa/cpv01.pdf. Accessed 19 May 2021

Sands P (1992) The United Nations framework convention on climate change. Rev Eur Comp Int'l Envtl L 1:270

Sarraf M (2002) Environment strategy assessing the costs of environmental degradation in the Middle East and North Africa region. World Bank. Available via http://documents1.worldbank.org/curated/en/780231468774275451/pdf/298630PAPER0As1Env0Strat0Note0no-09.pdf. Accessed 18 May 2021

SEI (2018) The sustainable development goals viewed through a climate lens. Available via The Stockholm Environment Institute. https://www.sei.org/publications/the-sustainable-development-goals-viewed-through-a-climate-lens/. Accessed 19 May 2021

Serdeczny O, Adams S, Baarsch F et al (2017) Climate change impacts in sub-Saharan Africa: from physical changes to their social repercussions. Reg Environ Chang 17(6):1585–1600. https://doi.org/10.1007/s10113-015-0910-2

Silva-Villanueva P (2019) What is human resilience and why does it matter? In: Sáenz-Herrero M (ed) Psychopathology in women. https://doi.org/10.1007/978-3-030-15179-9_2

Smith J, Deck L, McCarl B, Kirshen P et al (2013) Potential impacts of climate change on the Egyptian economy. Available via UNDP. https://www.adaptation-undp.org/sites/default/files/downloads/egypt.report_final.pdf. Accessed 19 May 2021

Thornton PK, Jones PG, Ericksen PJ et al (2011) Agriculture and food systems in sub-Saharan Africa in a 4°C+ world. Philos Trans R Soc A Math Phys Eng Sci 369:117–136. https://doi.org/10.1098/rsta.2010.0246

Troni J, Petersen C, Diouf HR (2018) Climate change adaptation in Africa: UNDP synthesis of experiences and recommendations. United Nations Development Programme, Bangkok Regional Hub, Thailand. https://www.undp.org/content/undp/en/home/librarypage/climate-and-disaster-resilience-/climate-change-adaptation-in-africa.html

Tubiello FN (2012) Natural resources management and environment department climate change adaptation and mitigation challenges and opportunities in the food sector. Natural Resources Management and Environment Department, FAO, Rome. Prepared for the High-level conference on world food security: the challenges of climate change and bioenergy, Rome, 3–5 June 2008. http://www.fao.org/docrep/016/i2855e/i2855e.pdf. Accessed 19 May 2021

UNECS (2013) UNICEF annual report 2013. Available via United Nations Economic and Social Council. un.org/en/ecosoc/qcpr/pdf/unicef_annual_report_2013.pdf. Accessed 19 May 2021

UNEP (2012) Africa's adaptation gap technical report climate-change impacts, adaptation challenges and costs for Africa. Available via UNEP. https://www.unep.org/resources/annual-report/unep-2012-annual-report. Accessed 19 May 2021

Union (2010) Report on climate change and development in Africa. Available via Prevention Web. https://www.preventionweb.net/files/13415_ReportonClimateChangeandDevelopment.pdf. Accessed 19 May 2021

Vag A (2009) Environment-society interactions and the effectiveness of environmental policies. In: Hideg E (ed) Futures studies in the interactive society Budapest.

WHO (2015) Climate and health country profile – Ghana. Available via https://www.afro.who.int/countries/ghana. Accessed 19 May 2021

Wilkinson S, Hajibandeh M, Remoy H (2016) Sustainable development. In: Noguchi M (ed) ZEMCH: toward the delivery of zero energy mass custom homes. Springer tracts in civil engineering. Springer, Cham. https://doi.org/10.1007/978-3-319-31967-4_1

Willis K (2018) The sustainable development goals. In: Cupples J, Marcela Palomino-Schalscha M, Prieto M (eds) The Routledge handbook of Latin American development, pp 121–131. https://doi.org/10.4324/9781315162935-11

World Bank (2010) The costs to developing countries of adapting to climate change. The global report of the economics of adaptation to climate change study. Available via World Bank. https://documents.worldbank.org/en/publication/documents-reports/documentdetail/667701468177537886/the-costs-to-developing-countries-of-adapting-to-climate-change-new-methods-and-estimates-the-global-report-of-the-economics-of-adaptation-to-climate-change-study. Accessed 19 May 2021

Yohe GW, Lasco RD, Ahmad QK et al (2007) Perspectives on climate change and sustainability. In: Parry ML, Canziani OF, Palutikof JP et al (eds) Climate change 2007: impacts, adaptation and vulnerability. Contribution of Working Group II to the fourth assessment report of the intergovernmental panel on climate change. Cambridge University Press, Cambridge

Chapter 3
Mathematical Models Ensuring Freshwater of Coastal Zones in Arid and Semiarid Regions

Ismail Abd-Elaty and Salvatore Straface

Abstract Freshwater resources are limited and account for only 3% of all Earth's water, of which 22% constitute groundwater resources. Sustainable management of groundwater resources is increasingly urgent with the widening gap between demand and available water supply. Water scarcity problems are amplified by climate change (CC). Today, exploitation of nonconventional water resources for water and food security is a major challenge. Brackish water is reliable and low cost; it may be obtained using renewable energy and has a low content of salinity. A mathematical model (SEAWAT) was applied to the coastal region of the Nile Delta, Egypt. Three scenarios were simulated: sea level rise (SLR), reduced surface water hydrographs, and overexploitation. Four management scenarios were considered: optimisation and allocation of abstraction rates (OA); treatment and recharge (TR); abstraction of brackish water, desalination, and recharge (ADR); and treatment of wastewater and recharge, abstraction of brackish water, and desalination (TRAD). The results indicated that SEAWAT is a powerful tool for simulating and predicting groundwater salinity and can be used for sustainable management and control of coastal aquifer salinity.

Keywords Saltwater intrusion · Sustainable water management · Coastal aquifers · Mathematical modelling · Nile Delta Aquifer · Egypt

I. Abd-Elaty (✉)
Water & Water Structures Engineering Department, Faculty of Engineering, Zagazig University, Zagazig, Egypt
e-mail: eng_abdelaty2006@yahoo.com

S. Straface
Department of Environmental Engineering, University of Calabria, Rende, Italy
e-mail: straface@unical.it

J. N. Furze et al. (eds.), *Earth Systems Protection and Sustainability*,
https://doi.org/10.1007/978-3-030-98584-4_3

3.1 Introduction

About 97% of water in the oceans is saline, while 3% of all water on Earth is represented by freshwater. Most of the freshwater is enclosed in glaciers and polar ice caps of Greenland and Antarctica. Freshwater is also groundwater and surface water of rivers and lakes which we use in our everyday consumption (Gleick 1996). Groundwater accounts for about 22% of all freshwater on Earth, 77% is polar ice and 0.30% is in rivers and lakes (Bear et al. 1999). The role of groundwater resources in the hydrological cycle is illustrated by the distribution of global water supplies (Fetter 2001).

Good water management is essential for life and the well-being of ecosystems, yet it can be very challenging. One of the most concerning global issues is the uneven distribution of water and water shortage, which provokes violations of human rights and issues of injustice and even leads to war. Causal factors of water shortage include climate change, population growth, overuse of water, and industrial pollution (Jones 2011). An efficient, integrated, and sustainable groundwater resource management plan is required. Management of water resources relies on a comprehensive database representing the characteristics of aquifer systems and modelling tools (Dawoud et al. 2005). Demand for water resources for human consumption, sanitation, agricultural irrigation, and production will continue to intensify with population growth and the acceleration of global urbanization, industrialization, and commercial development (Flint and Houser 2001).

Fresh groundwater (FG) plays a prominent role in supplying many areas that do not have sufficient surface water sources. FG supports different types of life forms and helps in the growth of human civilization. Around two billion people depend on groundwater sources. Groundwater sources are a renewable source that is recharged yearly from rainfall (Simlandy 2015). Today more strategies are needed to maintain optimal groundwater quality; the management of this vital natural resource has become a global priority (Andreo et al. 2005). The hydrologic water balance can be used as a preliminary estimate of the total inflow and outflow of groundwater flow systems and the resulting net storage change. The groundwater flow balance equation is applicable when the available data for use in sophisticated numerical groundwater flow models is insufficient (Mukhopadhyay et al. 1994).

3.2 Climate Change and Water Resources

Climate change (CC) is accelerating at an alarming rate as a result of human activity and natural processes. The effect of CC on various water resources and processes is discussed in this section.

3.2.1 Groundwater and Climate Change

Most climatologists believe that human activity contributes to climate change (CC) by increasing greenhouse gas emissions and the Earth's average temperature. Over centuries, CC can be responsible for melting large amounts of ice from glaciers and caps, sea level rise, coastal region flooding, erosion, loss of wetlands, and saltwater intrusion (SWI) as seen in Fig. 3.1. Rise in sea levels contributes to submergence of coastal and small island nations (Abd-Elhamid 2010; El-Raey 2010).

Scenarios within the Intergovernmental Panel on Climate Change (IPCC) Special Report on Emission Scenarios (SRES) define four storylines within two divergent tendencies: one group varies between strong economic values and strong environmental values, whilst the other is between increasing globalization and increasing regionalization (Nakicenovic et al. 2000). The outcome of the storylines and our current activities is a global rise in temperature of up to 5.8 °C by 2100; local fluctuations may be more or less, depending on their vulnerabilities and activities. Whatever the gravity of CC, impacts on water resources are inevitable.

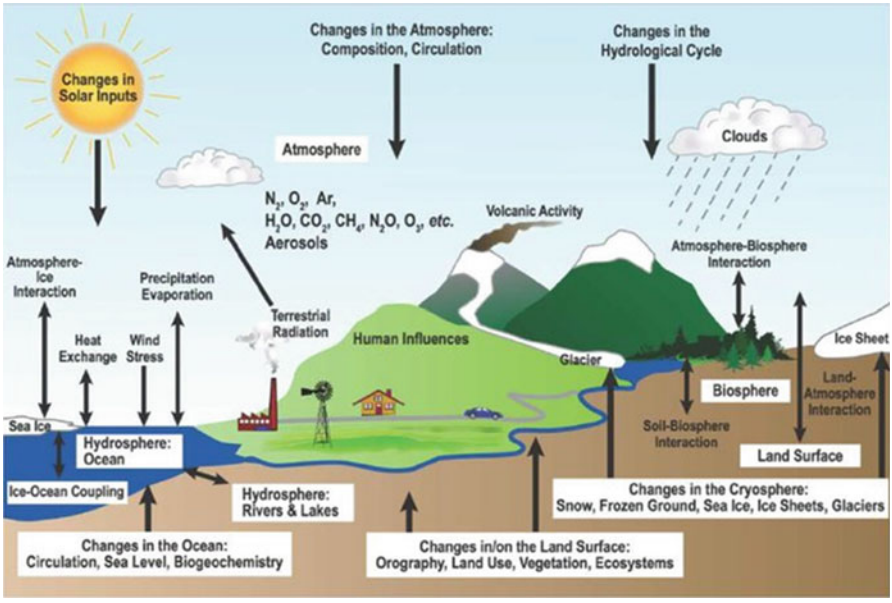

Fig. 3.1 Schematic view of the components of the climate system, their processes, and interactions (Treut et al. 2007)

3.2.2 Impact of Climate Change on Sea Level Rise (SLR)

Climate change has a major impact on coastal aquifers, leading to SLR, which directly affects SWI. Increased global temperature warms the land surface, bodies of water, and seas, further leading to decreased atmospheric pressure, which leads to an increase in water levels (IPCC 1996). SLR is a consequence of thermal expansion of oceans and seas and the melting of glaciers, ice caps, and Greenland and Antarctic ice sheets.

Satellite observations have indicated an acceleration of SLR. Field measurements of the tide level showed that the global mean sea level rose between 0.10 and 0.20 m in the twentieth century as shown in Fig. 3.2a.

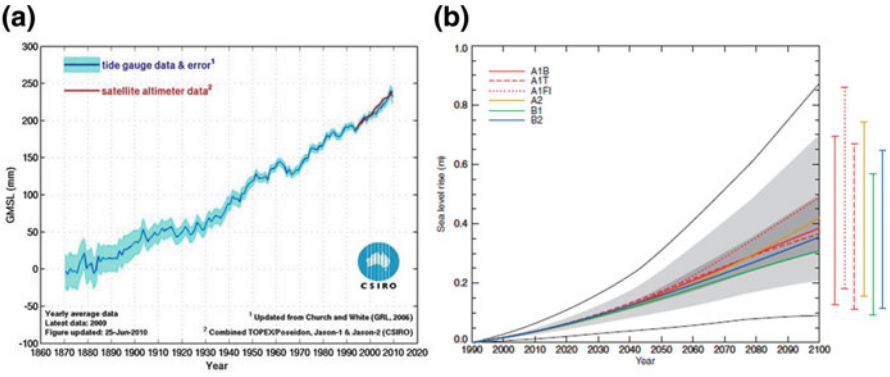

Fig. 3.2 Changing rates of SLR for (**a**) measured global mean sea level (GMSL) over the period 1870–2010 as observed by ground-based and satellite observations and (**b**) prediction for the twenty-first century (IPCC 2001)

The range of SLR reported in the second assessment report (SAR) by IPCC (1996) was 0.13–0.94 m for IS92 scenarios. Simple models have been developed to represent seawater expansion and the melting of ice sheets and glaciers and used in the third assessment report (TAR) for the estimation of the global average SLR, projecting from 0.09 to 0.88 m by 2100 relative to 1990 in SRES scenarios as shown in Fig. 3.2b (IPCC 2001). Moreover, SLR is expected to be between 18 and 58 cm by the end of this century (IPCC 2007).

3.2.3 Impact of Climate Change on Precipitation

Precipitation increased by 0.5–1% per decade in the middle and high latitudes of the continents of the northern hemisphere, and by 0.2–0.3% per decade over the tropical (10° N to 10° S) land areas, while it decreased by 0.3% in the subtropical areas of the northern hemisphere (10° N to 30° N). In parts of Asia and Africa, the frequency and intensity of droughts have increased in recent decades. The simulations and

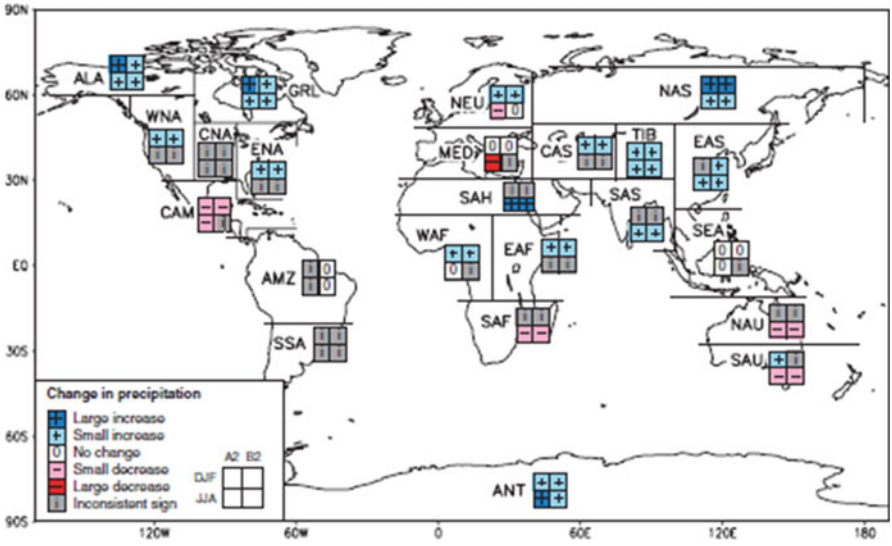

Fig. 3.3 Analysis of inter-model consistency in regional precipitation change (IPCC 2001)

scenarios of the global models are used to predict that the global average water vapor concentration and precipitation will increase in the twenty-first century. In the second half of the twenty-first century, winter precipitation is likely to increase in northern mid-to-high latitudes and in Antarctica, while there are both regional increases and decreases over land areas at low latitudes. Figure 3.3 shows changes in regional precipitation calculated by the IPCC (2001).

3.2.4 Impact of Climate Change on Hydrology and Water Resources

More than one-sixth of the world's population lives in river basins fed by glaciers or snowmelt and is influenced by a decrease in the amount of water stored in glaciers and snow, an increase in the ratio of winter to annual flows, and a decrease in low rivers caused by reduced glacier expansion. It is predicted that increased precipitation intensity and frequency will increase the risk of floods and droughts in many areas. Up to 20% of the world's population lives in river basins and may be affected by an increased risk of flooding in the course of global warming until the 2080s. By the middle of this century, the annual average river runoff and water availability will increase between 10% and 40% in high latitudes and in some tropical humid areas. In contrast, these parameters will decrease between 10% and 30% in some arid regions in mid-latitudes and in arid regions of the tropics, some of which are already water stressed (IPCC 2007; SNC 2010).

The goal of groundwater management is to obtain the maximum quantity of water to meet predetermined quality requirements at least cost. Aquifers can be conceptualized as large natural groundwater reservoirs. The abstraction of groundwater by localized wells can affect the quantity and quality of water that is available elsewhere within an aquifer. To manage FG (fresh groundwater), knowledge of water quantity that can be abstracted is a prerequisite. The equation of hydrologic equilibrium provides a quantitative statement of water balance (Todd 1980).

3.3 Groundwater Reservoirs

Geological formations of groundwater reservoirs are classified as aquifers, aquitards, and aquicludes.

3.3.1 Aquifers

Aquifers are rock or sediment bodies that release significant (economic) amounts of groundwater to the abstraction wells or springs. There are different types of aquifers (unconfined sedimentary, confined sedimentary, and confined fractured lava rock) depending on the geologic material coverage and depth.

Unconfined or free water table (atmospheric) aquifers are without overlying confining layers and are more highly subjected to contamination than confined aquifers. Confined aquifers are those overlain by a confining layer. Artesian aquifers of well flow result from pressure within the aquifer. The hydrogeological conditions subject groundwater to pressure. The artesian flow discontinues when the aquifer pressure is reduced, and the potentiometric surface drops below ground surface level. Partially or confined aquifers can be restricted to parts of their area being more confined than other (uncovered) types (Heath 1983; Berardinucci and Ronneseth 2002).

3.3.2 Aquitards

Aquifers consist of silt, clay, shale, or dense crystalline rock. They can be permeable, enabling flow of significant amounts of water at the regional level, but are incapable of supplying water to a production well. Aquitards store the groundwater but do not provide it in significant or economical quantities. Aquitards have confining layers which retard the vertical movement of groundwater flow, though some can be described as “leaky” (Heath 1983).

3.3.3 *Aquicludes/Aquifuges*

Aquicludes are impermeable geological units which do not transmit water. They absorb water slowly, can store water but cannot transmit it easily. Examples are metamorphic rocks. Aquifuges are a further even less permeable type where geological formation can neither absorb nor transmit groundwater (Heath 1983).

3.4 Groundwater Contamination

Although groundwater resources are more protected from contamination than surface water, they are still exposed to pollution. Following contamination, restoring it to the original unpolluted state is very hard and costly. Groundwater contamination is usually traced back to environmental, domestic, industrial, and agricultural sources (Bear 1979; EPA 2012).

Environmental pollution occurs by the flow of groundwater through carbonate rock, SWI, or the brackish groundwater invasion from adjacent aquifers. Domestic pollution occurs via accidental fractures in sewers, seepage from septic wastewater tanks, precipitation through contaminated land, and acid rain; additionally biological contaminants (including bacteria and viruses) occur through sewerage treatments. Industrial pollution resides in sewage and may contain heavy metals, non-deteriorating compounds, and radioactive materials. Agricultural pollution occurs through leaching of applied materials such as fertilizers, salts, herbicides, and pesticides.

3.4.1 *Saltwater Intrusion*

Saltwater intrusion (SWI) is a natural process in which coastal aquifers are connected to the sea due to the greater density of saline water relative to the freshwater in the aquifer. Dense saline water flows under the freshwater and forms a "wedge." The wedge occupies a position where the density and pressure forces from the sea pushing the wedge inland are balanced by the forces of pressure within the aquifer. Pressure forces are often imbalanced and erode the wedge at the interface between the freshwater and saltwater, as shown in Figs. 3.4 and 3.8. The saltwater wedge becomes a significant problem if it begins to move inland. It can contaminate water supply and/or irrigation wells. Excessive groundwater abstraction from the coastal aquifer causes wedge movement (Harman 2002). Contour maps of total dissolved solids (TDS) are one measure of salinity. The TDS location subjects the area to the influence of SWI (Abd-Elhamid 2010).

SWI is a serious problem in coastal regions. The degree of groundwater salinity depends on several natural and human parameters. The natural parameters include

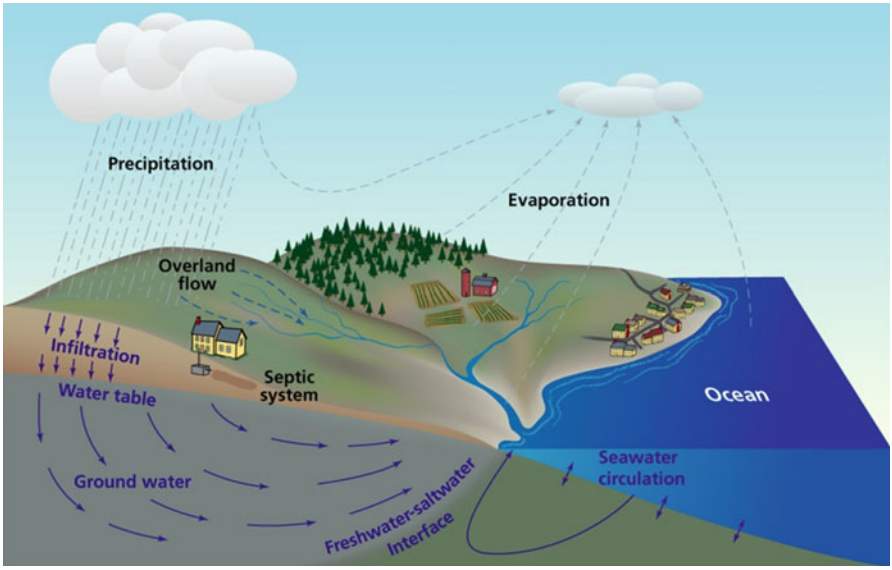

Fig. 3.4 Saltwater intrusion process

the geological aspects, aquifer geometry, sea depth, the hydrogeological and hydraulic parameters (specific yield, specific retention, effective and total porosity, permeability, specific storage and storage coefficient, groundwater heads, groundwater abstraction and recharge), the transport parameters (such as dispersivity, dispersion and diffusion coefficients), reaction processes, and the flow and contamination boundary conditions. Human parameters include overpumping, control of flooding runoff, land use, and artificial recharge of freshwater activities. The five types of SWI are lateral intrusion, downward seepage, upcoming deep saline seawater, alteration to natural barriers, and via improving groundwater quality due to abstraction (Callander 2011).

Coupling of groundwater fluid flow and solute transport models may be used to investigate and predict SWI in coastal aquifers. Problems for groundwater are overexploitation, mining, subsidence, water logging, seawater intrusion, and groundwater pollution (Kumar 2002). Investigation of coastal region salinity requires data of the hydrological and hydro-chemical parameters of aquifers. SWI has been investigated by both geophysical and geochemical methods (Bear et al. 1999). Experimental studies may be carried out in laboratories to ascertain the saline freshwater interface in order to obtain accurate values of the hydraulic heads in freshwater zones. Mathematical studies have been applied to simulate and predict the SWI using analytical and numerical models.

3.4.2 Population and Overexploitation

Over 70% of the world's population resides in coastal zones which are among the most densely populated areas in the world. These regions face serious hydrological problems such as freshwater scarcity, groundwater contamination, and seawater invasion. Coastal zones are subjected to serious hydrological problems including high stress of freshwater, pollution of groundwater by SWI, and overpumping by increasing groundwater abstraction due to growth in the global population (Abd-Elhamid 2010).

3.5 Groundwater Models

The modelling of groundwater enables an understanding of physical problems and entails conversion of physical systems into mathematical terms to quantify and qualify processes taking place in a hydrological system or to answer a specific question (Kumar 2002). The goals and methods of modelling depend on the nature of the query and the properties of the location or system. Details and accuracy of the system depend on the objectives of the natural resource sector. Models of groundwater are used in environmental assessments or other permit requirements. The use of numerical groundwater models enables and helps decision-makers to study and evaluate large and complex water resource development projects.

3.5.1 Classification of Groundwater Models

Groundwater models are used to simplify the hydrological groundwater system, which can be classified by physical or mathematical models. Physical modelling is made by "box tanks" replicating physical processes at smaller scales than in the field. These models are developed and used to simulate the groundwater flow and the solute transport of contamination and pollutants in the groundwater (Barnett et al. 2012). Rausch (2010) states groundwater models can be classified with respect to: (i) physical conditions, (ii) dimensionality, and (iii) solution method.

3.5.2 Types of Mathematical Models

A wide variety of modelling tools are available to simulate groundwater systems. These tools can be roughly grouped into analytical, numerical, and analytic element models.

Analytical models use exact solutions to describe the groundwater flow or the transport equation. To obtain exact solutions, flow or transport equations have to be simplified to apply to hydrological systems. The analytical models' advantage is the ease of use and transparency of such models, while the disadvantage is that application may be limited to relatively simple flow or transport problems (Wels 2012).

Numerical models solve the governing equations of groundwater flow and/or contaminant transport using numerical methods. The advantage of numerical models is that they solve complex systems; multi-layered aquifers have hydraulic parameters and boundary conditions and model time steps. The disadvantages are the cost, the time of solving, and the model complexity which reduces the transparency of calculations and may introduce uncertainty (Wels 2012; Barnett et al. 2012).

Analytic element models use the superposition of closed-form (analytical) solutions to the governing differential equation of groundwater flow to approximate both local (near-field) and regional (far-field) flow (Hunt et al. 1998). The process of selecting the appropriate mathematical model has been described (Bazrkar et al. 2017).

3.5.3 Solution Methods for Differential Equations

The objective of solutions of differential equations which physically govern the hydrological system is to find unknown parameters with associated boundary and initial conditions. Analytical and numerical methods are used to solve these equations.

3.5.3.1 Analytical Solution

The coupled fluid flow and the transport problems in porous media are solved using complex nonlinear partial differential equations. Numerical methods with approximate solutions may be preferred to the use of complex differentials (Abd-Elhamid 2010). However, analytical solutions can be used for simple boundary, initial conditions and homogeneity assumption (Rausch 2010).

3.5.3.2 Numerical Solution

Types of numerical methods used to solve the complex nonlinear partial differential equations of groundwater flow and transport models in porous media are finite difference and finite element methods (Abd-Elhamid 2010).

Finite difference method (FDM) is most frequently used in simulation of numerical groundwater flow and transport models. In most FDM models, the domain of space and time are divided on a rectangular grid (Fig. 3.5a), and model parameters such as hydraulic parameters and the hydrological boundary conditions are specified

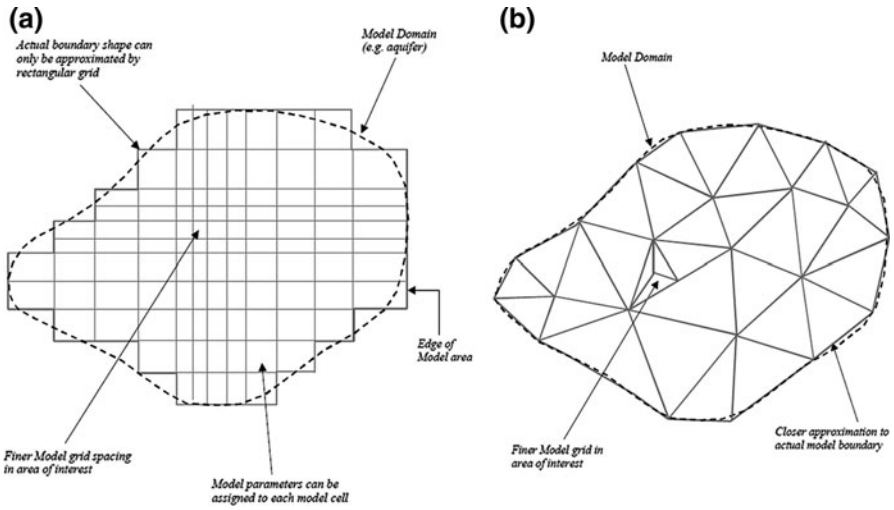

Fig. 3.5 Illustration of (**a**) finite difference method (FDM) and (**b**) finite element method (FEM) (NGCLC 2001)

by cell. The grid spacing represents the degree of accuracy of the model, representing lateral or vertical changes in the property values describing the system. The advantage of the FDM is its use for simple or regular geometry, while the disadvantage is that it may be less accurate for irregular model domains such as anisotropic and heterogeneous aquifers with irregular boundaries. In addition, it is difficult to change the grid spacing to increase model precision (Wels 2012; Istok 1989). FDM can be solved using a computer program or a spreadsheet, such as MODFLOW and SEAWAT.

Finite element method (FEM) uses a mesh of elements to divide the problem domain (Fig. 3.5b). FEM is a powerful numerical tool for the solution of a wide range of engineering problems. In the 1970s, the FEM was first used to solve flow and transport problems in porous media (Istok 1989). The fundamental idea of FEM is to produce a set of algebraic equations for each element and then collate all elements using a procedure called assembly to form the global matrix statement (Baker and Pepper 1991). A polynomial function may be used to approximate the variation in a model parameter across the model element. Complex geological boundary model domains are defined much better than in FDM. The mesh is easily modifiable and achieves great precision. Models of finite elements are less susceptible to numerical dispersion than finite difference models (Wels 2012). FEM is very popular (Logan 2002) as it may be used to simulate irregular and curved geometric domains, variable node spacing, variable element size, boundary conditions, anisotropic and heterogeneous porous media, nonlinear behavior, and dynamic effects (Cheung et al. 1996).

3.5.4 Numerical Model Codes

Numerical model code is used in groundwater modelling to solve groundwater flow or solute transport problems. The code facilitates the recording of the relevant input parameters of model such as model grids, aquifer hydraulic and hydrological parameters, and boundary conditions. Table 3.1 details code names and descriptions.

Numerical dispersion and numerical instability are the most common problems for groundwater solute transport models (Wels 2012).

Numerical dispersion problems are caused by insufficient discretization in space and time. Distortion effects are more pronounced in the vertical direction than horizontal. Reduced numerical dispersion can be achieved by using Lagrangian methods, decreasing the model grid spacing and time steps for the models solved by Euclidean methods, choice of initial or starting conditions, and convergence criteria.

Numerical instability can lead to numerical oscillations in space and time. Peclet and Courant numbers are used to estimate the maximum grid size and time step for solute transport models. In addition, sensitivity analyses may be used to check the effect of grid spacing and time step (Wels 2012).

Table 3.1 Available groundwater modelling codes (Barnett et al. 2012)

Serial	Model codes	Simulation type	Description
1	MODFLOW (McDonald and Harbaugh 1984)	Saturated groundwater flow	Open-source software of the US Geological Survey, based on FDM
2	MT3DMS (Zheng and Wang 1999)	Transport of multiple reactive solutes	Open-source software coupled with MODFLOW for coupling flow and transport
3	SEAWAT (Guo and Bennett 1998)	Saturated flow, transport of multiple solutes and heat	Open-source software combining MODFLOW and MT3DMS for density-coupled flow and transport
4	MODFLOW 2000	3D groundwater flow and contaminant transport	Commercial software supports MODFLOW packages, MODPATH, SEAWAT, MT3DMS, MT3D99, RT3D, PHT3D, MGO, PEST, MODFLOW-SURFACT, and MIKE 11
5	SUTRA (Voss 1984)	Saturated and unsaturated flow, transport and heat	Open-source software based on FEM, designed for density-coupled flow and transport
6	FEFLOW (Diersch 1996)	3D saturated and unsaturated flow, transport and heat, with integrated GUI	Commercial software based on the FED coupling to MIKE 11 to simulate flow in river and stream networks
7	GMS	GUI	Commercial software supports MODFLOW packages, MODPATH, MODAEM, SEAWAT, MT3DMS, RT3D, PEST, and FEMWATER

3.5.5 Water Modelling Packages

Visual MODFLOW 2010.1 is a 3D groundwater flow and solute transport model; it integrates MODFLOW-2000, SEAWAT, MODPATH, MT3DMS, MT3D99, RT3D, VMOD 3D-Explorer, WinPEST, Stream routing package, Zone Budget, MGO, SAMG, and PHT3D.

The main component of the governing groundwater flow equation is the law of mass balance plus Darcy's law (Kumar 2002). The mathematical treatment for the groundwater flow equation through a porous medium depends upon an equation that captures the essence of the physics of flow (Vandenbohede 2003). The partial differential equation of groundwater flow for constant density groundwater flow may be applied (McDonald and Harbaugh 1984) and is given in Eq. (3.1):

$$\frac{\partial}{\partial x}\left(K_{xx}\frac{\partial h}{\partial x}\right)+\frac{\partial}{\partial y}\left(K_{yy}\frac{\partial h}{\partial y}\right)+\frac{\partial}{\partial z}\left(K_{zz}\frac{\partial h}{\partial z}\right)=S_{\mathrm{s}}\frac{\partial h}{\partial t}\pm q \tag{3.1}$$

where K_{xx}, K_{yy}, and K_{zz} are values of hydraulic conductivity along the x, y, and z coordinate axes, h is the potentiometric head, t is time, and q is volumetric flux per unit volume representing source/sink terms, with $q < 0$ for flow out of the groundwater system and $q > 0$ for flow in. S_{s} is the specific storage coefficient defined as the volume of water released from storage per unit change in head per unit volume of porous material.

The mechanism of the equivalent freshwater head in a saline aquifer is based on the following assumptions: (i) validation of Darcy's law, (ii) it is applicable to specific storage in a confined aquifer, (iii) the diffusive approach based on Fick's law is applied, and (iv) prevailing isothermal conditions. The porous medium is assumed to be fully saturated with water. A single, fully miscible liquid phase of very small compressibility is also assumed (Guo and Langevin 2002).

The theory of variable-density groundwater flow is usually developed in terms of fluid pressure and density with an Eq. (3.2) developed in terms of equivalent freshwater head and fluid density. Figure 3.6 indicates the two piezometers which represent an aquifer containing saline water in which Piezometer A contains freshwater while Piezometer B contains saline aquifer water at point *N*.

The principle of mass conservation for fluid and solute is the rate of accumulation of mass stored in the reservoir and is equal to the algebraic sum of the mass fluxes across the faces of the element and the mass exchange due to sinks or sources. The governing equation for variable-density flow (Guo and Langevin 2002) in terms of freshwater head as used in SEAWAT is as follows in Eq. (3.2):

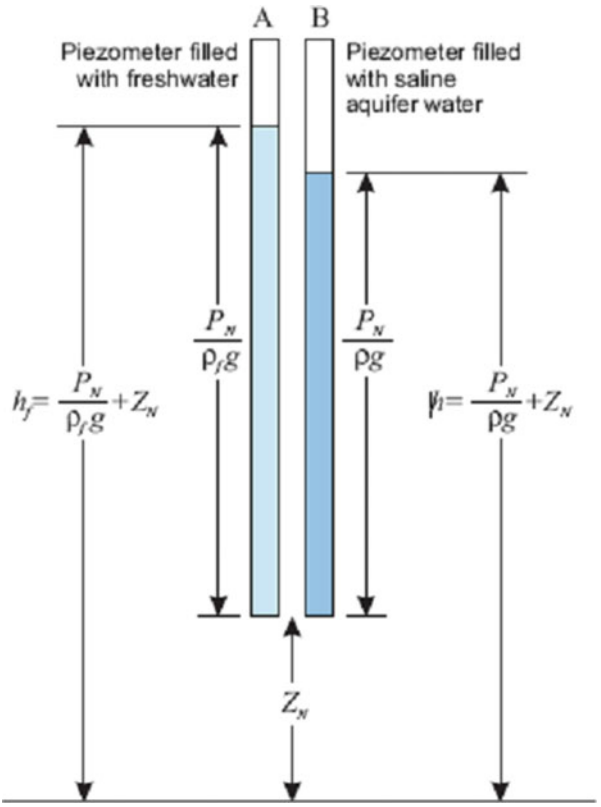

Fig. 3.6 Equivalent freshwater head in a saline aquifer (Guo and Langevin 2002)

$$\frac{\partial}{\partial x}\left(\rho K_{\mathrm{fz}}\left[\frac{\partial h_{\mathrm{f}}}{\partial x}\right]\right)+\frac{\partial}{\partial y}\left(\rho K_{\mathrm{fy}}\left[\frac{\partial h_{\mathrm{f}}}{\partial y}\right]\right)+\frac{\partial}{\partial z}\left(\rho K_{\mathrm{fz}}\left[\frac{\partial h_{\mathrm{f}}}{\partial z}+\frac{\rho-\rho_{\mathrm{f}}}{\rho_{\mathrm{f}}}\right]\right)$$
$$=\rho S_{\mathrm{sf}}\left(\frac{\partial h_{\mathrm{f}}}{\partial t}\right)+n\left(\frac{\partial \rho}{\partial C}\right)\left(\frac{\partial C}{\partial t}\right)-\frac{\rho}{q_{\mathrm{s}}} \tag{3.2}$$

where h_{f} is the equivalent freshwater head, h is the head, P_N is the pressure at point N, ρ is the density of saline groundwater at point N, ρ_{f} is the density of freshwater, S_{sf} is the specific storage in terms of freshwater head or the volume of water released from storage in a unit volume of aquifer per unit decline in freshwater head, t is time, n is the porosity (dimensionless), and C is solute concentration (parts per million).

Numerical models of groundwater are a strong and powerful tool to simulate groundwater in both flow and solute transport systems; they provide support in planning, design, and management of groundwater resources. Derivation of the advection-dispersion equation (ADE) is based on the law of conservation of mass. The derivation is based on Ogata (1970) and Bear (1972) and is presented in Freeze and Cherry (1979) and assumes that the porous medium is homogeneous, isotropic, and saturated, the flow is steady state, and Darcy's law applies.

The effects of pore pressure on fluid density are included in the storage term. An empirical relation between the density of saltwater and concentration (Baxter and Wallace 1916) is shown in Eq. (3.3):

$$\rho = \rho_{\mathrm{f}} + E * C \tag{3.3}$$

where E is a dimensionless constant having an approximate value of 0.7143 for salt concentrations ranging from zero to that of seawater at ρ_{f}, i.e., the freshwater density equal to 1000 kg/m^3.

3.6 Case Study: The Nile Delta Aquifer (NDA), Egypt

The Nile Delta Aquifer (NDA) is one of the largest groundwater reservoirs in the world and is subject to severe seawater intrusion from the Mediterranean. It has direct hydraulic contact with the ocean on its northern boundary (Negm et al. 2018; Abd-Elaty et al. 2021a). Groundwater resources in the Nile Delta are an important water supply for domestic, industry, and irrigation uses (Abd-Elaty et al. 2021b). Increasingly intensive agriculture practices require greater application of fertilizers in order to sustain food production, resulting in higher concentrations of pollutants in groundwater (Abd-Elaty et al. 2020a). The evaluation of water quality indicators is crucial in integrated water resource management, since potable water is an essential resource for world health and sustainable development (Abd-Elaty et al. 2019a).

A number of studies were carried out following various extraction rate scenarios. Voss (1984) and authors used a SUTRA code to identify the optimal distribution for additional production wells from the NDA. It was concluded that additional abstraction rates should be applied in the Middle Delta accompanied with a reduction in abstraction from eastern and western parts. Sherif and Al-Rashed (2001) investigated the quality of groundwater in the northern part of the Nile Delta and found that water quality has deteriorated over the last few decades due to excessive pumping. El Didy and Darwish (2001) simulated the SWI in the NDA using SUTRA code considering the effect of freshwater storage in the northern lakes of Manzala and Burullus, and confirmed that SWI occurred in the northern part despite freshwater lakes minimizing intrusion around the influence zone. Nowadays, Egypt is entering a new phase in which human food needs must harmonize with environmental and sustainable principles (Abd-Elaty et al. 2017).

Figure 3.7 shows the location of the NDA, with its contact with the sea on its northern boundary. Sefelnasr and Sherif (2014) simulated the effect of SLR on SWI in the NDA using a 3D finite element variable density FEFLOW model. Abd-Elaty et al. (2014a, b) used a 3D model (SEAWAT) considering scenarios featuring a rise in sea levels, reduced surface water systems, increased abstraction from production wells, and a combination of the three scenarios. Results indicated damage to the aquifer and a loss in quantity of freshwater due to SWI.

Fig. 3.7 The Nile Delta Aquifer (NDA), Egypt

Figure 3.8 shows the cross section of the NDA. Building on the established basic principles (Theis 1935), Abd-Elhamid et al. (2016) applied a 2D variable density model, and three scenarios were studied: SLR, reduction of freshwater heads due to increasing the abstraction at the land side, and the combination of the two scenarios. Results indicated that SWI was increased when the boundary conditions are altered. Moreover, Abd-Elhamid et al. (2016, 2018, 2019) and Abd-Elaty et al. (2018, 2019b, 2021c, d) investigated SWI in coastal aquifers using SEAWAT.

The NDA geometry and boundary conditions were presented by Abd-Elaty et al. (2014a, b). Figure 3.9 shows the NDA head boundary conditions using river and drain packages, while the brackish lakes including Idku, Burullus, and Manzala with direct connection to the Mediterranean Sea were assigned a constant head boundary.

A constant concentration value of 35,000 mg/L total dissolved solids (TDS) was assigned along the Mediterranean Sea, while the initial concentration of the groundwater was set to 0 mg/L. The model was calibrated; the results of the calculated groundwater head are shown in Fig. 3.10, the groundwater level between 14 m in the south and 0 in the north is in agreement with Abd-Elaty et al. (2014a). Figure 3.11 shows the solute transport where the intrusion length of iso-concentration line 3.5E4 intruded in the aquifer by a distance of 63.75 km from the shoreline. However, the iso-concentration line 1.0E3 in the NDA intruded to 93.75 km from shoreline with a transition zone of 30 km (Fig. 3.12).

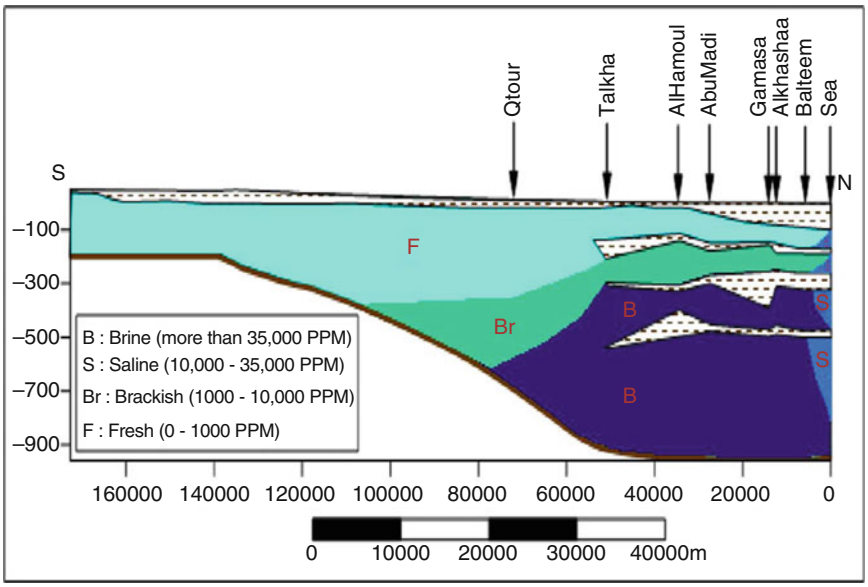

Fig. 3.8 Multi-wedge system of seawater intrusion in the Nile Delta Aquifer (NDA) (Nofal et al. 2015)

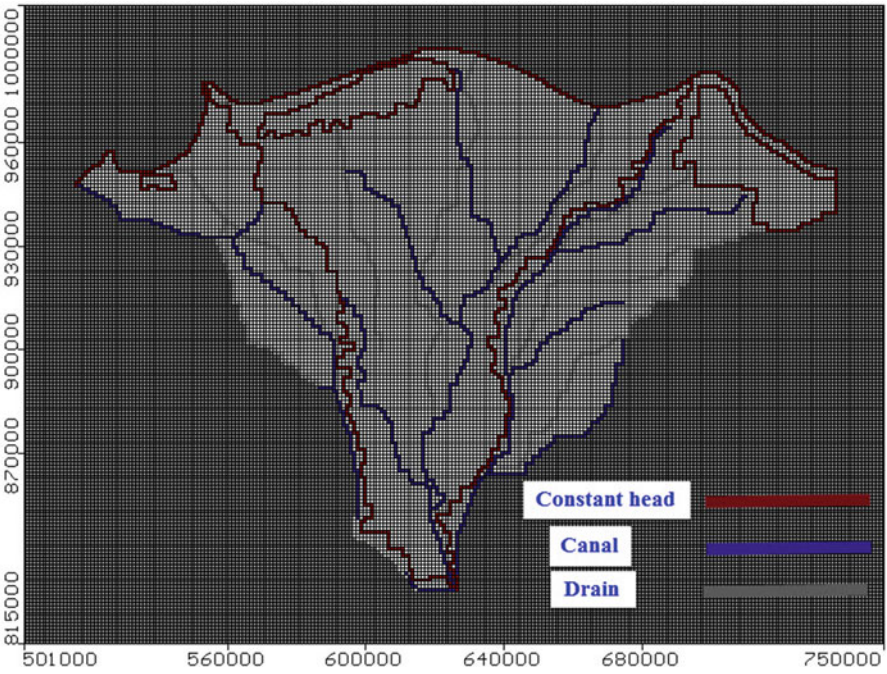

Fig. 3.9 Head boundary conditions for the Nile Delta Aquifer (NDA) in the numerical model

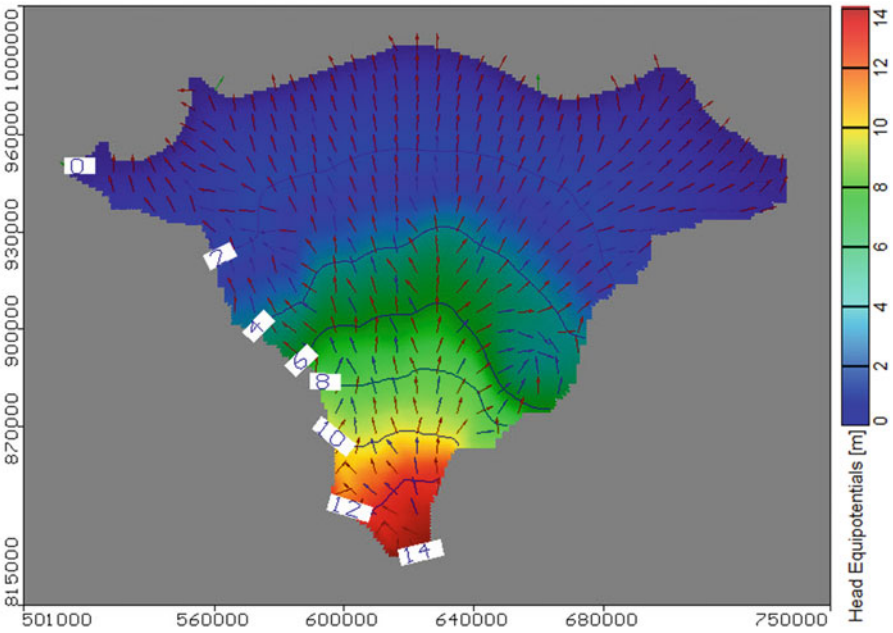

Fig. 3.10 Calculated groundwater level in the Nile Delta Aquifer

3.6.1 Simulations of Saltwater Intrusion (SWI) in the Northern Delta Aquifer

The case study continues to show the numerical code simulated on the NDA for the three cases of increasing sea level, reduction in surface water hydrograph, and increased aquifer abstraction rates. The results of these scenarios are presented in Table 3.2. The investigation of SWI under SLR, decreasing recharge, and overpumping concords with Abd-Elaty et al. (2014b).

Management scenarios were developed for sustainable water resources in coastal aquifers including optimisation and allocation of wells, treatment and recharge, and abstraction and desalination of brackish water. Further results are discussed in the remaining parts of the section.

3.6.1.1 Impact of Sea Level Rise

The results of increasing sea level by 50 cm are presented in Fig. 3.13.

In this scenario the intrusion reached 67 km from shoreline for iso-line 3.5E4, while it reached 96.25 km for iso-line 1.0E3.

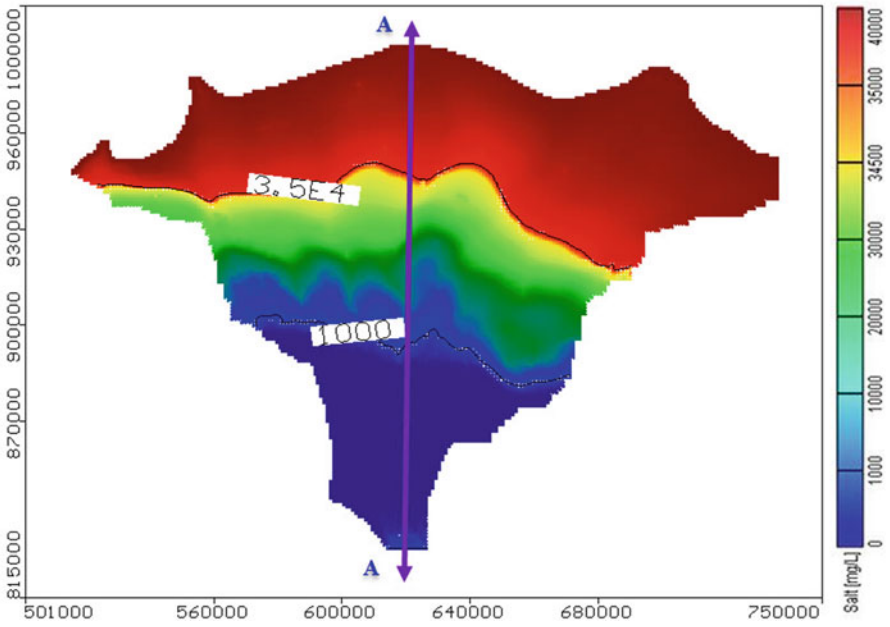

Fig. 3.11 Distribution of TDS in the NDA, on average depth ranges from 450 m in the north to 100 m in the south

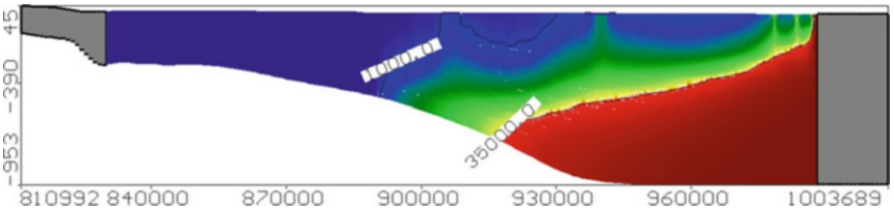

Fig. 3.12 Vertical distribution of TDS in the NDA for base case from the south to the north at section A-A

3.6.1.2 Impact on the Surface Water Hydrograph

The following scenario was developed by decreasing the surface water level by 50 cm. The results are shown in Fig. 3.14.

The intrusion reached 67 km for iso-line 3.5E4 and 96.50 km for iso-line 1.0E3, respectively. The decrease of the surface water level leads to an increase of SWI in the aquifer.

Table 3.2 Scenarios to investigate and control SWI in the Middle Nile Delta Aquifer (NDA)

Case	Scenario	Scenario description	Intrusion length (Km)	
			Iso-concentration line 3.5E4	Iso-concentration line 1.0E3
Investigation of SWI	I_1	Current situation	63.75	93.75
	I_2	50 cm by SLR	67	96.25
	I_3	50% by decreasing recharge	67	96.50
	I_4	50% by overabstraction	66.50	101.25
Management of SWI	M_1	50% recharge by treated wastewater (TR)	66.25	89
	M_2	50% recharge by desalinated brackish water (ADR)	67.75	90
	M_3	50% recharge by treated wastewater and desalinated brackish water (TRAD)	65.50	84.75

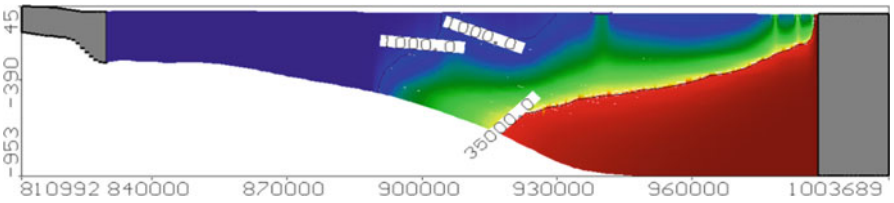

Fig. 3.13 Vertical distribution of TDS in the NDA due to a 50 cm sea level rise (SLR)

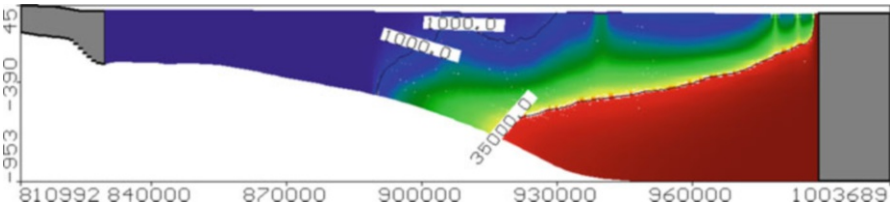

Fig. 3.14 Vertical distribution of TDS in the NDA due to a 50 cm decrease of the surface water hydrograph

3.6.1.3 Impact of Abstraction Rates

In the following graph the abstraction rates from groundwater were increased by 50% (Fig. 3.15).

The figure shows increasing extraction rate for increasing SWI in aquifer. Intrusion reached 66.50 km from shoreline for iso-line 3.5E4 and reached 101.25 km for iso-line 1.0E3, respectively.

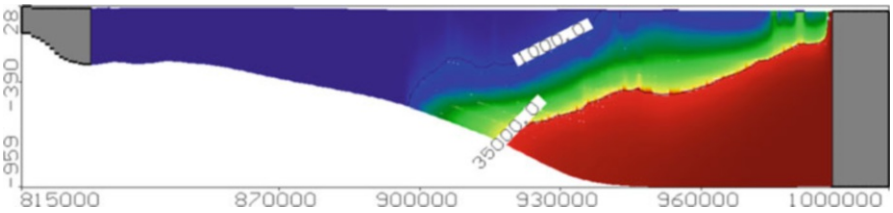

Fig. 3.15 Vertical distribution of TDS in the Nile Delta Aquifer (NDA) due to overpumping by 50%

3.6.2 Management of Saltwater Intrusion (SWI) in Coastal Aquifers

The identified future scenarios provided valuable information for prediction of the sustainable management of the NDA freshwater and for achieving food security. Subsequently, in Egypt, four techniques were applied to control SWI and protect the freshwater aquifer from salinity: optimisation and allocation of abstraction rates (OA); treatment and recharge (TR); abstraction, desalination, and recharge (ADR); and treatment and recharge, abstraction, and desalination (TRAD). Coastal aquifer mitigation is essential to increase the fresh groundwater resources in these regions (Abd-Elhamid et al. 2020).

3.6.2.1 Optimisation and Allocation of Abstraction Rates (OA)

Simulation-optimisation models (SOM) may be used to manage and control SWI in coastal aquifers. The numerical model of SEAWAT may be used to investigate the groundwater heads and salt concentrations for transient density-dependent cases, while the genetic algorithm optimisation technique estimates the optimal well locations, depths, abstraction, and recharge rates to minimize the total costs of the system construction and operation. The iterations of trial and error have been used to solve the optimisation problem, while the numerical simulation models overcame and examined a limited number of design options (Mohamed 2004; Abd-Elhamid 2010). SOM approaches also reduce the remediation costs of polluted land in numbers of a real case study with global coverage (Zheng and Bennett 2002).

Cheng et al. (2000) developed SOM to manage and optimise the abstraction for SWI mitigation based on a sharp interface. Hong et al. (2004) carried out SOM to examine the optimal well pumping rate and locations to achieve the sustainable water resources in coastal zones. Qahman et al. (2005) simulated the SWI using the SEAWAT code with SOM in the Gaza Aquifer, Palestine; also the model was used to study the different pumping rates on aquifer salinity. Reichard and Johnson (2005) carried out SOM to manage the SWI in the west coast basin of Los Angeles, USA, using recharge of freshwater via well injection and surface water ponds. Park et al. (2008) used SOM to optimize the abstraction rates in the aquifer to protect the fresh

groundwater by reducing pumping rates. Dokou et al. (2016) developed SOM to manage SWI in two unconfined coastal aquifers in Crete, Greece, by optimising the abstraction rates with fixed SWI using a GWM code. Rearrangement of abstraction wells can reduce the SWI and upconing (Abd-Elhamid and Javadi 2008), though it is costly; construction and placing of wells pose problems.

For the NDA in Egypt, total annual abstraction rates of 7 billion cubic meters in 2016 were reached (Molle et al. 2016). Such abstraction should be managed to optimise the uses of water resources and protect the aquifer from depletion. The NDA may be managed using linked SOM to control SWI rather than with the traditional methods of reduction.

3.6.2.2 Treatment and Recharge (TR)

TR is used to increase aquifer storage by treating wastewater and recharging it to the fresh groundwater, helping to increase groundwater storage and control of SWI. The recharge systems can be realized by means of infiltration surface ponds or deep wells. In regions of high abstraction rates, this system is costly and ineffective (Narayan 2002). Narayan et al. (2003) simulated the groundwater salinity using SUTRA in the Burdekin Delta Aquifer, Australia, for different abstraction and recharge conditions. The study indicated that the variation in pumping rate, artificial and natural recharge, affects the dynamic of SWI. Vandenbohede et al. (2006) simulated the SWI and control methods in the western Belgian coastal plain using natural recharge of ponds for sustainable water management. Abd-Elaty et al. (2021e) developed a numerical study to simulate the use of different well systems in the NDA in Egypt by reduction of current abstraction, treated wastewater recharge, abstraction of brackish water for desalination, and combination of these systems. The study indicated that these techniques are effective in the management of SWI.

In the NDA of Egypt, the use of recharge ponds was simulated using SEWAT to control SWI. The recharge water can be collected from treated water or storm water. The scenario of increasing the recharge by 50% was introduced. Results are shown in Fig. 3.16 where the intrusion length reached 66.25 and 89 km from shoreline for iso-line 3.5E4 and 1.0E3, respectively.

3.6.2.3 Abstraction, Desalination, and Recharge (ADR)

ADR involves abstraction of brackish water, desalination using renewable energy with novel desalination (reverse osmosis (RO), forward osmosis (FO)), and recharge using surface ponds or deep recharge wells. Developed by Abd-Elhamid and Javadi (2008), ADR can mitigate SWI in coastal aquifers. The method has low energy consumption, costs, and environmental impact and is capable of retarding SWI.

Abd-Elhamid and Javadi (2011) report the combined system (ADR) and individual abstraction or recharge technique; considering the total cost and salt

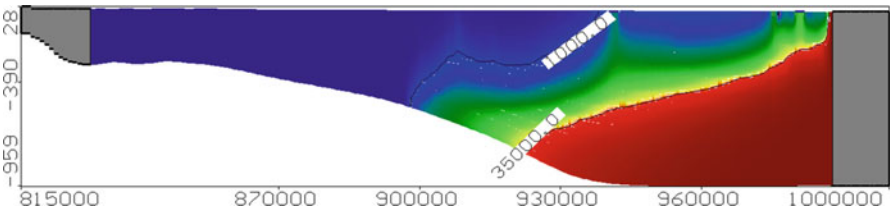

Fig. 3.16 Vertical distribution of total dissolved solids (TDS) in the Nile Delta Aquifer (NDA) due to 50% recharge by treated wastewater

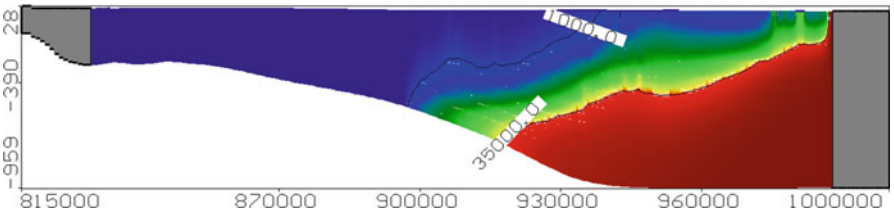

Fig. 3.17 Vertical distribution of TDS in the Nile Delta Aquifer (NDA) due to 50% recharge by use of desalinated abstracted water

concentration can reduce the aquifer salinity. The ADR system was significantly more efficient and sustainable than other systems. Javadi et al. (2013) simulated the SWI using SUTRA with a genetic algorithm (GA) to optimise the management of SWI in unconfined aquifers by combining abstraction of desalinated brackish water and recharge using surface ponds.

For the NDA of the case study in this chapter, control of SWI was developed by abstraction of brackish water by 50% from the total abstraction rates of aquifer. The SEWAT code was simulated (Fig. 3.17).

The iso-line 3.5E4 and 1.0E3 reached 67.75 and 90 km from shoreline, respectively, and the width of the transition zone covered 22 km.

3.6.2.4 Treatment, Recharge, Abstraction, and Desalination (TRAD)

This method is used to mitigate the SWI in coastal aquifers. It includes the treatment of wastewater, recharge to the aquifer to increase the storage of fresh groundwater, abstraction of brackish water to reduce the volume of saline water, and desalination to produce freshwater. The TRAD method overcomes the limitation of other methods, because the source of recharge systems includes the use of treated wastewater, storm water, or the desalinated water of desalination plants. Desalinated water may be used for different purposes to support the water demand or source aquifer freshwater recharge managing SWI. The technique of abstraction and recharge can control SWI toward the sea. Disposal of brine from the desalination plant can be used to produce salt or used in irrigation of certain crops or fisheries. The method has low

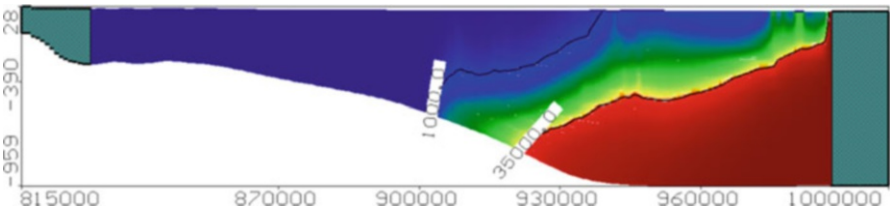

Fig. 3.18 Vertical distribution of total dissolved solids (TDS) in the Nile Delta Aquifer (NDA) due to 50% recharge by treated wastewater and desalination of abstracted water

cost and low environmental impacts, resultantly increasing the groundwater abstraction rates for freshwater supplies and managing flows to the sea (Abd-Elhamid 2010).

Javadi et al. (2015) developed a GA optimisation tool and simulated a SUTRA code to investigate the efficacy of TRAD method to manage SWI. The TRAD technique is efficient and mitigates SWI with low cost and produces the lowest salinity in the aquifer. Abd-Elaty et al. (2021f) used the SEAWAT code to investigate and manage SWI in coastal aquifers under climatic changes of humidity and hyper-aridity using the TRAD technique. The results showed that this system effectively manages SWI.

Abd-Elhamid and Abd-Elaty (2017) simulated the NDA of the chapter case study salinity using this method and found that it could be useful to control SWI where treated wastewater is used for recharge and the abstracted brackish water is used for desalination. The simulation was carried out for the NDA for a recharge and abstraction from brackish water increase of 50%. The results indicated that the iso-line 3.5E4 decreased to 65.50 km, while the iso-line 1.0E3 decreased to 84.75 km as shown in Fig. 3.18. Abd-Elaty et al. (2020b) applied the TRAD technique using a SEAWAT code in the Gaza Aquifer, Palestine, using TRAD with abstraction of brackish water and recharge of treated wastewater. The study showed that this system could retard intrusion of saline water and achieve management of SWI.

3.7 Conclusions

Today, the sustainable management of water resources is a key target for hydrological scientists around the world due to shortage of water resources and increases in water demands as a result of climatic change (CC) and overpopulation. SWI is a major challenge in the management of groundwater resources in coastal regions. Treatment of wastewater has a positive impact and overcomes the scarcity of water in arid regions. Desalinating brackish water using renewable energy sources such as solar energy in combination with reverse osmosis (RO) is an efficient methodology that requires relatively simple equipment and low energy. The freshwater in coastal

aquifers must be protected. Nowadays overpumping effects the growth in water demands from increasing coastal populations, increasing the SLR and aquifer salinity, threatening available groundwater supplies. The current study used a SEAWAT code to investigate the sustainable management of water resources in the NDA, Egypt, with mathematical advances. The latter developed a number of approaches – optimisation and allocation of abstraction rates (OA); treatment and recharge (TR); abstraction, desalination, and recharge (ADR); and treatment and recharge, abstraction, and desalination (TRAD). TRAD is a new and valuable method which pushes saline water toward the sea and improves environmental conditions of the aquifer in Egypt; we recommend its application (with adaptation) elsewhere to potentially ensure or contribute to water sustainability amidst increasingly extreme changes present on Earth today.

References

Abd-Elaty IM, Abd-Elhamid HF, Fahmy MR et al (2014a) Investigation of some potential parameters and its impacts on saltwater intrusion in Nile Delta aquifer. J Eng Sci 42(4): 931–955. https://doi.org/10.21608/JESAUN.2014.115039

Abd-Elaty IM, Abd-Elhamid HF, Fahmy MR et al (2014b) Study of impact climate change and other on groundwater system in Nile Delta aquifer, the Egyptian. J Eng Sci Technol Zagazig Univ Fac Eng 17(4):2061–2079

Abd-Elaty I, Negm AM, Sallam GAH (2017) Environmental impact assessment of subsurface drainage projects. In: Negm A (ed) Unconventional water resources and agriculture in Egypt. The handbook of environmental chemistry, vol 75. Springer, Cham. https://doi.org/10.1007/698_2017_123

Abd-Elaty I, Abd-Elhamid HF, Negm AM (2018) Investigation of saltwater intrusion in coastal aquifers. In: Negm A (ed) Groundwater in the Nile Delta. The handbook of environmental chemistry, vol 73. Springer, Cham. https://doi.org/10.1007/698_2017_190

Abd-Elaty I, Zelenakova M, Straface S et al (2019a) Integrated modelling for groundwater contamination from polluted streams using new protection process techniques. Water 11(11). https://doi.org/10.3390/w11112321

Abd-Elaty I, Sallam GA, Straface S et al (2019b) Effects of climate change on the design of subsurface drainage systems in coastal aquifers in arid/semi-arid regions: case study of the Nile delta. Sci Total Environ 672:283–295. https://doi.org/10.1016/j.scitotenv.2019.03.483

Abd-Elaty I, Pugliese L, Zelenakova M et al (2020a) Simulation-based solutions reducing soil and groundwater contamination from fertilizers in arid and semi-arid regions: case study the eastern Nile Delta, Egypt. Int J Environ Res 17(24):9373. https://doi.org/10.3390/ijerph17249373

Abd-Elaty I, Abd-Elhamid HF, Qahman K (2020b) Coastal aquifer protection from saltwater intrusion using abstraction of brackish water and recharge of treated wastewater: case study of the Gaza aquifer. J Hydrol Eng. https://doi.org/10.1061/(ASCE)HE.1943-5584.0001927

Abd-Elaty I, Saleh OK, Ghanayem HM et al (2021a) Assessment of hydrological, geohydraulic and operational conditions at a riverbank filtration site at Embaba, Cairo using flow and transport modeling. J Hydrol Reg Stud. https://doi.org/10.1016/j.ejrh.2021.100900

Abd-Elaty I, Said AM, Abdelaal GM et al (2021b) Assessing the impact of lining polluted streams on groundwater quality: a case study of the eastern Nile Delta aquifer, Egypt. Water 13(12): 1705. https://doi.org/10.3390/w13121705

Abd-Elaty I, Zeleňáková M, Krajníková K et al (2021c) Analytical solution of saltwater intrusion in coastal aquifers considering climate changes and different boundary conditions. Water 13(7): 995. https://doi.org/10.3390/w13070995

Abd-Elaty I, Shahawy AEL, Santoro S et al (2021d) Effects of groundwater abstraction and desalination brine deep injection on a coastal aquifer. Sci Total Environ 148928. https://doi.org/10.1016/j.scitotenv.2021.148928

Abd-Elaty I, Javadi A, Abd-Elhamid H (2021e) Management of saltwater intrusion in coastal aquifers using different wells systems: a case study of the Nile Delta aquifer in Egypt. Hydrogeol J. https://doi.org/10.1007/s10040-021-02344-w

Abd-Elaty I, Straface S, Kuriqi A (2021f) Sustainable saltwater intrusion management in coastal aquifers under climatic changes for humid and hyper-arid regions. Ecol Eng. https://doi.org/10.1016/j.ecoleng.2021.106382

Abd-Elhamid HF (2010) A simulation-optimization model to study the control of seawater intrusion in coastal aquifers. PhD Thesis, University of Exeter, UK

Abd-Elhamid HF, Abd-Elaty I (2017) Application of a new methodology (TRAD) to control seawater intrusion in the Nile Delta aquifer, Egypt solutions to water challenges in MENA region. In: Proceedings of the regional workshop, 25–30 Apr 2017, Cairo, Egypt

Abd-Elhamid HF, Javadi AA (2008) Mathematical models to control saltwater intrusion in coastal aquifer. In: Proceeding of GeoCongress, New Orleans, Louisiana, USA

Abd-Elhamid HF, Javadi AA (2011) A cost-effective method to control seawater intrusion in coastal aquifers. J Water Resour Manag 25:2755–2780. https://doi.org/10.1007/s11269-011-9837-7

Abd-Elhamid HF, Javadi A, Abdelaty I et al (2016) Simulation of seawater intrusion in the Nile Delta aquifer under the conditions of climate change. Hydrol Res 47(6):1198–1210. https://doi.org/10.2166/nh.2016.157

Abd-Elhamid HF, Abd-Elaty I, Negm AM (2018) Control of saltwater intrusion in coastal aquifers. In: Negm A (ed) Groundwater in the Nile Delta. The handbook of environmental chemistry, vol 73. Springer, Cham. https://doi.org/10.1007/698_2017_138

Abd-Elhamid H, Abdelaty I, Sherif M (2019) Evaluation of potential impact of grand Ethiopian renaissance dam on seawater intrusion in the Nile Delta aquifer. Int J Environ Sci Technol 16: 2321–2332. https://doi.org/10.1007/s13762-018-1851-3

Abd-Elhamid HF, Abd-Elaty I, Hussain MS (2020) Mitigation of seawater intrusion in coastal aquifers using coastal earth fill considering future sea level rise. Environ Sci Pollut Res 27: 23234–23245. https://doi.org/10.1007/s11356-020-08891-1

Andreo B, Goldscheider N, Vadillo I et al (2005) Karst groundwater protection: first application of a Pan-European approach to vulnerability, hazard and risk mapping in the Sierra de Líbar (Southern Spain). Sci Total Environ 357(1–3):54–73. https://doi.org/10.1016/j.scitotenv.2005.05.019

Baker AJ, Pepper DW (1991) Finite elements. McGraw-Hill Companies, Inc, New York

Barnett B, Townley LR, Post V et al (2012) Australian groundwater modeling guidelines||. Waterlines report series no. 82. National Water Commission, Canberra

Baxter GP, Wallace CC (1916) Changes in volume upon solution in water of halogen salts of alkali metals: IX. J Am Chem Soc 38:70–104

Bazrkar MH, Adamowski JF, Eslamian S (2017) Water system modelling. In: Furze JN, Swing K, Gupta AK et al (eds) Mathematical advances towards sustainable environmental systems. Springer, Cham. https://doi.org/10.1007/978-3-319-43901-3_4

Bear J (1972) Dynamics of fluids in porous media. American Elsevier Publishing Company, New York

Bear J (1979) Hydraulics of groundwater. McGraw-Hill, New York

Bear J, Cheng AH, Sorek S et al (1999) Seawater intrusion in coastal aquifers, concepts, methods and practices. Kluwer Academic Publisher, Dordrecht. ISBN 0-7923-5573-3

Berardinucci J, Ronneseth K (2002) Guide to using the BC aquifer classification maps for the protection and management of groundwater. British Columbia Ministry of Water, Land and Air

Protection. Electronic Report. Available via Water Stewardship Services. https://www.env.gov.bc.ca/wsd/plan_protect_sustain/groundwater/aquifers/reports/aquifer_maps.pdf. Accessed 15 May 2021

Callander P (2011) New Zealand guidelines for the monitoring and management of sea water intrusion risks on groundwater. Available via Envirolink. https://envirolink.govt.nz/assets/Envirolink/420-NLRC50-Guidelines-for-the-monitoring-and-management-of-sea-water-intrusion-risks-on-groundwater.pdf. Accessed 15 May 2021

Cheng AH-D, Halhal D, Naji A et al (2000) Pumping optimization in saltwater-intruded coastal aquifers. Water Resour Res 36(8):2155–2165. https://doi.org/10.1029/2000WR900149

Cheung YK, Lo SH, Leung AYT (1996) Finite element implementation. Blackwell Science Ltd, Oxford

Dawoud MA, Darwish MM, El-Kady MM (2005) GIS-based groundwater management model for Western Nile Delta. Water Resour Manag 19:1–20. https://doi.org/10.1007/s11269-005-5603-z

Diersch H-JG (1996) Interactive, graphics-based finite-element simulation system FEFLOW for modelling groundwater flow, contaminant mass and heat transport processes. FEFLOW user's manual version 4.50, April 1996. WASY Institute for Water Resources Planning and Systems Research Ltd, Berlin

Dokou Z, Dettoraki M, Karatzas G et al (2016) Utilizing successive linearization optimization to control the saltwater intrusion phenomenon in unconfined coastal aquifers in Crete, Greece. J Environ Model Assess. https://doi.org/10.1007/s10666-016-9529-z

El Didy SM, Darwish MM (2001) Studying the effect of Desalination of Manzala and BurullusLakes on Saltwater Intrusion in the Nile Delta, Water Science, National Water Research Center, Ministry of Water Resources and Irrigation, Egypt

El-Raey M (2010) Impact and implications of climate change for the coastal zones of Egypt. In: Michel D, Pandya A (eds) Coastal zones and climate change. Stimson Center, Washington, DC

EPA (2012) Safe and sustainable water resources strategic research action plan 2012–2016. Available via United States Environmental Protection Agency. https://www.epa.gov/research/safe-and-sustainable-water-resources-strategic-research-action-plan-2012-2016. Accessed 16 May 2021

Fetter CW (2001) Applied hydrogeology, 4th edn. Prentice Hall, New Jersey

Flint RW, Houser WL (2001) Living a sustainable lifestyle for our children's children. iUniverse, Campbell

Freeze RA, Cherry JA (1979) Groundwater. Prentice-Hall, Englewood Cliffs

Gleick PH (1996) Basic water requirements for human activities: meeting basic needs. Water Int 21:83–92. https://doi.org/10.1080/02508069608686494

Guo W, Bennett GD (1998) Simulation of saline/fresh water flows using MODFLOW. In: Poeter EP, Zheng C, Hill MC (eds) Proceedings of the MODFLOW '98 conference. Colorado School of Mines, Golden

Guo W, Langevin CD (2002) User's guide to SEAWAT: a computer program for simulation of three-dimensional variable-density ground-water flow. United States Geological Survey Techniques of Water-Resources Investigations 6-A7, Tallahassee

Harman C (2002) The effect of basement on heterogeneity on saltwater wedge- a physical and numerical modelling approach. The University of Western Australia, Crawley

Heath RC (1983) Basic ground-water hydrology. United States Geological Survey, Alexandria

Hong S, Park N, Bhopanam N et al (2004) Verification of optimal model of coastal pumping with sand-tank experiment. In: Proceeding of the 18th Salt Water Intrusion Meeting, Cartagena (Spain) 31 May – 3 June 2004

Hunt RJ, Anderson MP, Kelson VA (1998) Improving a complex finite difference groundwater flow model through the use of an analytic element screening model. Groundwater 36(6):1011–1017

IPCC (1996) Climate change 1995: the science of climate change. Contribution of Working Group I to the second assessment report of the Intergovernmental Panel on Climate Change. Cambridge University Press, Cambridge/New York

IPCC (2001) Climate change 2001: impacts, adaptations, and vulnerability contribution of Working Group II to the third assessment report of the Intergovernmental Panel on Climate Change. Cambridge University Press, Cambridge/New York

IPCC (2007) An Assessment of the intergovernmental panel on climate change, Adopted section by section at IPCC Plenary XXVII (Valencia, Spain, 12–17 November 2007), represents the formally agreed statement of the IPCC concerning key findings and uncertainties contained in the Working Group contributions to the Fourth Assessment Report

Istok JD (1989) Groundwater modelling by the finite element. American Geophysical Union, Washington, DC

Javadi AA, Hussain M, Sherif M (2013) Optimal control of seawater intrusion in coastal aquifers. In: International conference on computational mechanics (CM13), Durham, UK, 25–27 Mar 2013

Javadi AA, Hussain M, Sherif M et al (2015) Multi-objective optimization of different management scenarios to control seawater intrusion in coastal aquifers. Water Resour Manag, Springer; European Water Resources Association (EWRA) 29:1843–1857

Jones JAA (2011) Water sustainability – a global perspective. Oxford University Press, New York

Kumar CP (2002) Groundwater flow models. National Institute of Hydrology, Roorkee – 247667 (Uttaranchal)

Logan DL (2002) Finite element method, 3rd edn. Brooks, Cole, Pacific Grove

McDonald MG, Harbaugh AW (1984) A modular three-dimensional finite-difference ground-water flow model. United States Geological Survey. https://doi.org/10.3133/ofr83875

Mohamed MA (2004) Seawater level variation and its estimation along the Northern Egyptian coasts using artificial neural network model. PhD Thesis, Alexandria University, Egypt

Molle F, Gaafar I, El-Agha DE et al (2016) Irrigation efficiency and the Nile Delta water balance, water and salt management in the Nile Delta: report no.9. International Water Management Institute and Australian Center for International Agriculture Research

Mukhopadhyay A, Saha D, Saha AK (1994) Development of a groundwater-management model using the d-base facility. Comput Geosci 20(7–8):1065–1102. https://doi.org/10.1016/0098-3004(94)90064-7

Nakicenovic N, Alcamo J, Davis G et al (2000) Special report on emissions scenarios a special report of Working Group III of the Intergovernmental Panel on Climate Change. Cambridge University Press, Cambridge

Narayan D (2002) Empowerment and poverty reduction: a sourcebook. World Bank, Washington

Narayan KA, Schleeberger C, Charlesworth PB et al (2003) Effects of Groundwater Pumping on Saltwater Intrusion in the Lower Burdekin Delta, North Queensland. In Post, DA (ed.) MODSIM 2003 International Congress on Modelling and Simulation. Volume 2, pp 212-217. Modelling and Simulation Society of Australia and New Zealand, July 2003 at http://www.mssanz.org.au/modsim03/Media/Articles/Vol%201%20Articles/224-229. pdf accessed 9 March 2010

Negm AM, Sakr S, Abd-Elaty I et al (2018) An overview of groundwater resources in Nile Delta aquifer. In: Negm A (ed) Groundwater in the Nile Delta. The handbook of environmental chemistry, vol 73. Springer, Cham. https://doi.org/10.1007/698_2017_193

NGCLC (2001) National Groundwater and Contaminated Land Centre. Guide to good practice for the development of conceptual models and the selection and application of mathematical models of contaminant transport processes in the subsurface. NGCLC report NC/99/38/2

Nofal ER, Amer MA, El-Didy SM et al (2015) Sea water intrusion in Nile Delta in perspective of new configuration of the aquifer heterogeneity using the recent stratigraphy data. J Am Sci 11(6):281–292

Ogata A (1970) Theory of dispersion in a granular medium. Available via United States Geological Survey. https://pubs.usgs.gov/pp/0411i/report.pdf. Accessed 15 May 2021

Park N, Kim S, Shi L et al (2008) Field validation of simulation optimization model for protecting excessive pumping wells. In: Proceedings of 20th SWIM, Naples, Florida, USA

Qahman K, Larabi A, Ouazar D et al (2005) Optimal and sustainable extraction of groundwater in coastal aquifers. Stoch Environ Res Risk Assess 19:99–110. https://doi.org/10.1007/s00477-004-0218-0

Rausch R (2010) Groundwater modeling, an introduction to groundwater flow and solute transport modeling with application. Technische Universidad Darmstadt, Berlin

Reichard EG, Johnson TA (2005) Assessment of regional management strategies for controlling seawater intrusion. J Water Resour Plan Manag 131(4):280–291. https://doi.org/10.1061/(ASCE)0733-9496(2005)131:4(280)

Sefelnasr A, Sherif M (2014) Impacts of seawater rise on seawater intrusion in the Nile Delta aquifer, Egypt. Groundwater 52:264–276. https://doi.org/10.1111/gwat.12058

Sherif MM, Al-Rashed MF (2001) Vertical and horizontal simulation of seawater intrusion in the Nile Delta aquifer. In: Proceedings of the 1st international conference and workshop on saltwater intrusion and coastal aquifers, monitoring, modelling, and management (Morocco), 23–25 April 2001

Simlandy S (2015) Importance of groundwater as compatible with environment. Int J Ecosyst 5:89–92. https://doi.org/10.5923/c.ije.201501.13

SNC (2010) Egypt's second national communication, Egyptian environmental affairs agency (EEAA-May 2010), under the United Nations framework convention on climate change. Available via United Nations Framework Convention on Climate Change. https://unfccc.int/resource/docs/natc/egync2.pdf. Accessed 16 May 2021

Theis CV (1935) The relationship between lowering of the piezometric surface and the rate and duration of discharge of a well using groundwater storage. Trans Am Geophys Union 2:519–524. https://doi.org/10.1029/TR016i002p00519

Todd DK (1980) Groundwater hydrology, 2nd edn. John Wiley & Sons, New York

Treut HL, Somerville R, Cubasch U et al (2007) Historical overview of climate change science. In: Solomon S, Qin D, Manning M et al (eds) Climate change 2007: the physical science basis. Contribution of Working Group I to the fourth assessment report of the Intergovernmental Panel on Climate Change. Cambridge University Press, UK/New York, pp 104–105

Vandenbohede A (2003) Solute transport in heterogeneous aquifers parameter identification and its use in groundwater pollution and saltwater intrusion problems. Faculty Wetenschappen, Vakgroep Geology en Bodemkunde, University Gent, Ghent

Vandenbohede A, Luyten K, Lebbe L (2006) Effects of global change on heterogeneous coastal aquifers: a case study in Belgium. J Coast Res 24:160–170. https://doi.org/10.2112/05-0447.1

Voss CI (1984) A finite-element simulation model for saturated-unsaturated, fluid-density-dependent groundwater flow with energy transport or chemically-reactive single-species solute rransport. United States Geological Survey Water-Resources Investigation Report 84-4369

Wels C (2012) Guidelines for groundwater modelling to assess impacts of proposed natural resource development activities. Report No. 194001. Ministry of Environment, British Columbia

Zheng C, Bennett GD (2002) Applied contaminant transport modeling, 2nd edn. Wiley-Interscience, New York

Zheng C, Wang PP (1999) MT3DMS, A modular three-dimensional multi species transport model for simulation of advection, dispersion and chemical reactions of contaminants in groundwater systems: documentation and user's guide. U.S. Army Engineer Research and Development Center Contract Report SERDP-99-1, Vicksburg, MS. 202

Chapter 4
Multicriteria Decision-Making for Risks of Natural Disaster in Social Project Assessments

Claudio Garuti, Alicia Cerda, and Carolina Cabezas

Abstract This chapter presents a global index for risk disaster assessment in public infrastructure projects using the multicriteria method of analytic hierarchy process (AHP). The index gives a numerical account of the level of disaster risk associated with public investment projects in the territory and thus determines whether the project requires additional attention or investment associated with the mitigation of risk. Further, we provide representative natural hazards that impact a project's location, vulnerability, and resilience capacity and metrically combine a simple and easy implementation approach. From these conditions, we generate a global index of natural disaster risk level for different hazards, in association with a tolerable risk threshold, to be used as a tolerance reference limit for decision-making. The global risk indicator is designated IRDA (hazard disaster risk index), and the tolerable risk limit is designated URT (tolerable risk threshold). This work is the continuation and culmination of several institutions led by the Chilean Ministry of Social Development (MIDESO) with the United Nations (CEPAL) to incorporate the natural disaster risk variable in the social evaluation of public investment projects. It considers different natural hazards that a project may face for a given location including those occurring in the case of fire, tsunami, mass removal, and volcanoes.

Keywords AHP · Measurement rule · Cardinal rating scale · Multicriteria evaluation matrix · Theoretical and empirical threshold calculation · Compatibility index G · Natural disaster risk assessment

C. Garuti (✉)
Fulcrum Engineering, University of Chile, Santiago, Chile
e-mail: claudiogaruti@fulcrum.cl

A. Cerda
Department of Pre-inversion, Ministry of Health, Santiago, Chile
e-mail: altcerda@gmail.com

C. Cabezas
Department of Physical Resources, Health Service of Talcahuano, Talcahuano, Chile
e-mail: carolina.aja@gmail.com

J. N. Furze et al. (eds.), *Earth Systems Protection and Sustainability*,
https://doi.org/10.1007/978-3-030-98584-4_4

4.1 Introduction

Levels of global risk given specific hazards can be obtained in terms of the exposure (vulnerability) of the project as a result of its specific location in the territory (territory variables), further given the fragility (among other variables) due to the criticality of the type of project in the territory (project variables). Further, the capacity or resilience obtained by the physical characteristics of projects (project variables) and the capacities existing in the territory directly associated with the project (territory variables) are considered. The overall or final risk is a combination of physical hazards, vulnerability (increased risk by exposure and fragility of the project in the territory), its resilience (risk reduction elements or capabilities) that the project presents and possible capacities of the territory related to the project (Cutter et al. 2008; NIDM and GIZ 2013).

Global risk indicators require consideration of a range of ills which have both additive and subtractive effects on the final risk value; the selection of an inappropriate index leads to misuse of resources in governance and development (Visser et al. 2020). The global risk indicator defined as IRDA (hazard disaster risk index) combines a series of variables (criteria) that can be positive (risk-decreasing variables associated with resilience or capacities), or negative (risk-increasing variables associated with vulnerability). The variables contribute with different importance levels (weights) within the structure or assessment model that represents the risk measurement rule (Garuti 2007, 2014a). The IRDA represents the project's risk value due to each existing hazard within a territory. The model or measurement rule reflects a comprehensive knowledge of the different participants included in the natural disaster risk analysis (Bach et al. 2013). The analytic hierarchy process (AHP) method provides an index for consistency of the knowledge and a compatibility or proximity index between the relative positions of the different participants, and with respect to a consensual response (Garuti 2016). The latter represents the variability of responses due to different individual perceptions; these are pertinent in the development of all public projects with variable geographic settings (Saaty et al. 1982; Saaty et al. 1991; Alkhalidi et al. 2019).

Once the IRDA is assessed and interpreted, qualifiers must know whether the value obtained is good, acceptable, or bad. This implies being able to build thresholds of acceptability/non-acceptability and eventually complementary degrees.

A tolerable risk threshold (URT) is derived, to give a reference value with respect to a project's IRDA for comparison and qualification. The index range value is always between 0 and 1. For instance, if an IRDA of 0.35 is obtained, how should it be read? For the final user, it should be clear if the value implies that the project's natural disaster risk qualifies as high (unacceptable), moderate (acceptable but still important), or low (no need for action). Thus, if the threshold (URT) is less than 0.35, then the project is classified as of high risk (non-acceptable risk); otherwise, it is a tolerable risk project.

Risk comparison hierarchical assessment is shown in Fig. 4.1.

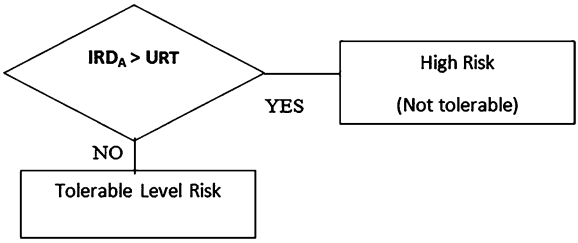

Fig. 4.1 Risk comparison

Index values are cardinal numbers (numerically significant), so is possible to classify a project's behavior. For instance, if we have a value of URT = 0.350, a project with an index value IRDA = 0.356 is very different from a project with an index value of IRDA = 0.750. Although both projects are classified as of high disaster risk level, as both indices exceed the URT, they are clearly not equivalent, especially if the risk is viewed in the long term. In the case that IRDA < URT, then the project does not require additional investment to prevent risk.

In consideration of application of the global risk index, it should be noted that we are working with priorities (with range between 0 and 1), under an absolute ratio scale (capable of integrating multiple variables of different nature), and as such, we are able to operate in weighted environments.

The determination of the maximum tolerable risk corresponds to the concept of threshold, and its calculation results from the application of the same characteristics exposed in the previous paragraph.

All the weights of the criteria within each model were obtained prior to the study, by limiting each pair-comparison matrix to its equilibrium point; eigenvector systematic operator (Garuti 2016). This process was performed through the collaboration of different expert groups and empirically tested over several projects in the Chilean context.

The objectives of this study are to show (i) the build of a metric for the estimation of natural risk (IRDA) to which a public investment project would be exposed as a function of its hazards, vulnerability, and resilience given its location and project characteristics, and (ii) the determination of the maximum URT and different levels of risk for different types of infrastructure (projects) and for each hazard, in the cardinal terms of an absolute ratio scale.

4.2 The Solution Approach Used to Solve Risk Assessment Factors

Bearing in mind the requirement for a metric estimating complex characteristics of risk and public investment, it is necessary to follow a stepwise solution approach (Garuti and Escudey 2005; Garuti and Spencer 2020). The main steps for natural disaster risk assessment problems, in the Chilean case, are:

- To determine whether the investment project is located in a natural hazardous area. This first step is performed through maps of the National Emergency Office of the Ministry of the Interior and Public Security, Government of Chile (ONEMI), viewer software, and/or specific ONEMI questionnaires and provides an initial filter to define if the project should apply to the IRDA natural disaster risk assessment.
- To assess the project's risk level, if located in a hazardous zone. To do this, the methodology proposes to estimate the risk level through hazard exposure, vulnerability, and resilience (or responsiveness) capacity.
- Identify and evaluate alternative risk reduction measures. In this regard, the methodology suggests to compare the project's disaster risk level with a defined maximum tolerable threshold and include risk management measures that allow effective reduction of the risk level to an acceptable one (ONEMI 2016, 2017).

4.3 Construction Scheme for IRDA (Hazard Disaster Risk Index)

The model for estimating the proposed IRDA includes risk element exposure to the hazard (hazard degree), vulnerability, and capacity or resilience. In other words, we seek to define the risk in functional terms as in Eq. (4.1):

$$\text{Risk} = f(\text{H}, \text{V}, \text{Re}) \tag{4.1}$$

where risk is equal to the function of hazards (H), vulnerability (V), and resilience (Re).

It should be considered that hazard and vulnerability are variables that are opposed to resilience (Borg et al. 2014). Therefore, models showing Poisson or other distributions are required for assessment, which can then be used to reflect the proportionate (degree) of the unit of measure.

The hazard risk model must have a functional type or scheme linking commonly distributed (positive and negative) indicators as follows:

$$\text{AR} = f(\text{exposure of the territory given the project},\ \text{fragility of the project given the territory}) \tag{4.2}$$

$$\text{DR} = f(\text{capacity of the project given the territory},\ \text{capacity of the territory given the project}) \tag{4.3}$$

where AR is augmented risk function with a range of 0–1 and DR is decreased risk function with a range of 0–1.

A possible measurable function between AR and DR is therefore:

$$\text{IRDA} = \text{AR}^{*}(1 - \text{DR}) \quad \text{Function range} : 0 - 1 \tag{4.4}$$

where IRDA is hazard disaster risk index.

It is important to validate that the proposed function meets the basic conditions via expert-based fact checking.

The IRDA must belong to the range 0–1.

The following conditions hold true:

If AR increases, the final risk level (IRDA) increases.
If DR increases, the final risk level (IRDA) decreases.

Therefore:

If AR is maximum (1) and DR minimum (0), then IRDA = 1 (maximum risk).
If AR is minimum (0) and DR maximum (1), then IRDA = 0 (zero risk).
If AR is minimum (0) and DR minimum (0), then IRDA = 0 (zero risk).

Any combination of variables should respect the three basic properties of commensurability (in order to make them comparable in measure); direction (in order to respect the system's behavior), and context (in order to respect the problem's boundary conditions).

Correspondingly the measurement scales and thresholds must align with the functions and their combinations. This leads us to the objective of constructing measurement scales and cardinal qualification thresholds.

4.4 Hazards, Vulnerability, and Resilience Models and Their Combination

Based on interactive work done in conjunction with different Chilean institutions (public and private), the following risk models or hierarchical structures were obtained for the assessment of public projects: mass removal flow, tsunami, volcanoes, and fire. These were assessed in terms of vulnerability and resilience in order to expediate/assess public projects (Bach et al. 2013; Wilson et al. 2014) and are discussed in the following subsections.

4.4.1 Mass Removal (Flows)

Mass removal or movement may be structural/geotechnical or involving any high-quantity flow (Pudasaini and Mergili 2019). There are two different but complementary models (Fig. 4.2). Each generation acts as a set within the flow producing a separate hazard; further there is an additional hazard per closeness or concentration

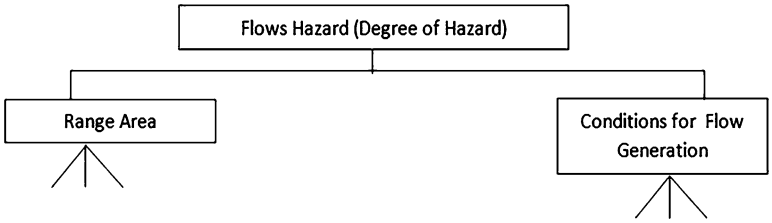

Fig. 4.2 Mass flow hazard scheme

of flow. This hazard is constantly received. The components of Fig. 4.2 act separately, with their own hazard thresholds and values.

Although Fig. 4.2 shows one hierarchy model, as can be seen there are two component models: range area and conditions for flow generation. Both affect the flow hazard in different ways and are evaluated independently (avoiding possible compensation); each has its own assessment and thresholds, criteria and sub-criteria (in certain cases sub-sub-criteria), and, beneath the terminal criteria, the evaluation scales (absolute ratio scales), entailing two separate rating models acting jointly (Saaty and Peniwati 2013).

As mentioned in the introduction section, the models are simple and direct for application. They are composed of two levels and three measurement indicators, plus the measurement scales themselves. However, this "simplicity" does not equate major errors for three main reasons:

- The general problem of disaster risk has been decomposed into several minor problems, and even minor problems (risk of flow hazard) have been decomposed again into two separate sub-problems that act together complementarily.
- The variables considered are the ones that have the greatest impact on the flow hazard; variables of lesser impact are left out.
- Several calibration tests have been performed with each sub-model to train the accuracy of their outcomes; it has been noted that they are sufficiently complex and realistic.

Each flow model is specifically concerned with one of the two relevant elements of flow hazards, that is, conditions for flow generation and the range area. Presenting a hazard value and an acceptance threshold for each independently, means a high area range risk is not compensated with a low generation risk or vice versa.

4.4.2 Tsunami

The tsunami model is a "mono-criterion" model defined as "flood depth." Therefore, only one specific scale of measurement was built to make it commensurable.

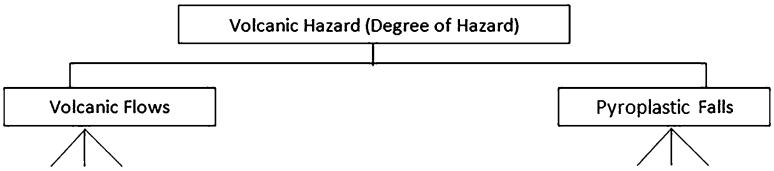

Fig. 4.3 Volcanic hazard

4.4.3 Volcano

For volcanoes, SERNAGEOMIN staff (Service of Geology and Mining) plus the support of the SERNAGEOMIN staff organization were deeply involved in modelling and defining measurement scales. Also, their existing volcanic risk maps were used to confirm project location exposure. A volcanic hazard assessment tree is shown in Fig. 4.3.

The main criteria have sub-criteria (in some case sub-sub-criteria) and beneath them terminal criteria and evaluation or rating scales (absolute ratio scales).

4.4.4 Fire

Due to the strong interrelationship between the variables in this model and their geographic vegetal character, a multiplicative territorial model (based on territorial cells) was built, whose algebraic expression is as follows:

$$\text{Hazard of Fire} = \sum\nolimits_i \{M_i{}^*(1 - D_i{}^*\text{Cos}(x_i))\} i = 1, \ldots n^\circ\text{cells} \qquad (4.5)$$

where

- M_i = Fuel mass of cell "i" (includes the cell mass flammability degree), range 0–1
- D_i = Distance from the project's nearest edge to the cell, range 0–1
- Cos (x_i) = Cosine function of the average slope between the project and the cell measured in degrees, range 0–90°

For each of the four hazard models, tolerable thresholds were calculated, both theoretically and empirically. Both calculated outcomes were compared using the compatibility function G, when the compatibility level was seen to be high enough (above 85% of compatibility between theoretical and empirical outcomes). The theoretical threshold value is considered acceptable to be used in the applicable hazard models.

All hazard models were tested with the hazard experts on known cases, and their results for both the hazard values and their comparison with the respective thresholds (classification of the value obtained) were very satisfactory.

4.4.5 Vulnerability Model

Although, there is one specific vulnerability model for each risk, there is also a general model (a control hierarchy) that combines the four vulnerability models of risk in only one measure. This vulnerability index is composed of physical vulnerability, functional vulnerability and characterists of the population as shown in Fig. 4.4.

As with the previous hierarchical models, the main criteria have layered sub-criteria (in some case sub-sub-criteria) and beneath them terminal criteria and evaluation or rating scales (absolute ratio scales).

4.4.6 Resilience Model

There is a specific resilience model for each hazard, There is also a general model (control hierarchy) that combine the 4 resilience models for resilience, composed by 3 strategic criteria: physical capacity of facilities, redundancies of the service and capacity of services, with a high level of hierarchical structure only is:

The same layered structure of Figs. 4.2, 4.3, and 4.4 is repeated in Fig. 4.5. The main criteria have sub-criteria (in some cases sub-sub-criteria) and beneath them the terminal criteria and the evaluation or rating scales (absolute ratio scales).

Having shown the evaluation models (hazards (H), vulnerability (V), and resilience (Re_i)), the risk formula is calculated as:

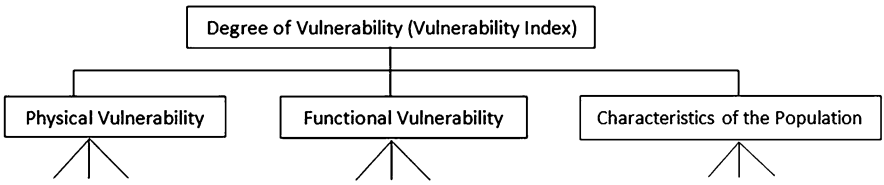

Fig. 4.4 General model for vulnerability

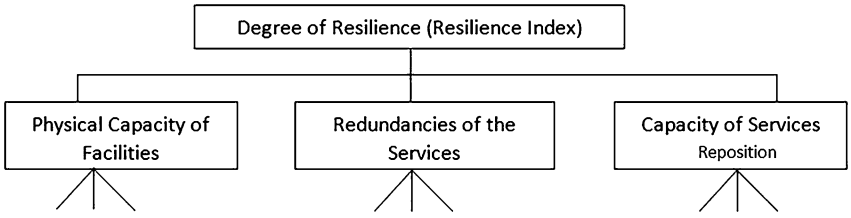

Fig. 4.5 General model for resilience

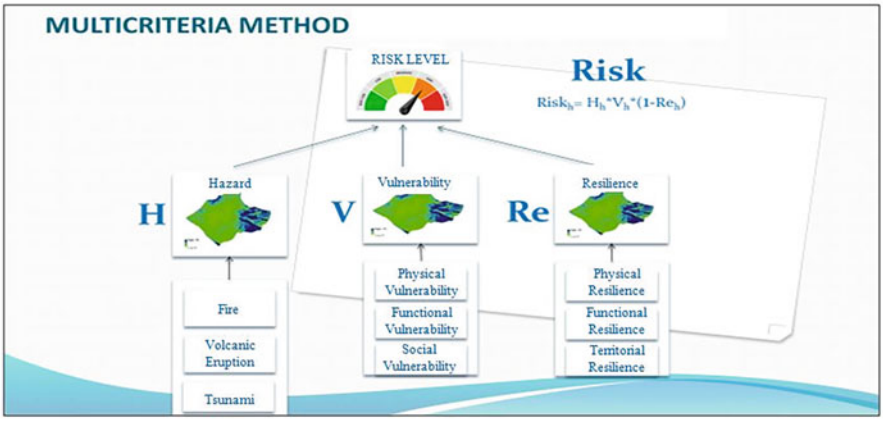

Fig. 4.6 Multicriteria method modelling general scheme. (MIDESO 2017)

$$\text{Risk}_{(i)} = H_i V_i (1 - \text{Re}_i) \quad i = 1, \ldots, 4 \tag{4.6}$$

Figure 4.6 shows the multicriteria scheme devised by MIDESO (2017). Formula (4.6) consolidates the values of different models and gives the global risk value. Finally, the risk level is quintile partitioned (very low, low, moderate, high, and very high), which results from comparing the global risk value obtained for the analyzed project with the global threshold value for each hazard. Details of this are shown in Fig. 4.7. In the next section, the process of model consolidation is described detailing the advantage of this formula over the classic forms of hazard risk assessment.

4.5 Model Consolidation Process (Hazard, Vulnerability, and Resilience)

Once the three main elements (H, V, and Re) associated with natural disaster risks are well defined (structured and weighted), they should be integrated into one mathematical expression (Garuti 2014b).

Expanding the general expression, Eq. (4.1) to the interrelation of project and territory, the expression takes the following form:

$$\text{TR}_i = \alpha_{p/t}\{A_i{}^* V_i(p) * (1 - C_i(p))\} + \alpha_{t/p}\{A_i{}^* V_i(t) * (1 - C_i(t))\} \quad \text{Range} : 0 - 1 \tag{4.7}$$

where:

TR_i = Total risk of hazard "i," given by the risk of the project due to the territory plus risk of the territory due to the project

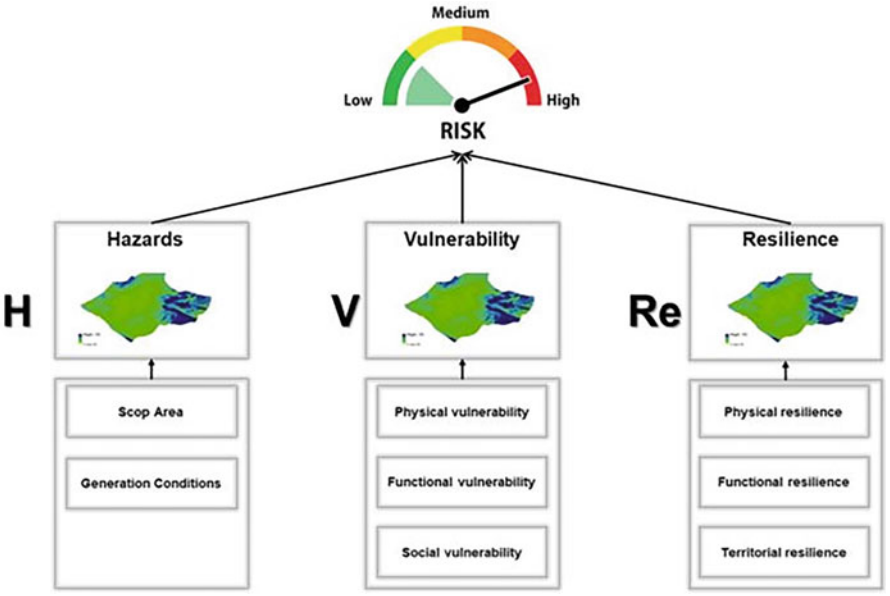

Fig. 4.7 The global risk scheme. (MIDESO 2017)

$\alpha_{p/t}$, $\alpha_{t/p}$ = Risk weights of the project given the territory and territory given the project. They represent the project importance given the territory and territory importance given the project respectively. With $\alpha_{p/t} + \alpha_{t/p} = 1$.

A_i = Different hazards considered, fire, tsunami, mass removal, and volcanoes; $i = 1,\ldots,4$

$V_i(p)$ and $V_i(t)$ = Project vulnerability given the territory and territory vulnerability given the project, for the "i^{th}" hazard.

$C_i(p)$ and $C_i(t)$ = Project capacity (or resilience) given the territory and territory capacity given the project for the "i^{th}" hazard.

Equation (4.7) integrates all parameters involved in the previous hazard, vulnerability, and resilience evaluation models. It should also be noted that for this study, only the first part of the Eq. (4.7) (the TR expression) applies. That is, TR assessment will only be done for the part related to the project due to the territory (and not the territory due to the project). Therefore, we adjust to:

$$\mathrm{RT}_i = A_i{}^{*} V_i(p) * (1 - C_i(p)) \left(\alpha_{p/t} = 1;\ \ \alpha_{t/p} = 0\right) \tag{4.8}$$

Note: If the reader wishes to perform global management risks of the land, he or she has to consider both parts of the risk equation (4.7).

Once the hazard parameters (A_i), vulnerability (V_i), and resilience (C_i) are determined, they are entered in the previous formula (4.8), and the project's risk level (R_i) is obtained for every hazard (A_i).

It is interesting to note that the global threshold of the risk integration model respects the thresholds of models (A_i and V_i). For instance, for a project that exceeds both limits (the thresholds for A_i and V_i) and assuming a lower resilience (C_i), then the formula will return a value for TR_i that will exceed the acceptable limit risk, since if $A_i > UA_i$ and $V_i > UV_i$, its multiplication ($A_i{*}V_i$) will also be greater than ($UA_i{*}UV_i$), obtaining an unacceptable risk value. However, if $A_i < UA_i$ and $V_i < Uv_i$, multiplication ($A_i{*}V_i$) will result in the global risk value returned by the TR formula being below the unacceptable threshold.

Finally, in the cases where only one of the two values (A_i, V_i) exceeds the threshold, then the total risk value with respect to its threshold will depend on the combination of the specific values of A (hazard), V (vulnerability), and C (capacity or resilience).

4.6 Case Study: Risk Disaster of the Hospital in the Locality of Tomé, South of Chile

The risk disaster analysis of Tomé Hospital in Chile follows. The study was carried out to show the vulnerability of the health infrastructure.

4.6.1 Conceptual Framework

The following analysis was developed in the context of the application of the Complementary Methodology for Risk Management and Disasters of Public Infrastructure Projects, validated in March 2017.

The political objective was to comply with the National Strategy for hazard risk assessment (MINVU 2016; MIDESO 2017); this political objective depends on the Ministry of Social Development (MIDESO) in association with the National Emergency Office of the Ministry of the Interior and Public Security (ONEMI), the Ministry of Housing and Urban Development (MINVU), the Ministry of Public Works (MOP), and the Research Center for Integrated Disaster Risk Management, Chile.

The technical main objectives of this complementary methodology are to safeguard the population and public investment, generating and implementing specific mitigation measures in each project, as consequence of what was learnt after the earthquake of February 27, 2010.

Following the objectives set by the government, the application consists of a multicriteria analysis (AHP) of the hazards, vulnerabilities, and resilience or capacities according to the following stages:

Step 1. Answer the questionnaire to determine the existence of the hazards
Identify one of the possible hazards. Given it confirms that the hazard exists, then it must be identified in the study area (ONEMI 2018) the functional unit and the site surface (geographically and socially).

Step 2. Risk assessment
Determine the level of exposure to the hazard, that is, the risk, and analyze the impact in terms of the vulnerability (V scheme) and resilience (Re scheme) of the project according to the structure of Figs. 4.7, 4.8, 4.9, and 4.10.

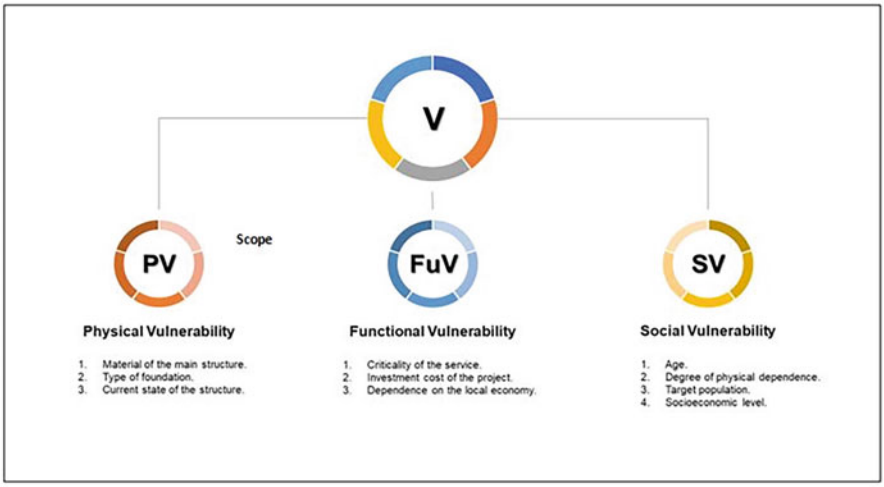

Fig. 4.8 Vulnerability model. (MIDESO 2017)

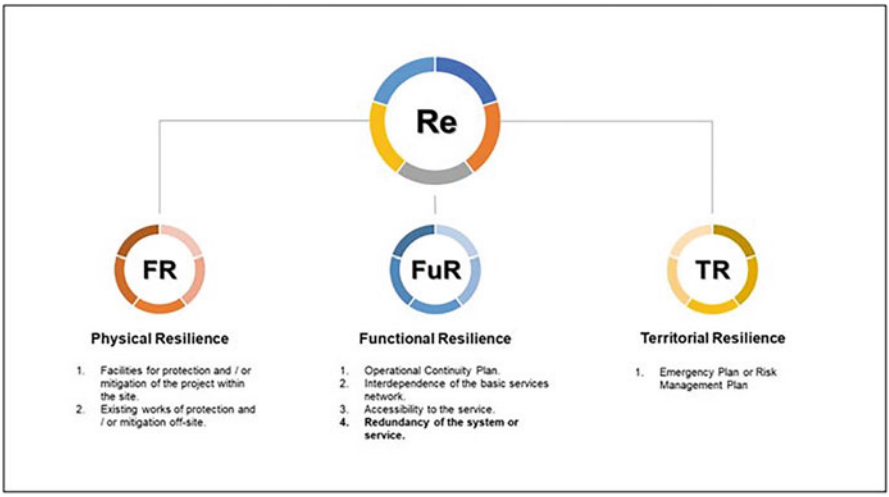

Fig. 4.9 Resilience model. (MIDESO 2017)

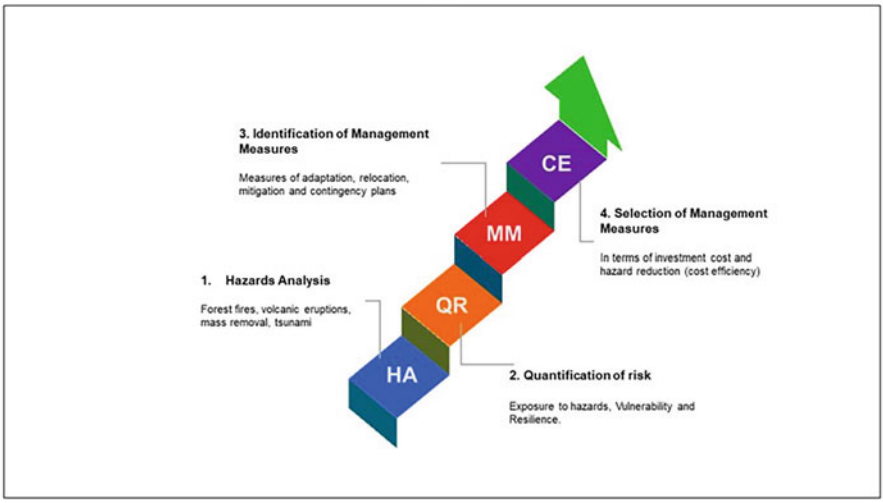

Fig. 4.10 Quantification and qualification of natural risk disaster. (MIDESO 2017)

Step 3. Identification of mitigation measures
According to the degree of criticality of the service, the vulnerability has a maximum threshold, if the calculation exceeds this threshold; it is not possible to continue delivering the service.

Step 4. Selection of management measures
These are defined in response to the results obtained from the quantification of risk (Step 2) with the objective of diminishing the impact of risks.

In summary the steps to follow of the methodology go from a general analysis to the particular in each project.

The final result of the analysis is explained in detail, in a locality in southern Chile.

4.6.2 Application of the Complementary Methodology of Risk Management

The case under study corresponds to a health facility of the health network of the Talcahuano Health Service, in the town of Tomé (Chile). The project is part of the Government Plan (2018–2022) and is currently in the pre-investment phase since 2018 (MINSAL 2018) details are seen in (Fig. 4.11 and Table 4.1).

Fig. 4.11 Geographic location of the city of Tomé in Chile

Table 4.1 Technical record of the health establishment

Name of the establishment	Hospital of Tomé
Complexity of the establishment	High
Country	Chile
Region	Biobío
Province	Concepción
Commune	Tomé
City	Tomé
Address	Mariano Egaña N°1640
No. of inhabitants serving	52524
Land surface	10.000 m^2
Built surface	8000 m^2
Number of beds	116
Number of consultations per year	9.177
Constructive history	1851 starts of its operation
	1939 temporary hospital is built (earthquake)
	1995 the current health establishment is inaugurated
Type of construction	Reinforced concrete
Number of officials *	420
Responsible administrator	Talcahuano Health Service

Step 1. Answering the questionnaire to determine the existence of the hazards (Table 4.2)

According to the geographical conditions and particular historical data, the survey showed that the health establishment is exposed to three dangers: tsunami flood, mass removal by flows, and forest fires. According to methodology, we identified the functional unit (FU) in which the Tomé Hospital is located. We excluded volcanic eruption as it does not exist in the functional unit.

Table 4.2 Questionnaire

1. Hazard	Yes/no	Which?
1.1 General		
(a) Is there a history of swells; heavy rains; floods; landslides; floods; forest fires; the existence of geologically active or potentially active faults; the process of subsidence or liquefaction; poor quality or soil instability due to natural conditions such as cliffs, sands, swamps, Magellanic swamps, and others of similar nature; waterlogging by groundwater; deteriorated land, by extinct human activities; or other danger that exposes the functional unit to disaster risk?	Yes	Saturday, 23 April 2016. Flood in the city of Tomé Collapse 4 March 2010 of Cerro Navidad (post 27F)
1.2 Hydrometeorological hazard		
(a) Is there sedimentation in streams or rivers that could be a danger to the functional unit?	Yes	
(b) Does the functional unit interfere with the flood plain of a riverbed?	Yes	
(c) Has the functional unit been affected by tsunami in the past?	No	
(d) Is the functional unit in an area near or close to slopes that can increase the risk?	Yes	Cerro Estanque
(e) Is there any terrain near or close to the functional unit with erosion process and that can enhance the risk?	No	
(f) Are there drainage problems in areas near or near the functional unit that can enhance the risk?	Yes	River Collén flows into the sea through the city of Tomé
1.3. Forest fire		
(a) Is there abundant plant cover in the functional unit that could expose it to fire risk?	Yes	
1.4 Others		
(a) Is it possible in view of climate change that a hazard situation occurs during the useful life of the project?	No	
(b) Is the project within the danger zone of lava flows/lahars, pyroclastic flows, and/or pyroclastic falls?	No	
(c) Is the volcano active?	No	

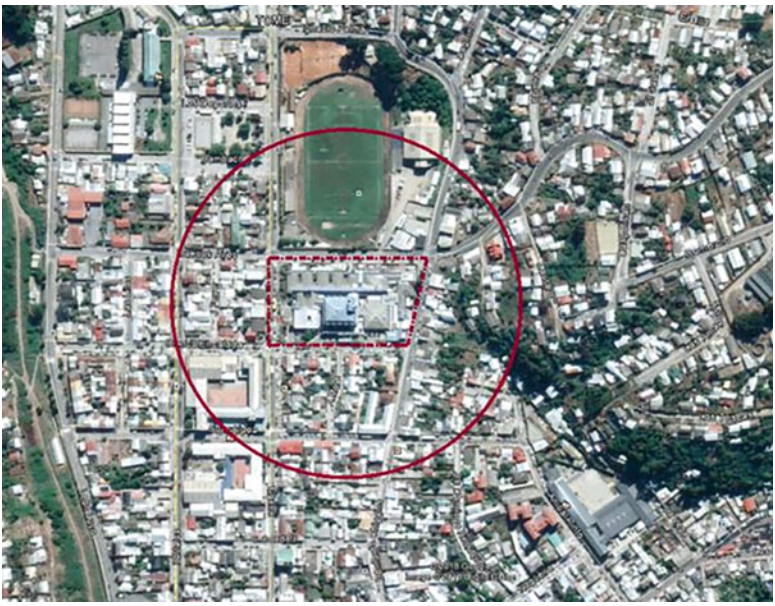

Fig. 4.12 Functional unit of Tomé Hospital

4.6.3 Functional Unit (FU)

The FU is located in the center of Tomé. It has a land area of 10.700 m^2 (red circle in Fig. 4.12).

Step 2. Hazard analysis and evaluation
After the earthquake off the coast of south-central Chile on the 27th February, 2010 (27F) and subsequent tsunami in the region, ONEMI redefined the levels of safe evacuation, delimiting the area affected by flood to level 20. The CITSU flood chart of the Hydrographic and Oceanographic Service of the Navy (SHOA) of the study area indicates that the establishment is in an area without risk.

Fig. 4.13 identifies the zone of tsunami flooding in red, covering flat areas of the coast of the commune; in this case the Hospital de Tomé is located at level 14, non-flood zone. Figure 4.14 shows the risk index score calculation.

4.6.4 Forest Fire Hazard

The hospital establishment is located in an area of medium risk, with respect to the average number of forest fires that occurred in the commune.

Fig. 4.13 Affected area. Chile's "Visor"

Fig. 4.14 Risk index score calculation

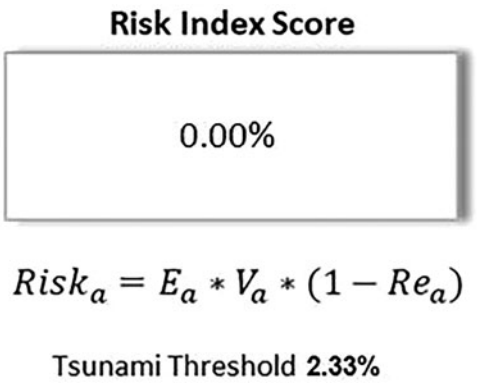

Figure 4.15 uses a red circle to show the functional unit.
Forest fire hazard map:

Red (high) = More than ten fires
Yellow (average) = Five to ten fires
Green (low) = One to four fires

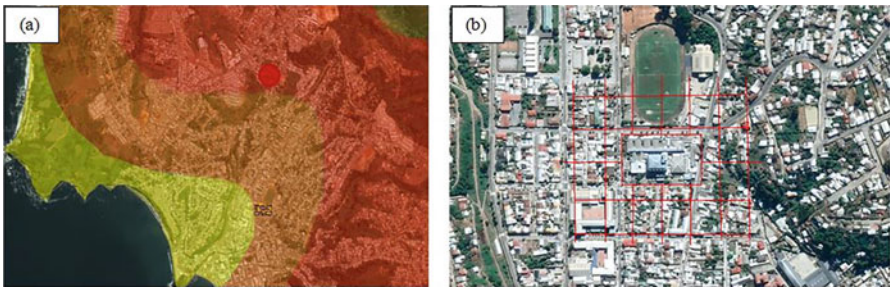

Fig. 4.15 Forest fire hazard map (**a**) and the surrounding mesh of Tomé Hospital (**b**). (Source: Visor Chile sw Prepared by ONEMI)

Fig. 4.16 Identification cells according to the methodology

	A	B	C	D	E	F	G	H	I	J
1										
2										
3		IE	SC	IR	IR	SC	IE			
4		SC	VE	VD	VD	VE	SC			
5		IR	VD	P	P	VD	IR			
6		IR	VD	P	P	VD	IR			
7		SC	VE	VD	VD	VE	SC			
8		IE	SC	IR	IR	SC	IE			
9										
10										

In Figs. 4.16 and 4.17, each grid cell has a specific coordinate and specific calculation formula for fire risk evaluation, assigned with the following names: project cell (P), direct neighbor cell (VD), neighbor corner cell (VE), indirect straight (IR) cell, horse jump (SC), and indirect corner cell (IR). In Fig. 4.17, codes of flammable land materials (to be used for cell calculation fire risk) are shown.

The evaluated area corresponds to the radius considered from the edge of the terrain up to 100 m, in cells of 50 × 50 m. Each cell of the grid of Fig. 4.15(b) corresponds with the cells of Figs. 4.16 and Fig. 4.17; hence, the affectation of forest fire is verified. The building material is identified, as well as the risk factor of the zones, type of construction, and type of coverage of the site. The risk of fire is obtained cell by cell in percentage (Fig. 4.18).

In conclusion, the fire risk index in the area of the functional unit of Tomé Hospital, according to the Hazard Evaluation Form, is 11.90% and exceeds the threshold only by 1.43%; according to the degree of criticality of this type of public service, there is a low percentage of vulnerability as shown in Fig. 4.19b.

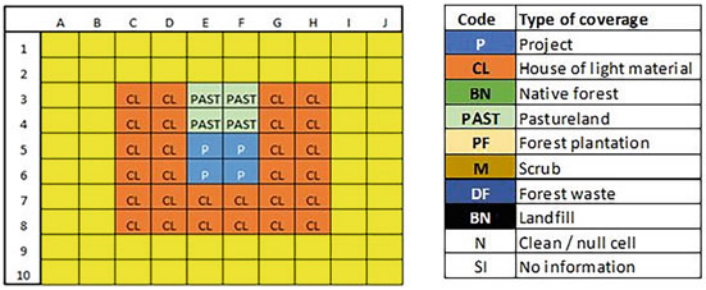

	A	B	C	D	E	F	G	H	I	J
1										
2										
3			CL	CL	PAST	PAST	CL	CL		
4			CL	CL	PAST	PAST	CL	CL		
5			CL	CL	P	P	CL	CL		
6			CL	CL	P	P	CL	CL		
7			CL	CL	CL	CL	CL	CL		
8			CL	CL	CL	CL	CL	CL		
9										
10										

Code	Type of coverage
P	Project
CL	House of light material
BN	Native forest
PAST	Pastureland
PF	Forest plantation
M	Scrub
DF	Forest waste
BN	Landfill
N	Clean / null cell
SI	No information

Fig. 4.17 Cell coverage types and distribution

Fig. 4.18 Synthesis of the forest fire hazard, cell by cell in percentage, colored by its level of risk

	A	B	C	D	E	F	G	H	I	J
1	0%	0%	0%	0%	0%	0%	0%	0%	0%	0%
2	0%	0%	0%	0%	0%	0%	0%	0%	0%	0%
3	0%	0%	17%	4%	2%	2%	0%	0%	0%	0%
4	0%	0%	22%	9%	6%	5%	3%	0%	0%	0%
5	0%	0%	25%	P	P	0%	4%	0%	0%	0%
6	0%	0%	25%	P	P	0%	10%	0%	0%	0%
7	0%	0%	22%	9%	9%	22%	8%	0%	0%	0%
8	0%	0%	3%	4%	9%	8%	0%	0%	0%	0%
9	0%	0%	0%	0%	0%	0%	0%	0%	0%	0%
10	0%	0%	0%	0%	0%	0%	0%	0%	0%	0%

(a)

Overall Result	Score (%)
Forest Fire Hazards	24.73
Physical Vulnerability	16.83
Functional Vulnerability	24.96
Social Vulnerability	16.53
Physical Resilience	0.00
Functional Resilience	16.13
Resilience for Local Risk Management	1.38

(b)

11.90%

$Risk_a = E_a * V_a * (1 - Re_a)$

Forest Fire Threshold 10.47%

Fig. 4.19 Hazard vulnerability scores (**a**) and calculation of risk (**b**) of fire

4.6.5 Hazards Due To Mass Movements, Removal and Flows

The Tomé Communal Regulatory Plan informs that less than 100 m is located at Cerro Estanque and its slope is classified as a mass slip zone (restricted area), the green area in Fig. 4.20.

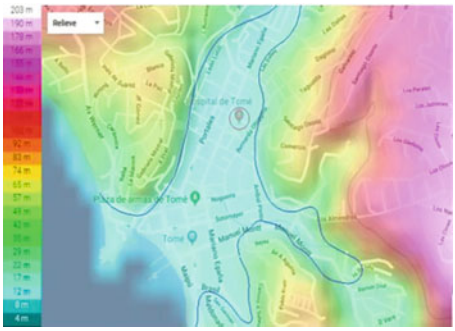

Fig. 4.20 Regulatory plan for the city of Tomé

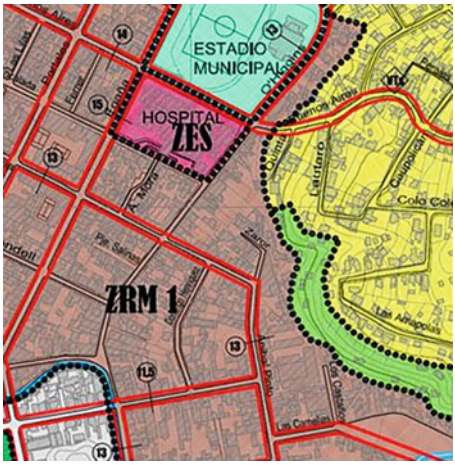

Fig. 4.21 Setoff of downtown of Tomé and functional unit

Height above sea level is shown in Fig. 4.21. The slope in the area of the functional unit is 2% (red circle with arrow); however, the slope of Cerro Estanque is 45%, according to Fig. 4.22 (right circle).

The Mass Removal Form concludes that there is a very high degree of risk. The maximum threshold of 7.33% is greatly surpassed, especially by the two first elements of the list, shown in Fig. 4.23.

The methodology concludes that the first danger is by mass removal and the second by forest fire.

Step 3. Identify mitigation measures (MM)

Forest Fire Hazards

Three mitigation measures have been identified to diminish further risk (Table 4.3):

MM 1. Dry and wet network project in the current hospital
MM2. Perimeter wall of reinforced concrete
MM3. Ventilation and air-conditioning project

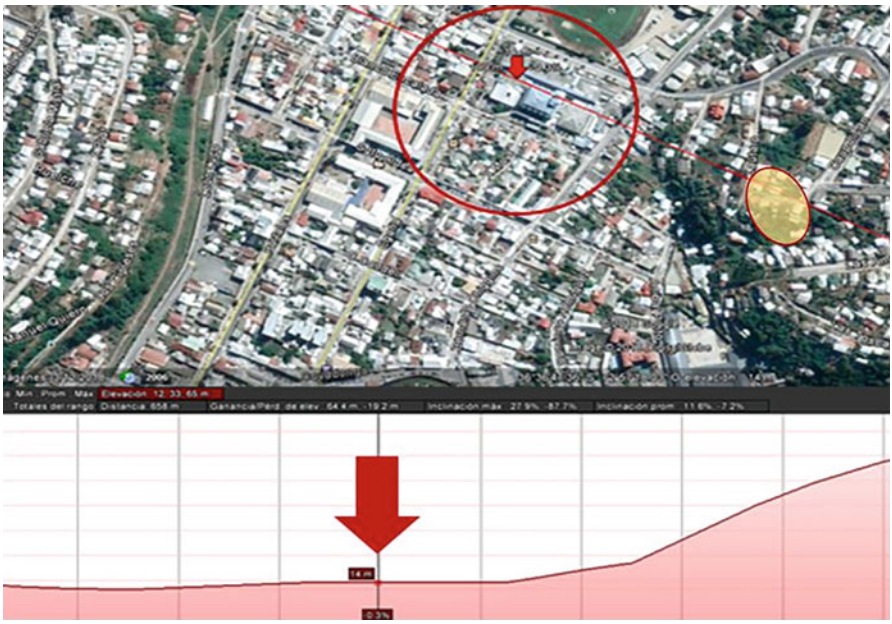

Fig. 4.22 Aerial photo of functional unit and its slope profile

(a)

Overall Result	Score (%)
Generation Constraints Hazards RM	81.17
Scope Area Hazards RM	30.20
Physical Vulnerability	11.60
Functional Vulnerability	24.96
Social Vulnerability	16.31
Physical Resilience	0.00
Functional Resilience	16.13
Resilience for Local Risk Management	1.38

(b)

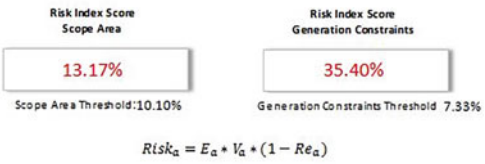

$$Risk_a = E_a * V_a * (1 - Re_a)$$

Fig. 4.23 Hazard vulnerability scores (**a**) and calculation of risk (**b**) of mass removal

Table 4.3 Cost evaluation

Generation constraints (Cost evaluation)	No MM	MM1	MM2	MM3
	11.90%	9.11%	11.24%	9.11%
Costs		$117,000,000	$26,000,000	$135,000,000

Mass Removal Hazards

Three mitigation measures have been identified to diminish further risk:

MM1. Hillside retaining wall
MM2. River diverts
MM3. Perimeter wall of reinforced concrete

Generation constraint evaluation (%)	No MM	MM1	MM2	MM3
	35.4	32.30	31.73	29.45
Scope area evaluation (%)	13.17	13.17	18.17	13.17
Costs (USD)		750000000	2300000000	280000000

Step 4. Selection of mitigation measures

Forest Fire Hazards

The calculations given by the methodology inform that MM1 and MM3 allow bringing the establishment below the threshold of generation constraint (10.47%).

In Fig.4.24 the mitigation measure (MM1) results in a 9.11% threshold of generation condition.

The investment of mitigation measures 1 and 3 are the most costly; MM1 is the least expensive.

Mass Removal Hazard

The calculations made by the methodology inform that MM1, MM2, and MM3 do not improve or allow the establishment to be left below the generation conditioning threshold (7.33%) (Figs. 4.25, 4.26, and 4.27).

In summary, according to what was defined by the methodology, the sequence of development of the four steps in the case study was as follows:

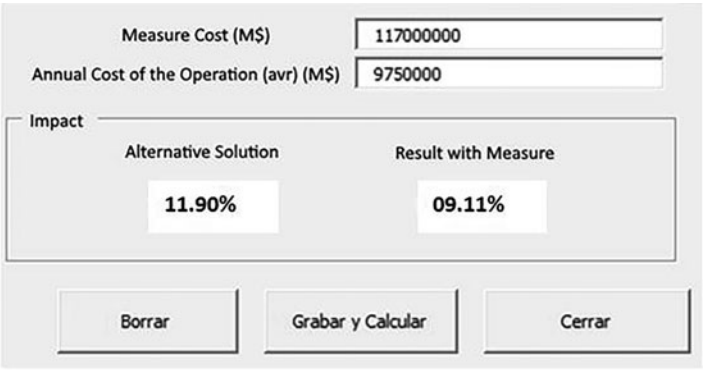

Fig. 4.24 Calculation of mitigation efficiency

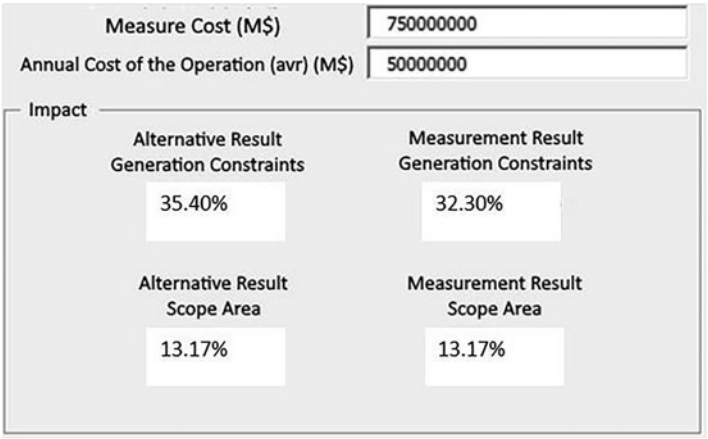

Fig. 4.25 Calculation of mitigation efficiency for MM1 hillside retaining wall

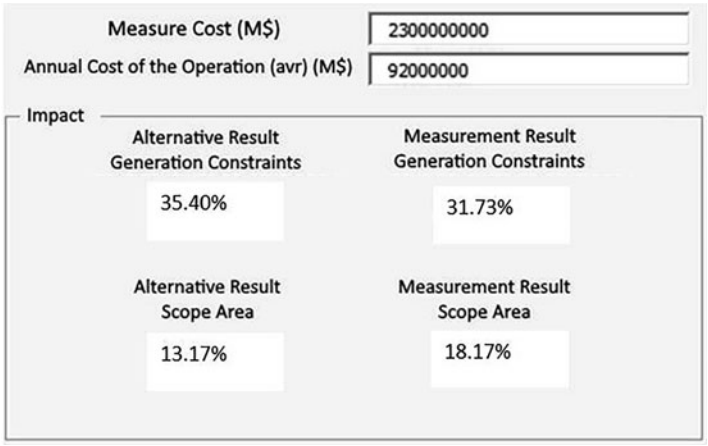

Fig. 4.26 Calculation of mitigation efficiency for MM2 river diverts

(i) Risk assessment of hazards.
(ii) Calculation to evaluate if risk is greater than tolerance threshold. If yes, then mitigation measures are required.
(iii) Re-evaluation of the risk with the mitigation measures included (repeat Step 1).
(iv) If the reassessment gives that the risk is less than the threshold, then generate economic valuation (according to indications of the manual of the methodology) of the management measures.

Notice that Step 4 is an iteration that is considered completed when the inclusion of mitigation measures shows that the total risk is below the risk threshold.

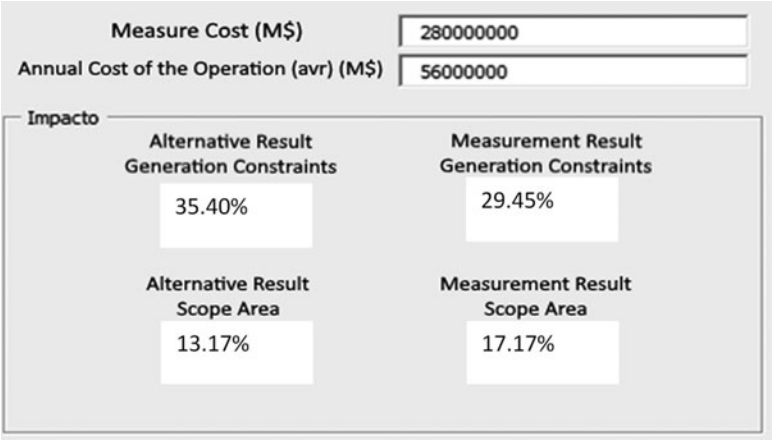

Fig. 4.27 Calculation of mitigation efficiency for MM3 perimeter wall of reinforced concrete

4.7 Conclusions

AHP multicriteria decision-making provides a solution for risk assessment in the most vulnerable conditions and generates a risk index with cardinal and balanced precision. The layered nature of the models shown in this work has succinct advantages over conventional methods in the following way: The well-applied AHP method assures the building of a valid metric rule to measure the elements of the TR enabling the inclusion and combination of tangible and intangible factors. Secondly, including expert knowledge enables consistency and compatibility with the changing natures of risks and hazards. Thirdly, as the hierarchical structure detailed in our AHP method includes the concept of threshold to qualify the risks in a simple and mathematically correct way, using the same AHP concepts assesses TR and applies the same rule of measurement to build it. This achieves the realization that every model has its own threshold calculation with the same variables and restrictions. In the case that parameters change, thresholds may be reassessed and recalibrated to new values, for which there is provision.

There are two different parts to be concluded. Initial conclusions (2017–2018) were made at the end of the study to decide if the project requires special attention (additional investment) due to the natural risk disaster level that the project was facing (the ex ante vision). Secondary (2018–2019), final conclusions were made in order to test if the decision made in the initial conclusions was the right one (the ex post vision). A double-timed assessment enables a conclusion with short- (initial) and longer-term (final) significance.

As an initial conclusion (2017–2018), the Institutional Policy of the governing unit will determine the acceptance or rejection of projects with the TR below the threshold's risk, but with "A" (hazard) or "V" (vulnerability) values above the limit.

Risk evaluation should be reviewed before being accepted in cases where A or V are above their limits although global risk is below its limit. The validation of the method is achieved using additional cases. Fifteen test cases were made in 2017–2018, being social investment projects from different institutions of the Ministry of Public Works (MOP), Chile, with its sub-directions of airports, roads, and water according to the Ministry of Housing and Urbanism (MINVU); the National Emergency Office (ONEMI), Chile; the Ministry of Health (MINSAL), Chile; and the Ministry of Social Development (MIDESO). In all cases, after minimal corrections, satisfactory results were obtained. Correct calculation of threshold values is of principle importance as they meet the basic aims of the study in establishing (as objectively as possible) if a project requires extra financing due to its disaster risk exposition.

The test phase establishing different threshold values and the operative process for risk evaluation of social projects will continue nationally in Chile, until sufficient confidence with the risks models is reached. Such testing is required before writing legislature officially for the social project assessment of the MIDESO. The primary results shown in this chapter provide great promise.

The final/long-term conclusion is that after a year of intensive tests applying the models, the integration formula and (especially) the calculated thresholds have proven to be very good decision-making tools to establish if initial projects require an additional investment due to disaster risk. The formula and process of this chapter have been tested in different public health infrastructures (critical infrastructure in general), and the model presented produced outcomes according to the expected results (below threshold values were obtained where they were expected to be low, and above threshold values were obtained where they were expected to be high). Examples of tested sites are the Hospital of Illapel, Hospital of Tolten, Hospital of Coronel, Hospital of Tomé, CESFAM of Vichuquen, and the primary health room of Ensenada. They were tested against hazards of fire, tsunami, mass removal, and/or volcanoes, according to their geographical location.

Finally, when compared with the classical expression for TR assessment, $R = AV/Re$, the risk models and testing shown in this chapter present several advantages. This is pertinently seen as the classic formula has no borders (no range); if Re (resilience) comes close to 0, then R becomes infinite, which is not a measureable value (and difficult to be interpreted). Also, if A, V, or Re are not defined in a measurable range, then R becomes very large (or very small) and again is difficult to be interpreted.

In the history of natural hazard risk analysis, there is no methodology (with explicit formulae) that takes into consideration the interrelation between project and territory for different kinds of hazards and its combination, in the explicit way shown in this chapter. Lastly, the consolidation of hazards, vulnerability, and resilience with equation (4.6) is highly effective due to its construction process, equation (4.7) well-defined borders may be used as a tool for territory planning under natural disaster risk, since it considers the complete interrelation between territory and project in both senses, territory over the project and project over the territory.

Further application of the set basis shown within the precise, consolidated methods of this chapter removes the need for overcomplications and wasted resources in managing risk and development, thus ensuring protection of our communities into the future amidst changing conditions brought on through our activities and increasingly unstable climatic risks.

References

Alkhalidi A, Tahat S, Smadi M et al (2019) Risk assessment using the analytic hierarchy process while planning and prior to constructing wind projects in Jordan. Wind Eng 44(3):282–293. https://doi.org/10.1177/0309524X19849862

Bach C, Gupta AK, Nair SS et al (2013) Critical infrastructures and disaster risk reduction (in the context of Natural Hazards). New Delhi 72p

Borg P, Indirili M, Romagnoli F et al (2014) The android case study: Venice and its territory: vulnerability and resilience in multihazard scenarios. Procedia Econ Finance 18:825–836. https://doi.org/10.1016/S2212-5671(14)01008-9

Cutter SL, Barnes L, Berry M et al (2008) A place-based model for understanding community resilience to natural disasters. Glob Environ Chang 18(4):598–606. https://doi.org/10.1016/j.gloenvcha.2008.07.013

Dey PK (2010) Managing project risk using combined analytic hierarchy process and risk map. Appl Soft Comput 10(4):990–1000. https://doi.org/10.1016/j.asoc.2010.03.010

Garuti C (2016) Consistency & compatibility two sides of the same coin (but with different implications). ISAHP 2016 International Symposium of the Analytic Hierarchy Process. https://doi.org/10.13033/isahp.y2016.049

Garuti C (2014a) Measuring in weighted environments: moving from metric to order topology (knowing when close really means close). In: De Felice F, Petrillo A, Saatay T (eds) Applications and theory of analytic hierarchy process decision making for strategic decisions. IntechOpen

Garuti C (2014b) Compatibility of AHP/ANP vectors with known results. Presentation of a suggested new index of compatibility in weighted environments. ISAHP2014 International Symposium of the Analytic Hierarchy Process, Washington DC

Garuti CA (2007) Measuring compatibility in weighted environments: when close really means close? International Symposium on AHP, 9, Viña del Mar, Chile

Garuti CA, Spencer I (2020) Risk disaster management in public investment of highways. Why is important to prioritize critical projects for a sustainable investment? Deutsche Zusammenarbeit (GIZ)

Garuti C, Escudey M (2005) Decision making in complex scenarios Santiago de Chile, Chile, Editorial Universidad de Santiago

NIDM, GIZ (2013) Critical infrastructures and disaster risk reduction. Training module. Available via UNDRR, Prevention Web. https://preventionweb.net/educational/view/36182. Accessed 14 May 2021

MIDESO (2017) Complementary methodology for disasters risk assessment of public infrastructure projects. Division of Social Evaluation of Investments

MINVU (2016). D.S. N°47, de 1992. General urban planning and construction ordinance. (Updated at March 21, 2016 - including a modification to D.S. N°50 - D.O. 04.03.16 y D.S. N°37 - D.O. 21.03.16)

MINSAL (2018) Communication, (Ministery of Health): development of actual example application

ONEMI (2018) Results of the survey application of the factors underlying the risk of disasters at the community level. (Final report). NATIONAL PLATFORM FOR DISASTER RISK REDUCTION. Part I (Chile, 2018)

ONEMI (2017) Operational continuity plan. PENGRD 2015-2018. National Platform for Disaster Risk Reduction

ONEMI (2016) Service Order No. 10. Ref. Refers definitions of Disaster Risk, action defined in the National Strategic Plan for Disaster Risk Management. 26 December 2016

Pudasaini SP, Mergili M (2019) A multi-phase mass flow model. JGR Earth Surface 124(12): 2920–2942. https://doi.org/10.1029/2019JF005204

Saaty TL, Peniwati K (2013) Group decision making: drawing out and reconciling differences. RWS Publications

Saaty TL, Thomas L, Luis G (1982) The logic of priorities applications of business, energy, health and transportation. Springer Science and Business Media, New York

Saaty TL, Vargas LG, Kearns KP (1991) The logic of priorities and analytical planning—the Organization of Systems. RWS Publications

Visser H, de Bruin S, Martens A et al (2020) What users of global risk indicators should know. Glob Environ Chang. https://doi.org/10.1016/j.gloenvcha.2020.102068

Wilson G, Wilson TM, Deligne NI et al (2014) Volcanic hazard impacts to critical infrastructure: a review. J Volcanol Geotherm Res 286:148–182. https://doi.org/10.1016/j.jvolgeores.2014.08.030

Part II
Indonesia – Visitors Learning to Conserve and Appreciate Pearls of the Forest

Species names are provided tentatively, though may require further taxonomical and ecological characterisation as we struggle to keep pace with the loss of diversity and its functional services. Photographic figures feature images between 2017 and 2021. Material was provided in 2021 by resident conservation leader Hally Day in the hope that the unique diversity and rare endemic species of diversity hotspots can be sustained and protected.

Fig. 1 Jungle skills teaching group, Lapago Forest, Buton Island, July 2019
Fig. 2 Students from Birmingham University, United Kingdom butterfly catching, farmland of Labundo-Bundo, Buton Island, July 2018
Fig. 3 Resident conservation leader with international student volunteers, Bala Camp, Buton Island, August 2019
Fig. 4 Local guide for expeditions of Operation Wallacea, Lambusango Forest, Buton Island, June 2019
Fig. 5 Monitor Lizard – *Varanus salvator/celebensis* species complex) of the Mangrove habitat, Kakenauwe, Buton Island, April 2017
Fig. 6 Asian water monitor (*Varanus salvator*) by the river, Ladongkula, Buton Island, April 2019
Fig. 7 Tarantula species (*Lyrognathus giannisposatoi* sp. nov.), Lapago Camp, Buton Island, May 2017
Fig. 8 Giant Indonesian Blue Forest Scorpion (*Heterometrus longimanus*), Lambusango Forest, Buton Island, May 2017
Fig. 9 Sulawesi Toad (*Ingerophrynus celebensis*), endemic, Matareao Forest, Buton Island, June 2018
Fig. 10 Celebes Flying Frog (*Rhacophorus edentulus*), Lapago Forest, Buton Island, March 2018
Fig. 11 Sulawesi Knobbed Hornbill (*Rhyticeros cassidix*), endemic, Lambusango Forest, Buton Island, May 2019
Fig. 12 Blue-backed Parrot (*Tanygnathus everetti*), endangered, Lambusango Forest, Buton Island, September 2019
Fig. 13 Golden-bellied Flycatcher (*Microeca hemixantha*), Lambusango Forest, Buton Island, June 2019
Fig. 14 Sulawesi Hawk Cuckoo (*Cuculus crassirostris*) on farmland, Labundo-Bundo, Buton Island, August 2019
Fig. 15, **Fig. 16** Sulawesi Hawk Eagle (*Nisaetus lanceolatus*), Lambusango Forest, Buton Island, January 2020
Fig. 17 Sulawesi Goshawk (*Accipiter griseiceps*), an endemic species, Lambusango Forest, Buton Island, April 2020
Fig. 18 Sulawesi Serpent-Eagle (*Spilornis rufipectus*), an endemic species, Lambusango Forest, Buton Island, May 2020
Fig. 19 Rusty-backed Thrush (*Geokichla erythronota*), on farm land, Lambusango Forest, Buton Island, August 2019
Fig. 20 Lapago Forest, Buton Island, July 2019
Fig. 21 Small Sulawesi Cuscus (*Strigocuscus celebensis*), an endemic,decreasing, near threatened species, risked by hunting, habitat loss and the pet trade. Little is known of Cuscus species. Pictured in the upper forest canopy of Kakenauwe Forest Reserve, Buton Island, February 2017

Fig. 1

Fig. 2

Fig. 3

Fig. 4

Fig. 5

Fig. 6

Fig. 7

Fig. 8

Fig. 9

Fig. 10

Fig. 11

Fig. 12

Fig. 13

Fig. 14

Fig. 15

Fig. 16

Fig. 17

Fig. 18

Fig. 19

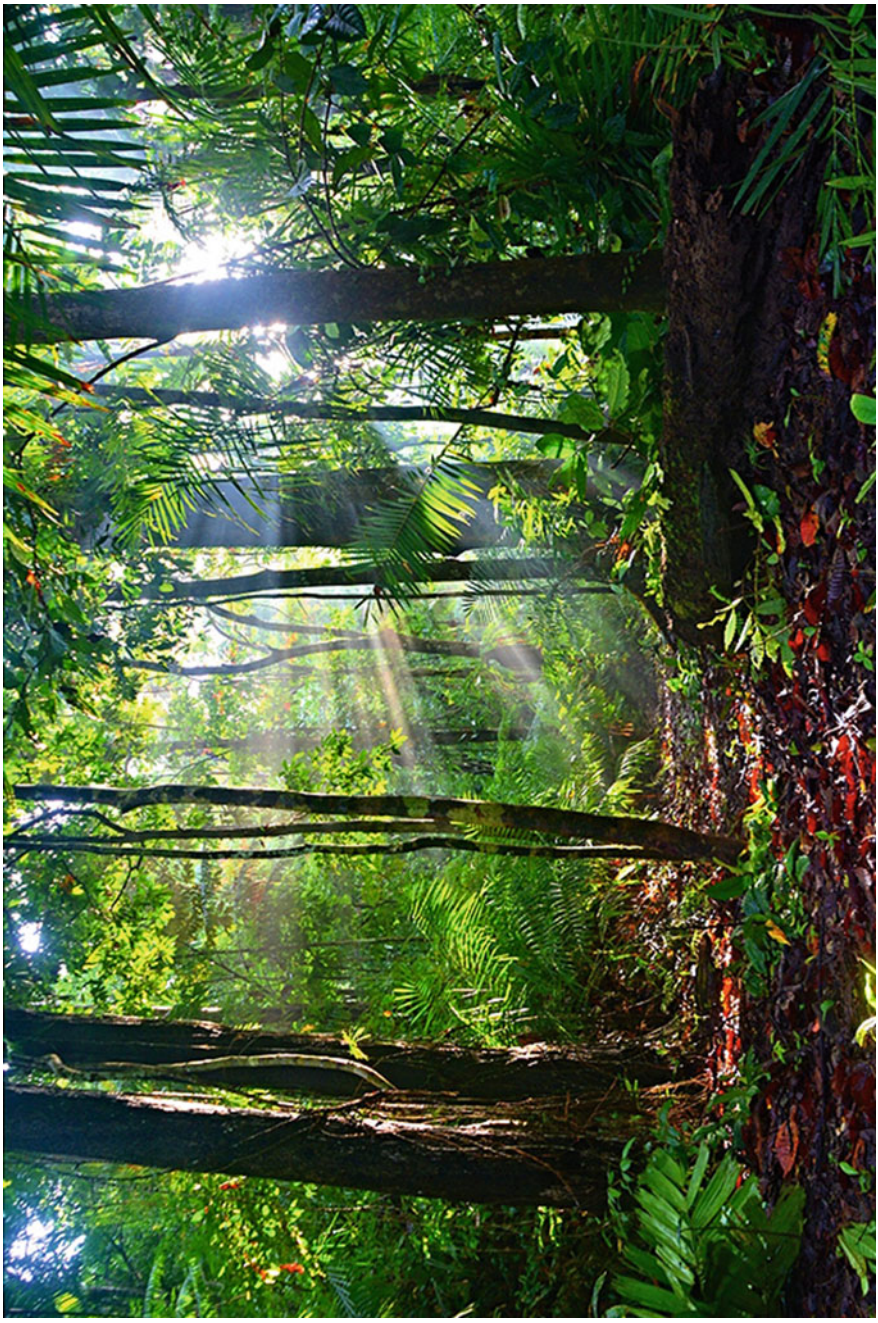

Fig. 20

Fig. 21

Chapter 5
Mathematical Modelling and Simulation of Chemical and Biological Reaction in Peat Solidification Work for Environmental Sustainability

Junita Abd Rahman, Radin Maya Saphira Radin Mohamed, Nor Haakmal Ab Durahim, Syafik Akmal Tajuddin, and Adel Ali Saeed Al-Gheethi

Abstract Understanding the chemical and biological mechanisms of peat solidification is vital to protect the environment during geotechnical works. The alteration of peat to increase its strength for the preparation of road construction requires an admixture to be added to the soil. Changes in peat properties affect proximal ecosystems. Peat has a high water content of up to 2000%, is high in fibre and microorganisms and has a low shear strength of around 4–12 kPa. Normal construction work requires around 300 kPa of soil bearing capacity. The addition of admixtures, usually cement, retards bacterial activities, changes the pH from acidic to alkaline and reduces moisture content significantly. Changes in solidified peat may be observed physically by measuring unconfined compressive strength (UCS) followed by scanning electron microscopy (SEM). Chemical reactions are quantified using X-ray diffraction (XRD), X-ray fluorescence (XRF), Fourier transform infrared spectroscopy (FTIR), pH and energy-dispersive X-ray (EDX), while biological reactions may be enumerated by bacterial counts and enzymatic activities. Mathematical modelling may be used to elucidate chemical and biological reactions and understand the kinetics of strength improvement. The Michaelis-Menten equation is applicable as enzymes secreted by bacteria in peat dissolve hydration products in solidified peat. Affirmation of the theory used in determining chemical and biological mechanisms is critical in helping geotechnical engineers to choose the best method of peat solidification with minimal environmental impact.

Keywords Peat solidification · Mass balance of peat · Mathematical modelling · Michaelis-Menten equation

J. A. Rahman · R. M. S. R. Mohamed (✉) · N. H. A. Durahim · S. A. Tajuddin · A. A. S. Al-Gheethi
Micropollutant Research Centre (MPRC), Institute for Integrated Engineering (I²E), Universiti Tun Hussein Onn Malaysia, Parit Raja, Batu Pahat, Johor, Malaysia
e-mail: junita.abdrahman@gmail.com; maya@uthm.edu.my; norhaakmal@gmail.com; akmalsyafik93@gmail.com; adel@uthm.edu.my

J. N. Furze et al. (eds.), *Earth Systems Protection and Sustainability*,
https://doi.org/10.1007/978-3-030-98584-4_5

5.1 Introduction

Geotechnical works in peat areas are always a challenge to engineers. Roads or buildings constructed on peat often encounter settlement issues. Peat treatment has been introduced by researchers to harden the peat prior to engineering works. The chemical reaction that strengthens soil particles due to mixing peat with chemical admixtures has not yet been highlighted by geotechnical engineers. The reaction can be elucidated using mathematical modelling and simulation. In this chapter, the nature of peat and possible strengthening agents are discussed before mathematical modelling and simulation are introduced to clarify the chemical reaction that happens during peat treatment work. Awareness may safeguard our environment before work is done on-site; the use of possible chemical pollutants shoud be reduced, and the problem of dissolved transmissible chemical additives used for peat solidification transferred to neibouring areas should be solved or minimised.

5.2 Peat and Its Engineering Challenges

Peat is the cumulative product of decayed plants known as soft soil among geotechnical engineers. Peat contains up to 1800% moisture. According to the nature and management of tropical peat soils (Andriesse 1988), soil consisting of more than 65% organic matter is classified as peat soil. ASTM D 2607–69 (ASTM 1990) states that peat is soil with organic content greater than 75%. Overall, peat can be defined as a brownish or black-coloured soil, depending on the location it is formed and climatic conditions. It is formed by accumulation of decomposed organic matter over thousands of years, under anaerobic conditions. Waterlogging promotes formation. A large amount of porous spaces filled with water makes peat easily compressible. These unique characteristics make construction work on it very challenging to engineers. It is suggested that peat should be treated before any construction work is done.

It is estimated that 4.5% of total land areas or 1 billion acres of land in the world consists of peat. A total area of 25,000 km^2 peat soil in Malaysia is shown in Table 5.1, ranking the country ninth with the biggest total area of peat soil (Mesri and Ajlouni 2007). The characteristics of peat depend on the original plant material, e.g. moss or fern, and the climate of specific locations. In most European countries,

Table 5.1 Peat areas in different countries

No.	Country	Area (km^2)		No.	Country	Area (km^2)
1	Canada	1,500,000		6	Sweden	70,000
2	USSR	1,500,000		7	China	42,000
3	United States	600,000		8	Norway	30,000
4	Indonesia	170,000		9	Malaysia	25,000
5	Finland	100,000		10	Germany	16,000

peat originates from bogs and fens. There is variability in microbial communities of peat. In European regions it is normally wet and records constant or similar moisture content throughout the year. Although peats in temperate regions, with tropical climates, are saturated during wet seasons and of low moisture content in dry seasons, peats are easily ignited and are fire hazards (American Coal Ash Association 2007).

Around 2.4 million hectares of Malaysian land area is covered with tropical peat. Sarawak is the state that has the largest peat area, 69.5% of the total peat area in Malaysia (Mutalib et al. 1992). In peninsular Malaysia, the peat area of Pahang, Perak and Selangor states comprises 17.2% of the total land area (Mesri and Ajlouni 2007).

Peat has a low shear strength of 5–17 kPa when tested using vane shear; it is not a favourable soil for construction work (Hebib and Farell 2003; Wong et al. 2009). One of the reasons for the low strength of peat is its high porosity, affecting all peat types worldwide (Al-Ani et al. 2013). In construction work, there is a minimum strength of soil required before a basement is considered safe; however, no specific guideline has been established for construction in peat areas. The New Zealand Building Code proposed that other types of soil have an 'allowable bearing' pressure of 100 kPa before building (New Zealand Building Code Requirements 2011). Building codes of New York City (2008) and New Zealand Building Code (2011) advise a mass stabilisation or vertical piling for construction on peat areas.

As peats are prone to shrinkage and have a very low bearing capacity, they are not suitable for building on (Islam and Hashim 2010). Dramatic peat shrinkage occurs during drier seasons, leaving buildings 'hanging' on piling structure or facing settlement issues. The high moisture content of peat effects shrinkage of a few metres beneath the original level during droughts (Holden et al. 2004; Lindsay et al. 2015). When natural organic soils are drained, subsidence caused by consolidation may occur (Van Hardeveld et al. 2017). Perpetually, after the water table is lowered, saturated organic layers are compacted due to a loss of buoyancy (Wösten et al. 1997). When a high negative water pressure occurs due to loss of water, organic materials above water level experience shrinkage and rapid decomposition. Compaction follows decomposition processes when biochemical oxidation takes place (PS Konsultant 1998).

In most countries, peat areas are abandoned as treatment of peat incurs a high cost. However, Brazil, Canada and Denmark take advantage of peat's natural carbon stock making beneficial products such as peat bricks, peat fuel and supplements for agricultural activity (Peat Society 2015). In Malaysia and in other developed countries such as Sweden, the study of peat treatment has become important. According to Pontian District Municipal Council in a 2014–2018 report, Johor Bahru, Malaysia, (town) has a residential growth of 280% from 2003 to 2013 compared to other peat-based areas in the district with only 10% growth in the same time interval. This highlights the importance of peat treatment to the ministry for the purpose of balanced urbanisation. Knowledge of peat decomposition level is essential as it infers or leads to accurately predict the potential of any physical modification on

peat soil (Mohamed et al. 2002). Treatment studies should consider all peat types, to give solutions that suit all peat areas.

Peats originate from organic matter, some of which contains complex aromatic macromolecules known as humic substances that contribute to odour, taste and acidity in water supplies (Fong and Murtedza 2007). The chemical and physical properties of soils involve humic substances, the most chemically active fractions of peat with a high surface area and surface charge (Santagata et al. 2008). Stabilisation may be carried out using the agent ordinary Portland cement (OPC), though hydration processes are interrupted by humic acid, organic matter with a low pH. Stabilisation is disrupted when acid reacts with calcium from cement hydrolysis, resulting in insoluble calcium humic acid, which makes calcium crystallisation a challenging process. Calcium crystallisation products provide the key strengthening of cemented soil (Santagata et al. 2008; Hashim and Islam 2008).

Peat is classified according to its decomposition level. Categories of less decomposed (more than 66% fibre), moderately decomposed (33–66% fibre) and most decomposed (less than 33% fibre) peat are known as fibric, hemic and sapric respectively. The structure of decomposed peat varies in its degree of humification. Physical properties of peat vary with decomposition level. Peat moisture content alone cannot be used to predict decomposition as it changes with location, original vegetation, climate and water table (Rahman and Chan 2013). Abd Rahman (2015) confirms the relationship between peat decomposition level and the solidification process. The amount of fibre in peat determines the amount of filler needed for peat treatment.

The degree of decomposition varies between peat mosses depending on the resistance degree of plants and environmental factors such as the presence of hydrolytic enzymes produced by decomposing microorganisms. Factors affect microbial activity directly and then indirectly on the decomposition process. These include biochemical stability of the peat, water activity, temperature, pH and aeration (Huat 2004). Variations give a wide range of physical properties to peat including colour, texture, density, specific gravity, porosity and pore size, which are all related to the degree of decomposition. Higher decomposition levels of peat lead to a decrease in the particle size of organic matter (Boelter 1968). Microorganisms have more activity with increases in water content and aeration (Wolińska and Stępniewska 2012). Based on the degree of decomposition for each type, fibric peats are rich with organic matter and have a high porosity due to the large pore size, while sapric peats have a small pore size and low organic matter. Figure 5.1 depicts peat layers: The remnants of logs and woody plants can be seen clearly in fibric peat; the remnants of decomposing wood and trunks can also be noted in hemic peat, but both are absent in sapric peat. The decomposition of peat is organised and represents the peat profile, where fibric peat is normally found at the top of the peat soil layer (Abd Rahman 2015).

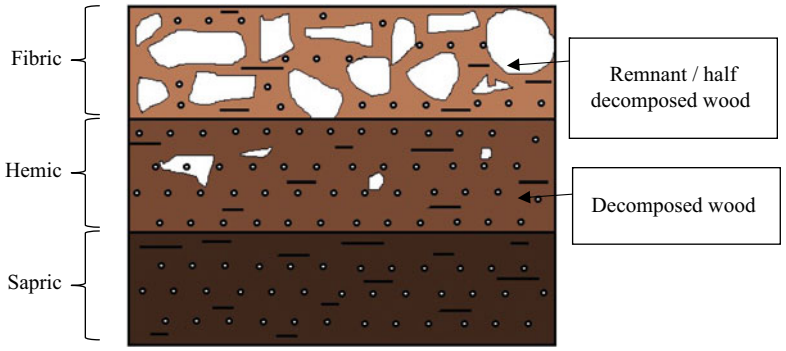

Fig. 5.1 Profile morphology of organic soil

5.3 Peat Solidification Theory

Any soil that is not stable, strong and durable is considered weak and unable to bear high load. Soil solidification, stabilisation or modification is the process of improving the physical and engineering properties of a soil to predetermined targets (Eisazadeh et al. 2010). Soil stabilisation is a solution that increases the bearing capacity and strength of the soil. Stabilisation also refers to the selection of the stabiliser in order to achieve target strengths or stiffness values in addition to modification (Makusa 2012).

The challenge in peat stabilisation is finding the best binder, filler and ratio for the admixture. Several studies on binder and filler for soft soil stabilisation have been conducted, which include the use of recycled waste products, rice husks and many more (Huat 2004). According to Makusa (2012), there are two types of soil stabilisation methods: mechanical and chemical stabilisation. Mechanical stabilising methods include induced vibration or compaction, as well as adding other physical properties like barriers and nails. These are best suited for coarse-grained soils or aggregates at optimum or below optimum moisture contents (Dhakal 2012) and are not suitable for peat soils. Chemical stabilisation, often known as soil stabilisation, is based on a chemical reaction between a stabiliser and the minerals in the soil. There are two groups of chemical stabiliser – traditional and non-traditional. Liu et al. (2011) stated that traditional stabilisers such as cement and lime are more common as compared to non-traditional stabilisers including liquid polymers, silicates and lignin derivatives. This may be due to the cheap price of traditional stabilisers especially if the stabilisation needed to cover a large area is easily obtained. According to Dhakal (2012), clayey soil is the most effective for chemical stabilisation. The selection of stabilisation technique depends on the soil type and its condition.

The water content; the physical, chemical and mineralogical properties of peats; the nature and amount of organic matter included; and the pH of pore water all play a

role in peat stabilisation. As different types of peat have their own unique characteristics, no absolute ratio of properties can be used to indicate solidification. The qualities of treated organic soils by binders and fillers are dependent on both the concentration of organic matter and the nature and type of organic matter (Tremblay et al. 2002). The degradation of biodegradable chemicals also affects the strength gained. Fine-grained soils' engineering behaviour is governed by their specific surface area (Santamarina et al. 2002). A study by Kazemian et al. (2009) found that sapric, hemic and fibric peats have specific surface areas of 93, 69 and 50 m^2/g, respectively. On a unit mass or volume basis, as the specific surface of sapric peat increases, more surface area is accessible for reaction. A higher shear strength is obtained in comparison with fibric and hemic peats (Kazemian et al. 2009). In the following subsections, the solidification of peats will be reviewed and evaluated.

5.3.1 Techniques in Peat Solidification

In many soil solidification studies, cement is used as a binder (Tremblay et al. 2002; Consoli et al. 2000; Rotta et al. 2003; Rao and Shivananda 2005; Ahnberg 2006). Cement is a hydraulic binder. A hydraulic binder is self-curing when in contact with water, while a non-hydraulic binder requires a catalyst to initiate curing. A hydraulic binder will stabilise almost any soil. When a binder interacts with soft soil, it creates a substance with greater engineering qualities than the original soil (Hebib and Farell 2003). The finer the grain size of cement, the more reactive it will be (Kazemian et al. 2009).

Cement is commonly used to alleviate soil acidity, as well as to improve the physical condition of the soil (Rotta et al. 2003). The pozzolanic reaction increases the pH of pore water due to dissolution of hydrated lime. The strong base dissolves both soil silica and alumina from soil minerals (Rao and Shivananda 2005). Care must be taken to ensure homogeneous mixing; unlike lime cement does not diffuse into soil mass (Ahnberg 2006). Thermogravimetric analysis (TGA) is often use to determine the presence of $Ca(OH)_2$ in OPC or solidified soil. Weight loss between 450 and 580 °C was used to determine the $Ca(OH)_2$ composition (El-Jazairi and Illston 1977; Wang et al. 2004). The change of cementitious products can be indicated by the change of $Ca(OH)_2$ by hydration process which produces ettringite (Horpibulsuk 2012).

Beside cement, researchers mix peat with a variety of pozzolan materials to enhance secondary reactions and reduce the cement cost. Pozzolan is a material made up of siliceous or siliceous and aluminous materials with little to no cementitious value. Pozzolan reacts chemically with calcium hydroxide at room temperature in the presence of water to generate cementitious compounds (Mehta 1987). Small amounts of secondary pozzolanic materials are added to admixtures to promote secondary pozzolanic reactions. Fly ash is commonly known as a good pozzolan for soil stabilisation (Wongsa et al. 2016).

Sodium silicate is an admixture used in peat solidification studies (Kazemian et al. 2011a, b, c). According to Karol (2003) and the US Army Corps of Engineers (USACE 1995), when sodium silicate solution and an adequate solution of alkali metal salt (sodium and potassium) are mixed, the reaction generates a gel instantly. As the reaction is fast, solutions do not completely contact with each other; unstable interfaces ensure that enough contact occurs to form a continuous gel network that can be followed through stabilised soil. The study by Kazemian et al. (2009) found that sodium silicates can solidify peat and achieve higher strength; more than 50% of the strength is gained when solidifying using OPC in controlled acidic media. The sodium silicates, however, react more in hemic and sapric peats compared to fibric peat.

The ground granulated blast furnace slag (GGBS), calcium oxide (CaO) and sodium bentonite are among secondary pozzolans that are used in peat. These admixtures are good binders with cement. Most secondary pozzolans cannot achieve significant strength without cement as no hydrolysis takes place; no ettringite is formed to bind the soil particles. Combinations of GGBS and cement lengthen the curing effect as it is reactive for long durations (after years). The mixture was found to be efficient in gaining strength in peat solidification studies (Axelsson et al. 2002; Mass Stabilization Manual 2005). Calcium oxide, on the other hand, works differently. Calcium oxide reacts well with water to produce slake lime. Slake lime is very reactive to carbon dioxide, producing mortar. Mortar is a paste that gradually hardens and cements bricks together. The use of calcium oxide in soil treatment is limited to the soil natural water content; however, in the case of peat, a high water content enables mortar formation when calcium oxide is used.

5.3.2 Stabilisation of Peat by Cement

Organic soils have been shown to slow or prohibit the hydration of binders such as cement in binder-soil mixes (Hebib and Farell 2003). With a high organic content and less solid particles in peat, cement alone as a chemical admixture is insufficient to provide peat stabilisation. Peat has a significantly lower content of clay particles that enter secondary pozzolanic reactions than clay and silt (Janz and Johansson 2002). As such, the interaction between hydrated lime Ca(OH) and the soil is less effective in secondary pozzolanic reactions. Unless a sufficient amount of cement is put to the soil, peat stabilisation by cement will not lead to a significant increase in strength. A study by Ahnberg et al. (1995) found that peat achieves the lowest shear strength with cement stabilisation compared to other types of soil. Similarly, with the highest water/cement ratio (wcr), cement-stabilised peat demonstrated the lowest shear strength compared to other types of soil (Ahnberg et al. 1995). Evidence from both figures shows that less solid particles and high organic matter make peat soil porous and spongy in nature; the organic matter tends to impede the hydration of cement when it is used to stabilise soil (Wolińska and Stępniewska 2012).

Abd Rahman (2015) discusses the concept of natural water content in peat. As peat is naturally acidic, containing humic acid, the concept of water consumption in peat solidification is varied. Water in the peat increases after neutralisation of humic acid takes place. The neutralisation produces water, which will react with OPC to form ettringite. Neutralisation is a process involving a reaction between acid and alkaline, producing water and salt as shown in Eq. (5.1).

$$\text{Acid} + \text{Alkaline} \rightarrow \text{Water} + \text{Salt} \tag{5.1}$$

Neutralisation can be detected by pH 7 of a mixture and an increasing amount of water as the result of combination of the aqueous solution from both acid and alkaline. An exact quantity of acid and base (OH^- ion) is needed to achieve neutralisation. Exceeding the neutralisation limit by any of the elements causes the material to be dominant by the respective element, either acid or base. The pH of solidified peats was found to be alkaline (Fig. 5.6). OH^- ions contained in the alkaline binder dominate the pH mixture. The pH value is determined based on the number of OH^- ions present in the solution.

The pH of Pontian peat is around 3–4 and represents the high number of H^+ ions in humic acid (Abd Rahman 2015). Humic acid is a weak acid; direct exposure to peat does not give irritation or corrosion. Moisture in peat contains an aqueous humic acid. Since ettringite is formed by the interaction between cement and water, neutralisation does not occur in a mixture of solidified peat. The amount of water present in the mixture depends on the neutralisation process. Studies by Ali et al. (2010), Akol (2012), Wong et al. (2013a, b) and Abd Rahman (2015) show that peat is acidic by nature, while solidified peat is alkaline with a pH range from 8.83 to 12.11 (Fig. 5.2). The alkaline condition is important for the reaction between OPC and water, interlocking the hydration product and soil particles.

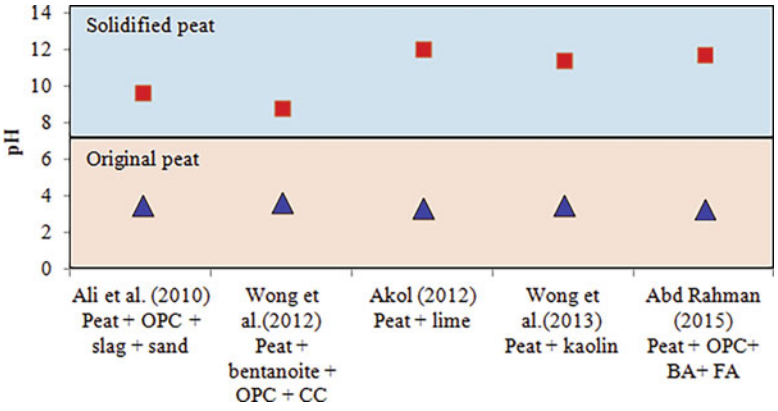

Fig. 5.2 pH of peat and solidified peat. **CC* calcium carbonate, *OPC* ordinary Portland cement, *BA* bottom ash, *FA* fly ash

The presence of black humic acid and fulvic acid in peat soil makes cementation and hardening of peat-cement admixtures difficult. Wherever calcium is present in solution, black humic acid interacts with it to generate insoluble calcium humic acid (Rahman and Chan 2013). Calcium crystallisation is hard due to the combination of humic acid and calcium ions created during cement hydration; yet, crystallisation increases the strength of the peat soil-cement mixture (Rahman and Chan 2013). Exposure of cement to fulvic acid solutions generates the hydration of cement. The chemical reaction between fulvic acid and cement minerals results in an absorbed layer, which obstructs the hydration process. Furthermore, existing crystals such as calcium aluminate hydrate, calcium sulfate-aluminate hydrate and calcium ferrite-aluminate hydrate are decomposed by fulvic acid, inhibiting the creation of a soil-cement structure (Rahman and Chan 2013). The acids lower the pH of the soil, which has an adverse effect on the binder's reaction rate, resulting in a slower strength gain in the peat (Axelsson et al. 2002).

Organic acids, when mixed with soil and cement, generate a pH lower than 9 in porous solutions, preventing the creation of cementing products because the pH has become too low to support secondary mineral formation (Liu et al. 2011). The process of soil stabilisation will be slowed unless a large amount of cement is mixed with the soil to neutralise the acids. It is uneconomical to add a big amount of cement to the soil to improve peat ground. As a result, it is obvious that the physico-chemical reactions that occur, such as cement hydration and hardening, as well as interactions between components in the soil and cement hydration products, are responsible for the increased strength of cement-stabilised soil (Abd Rahman 2015).

Excessive organic matter in peat effects a high water retention capacity, and organic particles on the surface of cement and solid soil particles absorb water during cement hydrolysis in the soil. Both the development of cement hydration products and the hydration of solid soil particles and hydration products are hampered by this (Abd Rahman 2015). As a result, only limited increments can be achieved in peat-cement admixture strength. This was evident when Chen and Wang (2006) mentioned that the strength of peat did not reach 300 kPa with deep mixing with a cement ratio of up to 30%, in a foundation reinforcing project on peat undertaken in 1985. A clear understanding on the behaviour of organic matter in the process of stabilisation of peat by suitable chemical admixtures is vital in order to outline effective peat stabilisation.

5.3.3 Effect of Pozzolan as a Secondary Additive in Peat Stabilisation

To increase the secondary pozzolanic reaction in the stabilised soil, small amounts of pozzolans such as kaolinite, sodium bentonite and fly ash can be added to the cement-stabilised peat (Torkittikul et al. 2017). Under specific conditions, both

cement and pozzolan used for peat stabilisation react with water in the soil to generate a high-strength product that binds soil particles together. However, the ratio of lime to silica ($Ca(OH)_2$:SiO_2) affects reactivity. The material is more hydraulic if the ratio is higher (Janz and Johansson 2002).

5.4 Gaps in Peat Improvement Studies

It can be concluded that the effectiveness and dosage of binder type on the stabilisation of peat are site specific since the properties of peat differ geographically. Different types of peat react with different types of binder at certain binder dosage to achieve effective stabilisation. The unconfined compressive strength gain of stabilised soil rose with an increase in binder dosage, filler and curing time, according to a review of numerous experimental examinations of stabilised peat. Abd Rahman (2015) shows that peat strength can be improved. However, two patterns manifest during stabilisation effecting optimum and non-optimum mixtures during the treatment process (Fig. 5.3). The same pattern was detected by Kido et al. (2009), Kalantari et al. (2013) and Huat et al. (2014) where the peat was of less strength after a certain curing period. Most studies stop at this engineering finding. The chemical reaction, other than hydration, is expected to be the main cause of peat solidification. The alteration of the chemical bond in solidified peat may lead to a new product, potentially a more cost-effective and efficient solution.

The role of the microbial community in peat decomposition of plants has not been considered. Researchers estimate that microbial activity is frozen during the stabilisation process. However, current research in concrete studies introduces self-healing concrete, where microbes are used to react with chemicals from concrete to self-paste the leaking concrete. The concrete research used $CaCO_3$, the main element found in OPC.

5.5 Biological Reaction in Peat Solidification

5.5.1 Microbes in Peat

Microorganisms are responsible for the decomposition of plants in peat. Edaphic communities are varied and comprised of bacteria, actinomycetes, fungi, algae and protozoa. Peat lands contain large microbial populations of a wide metabolic diversity (Williams and Crawford 1983). Studies by Kraigher et al. (2006) and Ausec et al. (2009) explore relationships in microbial activity and structure in two fens and one bog. The result from the studies shows that from the 16S rRNA genes, *Proteobacteria* and *Acidobacteria* dominate fen and bog soils (Thrash and Coates 2011). However, bog and fen soils show a clear distinction in their bacterial communities despite sharing dominant phyla. A significant difference can be

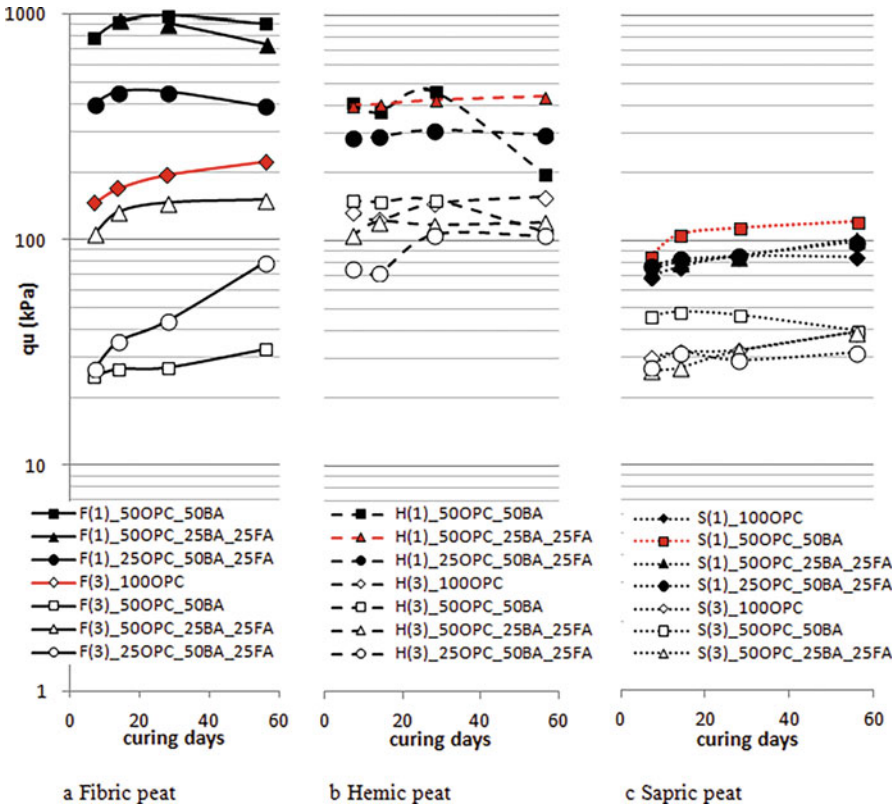

Fig. 5.3 Strength (q_u) versus curing days (Abd Rahman 2015). This infers a potential reaction between microbes and solidified peats. *Red lines indicate optimum mixture

observed at the level of relative abundance of species affiliated with the phylum *Acidobacteria*, 23% in the fen and 40% in the bog gene library respectively.

The types of vegetation from which peat originates cause differences in microbial community makeup. Ombrotrophic bogs are made up of slow-decomposing mosses and shrubs that get their nutrients from both dry and wet deposition (Aerts et al. 1999). Minerotrophic fens, on the other hand, are made up of more easily decomposable sedges, plants and shrubs that get their nutrients from groundwater (Bragazza et al. 2007). According to Tamburini et al. (2017), microorganisms using degraded cellulose by a depolymerisation step allow a metabolisation step. Table 5.2 lists the variety of microbes found in different regions of peat.

All microbes have unique characteristics; some are pathogenic and can be harmful to people. The microbes in Pontian peat may be different from peat from Europe countries as studied by Liimatainen et al. (2018), Novak et al. (2018) and Lorenz and Lal (2018).

Table 5.2 Variety of microbes found in different regions of peat

Microbe	Location	Vegetation	Reference
Arthrobacter, *Bacillus* spp.	Riviere-du-Loup, Quebec, Canada	Finnish *Sphagnum*	Boehm et al. (1993)
Bacillus acidicola ssp. Nov	Wisconsin, USA	Not reported	Albert et al. (2005)
Rhizobium, *Agrobacterium*, *Acidobacteria*	Latvia, Denmark and Ireland	Not reported	Hunter et al. (2007)
Proteobacteria, *Acidobacteria*	Ljubljana, Slovenia	*Sphagnum* sp. *Arrhenatherum elatius*, *Dactylis glomerata*, *Festuca rubra*, *Equisetum palustre*, *Galium mollugo*, *Ranunculus repens*, *Achillea millefolium*, *Leucanthemum ircutianum* and *Centaurea jacea*	Mandic-Mulec et al. (2014)
Actinobacteria, *Bacteroidetes*	Svalbard	Not reported	Žifčáková et al. (2016)
Acidobacteria	Xistral Mountains (Northwestern Spain)	*Sphagnum subnitens* Russ & Warnst., *Molinia caerulea* (L.), *Carex duriaeui* Steud. ex Kunze, *Agrostis stolonifera* L. and *A. curtisii* Kerguélen., *Potentilla erecta* (L.), *Erica mackaiana* Bab., *Deschampsia flexuosa* (L.), *Carex panicea* L. and *Calluna vulgaris* (L.), *Eriophorum angustifolium*	Guanlin et al. (2017)
Thiobacillus	Finland	Not mentioned	Hartikainen et al. (2002)
Burkholderia gladioli	Riau, Indonesia	Not mentioned	Istina et al. (2015)
Methanotrophs	Not mentioned	*Sphagnum* mosses	Kip et al. (2010)
B. phenazinium	Germany	Not mentioned	Al-Sadi et al. (2016)

5.5.2 *Microbes in Solidified Soil*

The study of microbes in solidified soil has attracted interest since the last turn of the century. Most studies focus on utilising bacteria in soil treatment (Ivanov and Chu 2008; Kim et al. 2013; Abo-El-Enein 2013; Ismail et al. 2014; Ng et al. 2012). The biocementation concept where microbes and cement are mixed to form a cementation product lessens the void in soil. The bioclogging process was introduced by Ng et al. (2012) where the soil void is filled by microbial-induced biochemical products. In the study, Ng et al. (2012) concentrate used uratic bacteria that are naturally found

to produce a cemantitious product. Urase activity was found to increase rapidly in mediums with pH 6–8.

In a study by Ivarson (1977), it was shown that the number of microbes in surface peat (normally fibric peat) was higher compared to those from subsurface (hemic peat) and subsoil (sapric peat). It was recorded that fibric and hemic types have microbe counts of 25×10^5 CFU/g and 5×10^5 CFU/g, respectively. However, when lime was introduced to peat, the number of microbes increased dramatically to 6540×10^5 CFU/g for fibric peat and 2940×10^5 CFU/g for hemic peat. This leads to biocementation where the lime content from cement can be expected to stimulate the microbes in peat.

Ivanov and Chu (2008) investigated the potential of biocementation, which is described as a method that uses microbial activity or products to improve the strength and stiffness properties of soils and rocks. Ivanov and Chu (2008), however, limit their research to clay and sand only. Kucharski et al. (2005) filed a patent application for microbial biocementation, which involves combining a permeable material with a biomass of urease-producing microbes, urea and soluble calcium salts to make a high-strength cement. Microorganisms enable rapid urea hydrolysis, raise pH during urea-to-ammonia hydrolysis and create calcite in soils and rocks. Compressive strength of the cement produced was up to 5 MPa. Conglomerate, breccia, sandstone, siltstone, shale, limestone, gypsum, peat, lignite, sand, soil, clay, sediments and sawdust are among the materials treated by biocementation. *Bacillus*, *Sporosarcina*, *Sporolactobacillus*, *Clostridium* and *Desulfotomaculum* are among the urease-producing bacteria used in the study (Ivanov and Chu 2008).

The process of producing urease for the hydrolysis of urea CO $(NH_2)_2$ into carbonate (CO_3^{2-}) and ammonium (NH_4^+) is as follows (Karthik and Rao 2016):

$$CO(NH_2)_2 + H_2O \rightarrow NH_2\,COOH + NH3$$
$$NH_2\,COOH + H_2O \rightarrow NH_3 + H_2CO_3$$
$$H_2CO_3 \rightarrow HCO_3^- + H^+$$
$$2\,NH_3 + 2\,H_2O \rightarrow 2\,NH_4^+ + 2\,OH^-$$
$$H\,CO_3^- + H^+ + 2\,NH_4^+ + 2\,OH^- \rightarrow CO_3^{2-} + 2\,NH_4^- + 2\,H_2O$$

These reactions increase the pH and form carbonate ions (Ramakrishnan et al. 1998).

5.5.3 *Microbes in Cement Study*

Recent trends in concrete or cement studies utilise microbes to develop self-healing concrete. Basically, microbes are known to have unique characteristics which are vulnerable to environmental changes. However, microbes can survive in extreme conditions. The process of self-healing concrete requires adding microbes to the cement before pouring it into the concrete material. In crack-sealing, bacterial

concrete is formed via the metabolic conversion of calcium lactate to calcium carbonate (Jonkers et al. 2010; Kim et al. 2013). Whenever cracking occurs in concrete, rainwater fills the crack, stimulating the inserted microbe and reactivating it to produce more carbon dioxide. The carbon dioxide reacts with calcium lactate and produces calcium carbonate which hardens the material (Jonkers 2011). Ismail et al. (2014) and Pradeep Kumar et al. (2015) have confirmed the success of this hypothesis. Small cracking was found to take about 100 days to recover (Joshi et al. 2017). *Bacillus* spp. work well with cement and are easily obtained in the soil (Ivanov and Chu 2008; Jonkers 2011). Table 5.3 summarises the bacteria that have been used in concrete studies.

Table 5.3 Summary of bacteria used in concrete studies

Bacteria and products	Findings	References
Escherichia coli; *Shewanella*	Mortar specimens induced with *Shewanella* show an increase in strength. The growth of fibres within the pores was observed under SEM and supported strength in increments.	Ghosh et al. (2005)
Bacillus sphaericus	SEM showed the presence of carbonate crystals on the mortar surface.	De Muynck et al. (2008)
EM product	The reaction of bacteria with cement was not well explained. Compressive strength increased in concrete specimens. No microstructural examination reported.	Jamaludin et al. (2009)
Shewanella	Bacteria mortar shown is different compared to control specimens without bacteria when analysed using environmental scanning electron microscopy (ESEM). XRD analysis confirmed the formation of silicates in the mortar containing bacteria.	Ghosh et al. (2009)
EM product EM ceramic	Mechanism of cement hydration was not explained due to bacterial activity. Compressive strength increased by an average of 28% in EM concrete. SEM was used to examine corrosion due to bacteria.	Bang et al. (2010)
Bacillus pseudofirmus; *Bacillus cohnii*	Bacterial spores were observed using ESEM when *Bacillus pseudofirmus* and *Bacillus cohnii* were isolated in cement stone specimens.	Jonkers et al. (2010)
Bacillus subtilis	The presence of silica and the peak of the quartz were detected using XRD analysis.	Afifudin et al. (2011)
Sporosarcina pasteurii	SEM showed the presence of crystalline calcium carbonate associated in microbed concrete containing silica fume. XRD and EDX results confirmed the presence of calcite with results of high amounts of calcium.	Chahal et al. (2012)
Alkalophilic species	SEM and EDS results indicated the peak of calcite in microbially induced precipitated microbed cement containing sandstones as aggregate. SEM micrograph showed the bottom region is denser than the top region.	Rong et al. (2012)

(continued)

Table 5.3 (continued)

Bacteria and products	Findings	References
EM product	Compressive strength and indirect tensile strength increased in concrete specimens. However, flexural strength results are similar to control specimens. No microstructural examination and chemical phases reported. Confirmed the presence of silica and quartz detected using XRD analysis.	Andrew et al. (2012)
Sporosarcina pasteurii *Bacillus sphaericus*	SEM featured the calcium carbonate precipitated on the surface of microbed normal and lightweight concrete. Calcite crystals with little vaterite crystals for both types of bacteria were indicated in XRD pattern.	Kim et al. (2013)
Sporosarcina pasteurii	SEM with energy-dispersive X-ray analyser (EDAX) depicts that $CaC0_3$ is precipitated within the cement mortar matrix. XRD was not used to quantify the minerals.	Abo-El-Enein (2013)
Effective microorganism (EM)	Compressive strength improved with curing days and amount of microbes. SEM micrograph of microbed cement paste had less voids and was denser compared to control cement paste.	Ismail et al. (2014)

Since microbes were reported to be part of the solidification product, microbes present in peat may work the same in solidified peat. However, no successful biocementation field applications have been reported.

5.6 Chemical Reactions in Peat Solidification

5.6.1 Chemical Bonding/Sketching for Raw Peat

The chemical bonding of all materials is known as a fingerprint of a substance. Different materials have unique molecular structure. Peat in particular is very dynamic. It consists of several types of plant origin and has different decomposition levels, a wide range of acidity and microbial presence. These parameters have limited the sketching of chemical bonds in peat. A general sketching for peat according to its functional group was introduced by Koch (1982) as seen in Fig. 5.4. In 1993, Yonebayashi et al. (1994a, b) used nuclear magnetic resonance (NMR) and infrared (IR) spectroscopy to locate the functional group of peat. However, Yonebayashi et al. (1994a, b) were unable to sketch the molecular structure of the peat, there was no absolute chain in peat from all three sampling locations and the C/N ratio was unstable. Stevenson (1994) has sketched the molecular bonding of humic acid, a typical acid present in peat soil (Fig. 5.5).

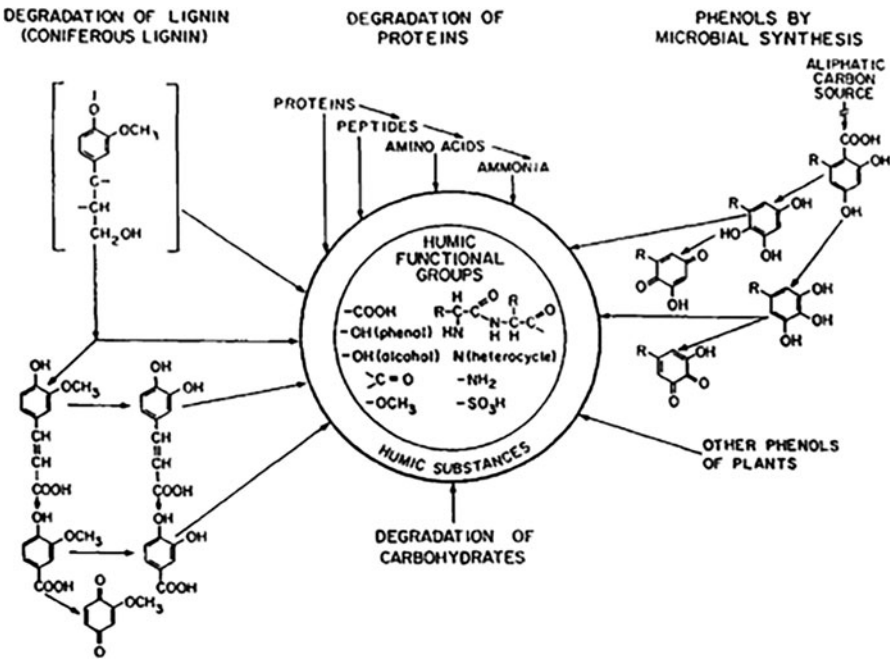

Fig. 5.4 Degradation of plant residues and the formation of humic substances in peat. (Koch 1982)

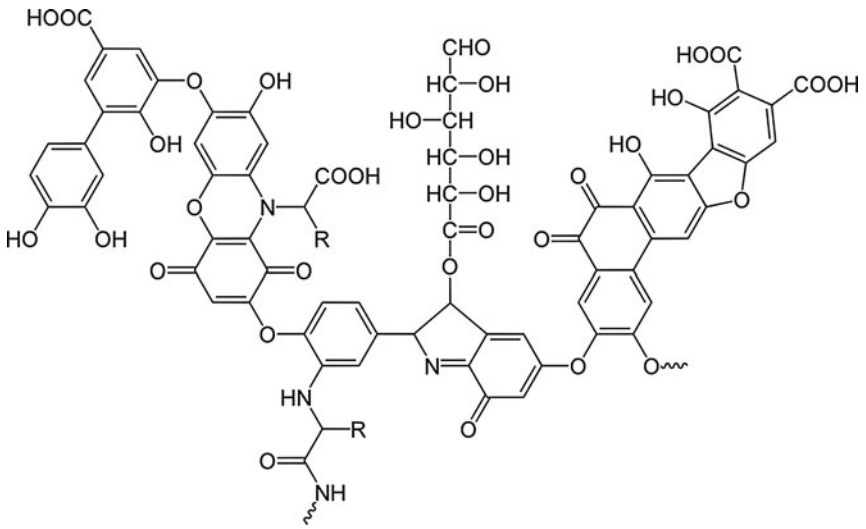

Fig. 5.5 A typical humic acid with a range of components such as quinone, phenol, catechol and sugar moieties in peat. (Yonebayashi et al. 1994a, b)

5.6.2 *Fourier Transform Infrared (FTIR), Nuclear Magnetic Resonance (NMR) and X-Ray Diffraction (XRD) Analysis Explain Chemical Alteration in Peat*

FTIR and XRD are used in determining the chemical and mineral elements in samples. FTIR determines the absorbance of infrared rays in a sample. Different functional groups will give different absorbance values and normally read in ranges. XRD works by determining minerals in samples by dispersing X-rays. The combination of information gained by both FTIR and XRD could be utilised to obtain the chemical sketching of specific peat samples. Yonebayashi et al. (1994a, b) examined the occurrence of carboxyl, carbonyl, phenolic hydroxyl and alcoholic hydroxyl groups in humic acids. It has been shown that the amount of lignin and cellulose decreases with increasing humic acid in peat. Yonebayashi et al. (1994a, b) used NMR to classify the chemical in the sample. It was concluded that humic acids from tropical peat have long aliphatic chains due to the origin of their plant source.

Kyziol (2002) used FTIR to determine functional groups in peat from three different locations. Peat from different sites has the same functional group at wavelength 2900, 2780, 2350, 1480 cm^{-1} and more minor peaks in the range 800–1300 cm^{-1} (Fig. 5.6). Table 5.4 summarises the techniques used to consider chemical bonding.

5.6.3 *Chemical Reaction Models of Peat Processes*

To model chemical reactions that take place in peat solidification, an understanding of the concept of chemical reaction is essential. The kinetics behind chemical reactions are influenced by the rate of reaction, reversible or non-reversible reaction, rate constant, reaction order and reaction mechanism.

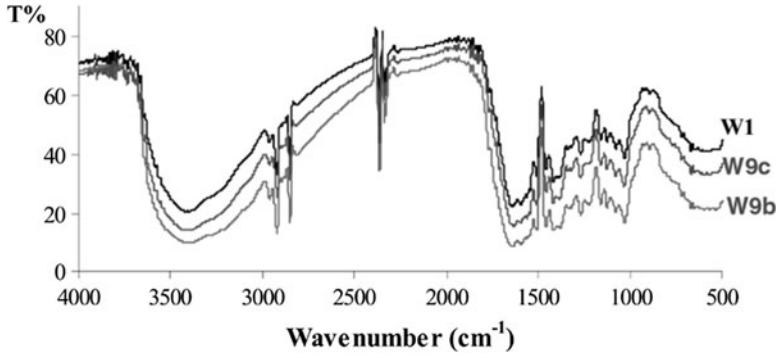

Fig. 5.6 FTIR spectra of selected peats. (Kyziol 2002). W1 Alder Peat Humus, W9b Brushwood Peat Humus, W9c Rush (Reed-Sedge) Peat

Table 5.4 Techniques used to determine chemical bonding in peat

References	Technique used	Findings
Yonebayashi et al. (1994a, b)	Proton NMR spectra	The atomic ratios of C, H, N and H/C in tropical peat humic acids ranged from 54% to 63%, 4.5% to 7.1%, 1.1% to 3.9% and 0.96% to 1.35%, respectively
		Humic acids from tropical peats have concentrations of carboxyl, carbonyl, phenolic hydroxyl and alcoholic hydroxyl groups ranging from 3.1 to 5.1, 1.0 to 5.3, 0.03 to 1.1 and 3.1 to 23.5 mol kg^{-1}, respectively
		The methoxyl group, lactone ring and aromatic ring proton percentages of tropical peat humic acids ranged from 16% to 57%, 6% to 41% and 4% to 17%, respectively
		The percentages of aliphatic protons linked to carbon atoms, fJ to aromatic rings and terminal methyl protons were 1–6, 13–39 and 4–14%, respectively
Kyziol (2002)	Functional group – FTIR	Product of humification process of organic matter has similar chemical structure when compared with other peat samples from different regions
Romão et al. (2007)	XRD	Peat samples give an amorphous pattern which indicates no presence of absolute mineral in peat

The reaction mechanism of materials takes place via adsorption, desorption and surface reaction. These reactions are spurred by temperature, pressure and biological elements. All parameters mentioned must be considered when modelling the chemical reaction of a material. There are chemical reaction models which use conventional equations or mathematical models using software in explaining the reaction that takes place in particular samples.

As peat is derived from plant materials and affected by microbial activity, a biochemical reaction model is suitable for clarifying the reaction inside the solidified peat. The majority of soil biochemical reactions take place in organic dominated layers (McLaren and Peterson 1967). Table 5.5 summarises modelling and simulation of chemical reactions as discussed by Higham (2008).

5.6.4 Chemical Reactions Behind Soil Improvements

Eisazadeh et al. (2012) used NMR and FTIR techniques to analyse the functional group and local bonding of lime-treated soil. The study treated green bentonite and laterite soil (rich with iron) by using lime in various ratios and curing periods. As bentonite and laterite soils are rich with minerals, changes in clay minerals were expected. Conversely, the silica in quartz was found not to be affected by the presence of lime. The study on the effect of curing period of treated clay found a promising strengthening effect for all types of mixing up to 8 months of curing. However, the NMR and FTIR analysis for all mixing portions and curing periods did

Table 5.5 Summary of mathematical modelling and simulations of chemical reaction

Model/ simulation	Explanation	Relation with solidified peat study
Michaelis-Menten equation	Associate with a system involving four species: 1. A substrate, S_1 2. An enzyme, S_2 3. A complex, S_3 4. A product, S_4 $S_1 + S_2 \overset{c_1}{\rightarrow} S_3$, $S_3 \overset{c_2}{\rightarrow} S_1 + S_2$, $S_3 \overset{c_3}{\rightarrow} S_4 + S_2$.	Microbes in peat secrete enzyme that will eventually react with chemical additives and peat soil itself
	Expectation: 1. Reaction happens when $S1$ molecules meet $S2$ molecules. 2. c_1 is a scaling factor that takes into account the fact that not all collisions result in a reaction, 3. Two molecules from the same chemical species interact.	
	$\frac{dP(\mathrm{x},t)}{dt} = \sum_{j=1}^{M} \left(a_j(\mathrm{x}-v_j)P(\mathrm{x}-v_j,t) - a_j(\mathrm{x})P(\mathrm{x},t)\right)$. For probability that a happens, happens j is a certain vector	
Stochastic simulation algorithm (SSA)	Rather than computing the complete probability distribution, single realisations of the state vector are computed $p(\tau, j\|\mathrm{x},t) = \frac{a_j(\mathrm{x})}{a_{\mathrm{sum}}(\mathrm{x})} a_{\mathrm{sum}}(\mathrm{x}) e^{-a_{\mathrm{sum}}(\mathrm{x})\tau}$. Depending on the next reaction index and time for next reaction	Assumption of reaction rate can be calculated using an algorithm; however, as peat is complex, single algorithms are expected to be insufficient, and so must be applied in sequence pending variations
Tau-leaping	$\mathrm{X}(t+\tau) = \mathrm{X}(t) + \sum_{j=1}^{M} v_j P_j\left(a_j(\mathrm{X}(t)), \tau\right)$, To advance SSA. Applicable when τ is sufficiently small that relatively few reactions take place	When peat solidification takes place, lots of reaction step are expected. The mixture of peat and cement itself is exorthermal
Chemical Langevin equation	$\mathrm{Y}(t+\tau) = \mathrm{Y}(t) + \tau \sum_{j=1}^{M} v_j a_j(\mathrm{Y}(t)) + \sqrt{\tau} \sum_{j=1}^{M} v_j \sqrt{a_j(\mathrm{Y}(t))} Z_j$. Using real values and can do a large number of iterations. Knowledge of a large number of molecules present in the reaction is needed	The possibility in using this model in interpreting the reaction during solidification is there since complex molecule is expected

not reveal any new element in the mixtures. Comparison between non-treated clay and treated clay differed with a new peak identified as a Ca-OH bond. Ca-OH is a functional group of lime. No new element was found in the treated clay that can explain the strengthening effect gained. According to Eisazadeh et al. (2012), lime treatment did not result in significant changes in functional groups in the soil structure component. The pozzolanic reaction expected happened over the curing period though it was not clearly resolved using FTIR and NMR.

Clay soil is known for its homogeneity in size, pores and retained controllable water. However, peat compounds contain several functional groups, and its chemical structure is hard to be visualised; chemical changes in peat are complex to explore and explain.

5.7 Case Study in Pontian, Johor, Malaysia

A case study was carried out in Pontian, Johor, Malaysia where three types of peat – fibric, hemic and sapric – were sampled, solidified and tested for strength (q_u), bacterial count and crystallite (using XRD) for curing in 7, 14, 28 and 56 days. Two mixing formulations were used following Rahman et al. (2015) for the two patterns of strengthening effects owned by solidified peat. Table 5.7 shows the mixed design for both formulations. This differentiates the chemical and biological reactions that happen when samples steadily increase in strength over the curing period (Mixing 1, M1) and samples that show increase in strength for curing days 7, 14 and 28 while decreasing its strength on day 56 (Mixing 2, M2).

Figures 5.7 and 5.8 show the pattern of bacterial counts and the strength of solidified peat over the curing period for both M1 and M2. In M1 bacteria are depleted but remain present in solidified peat; the depleted colony bears a strong relation with the strength. The stronger the solidified peat, the least bacteria count recorded and vice versa.

The finding from XRD showed that the amount of crystallite formed in solidified peat related with the strength of the sample (Fig. 5.9). The samples were found to be stronger when more crystallite formed and vice versa. The dominant crystal present in all samples was identified as pargasite ($NaCa_2[Mg_4Al](Si_6Al_2)O_{22}(OH)_2$) which

Table 5.7 Mixed design for solidified peat (Rahman et al. 2015)

	Fibric peat	Hemic peat	Sapric peat
Mixing 1	OPC with equal amount of dry peat FA 25% Addition of BA to give the coarse particle 23–34% of the total mixtures		
Mixing 2	w/b = 1 50% OPC 25% BA 25% FA	w/b = 3 50% OPC 50% BA	w/b = 3 50% OPC 50% BA

w/b water-to-binder ratio, *FA* fly ash, *BA* bottom ash, *OPC* ordinary Portland cement.

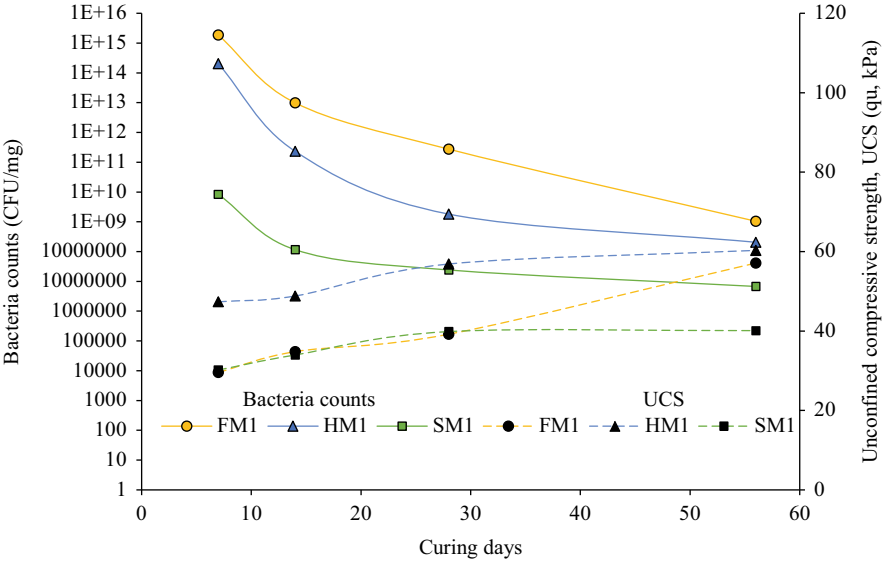

Fig. 5.7 Pattern of bacteria colony in peat and UCS – Mixing 1

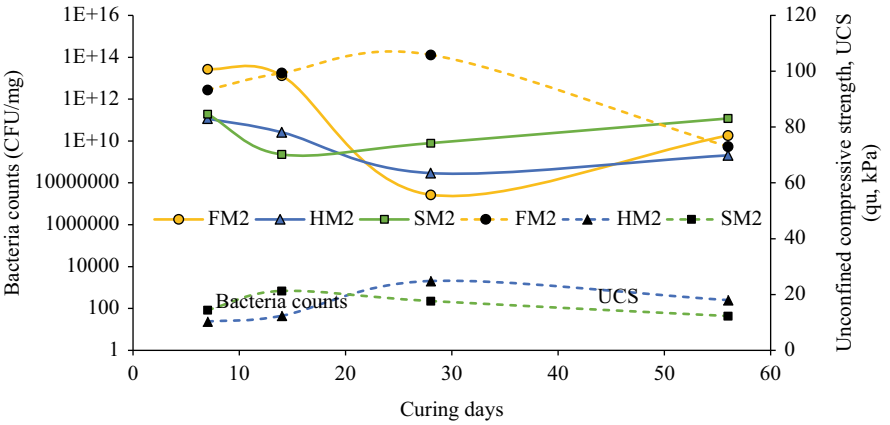

Fig. 5.8 Pattern of bacteria colony in peat and UCS – Mixing 2

has similar physical characteristics with ettringite ($Ca_6Al_2[(SO4)_3(OH)_{12}]$•(24 + 2) H_2O) that is normally found in solidified clay as a result of hydration processes.

The bacteria in this case study were identified as *Bacillus* sp. and were tested using cellulose agar. This medium allows bacteria secreting the enzyme cellulose to grow. The cellulose was monitored using Congo red, and bacterial activity was recorded, as shown in Table 5.8.

Peat solidification work highlights the formation of crystallite as the product of reaction between OPC, bottom ash (BA), fly ash (FA) and acidic peat. Since bacteria

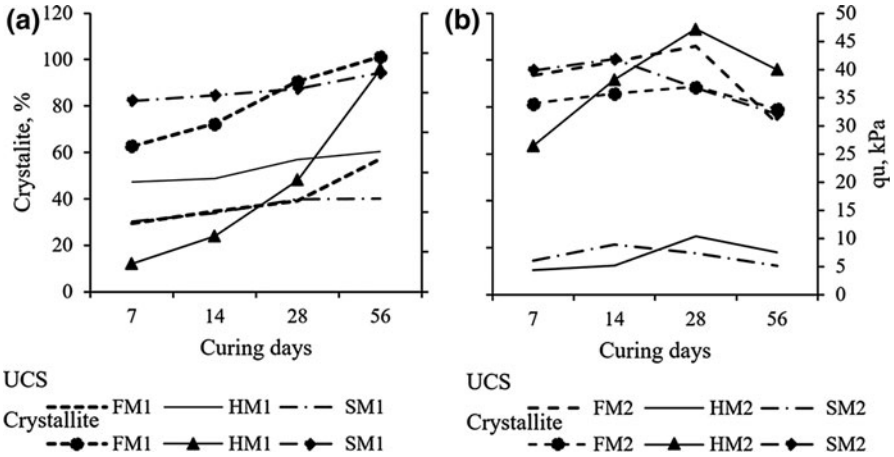

Fig. 5.9 Pattern of strength and percentage of crystallite formed over curing period for solidified peat using M1 and M2 formulations. (**a**) Strength and percentage of crystallite formed increase over curing period of solidified peat for Mixing 1. (**b**) Strength and percentage of crystallite formed increase for D7 and D14 but decrease on D28 and D56 for Mixing 2

Table 5.8 Enzyme activities in peat solidification study

		FM1	HM1	SM1	FM2	HM2	SM2
Halo zone	D7	–	++	++	+	+	+
	D14	–	++	++	–	–	+
	D28	–	++	+	–	–	–
	D56	–	+	–	+	+	+

Negative (–), positive (+), high production (++)

is abundantly present in the peat, the solidification work was not an absolute success as the enzyme secreted by the bacteria was found to dissolve the crystallite formed in M2. This phenomenon may be described using the Michaelis-Menten equation and was used by Cordero et al. (2019) and Sihi et al. (2019) to describe soil enzyme activity.

$$\underset{\text{(a substrate)}}{\text{Crystallite}} + \underset{\text{(an enzyme)}}{\text{cellulase}} \rightarrow \underset{\text{(a complex)}}{\text{weak solidified peat}}$$

$$\left(NaCa_2[Mg_4Al](Si_6Al_2)O_{22}(OH)_2\right) + \text{cellulase} \rightarrow \text{breakdown of} = O \text{ and} - OH^-$$

This finding helps engineers to understand the nature of peat before construction work. It contributes to environmental sustainability by limiting the trial and error during road and basement installation work.

5.8 Conclusion

It can be concluded that the effectiveness and dosage of binder type on the stabilisation of peat are site specific since the properties of peat differ from site to site. Furthermore, different types of peat react with different types of binder at certain binder dosage to achieve effective stabilisation. The unconfined compressive strength gain of the stabilised soil rose with an increase in binder dosage, filler and curing time, according to a review of numerous experimental examinations of stabilised peat. Most studies stop at this engineering finding with little knowledge exploration of cement hydration theory. The chemical reaction other than hydration theory is expected to be the main reason of peat solidification. The alteration of the chemical bond in solidified peat may lead to a new product finding with more cost-effective and cost-efficient solution.

Although it was previously estimated that microbial activity in peat is frozen during the stabilisation process, current research in concrete studies introduce self-healing concrete where microbes are used to react with chemicals from concrete to self-paste the leaking concrete. The concrete research used $CaCO_3$, the main element also found in OPC. This leads to a reaction between microbes and solidified peat being likely. The Michaelis-Menten equation was found to fit well with peat solidification work. Computational modelling may be developed beyond singular stochastic algorithms. Finally, different types of admixture could be proposed to find the pattern of enzymes reacting with induced chemicals in solidification. The study and nature of microbial activity in peat processes and its optimisation may well prove useful in use and transformation of land resources far into the future.

References

Abd Rahman J (2015) Relationship between decomposition level and induced solidification of peat based on laboratory investigation. Master Degree Thesis. Universiti Tun Hussein Onn Malaysia

Abo-El-Enein SA (2013) Application of microbial biocementation to improve the physico-mechanical properties of cement mortar. Housing and Building National Research Centre

Aerts R, Verhoeven JTA, Whigham DF (1999) Plant-mediated controls on nutrient cycling in temperate fens and bogs. Ecology 80(7):2170–2181. https://doi.org/10.2307/176901

Afifudin H, Hamidah MS, Noor Hana H et al (2011) Microbial participation in the formation of calcium silicate hydrated (CSH) from *Bacillus subtilis*. Procedia Eng 20:159–165. https://doi.org/10.1016/j.proeng.2011.11.151

Ahnberg H (2006) Consolidation stress effects on the strength of stabilised Swedish soils. Proc Inst Civ Eng Ground Improv 10(1):1–13. https://doi.org/10.1680/grim.2006.10.1.1

Ahnberg H, Ljungkratnz C Holmqvist L (1995) Deep stabilization of different types of soft soils. Proceedings XI ECSMFE, Copenhagen, 7:167–172, 28 May – 1 June 1995

Akol AK (2012) Stabilization of peat soil using lime as a stabilizer. Project Dissertation. Civil Engineering Programme Universiti Teknologi PETRONAS

Al-Ani H, Oh E, Chai G (2013) Engineering properties of peat in estuarine environment. In: 1st International Conference on Foundation and Soft Ground Engineering Challenges in Mekong Delta. 181–191. Thu Dau Mot University, Binh Duong City, Vietnam on June 5–6, 2013

Albert RA, Archambault J, Rossello-Mora R et al (2005) *Bacillus acidicola* sp. nov., a novel mesophilic, acidophilic species isolated from acidic sphagnum peat bogs in Wisconsin. Int J Syst Evol Microbiol 55(5):2125–2130. https://doi.org/10.1099/ijs.0.02337-0

Ali F, Wong LS, Hashim R (2010) Engineering properties of improved fibrous peat. Sci Res Essay 5(2):154–169

Al-Sadi AM, Al-Zakwani HA, Nasehi A et al (2016) Analysis of bacterial communities associated with potting media. Springerplus 5(1):74. https://doi.org/10.1186/s40064-016-1729-0

Alwi A (2008) Ground improvement of Malaysian peat soils using stabilized peat column techniques. PhD thesis, University of Malaya, Kuala Lumpur, Malaysia

American Coal Ash Association (2007) Coal combustion product (CCP) production and use survey. Available via www.acaa-usa.org. Accessed 13 Feb 2009

Andrew TCS, Syahrizal II, Jamaluddin MY (2012) Effective microorganisms for concrete (EMC) admixture–its effects to the mechanical properties of concrete. In: Awam International Conference on Civil Engineering (AICCE'12) Geohazard Information Zonation (GIZ'12), 28–30 Aug 2012

Andriesse JP (1988) Nature and management of tropical peat soils (No. 59). Food and Agriculture Organization

ASTM International (2005) ASTM Standards: Standards Test Methods and Definitions for Mechanical Testing of Steel Products (A370–02). American Society for Testing and Materials

ASTM (1990) 2607–69. Standard classification on peat, mosses, humus and related products (approved April 25, 1966) 1989 Annual Book of ASTM Standards. American Society for Testing and Materials

Ausec L, Kraigher B, Mandic-Mulec I (2009) Differences in the activity and bacterial community structure of drained grassland and forest peat soils. Soil Biol Biochem 41(9):1874–1881. https://doi.org/10.1016/j.soilbio.2009.06.010

Axelsson K, Johansson SE, Anderson R (2002) Stabilization of organic soils by cement and pozzolanic reaction-feasability study. Swedish Deep Stabilization Research Centre, Report 3, 1–51

Banadaki AD, Ahmad K, Ali N (2013) Influence of natural fillers on shear strength of cement treated peat. Gradevinar 65:633–640

Bang SS, Lippert JJ, Yerra U et al (2010) Microbial calcite, a bio-based smart nanomaterial in concrete remediation. Int J Smart Nano Mater 1(1):28–39. https://doi.org/10.1080/19475411003593451

Billong N, Melo UC, Louvet F et al (2009) Properties of compressed lateritic soil stabilized with a burnt clay-lime binder: effect of mixture components. Constr Build Mater 23:2457–2460. https://doi.org/10.1016/j.conbuildmat.2008.09.017

Boehm MJ, Madden LV, Hoitink HAJ (1993) Effect of organic matter decomposition level on bacterial species diversity and composition in relationship to pythium damping-off severity. Appl Environ Microbiol 59(12):4171–4179

Boelter DH (1968) Important physical properties of peat materials. Proceedings of the Third International Peat Congress. Quebec, Canada 150–156, 18–23 August 1968

Bragazza L, Siffi C, Iacumin P et al (2007) Mass loss and nutrient release during litter decay in peatland: the role of microbial adaptability to litter chemistry. Soil Biol Biochem 39(1):257–267. https://doi.org/10.1016/j.soilbio.2006.07.014

Caldarone MA (2014) High-strength concrete: a practical guide. CRC Press

Chahal N, Siddique R, Rajor A (2012) Influence of bacteria on the compressive strength, water absorption and rapid chloride permeability of fly ash concrete. J Constr Build Mater 28(1):351–356. https://doi.org/10.1016/j.conbuildmat.2011.07.042

Chen H, Wang Q (2006) The behaviour of organic matter in the process of soft soil stabilization using cement. Bull Eng Geo Environ 65(4):445–448. https://doi.org/10.1007/s10064-005-0030-1

Cordero I, Snell H, Bardgett RD (2019) High throughput method for measuring urease activity in soil. Soil Biol Biochem 134:72–77. https://doi.org/10.1016/j.soilbio.2019.03.014

Consoli NC, Zortéa F, De Souza M et al (2011) Studies on the dosage of fiber-reinforced cemented soils. J Mater Civ Eng:1624–1632. https://doi.org/10.1061/(ASCE)MT.1943-5533.0000343
Consoli NC, Rotta GV, Prietto PDM (2000) Influence of curing under stress on the triaxial response of cemented soils. Geotechnique. https://doi.org/10.1680/geot.2000.50.1.99
De Muynck W, Cox K, De Belie N et al (2008) Bacterial carbonate precipitation as an alternative surface treatment for concrete. J Constr Build Mater 22(5):875–885. https://doi.org/10.1016/j.conbuildmat.2006.12.011
Dhakal SK (2012) Stabilization of very weak subgrade soil with cementitious stabilizers. Master Degree Thesis Louisiana State University and Agricultural and Mechanical College, USA
Douglas PR (2004) Properties of self-consolidating concrete containing type F fly ash. Master Degree Thesis. Northwestern University, USA
El-Jazairi B, Illston JM (1977) A simultaneous semi-isothermal method of thermogravimetry and derivative thermogravimetry, and its application to cement plates. Cem Concr Res 7:247–258
Eisazadeh A, Kassim KA, Hadi H (2010) Physicochemical characteristics of phosphoric acid stabilized bentonite. Electron J Geotech Eng 15:327–355
Eisazadeh A, Kassim KA, Nur H (2012) Solid-state NMR and FTIR studies of lime stabilized montmorillonitic and lateritic clays. Appl Clay Sci 67:5–10. https://doi.org/10.1016/j.clay.2012.05.006
Fong SS, Murtedza M (2007) Chemical characterization of humic substances occurring in the peats of Sarawak, Malaysia. Org Geochem 38(6):967–976. https://doi.org/10.1016/j.orggeochem.2006.12.010
Ghosh P, Mandal S, Mandal BD et al (2005) Use of microorganism to improve the strength of cement mortar. J Cem Concr Res 35:1980–1983. https://doi.org/10.1016/j.cemconres.2005.03.005
Ghosh S, Biswas M, Chattopadhyay BD et al (2009) Microbial activity on the microstructure of bacteria modified mortar. J Cem Concr Comp 31(2):93–98. https://doi.org/10.1016/j.cemconcomp.2009.01.001
Green DH, Echavarri-Bravo V, Brennan D et al (2015) Bacterial diversity associated with the coccolithophorid algae *Emiliania huxleyi* and *Coccolithus pelagicus* f. *braarudii*. BioMed Res Int. https://doi.org/10.1155/2015/194540
Guanlin LI, Seongjun KIM, Minji PARK et al (2017) Short-term effects of experimental warming and precipitation manipulation on soil microbial biomass C and N, community substrate utilization patterns and community composition. Pedosphere 27(4):714–724. https://doi.org/10.1016/S1002-0160(17)60408-9
Hartford RA (1993) Smoldering combustion limits in peat as influenced by moisture, mineral content, and organic bulk density. Master Degree Thesis, University of Montana
Hartikainen T, Martikainen PJ, Olkkonen M et al (2002) Peat biofilters in long-term experiments for removing odorous sulphur compounds. Water Air Soil Pollut 133(1–4):335–348. https://doi.org/10.1023/A:1012966705004
Hashim R, Islam S (2008) A Model Study to Determine Engineering Properties of Peat Soil and Effect on Strength after Stabilization. Eur J Sci Res 2:205–215
Hebib S, Farell ER (2003) Some experiences on the stabilisation of Irish peats. Can Geotech J 40:107–120. https://doi.org/10.1139/t02-091
Higham DJ (2008) Modelling and simulating chemical reactions. SIAM Rev 50(2):347–368. https://doi.org/10.1137/060666457
Holden J, Chapman PJ, Labadz JC (2004) Artificial drainage of peatlands: hydrological and hydrochemical process and wetland restoration. Prog Phys Geogr 28(1):95–123. https://doi.org/10.1191/0309133304pp403ra
Horpibulsuk S (2012) Strength and microstructure of cement stabilized clay, scanning electron microscopy. InTech, ISBN: 978-953-51-0092-8
http://ppsj.johor.gov.my/johor-sepintas-lalu/maklumat-asas-negeri-johor (2018) Accessed 12 May 2021
Peat Society (2015). http://www.peatsociety.org. Accessed 12 May 2021

Huat BBK, Kazemian S, Prasad A et al (2011) A study of the engineering behavior of peat stabilized by DMM: lab model and FE analysis. Sci Res Essays J 6(1):196–204
Huat BBK (2004) Organic and peat soil engineering. University Putra Malaysia Press, Serdang
Huat BBK, Prasad A, Asadi A et al (2014) Geotechnics of organic soils and peat. CRC Press, London
Hunter WJ, Kuykendall LD, Manter DK (2007) *Rhizobium selenireducens* sp. nov.: a selenite-reducing α-proteobacteria isolated from a bioreactor. Curr Microbiol 55(5):455–460. https://doi.org/10.1007/s00284-007-9020-9
Islam MS, Hashim R (2010) Behaviour of stabilised peat: a field study. Sci Res Essays 5(17): 2366–2374
Islam S, Hashim R (2008) Stabilization of peat by deep mixing method: a critical review of the state of practice. Electron J Geotech Eng 13:1–9
Ismail N, Mohd Saman H, Kamaruddin K et al (2014) The cement hydration, chemical phases and its microstructural examination of microbed cement based material. In: 2014 IEEE Colloquium on Humanities, Science and Engineering Research (CHUSER 2014), Penang, Malaysia
Istina IN, Widiastuti H, Joy B et al (2015) Phosphate-solubilizing microbe from saprists peat soil and their potency to enhance oil palm growth and P uptake. Procedia Food Sci 3:426–435. https://doi.org/10.1016/j.profoo.2015.01.047
Ivanov V, Chu J (2008) Applications of microorganisms to geotechnical engineering for bioclogging and biocementation of soil in situ. Rev Environ Sci Biotechnol 7(2):139–153. https://doi.org/10.1007/s11157-007-9126-3
Ivarson KC (1977) Changes in decomposition rate, microbial population and carbohydrate content of an acid peat bog after liming and reclamation. Can J Soil Sci 57(2):129–137
Jamaludin M, Ismail YM, Rahman WA et al (2009) Performance of concrete containing effective microorganisms (EM) under various environments. In: Joint Conference of 7th Asia Pacific Structural Engineering and Construction Conference 2009 (APSEC2009) and 2nd European Asian Civil Engineering Forum (EACEF 2009), Malaysia
Janz M, Johansson S (2002) The function of different binding agents in deep stabilization. Report 9, Swedish Deep Stabilization Research Center, Linköping, Sweden. 1-47
Jonkers HM (2011) Bacteria-based self-healing concrete. Heron 56(1/2):1–12
Jonkers HM, Thijssen A, Muyzer G et al (2010) Application of bacteria as self-healing agent for the development of sustainable concrete. Ecol Eng 36:230–235. https://doi.org/10.1016/j.ecoleng.2008.12.036
Joshi S, Goyal S, Mukherjee A et al (2017) Microbial healing of cracks in concrete: a review. J Ind Microbiol Biotech 44(11):1511–1525. https://doi.org/10.1007/s10295-017-1978-0
Kalantari B, Prasad A, Huat BBK (2013) Cement and silica fume treated columns to improve peat ground. Arab J Sci Eng 38:805–816. https://doi.org/10.1007/s13369-012-0369-0
Karim MR, Zain MFM, Jamil M et al (2011) Strength development of mortar and concrete containing fly ash: A review. Int J Phys Sci 6(17):4137–4153
Karol RH (2003) Chemical grouting and soil stabilization, revised and expanded, vol 12. CRC Press
Karthik C, Rao RM (2016) Properties of bacterial-based self-healing concrete- A review. Int J ChemTech Res 9(2):182–188
Kazemian S, Huat BBK, Prasad A et al (2011a) A state of art review of peat: Geotechnical engineering perspective. Int J Phys Sci 6(8):1974–1981
Kazemian S, Huat BK, Prasad A et al (2011b) Effect of peat media on stabilization of peat by traditional binders. Int J Phys Sci 6(3):476–481
Kazemian S, Prasad A, Huat BB et al (2011c) Influence of cement–sodium silicate grout admixed with calcium chloride and kaolinite on sapric peat. J Civ Eng Manag 17(3):309–318. https://doi.org/10.3846/13923730.2011.589209
Kido Y, Nishimoto S, Hayashi H et al (2009) Effects of curing temperatures on the strength of cement-treated peat. International Symposium on Deep Mixing and Admixture Stabilization, Okinawa, 2009

Kim HK, Park SJ, Han JI et al (2013) Microbially mediated calcium carbonate precipitation on normal and lightweight concrete. J Constr Build Mater 38:1073–1082. https://doi.org/10.1016/j.conbuildmat.2012.07.040

Kip N, Van Winden JF, Pan Y et al (2010) Global prevalence of methane oxidation by symbiotic bacteria in peat-moss ecosystems. Nat Geosci 3(9):617–621. https://doi.org/10.1038/ngeo939

Koch W (1982) Findings with operation of biofilters for reduction of odourmtensive emissions. (original in German), Die Fleischmehl-Indusrtie. £, 165–175 (1982) in Domenico M.S. Delicato, Physical-Chemical Properties and Sorption Characteristics of Peat. PhD Thesis, Dublin City University

Kraigher B, Stres B, Hacin J et al (2006) Microbial activity and community structure in two drained fen soils in the Ljubljana Marsh. Soil Biol Biochem 38(9):2762–2771. https://doi.org/10.1016/j.soilbio.2006.04.031

Kucharski ES, Winchester W, Leeming WA et al (2005) Microbial biocementation. Patent Application WO/2006/066326; International Application No.PCT/AU2005/001927

Kyziol J (2002) Effect of physical properties and cation exchange capacity on sorption of heavy metals onto peats. Pol J Environ Stud 11(6):713–718

Liimatainen M, Voigt C, Martikainen PJ et al (2018) Factors controlling nitrous oxide emissions from managed northern peat soils with low carbon to nitrogen ratio. Soil Biol Biochem 122:186–195. https://doi.org/10.1016/j.soilbio.2018.04.006

Lindsay R, Birnie R, Clough J (2015) Impacts of artificial drainage on peatlands. IUCN UK Committee Peatland Programme Briefing Note No. 3. National Committee, United Kingdom

Liu J, Shi B, Jiang H, Huang H et al (2011) Research on the stabilization treatment of clay slope topsoil by organic polymer soil stabilizer. Eng Geol 117(1):114–120. https://doi.org/10.1016/j.enggeo.2010.10.011

Lorenz K, Lal R (2018) Carbon sequestration in wetland soils. In: Carbon sequestration in agricultural ecosystems. Springer, Cham. https://doi.org/10.1007/978-3-319-92318-5_5

Makusa GP (2012) Soil stabilization methods and materials in engineering practice. Lulea University of Technology, Lulea, Sweden

Mandic-Mulec I, Ausec L, Danevčič T et al (2014) Microbial community structure and function in peat soil. Food Technol Biotechnol 52(2):180–187

Mass Stabilization Manual (2005) Idea Chip and Ramboll Finland

McLaren AD, Peterson GH (1967) Introduction to the biochemistry of terrestrial soils. Soil Biochemistry 1:1–15

Mehta PK (1987) Natural pozzolans: Supplementary cementing materials in concrete. CANMET Special Publication 86:1–33

Mesri G, Ajlouni M (2007) Engineering properties of fibrous peats. J Geotech Geoenviron Eng 133:850–866. https://doi.org/10.1061/(ASCE)1090-0241(2007)133:7(850)

Mohamed M, Padmanabhan E, Mei BLH et al (2002) The Peat Soils of Sarawak. Strapeat- status report, University Malaysia Sarawak

Mousavi SE (2018) Utilization of silica fume to maximize the filler and pozzolanic effects of stabilized soil with cement. Geotech Geol Eng 36(1):77–87. https://doi.org/10.1007/s10706-017-0305-x

Muhardi Marto A, Kassim KA, Maktar AM et al (2010) Engineering characteristics of Tanjung Bin coal ash. Electron J Geotech Eng 15:1117–1129

Mutalib AA, Lim JS, Wong MH et al (1992) Characterization, distribution and utilization of peat in Malaysia. In: Aminudin BY (ed) Proceeding of the International Symposium on Tropical Peatland, Serdang: MARDI. 7-16. In: Mohamed M, Padmanabhan E, Mei BLH, Siong WB (2002). The Peat Soils of Sarawak. Strapeat- status report, Universiti Malaysia Sarawak

New York City Building Code (2008) Code Counsel, New York, U.S.A

New Zealand Building Code Requirements (2011) Bearing capacity and geotechnical investigation requirements for buildings. Gisborne District Council, New Zealand

Ng WS, Lee ML, Hii SL (2012) An overview of the factors affecting microbial-induced calcite precipitation and its potential application in soil improvement. World Acad Sci Eng Technol. https://doi.org/10.5281/zenodo.1084674

Novak M, Stepanova M, Buzek F et al (2018) The fate of 15 N tracer in waterlogged peat cores from two central european bogs with different N pollution history. Water Air Soil Pollut 229(3):70. https://doi.org/10.1007/s11270-018-3731-3

Konsultant PS (1998) Detailed Design and Construction Supervision of Flood Protection and Drainage Facilities for Balingian RGC Agricultural Development Project, Sibu Division, Sarawak (Inception Report). Department of Irrigation and Drainage, Kuching

Pradeep Kumar A, Akila D, Anestraj S, Arun S, Santhoshkumar A (2015) An experimental work on concrete by adding Bacillus Subtilis. Int J Emerging Technol Adv Eng 2(4):69–73

Rahman JA, Chan CM (2013) Influence of temperature on the mass losses of tropical peat at different decomposition level. In: Soft Soil Engineering International Conference

Rahman ZA, Lee JY, Rahim SA, Lihan T, Idris WMR (2015) Application of gypsum and fly ash as additives in stabilization of tropical peat soil. J Appl Sci 15(7):1006

Ramakrishnan V, Bang SS, Deo KS (1998) A Novel technique for repairing cracks in high performance concrete using bacteria. In: Proceedings of International conference on high performance high strength concrete. Perth, Australia, pp 597–518

Rao SM, Shivananda P (2005) Compressibility behaviour of lime-stabilized clay. Geotech Geol Eng 23(3):309–319. https://doi.org/10.1007/s10706-004-1608-2

Rashid ZA, Alias AB, Aris MJ et al (2010) Hazardous waste management: current status and future strategies in Malaysia. Int J Environ Eng 2(1):139–158. https://doi.org/10.1504/IJEE.2010.029825

Robert HK, Rober LK (1996) Treatment wetlands. Lewis Publishers, Boca Raton, New York

Romão LP, Lead JR, Rocha JC et al (2007) Structure and properties of Brazilian peat: analysis by spectroscopy and microscopy. J Braz Chem Soc 18(4):714–720. https://doi.org/10.1590/S0103-50532007000400008

Rong H, Qian CX, Li LZ (2012) Study on microstructure and properties of sandstone cemented by microbe cement. J Constr Build Mater 36:687–694. https://doi.org/10.1016/j.conbuildmat.2012.06.063

Rotta GV, Consoli NC, Prietto PDM et al (2003) Isotropic yielding in an artificially cemented soil cured under stress. Geotechnique 53(5):493–501. https://doi.org/10.1680/geot.2003.53.5.493

Rybicki E (1990) The classification of organisms at the edge of life, or problems with virus systematics. S Afr J Sci 86:182–186

Santagata M, Bobet A, Johnston CT et al (2008) One-dimensional compression behavior of a soil with high organic matter content. J Geotech Geoenviron Eng 134(1):1–13

Santamarina JC, Klein KA, Wang YH et al (2002) Specific surface area: determination and relevance. Can Geotech J 39:233–241. https://doi.org/10.1139/t01-077

Sihi D, Inglett PW, Inglett KS (2019) Warming rate drives microbial nutrient demand and enzyme expression during peat decomposition. Geoderma 336:12–21. https://doi.org/10.1016/j.geoderma.2018.08.027

Sposito G (2008) The chemistry of soils, 2nd edn. Oxford University press Inc

Stevenson FJ (1994) Humus chemistry: genesis, composition, reactions. Wiley

Tamburini D, Łucejko JJ, Zborowska M et al (2017) The short-term degradation of cellulosic pulp in lake water and peat soil: a multi-analytical study from the micro to the molecular level. Int Biodeterior Biodegradation 116:243–259. https://doi.org/10.1016/j.ibiod.2016.10.055

Report TBPP (2010) Malakoff Berhad. Johor, Malaysia

The Fly Ash Resource Center (2010) The fly ash resource center. Available via http://www.rmajko.com/flyash.html. Accessed 6 Apr 2010

Thrash JC, Coates JD (2011) Acidobacteriaceae fam. nov. Bergey's Manual of Systematic Bacteriology 4:728

Torkittikul P, Nochaiya T, Wongkeo W et al (2017) Utilization of coal bottom ash to improve thermal insulation of construction material. J Mater Cycles Waste Manag 19(1):305–317. https://doi.org/10.1007/S10163-015-0419-2

Tremblay H, Duchesne J, Locat J et al (2002) Influence of the nature of organic compounds on fine soil stabilization with cement. Can Geotech J 39(3):535–546. https://doi.org/10.1139/t02-002

USACE (1995) Chemical grouting [R]. US Army Corps of Engineers. Manual No. 1110-1-3500, Washington D C, USA

Van Hardeveld HA, Driessen PPJ, Schot PP et al (2017) An integrated modelling framework to assess long-term impacts of water management strategies steering soil subsidence in peatlands. Environ Impact Assess Rev 66:66–77

Wang KS, Lin KL, Lee TY et al (2004) The hydration characteristics when C_2S is present in MSWI fly ash slag. Cem Concr Res 26:323–330. https://doi.org/10.1016/j.jhazmat.2004.03.014

Williams RT, Crawford RL (1983) Microbial diversity of Minnesota peatlands. Microb Ecol 9(3): 201–214. https://doi.org/10.1007/BF02097737

Wolińska A, Stępniewska Z (2012) Dehydrogenase activity in the soil environment. In: Dehydrogenases. InTech

Wong LS (2015) Formulation of an optimal mix design of stabilized peat columns with fly ash as a pozzolan. Arab J Sci Eng 40(4):1015–1025. https://doi.org/10.1007/s13369-015-1576-2

Wong LS, Hashim R, Ali F (2008) Engineering behaviour of stabilized peat soil. Eur J Sci Res 21(4):581–591

Wong LS, Hashim R, Ali F (2009) Unconfined compressive strength of cemented peat. Aust J Basic Appl Sci 3(4):3850–3856

Wong LS, Hashim R, Ali F (2013a) Utilization of sodium bentonite to maximize the filler and pozzolanic effects of stabilized peat. Eng Geol 152(1):56–66

Wong LS, Hashim R, Ali F (2013b) Improved strength and reduced permeability of stabilized peat: focus on application of kaolin as a pozzolanic additive. Constr Build Mater 40:783–792. https://doi.org/10.1016/j.conbuildmat.2012.11.065

Wongsa A, Zaetang Y, Sata V et al (2016) Properties of lightweight fly ash geopolymer concrete containing bottom ash as aggregates. Constr Build Mater 111:637–643. https://doi.org/10.1016/j.conbuildmat.2016.02.135

Wösten JHM, Ismail AB, Van Wijk ALM (1997) Peat subsidence and its practical implications: a case study in Malaysia. Geoderma 78(1–2):25–36. https://doi.org/10.1016/S0016-7061(97)00013-X

Yonebayashi K, Okazaki M, Pechayapisit J et al (1994a) Distribution of heavy metals among different bonding forms in tropical peat soils. Soil Sci Plant Nutr 40(3):425–434. https://doi.org/10.1080/00380768.1994.10413320

Yonebayashi K, Pechayapisit J, Vijarnsorn P et al (1994b) Chemical alterations of tropical peat soils determined by Waksman's proximate analysis and properties of humic acids. Soil Sci Plant Nutr 40(3):435–444. https://doi.org/10.1080/00380768.1994.10413321

Žifčáková L, Větrovský T, Howe A et al (2016) Microbial activity in forest soil reflects the changes in ecosystem properties between summer and winter. Environ Microbiol 18(1):288–301. https://doi.org/10.1111/1462-2920.13026

Chapter 6
Green Energy Conversion Systems

Anand Kumar, Sachin Kumar, R. K. Saket, R. Rajendran, and Saeid Eslamian

Abstract This chapter develops a technological solution for waste management at the source. A device containing a soil microbial fuel cell (MFC) is designed for reliable renewable energy production using kitchen waste. The innovative methodology and constructed green energy conversion system produces 'eco-friendly' electricity by capturing energy produced by naturally occurring microbial metabolism of organic materials such as food scraps, manure and plant waste. Biomass that may be used includes municipal solid waste and agricultural by-products. The electricity generated by soil MFCs can be utilized immediately by USB devices. The developed system removes and sequesters carbon dioxide and methane gas, creating a clean, environmentally responsible supply of multiple power types. The overall process provides an option for current power generation and alleviates the need for

A. Kumar (✉)
Department of Electrical Engineering, Indian Institute of Technology Banaras Hindu University, Varanasi, Uttar Pradesh, India

Electrical Division, CSIR-National Aerospace Laboratories, Bangalore, Karnataka, India
e-mail: anand_kumarks@nal.res.in

S. Kumar · R. K. Saket
Department of Electrical Engineering, Indian Institute of Technology Banaras Hindu University, Varanasi, Uttar Pradesh, India
e-mail: sachinkumar.rs.eee18@itbhu.ac.in; rksaket.eee@itbhu.ac.in

R. Rajendran
Propulsion Division, CSIR-National Aerospace Laboratories, Bangalore, Karnataka, India
e-mail: raghavanrajendran@gmail.com

S. Eslamian
Department of Water Engineering, College of Agriculture, Isfahan University of Technology, Isfahan, Iran
e-mail: saeid@iut.ac.ir

J. N. Furze et al. (eds.), *Earth Systems Protection and Sustainability*,
https://doi.org/10.1007/978-3-030-98584-4_6

fossil fuels. Green energy conversion systems enable domestic power generation and create the possibility for reduced dependence on imports for energy needs.

Keywords Kitchen organic waste · Soil microbial fuel cell · Bioelectricity

6.1 Introduction

The microbial fuel cell (MFC) is a novel and sustainable approach to harvest electricity through a natural route. This green energy conversion system (GECS) utilizes organic-rich waste; predominantly carbohydrates are used as an electrolyte, and metabolic decay produces electrical energy (Logan and Regan 2006; Ren et al. 2014). The MFC couples with conventional electrochemical cells allowing the bio-catalytic action of microbes to harvest the bioelectricity. Potter (1911) proposed the concept of metabolic electricity, to draw electricity using exoelectrogens' bio-catalytic life (Borole et al. 2009). Recently the microorganism potential has emerged as a multi-dimensional technology due to its numerous advantages over conventional energy resources and existing waste treatment systems (Bond et al. 2002; Bond and Lovley 2003). MFC technology has received increased research interest in recent years because of its potential, particularly for bio-energy production and waste treatment (Hai et al. 2007). Microbial fuel cells are a novel addition to the inventory of alternative energy sources which have minimal or no net carbon dioxide emission (Shukla et al. 2004).

Electricity production using microbial cultures was first reported early last century by Potter (1911). MFCs have been described as bioreactors that convert energy in chemical bonds of organic compounds, into electrical energy through the catalytic activity of microorganisms under anaerobic conditions (Du et al. 2007). MFC technology represents a novel approach of using bacteria for the generation of bioelectricity by oxidation of organic waste and renewable biomass (Lovley 2006). In the MFC, the energy stored in chemical bonds in different organic compounds is indirectly converted into electrical energy through enzymatic reactions conducted by microorganisms (Kumar et al. 2016b). Exoelectrogenic bacteria commonly exist in the soil and can transfer electrons outside their cells through direct contact (Nicholls 1982; Kumar et al. 2016a). Most of the smallest and most interesting organisms on Earth are in the soil (Rabaey et al. 2004). The performance of MFCs depends on several factors, including microbial activity, substrate type, concentration and electrode material (Yong et al. 2014). Several factors can improve MFC performance to produce electricity (Moat et al. 2002; Kim et al. 2007; Yangyue et al. 2014). Determining which specific factors and conditions affect MFCs is crucial.

This chapter investigates an MFC in peat soil bioelectricity production, with organic kitchen waste being used as an electrolyte solution to moisturize the soil. Peat soils are widely found in southern Indian regions, local potential may be optimised for renewable electricity generation.

6.2 Microbial Use for Dual Purposes

Soil, manure or cow dung is beginning to attract research attention as suitable inoculums for MFCs designed for the dual purposes of remediation and electricity generation. This chapter explains and compares the fundamental design features of MFCs for waste management at the source level. Herein the concept has been targeted at generating electricity from peat soil and cow dung, utilizing microorganisms present in the ground and investigating the performance of the soil microbial fuel cell across varied external loads.

6.2.1 Soil Microbial Fuel Cell (SMFC) Design

The SMFC dimensions used in this study were 25 cm × 12 cm × 50 cm. The electrodes used in the unit were air cathodes of activated carbon and anodes of galvanized iron, which were round-shaped, installed sequentially, as shown in Fig. 6.1a, b.

The fuel cell contained a capacity of 2.5 kg of peat soil. The electrode's dimensions had a length of 25 cm and a radius of 2.5 cm. The fuel cell unit consisted of one positive electrode and one negative electrode.

The developed SMFC of Fig. 6.1 was used with the addition of 1 kg of organic waste, as shown in Fig. 6.2a, b.

Organic waste was added to the soil to increase humidity and supply nutrients, thereby increasing microbial populations. To investigate the effect of organic debris on the electricity generated, we measured the electrical potential of the SMFC for 30 days. Measurement of voltage and current was carried out every 24 hours. Voltage and current data are seen in Table 6.1.

Voltage and current generated using organic waste are higher than regular peat soil (contact authors for details). Organic waste contains minerals with positively

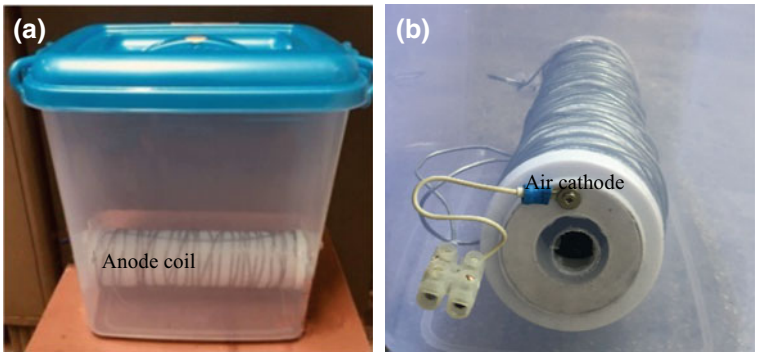

Fig. 6.1 Soil microbial fuel cell with: (**a**) anode coil; (**b**) air cathode

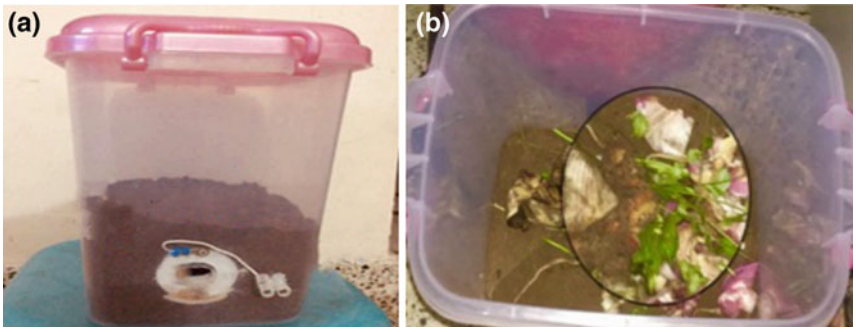

Fig. 6.2 Soil microbial fuel cell with: (**a**) peat; (**b**) kitchen wet waste

and negatively charged ions. Thus, the electrochemical process or change of chemical energy into electrical energy becomes significant because the electrodes become more conductive and less resistant. The SMFC contained 2.5 kg peat soil and 1 kg mixed organic waste which was obtained from kitchen sources in this study. An air vent system was fitted on the top side of the cover of the unit to trap moisture from the organic waste and release water as an electrolyte, increasing the humidity of soil (Wetser et al. 2015). Voltage and current are known to be higher in moist conditions (Reguera et al. 2006). The voltage and current generated from the SMFC in different ambient conditions were investigated. An ongoing objective of this and other studies is to determine the optimum conditions in which the SMFC produces voltage and current values (Mulyadi and Arsianti 2018; Sedighi et al. 2018; Truong et al. 2019; Lee et al. 2020), as shown in Fig. 6.3.

This study chose an SMFC with a boost converter circuit, to raise the generated voltage and current to a practical level.

6.2.2 Design of Boost Converter

The boost converter circuit was used to raise the direct current voltage level to a higher level direct current voltage produced by the SMFC. The circuit design is shown in Fig. 6.4a, b.

The SMFC was connected to a 3 W LED lamp load. The set parameters of the boost converter were output voltage 4.7 V, with efficiency (η) of 85%. The minimum voltage was 0.4–0.8 V. The duty cycle is determined using Eq. (6.1). The resultant calculation of our experiment is also shown.

$$D = 1 - \frac{V_{\text{in}}(\min) * \eta}{V_{\text{out}}} \tag{6.1}$$

Table 6.1 Soil microbial fuel cell voltage and current measured outdoors at ambient temperature for 30 days

Day	Open circuit voltage Volts (V)	Short circuit current density Amps (A)	Ambient temperature (°C)	Remarks
1	0	0	21	No voltage and current developed
2	0.16	2	25	Microamps
3	0.20	21	24	Microamps
4	0.30	100	21	Microamps
5	0.35	150	23	Microamps
6	0.40	200	21	Microamps
7	0.45	250	22	Microamps
8	0.49	350	21	Microamps
9	0.50	500	21	Microamps
10	0.56	700	26	Microamps
11	0.58	1	21	Milliamps
12	0.60	2	21	Milliamps
13	0.65	5	20	Milliamps
14	0.69	10	21	Milliamps
15	0.75	13	21	Milliamps
16	0.78	15	23	Milliamps
17	0.80	17	21	Milliamps
18	0.85	20	23	Milliamps
19	0.88	21	23	Milliamps
20	0.90	22	24	Milliamps
21	0.92	23	26	Milliamps
22	0.93	40	28	Milliamps
23	0.95	45	31	Milliamps
24	0.85	32	22	Milliamps
25	0.83	29	23	Milliamps
26	0.82	25	21	Milliamps
27	0.81	31	22	Milliamps
28	0.80	32	22	Milliamps
29	0.75	33	21	Milliamps
30	0.78	35	21	Milliamps

$$D = 1 - \frac{0.5^{*}0.8}{3.2}$$

$$D = 0.86718$$

The ripple current on the inductor load (I_L) can be obtained through Eq. (6.2):

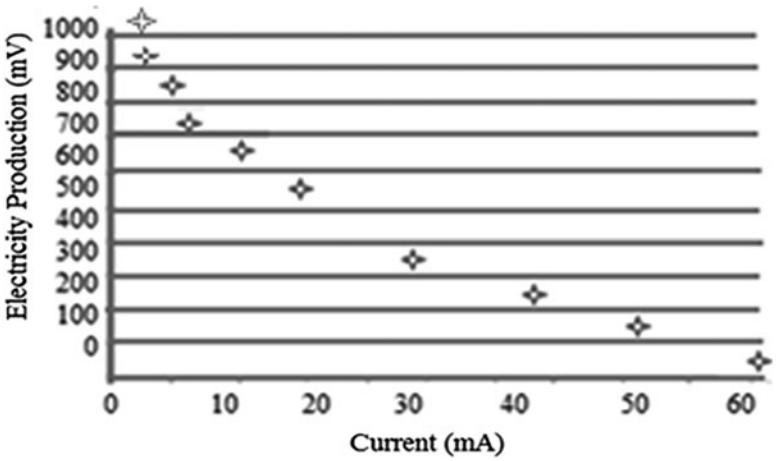

Fig. 6.3 Characteristic curve and electricity production measured as a function of voltage in millivolts (mV) and current in milliamps (mA)

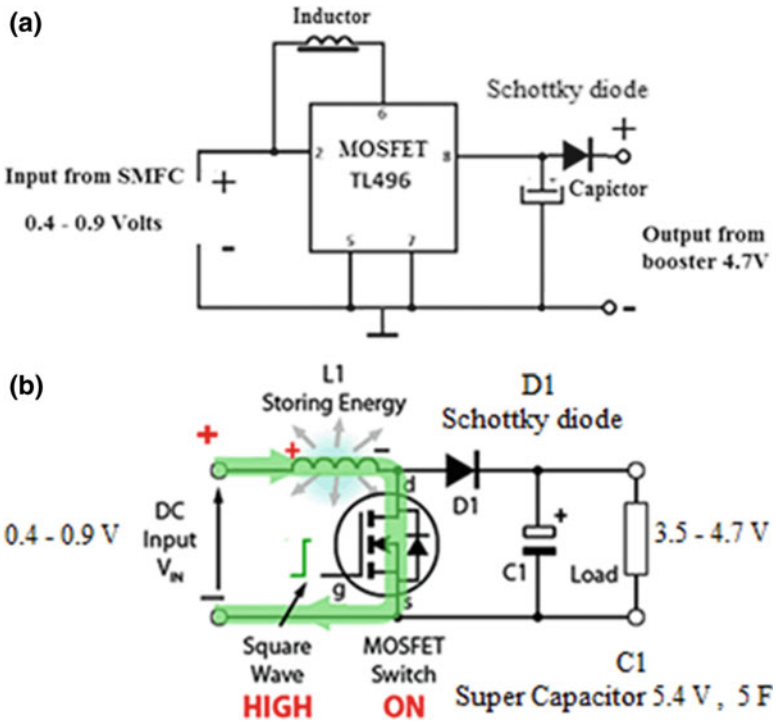

Fig. 6.4 Circuit diagram of the boost converter: (**a**) circuit representation; (**b**) direct current boosting and energy storage

$$\Delta I_L = \frac{V_{\text{in}} * (V_{\text{out}} - V_{\text{in}})}{L * \text{fs} * V_{\text{out}}} \tag{6.2}$$

where L is load of the inductor, fs is switching frequency and V_{in} and V_{out} are voltage in and out, respectively.

The ripple current on the inductor was obtained as shown in Eq. (6.3). A 940 micro-henry (μH) inductor was used in this circuit. A switching frequency of 20 kHz was used.

$$\Delta I_L = \frac{0.5 * (3.2 - 0.5)}{940 * 10^{-6} * 20 * 10^3 * 3.2}$$

$$\Delta I_L = 0.0224 \text{ Amps} \tag{6.3}$$

The capacitor value in the boost converter circuit can be obtained by using Eq. (6.4). The maximum output current (I_{OUT} max) was 0.25 A.

$$C_{\text{out (min)}} = \frac{I_{\text{out (max)}} * D}{\text{fs} * V_{\text{out}}} \tag{6.4}$$

$$C_{\text{out (min)}} = \frac{0.25 * 0.8671}{20 * 10^3 * 3.2}$$

$$C_{\text{out (min)}} = 3.3874 \text{ μF}$$

6.2.3 *Experimental Test of the Soil Microbial Fuel Cell*

The SMFC with a booster circuit was tested for transfer of the electrical loads. The SMFC with booster circuit schemes can be seen in Fig. 6.5.

Figure 6.6a–c shows the SMFC with a 3 W USB LED lamp, 1 W USB LED light and 1 W USB fan, respectively, demonstrating the versatility and potential uses of the system.

6.3 Results and Discussion of Soil Microbial Fuel Systems: Potential for Membership in Renewable Energy Mixes

We investigated the performance of the SMFC with the 3 W LED lamp load for 7 days. Measurement of the generated voltage and current by the SMFC was taken daily at 10-minute intervals for 1800 minutes. The voltage and current data

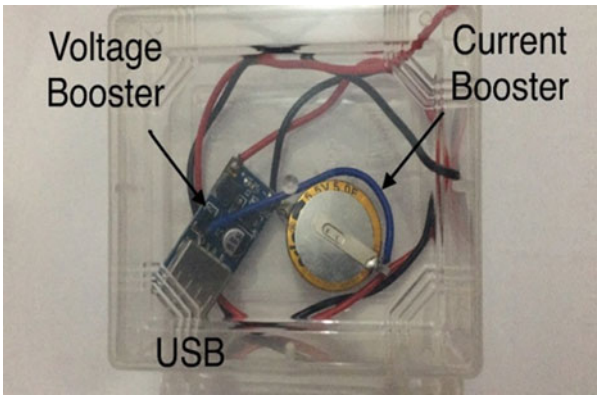

Fig. 6.5 Voltage and current boost converter

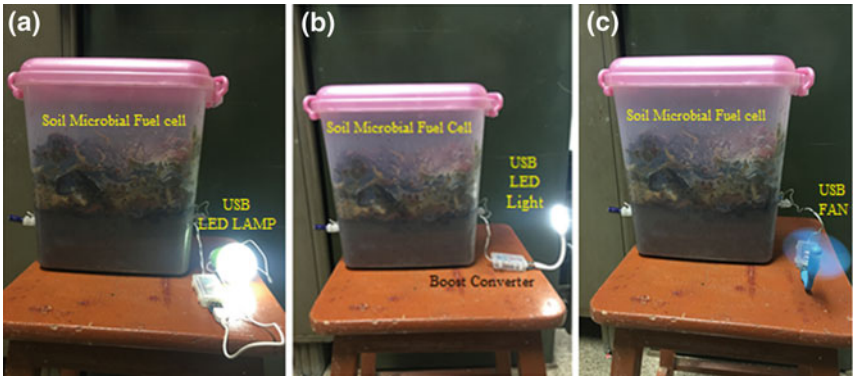

Fig. 6.6 Electrical loads powered by the soil microbial fuel cell: (**a**) a 3 W USB LED lamp; (**b**) a 1 W USB LED light; (**c**) a 1 W USB fan

generated by SMFC can be seen in Figs. 6.7 and 6.8. The output voltage generated by the SMFC in the first minute reached 1.00 V. This was the peak voltage generated by the SMFC with no load. The voltage value reached stability at 0.58 V in 120 minutes duration. The load voltage continued to be stable at 0.29 V until the seventh day at 1800 minutes. The boost converter circuit increased the SMFC load voltage from 0.29 V to 3.7 V.

Example data of the voltage of the SMFC can be seen in Fig. 6.7. Example data of the SMFC current measurement for 7 days can be seen in Fig. 6.8. In the first minutes, the current produced by the SMFC was 45 mA under a short circuit. The current continued to supply to the load for 7 days, the peak current of the SMFC under load was 23 mA.

The electricity power generated by the SMFC is shown in Fig. 6.9. The maximum power of the SMFC with no load was 17 mW. Electricity generated decreased. However, the SMFC's electrical power lasted up to 1800 minutes; the minimum value produced without load was 11.98 mW and 5.11 mW with load.

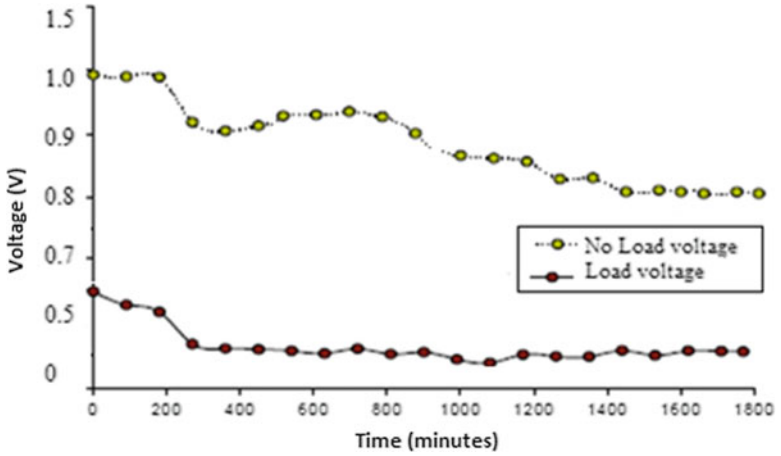

Fig. 6.7 The soil microbial fuel cell power generation

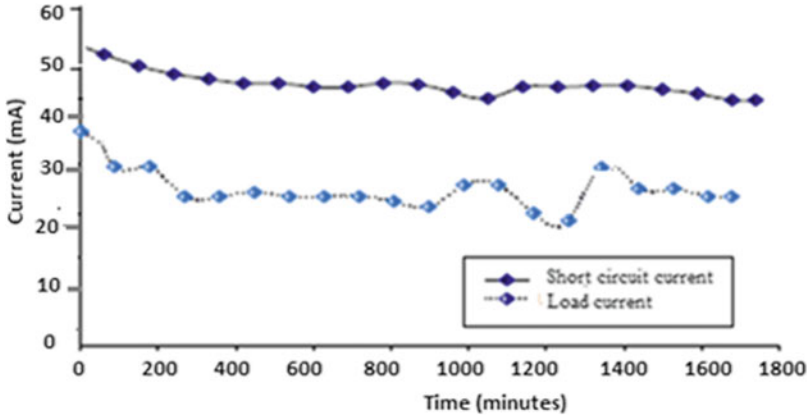

Fig. 6.8 Short circuit current and load current density of the soil microbial fuel cell

Although the substrate retrieval interval requires measurement, organic compound content and capacity to generate power decrease due to continual microbial degradation. Further, incremental internal resistance caused the decline in electricity generated by the SMFC. Using a conventional battery voltage source, the output of the LED lamp light intensity was 270 lumens; when powered by the SMFC it was 26 lumens in the first minute. Using a 3.7 V lithium-ion battery, the LED lamps lit up for 1500 minutes with a minimum light strength of 32 lumens; the SMFC powered the LED lights for up to 900 minutes with a last-minute light intensity of 25 lumens. The light intensity achieved with the SMFC is seen in Fig. 6.6a. The output of light produced is strongly influenced by voltage and current of the source.

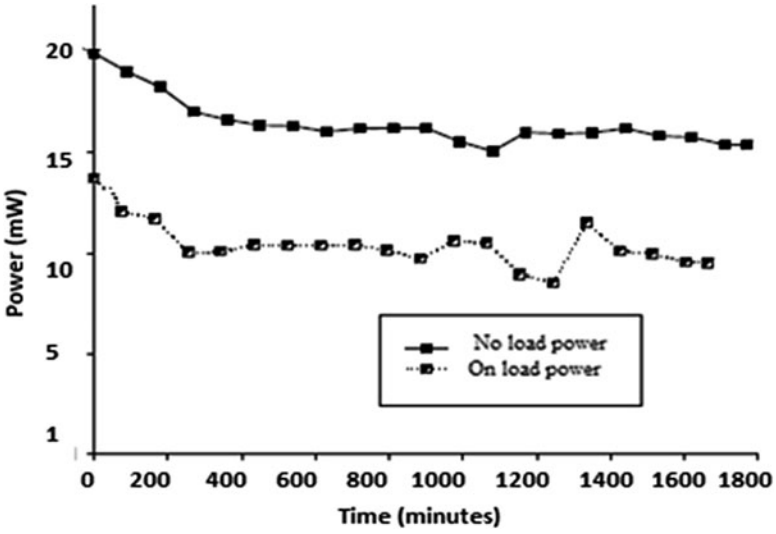

Fig. 6.9 Power delivered by the soil microbial fuel cell with and without load demand

The voltage and current generated by the SMFC were 0.50 V and 36 mA. The current produced by the SMFC was half of the current obtained by the battery source. This caused the light intensity produced by SMFCs to be lower. The SMFC may be proposed as a renewable energy mechanism for hybrid street lights, emergency lamps, USB device chargers, mobile chargers and remote areas that have not obtained an electrical network (Shantaram et al. 2005).

6.4 Conclusion

The present chapter demonstrated a prototype SMFC, an activated carbon block-based microbial fuel cell that used a kitchen based organic waste with soil: biodegradable hydrocarbon contaminant assisted bioelectricity generation. On average, a 250 mW/m^2, 550 mV increase in energy production efficiency resulted from the use of biodegradable contaminants. This study indicates that the SMFC is feasible for the treatment of organic waste contaminants. The SMFC with the current booster circuit can produce stable electricity of 17.2 mW and can power LED lights for 90 minutes with the highest and the lowest light intensity of 260 lumens and 12 lumens, respectively. Future work should investigate the composition of microbial communities with differing substrate addition to effect electrical power generation. The SMFC can be proposed as an alternative renewable energy mechanism under bio-energy. The SMFC is effective with low cost and simple maintenance, and may be used to produce low-power electricity for public street lighting or domestic settings. The importance of bioelectricity generation in treating complex and

recalcitrant compounds of organic waste has been illustrated. Biodegradation effected a range of high power output to low power output. The data of voltage and current measured from the analysis of SMFC for 30 days analysis also illustrates the sustainable capacity of SMFCs. SMFCs may be optimised in terms of their microbial populations. Green energy conversion systems hold great potential for future power generation.

References

Bond DR, Holmes DE, Tender LM et al (2002) Electrode-reducing microorganisms that harvest energy from marine sediments. Science 295:483–485. https://doi.org/10.1126/science.1066771

Bond DR, Lovley DR (2003) Electricity production by *Geobacter sulfurreducens* attached to electrodes. Environ Sci Technol 69(3):1548–1555. https://doi.org/10.1128/aem.69.3.1548-1555.2003

Borole AP, Hamilton CY, Vishnivetskaya T et al (2009) Improving power production in acetate-fed microbial fuel cells via enrichment of exoelectrogenic organisms in flow-through systems. Biochem Eng J 48(1):71–80. https://doi.org/10.1016/j.bej.2009.08.008

Du Z, Li H, Gu T (2007) A state of the art review on microbial fuel cells: a promising technology for wastewater treatment and bioenergy. Biotechnol Adv 25:464–482. https://doi.org/10.1016/j.biotechadv.2007.05.004

Hai FI, Yamamoto K, Fukushi K (2007) Hybrid treatment systems for dye wastewater. Crit Rev Environ Sci Technol 37(4):315–377. https://doi.org/10.1080/10643380601174723

Kim BH, Chang IS, Gadd GM (2007) Challenges in microbial fuel cell development and operation. Appl Microbiol Biotechnol 76:485–494. https://doi.org/10.1007/s00253-007-1027-4

Kumar R, Singh L, Wahid ZA (2016a) Exoelectrogens: recent advances in molecular drivers involved in extracellular electron transfer and strategies used to improve it for microbial fuel cell applications. Renew Sust Energ Rev 56:1322–1336. https://doi.org/10.1016/j.rser.2015.12.029

Kumar R, Singh L, Zularisam AW et al (2016b) Potential of porous Co3O4 nanorods as cathode catalyst for oxygen reduction reaction in microbial fuel cells. Bioresour Technol 220:537–542. https://doi.org/10.1016/j.biortech.2016.09.003

Lee M, Kondaveeti S, Jeon T et al (2020) Influence of humidity on performance of single chamber air-cathode microbial fuel cells with different separators. PRO 8. https://doi.org/10.3390/pr8070861

Logan BE, Regan JM (2006) Electricity producing bacterial communities in microbial fuel cells. Trends Microbiol 14(12):512–518. https://doi.org/10.1016/j.tim.2006.10.003

Lovley DR (2006) Bug juice: harvesting electricity with microorganisms. Nat Rev Microbiol 4:497–508. https://doi.org/10.1038/nrmicro1442

Moat AG, Foster JW, Spector MP (eds) (2002) Microbial physiology, 4th edn. Wiley, New York

Mulyadi, Arsianti RW (2018) Low power electrical generator from soil microbial fuel cell. 2018 Electrical Power, Electronics, Communications, Controls and Informatics Seminar (EECCIS). https://doi.org/10.1109/EECCIS.2018.8692948

Nicholls DG (1982) Bioenergetics – an introduction to the chemiosmotic theory. Academic Press, London

Potter M (1911) Electrical effects accompanying the decomposition of organic compounds. Proc R Soc Lond B 84:260–276. https://doi.org/10.1098/rspb.1911.0073

Rabaey K, Boon N, Siciliano D et al (2004) Biofuel cells select for microbial consortia that self-mediate electron transfer. Appl Environ Microbiol 70(9):5373–5382. https://doi.org/10.1128/AEM.70.9.5373-5382.2004

Reguera G, Nevin KP, Nicoll JS et al (2006) Biofilm and nanowire production leads to increased current in *Geobacter sulfurreducens* fuel cells. Appl Environ Microbiol 72(11):7345–7348. https://doi.org/10.1128/AEM.01444-06

Ren L, Ahn Y, Logan BE (2014) A two-stage microbial fuel cell and anaerobic fluidized bed membrane bioreactor (MFC-AFMBR) system for effective domestic wastewater treatment. Environ Sci Technol 48(7):4199–4206. https://doi.org/10.1021/es500737m

Sedighi M, Aljlil SA, Alsubei MD et al (2018) Performance optimisation of microbial fuel cell for wastewater treatment and sustainable clean energy generation using response surface methodology. Alex Eng J 57(4):4243–4253. https://doi.org/10.1016/j.aej.2018.02.012

Shantaram A, Beyenal H, Veluchamy R et al (2005) Wireless sensors powered by microbial fuel cells. Environ Sci Technol 39:5037–5042. https://doi.org/10.1021/es0480668

Shukla A, Suresh P, Berchmans S et al (2004) Biological fuel cells and their applications. Curr Sci 87:455–468

Truong VM, Duong NB, Wang CL et al (2019) Effects of cell temperature and reactant humidification on anion exchange membrane fuel cells. Materials (Basel) 12(13):2048. https://doi.org/10.3390/ma12132048

Yangyue J, Xu Y, Yang Q et al (2014) Power generation using polyaniline/multi-walled carbon nanotubes as an alternative cathode catalyst in microbial fuel cells. Int J Energy Res 38:1416–1423. https://doi.org/10.1002/er.3155

Yong XY, Feng J, Chen YL et al (2014) Enhancement of bioelectricity generation by cofactor manipulation in microbial fuel cell. Biosens Bioelectron 56:19–25. https://doi.org/10.1016/j.bios.2013.12.058

Wetser K, Sudirjo E, Buisman CJN et al (2015) Electricity generation by a plant microbial fuel cell with an integrated oxygen reducing biocathode. Appl Energy 137:151–157. https://doi.org/10.1016/j.apenergy.2014.10.006

Chapter 7
Flood Risk Estimation and Mapping: Present Status and Future Challenges

Mohit Prakash Mohanty and Subhankar Karmakar

Abstract Several regions of the globe are projected to experience elevated risks from flooding attributable to concomitant climate change and alterations in socio-economic dynamics. These impacts present major challenges to comprehensively quantify flood risk, which will facilitate building flood mitigation infrastructures, improve land use/urban planning, and assist the prioritization of emergency response strategies. Flood risk is built on two major components, namely, *hazard* and *vulnerability*. Most research conducted so far on vulnerability is limited to themes, such as physical, economic, and infrastructure vulnerabilities, and has frivolously excluded social vulnerability. Such works are solely based on a technocratic perspective rather than from a socio-technocrat's perspective. It is a fact that social vulnerability is less amenable to quantification because it is linked to the resilience of an individual, a community, or a society, which is acquired as a result of their perception, attitude, and coping capacity. The procedures for flood risk mapping are data-intensive, posing a difficulty in generating maps for middle- and low-income nations. Essentially, flood risk mapping is truly multidisciplinary in nature and requires inputs from engineers, social scientists, policymakers, and the general public.

Keywords Climate change · Flood risk · Hazard · Riverine flooding · Vulnerability

M. P. Mohanty
Department of Water Resources Development and Management, Indian Institute of Technology Roorkee, Roorkee, India
e-mail: mohit2012.env@gmail.com

S. Karmakar (✉)
Centre for Environmental Science and Engineering (CESE), Inter Disciplinary Program in Climate Studies, Centre for Urban Science & Engineering (C-USE), Indian Institute of Technology Bombay, Mumbai, India
e-mail: skarmakar@iitb.ac.in; subhankar.karmakar@gmail.com

J. N. Furze et al. (eds.), *Earth Systems Protection and Sustainability*,
https://doi.org/10.1007/978-3-030-98584-4_7

7.1 Introduction

Floods continue to affect more nations than before and cause widespread human and economic damages with each passing year (Blaikie et al. 2014; Dottori et al. 2016; Vousdoukas et al. 2018). With the statistics documented in various global reports on natural disasters such as Centre for Research on the Epidemiology of Disasters (CRED) (https://www.cred.be/), International Federation of Red Cross and Red Crescent Societies (IFRC) (https://media.ifrc.org/ifrc/), The International Charter Space and Major disasters (https://disasterscharter.org/web/guest/home), The United Nations office for disaster risk reduction (UNDRR) (https://www.unisdr.org/), and The Global Flood detection system (http://www.gdacs.org/flooddetection/overview.aspx) and a plethora of notable research articles (Alfieri et al. 2015a, b; Berghuijs et al. 2017), it is now a well-established fact that the occurrence (frequency) and severity (socioeconomic losses and human death count) of floods have escalated in the recent decades.

Among other factors, the concomitant climate change and booming urbanization are identified as the root causes to the rising flood risk. The projected precipitation changes from regional and global climate models indicate a possible rise in the frequency of extreme precipitation. This is observed in the tropical regions and high latitudes and mid-latitudes of northern regions in winter (IPCC 2012). Pall et al. (2011) and Schiermeier (2011) reported that anthropogenic greenhouse gas emissions contribute to the increasing severity of flood risk. Also, rising sea levels and land subsidence due to climate change may influence future flood risk in coastal urban cities (Hallegatte et al. 2013; Jonkman 2013). The second root cause of increased flood risk is rising urbanization. Moreover, it is highlighted that if economic and infrastructural damages due to flood disasters can be recovered in the short term, social damages may be irreparable. Hence, economically poor countries with a low gross domestic product (GDP) may find it extremely difficult to cope with such disasters due to low resilience. Keeping these various things in mind, the present chapter highlights the practiced ways of flood risk estimation and mapping. The chapter also describes the major challenges associated with flood risk estimation while considering its two vital components, i.e., hazard and vulnerability, and the exigent need of considering a system that provides an equal weightage to them in the flood risk estimation (Bohle 2001). The importance of the new flood risk mapping approach is demonstrated on a severely flood-prone region residing inside a large river basin in India.

7.2 Flood Risk Management: A Risk-Based Approach to Managing Floods

Flood risk management is a complex decision-making process. Recent decades have diverted the conventional "flood management" to "flood risk management" approach in which flood risk analysis exists in the core (Schanze 2006). Under flood risk management, there are three major tasks: flood risk analysis, flood risk assessment, and flood risk reduction. These components are described in the subsequent subsections. The basic framework of flood risk management is given in Fig. 7.1.

7.2.1 Flood Risk Analysis

Flood risk analysis considers the past, current, and possible future risks associated with the community and environment (Apel et al. 2009). It is built on two major components: *flood hazard* and *vulnerability* (Apel et al. 2004; Kron 2005; Gotham et al. 2018). Narayan et al. (2011) proposed a Source-Pathway-Receptor-Consequence-Model (SPRC-Model) to demonstrate the flood risk system as illustrated in Fig. 7.2. The chain links physical processes, namely, "source," "pathway," and "receptor" with the societal values "consequence." Within the context of flood risk, "source" and "pathway" indicate the flood hazard. Here "source" is quantified as the probability (p) of an event to occur and several other features (m). To minimize the risk, early warning system (w) and the adaptive capacity (t) are considered vital. The "pathway" is defined by the inundation which can arise from

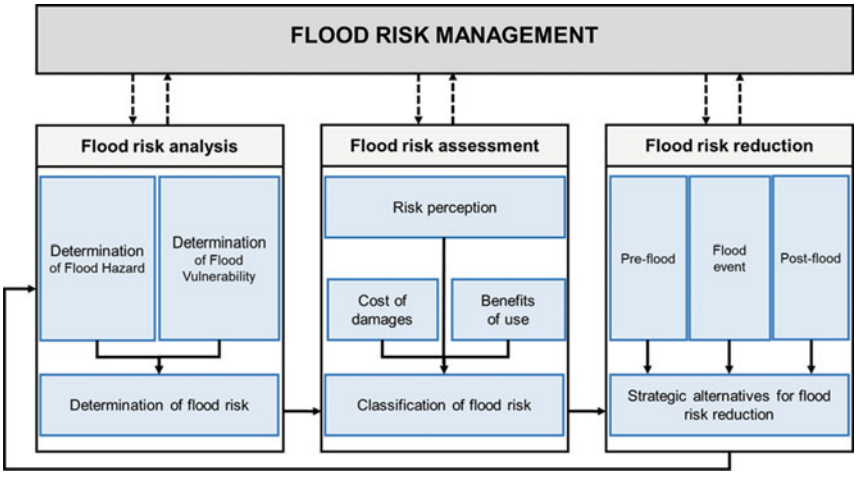

Fig. 7.1 Basic framework of flood risk management

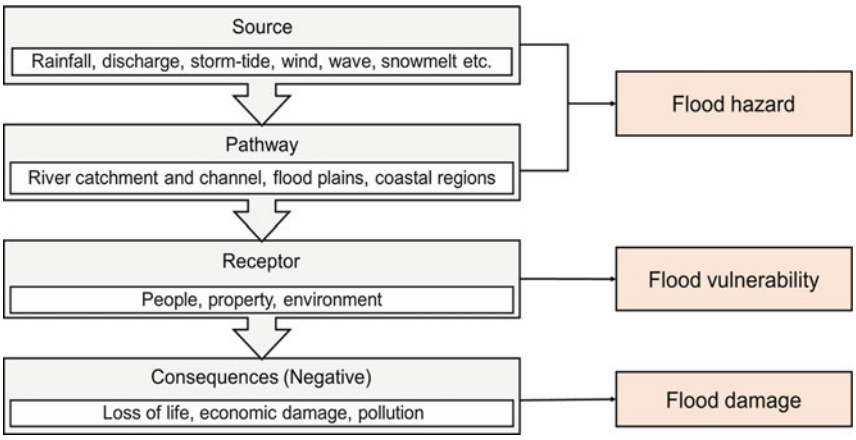

Fig. 7.2 Source-Pathway-Receptor-Consequence-Model (SPRC-Model). (Narayan et al. 2011)

various flood drivers such as discharge overflow, coastal impacts, and others (i), along with their attributes (a) and interventions available if any for flood control (c). Lastly, "receptor" is defined by the susceptibility (s) depending on the resistance and resilience (r) of the system. "Consequence" is nothing but the damage (v) with possible options to eliminate or reduce (d). Mathematically, flood risk can be expressed by the following equation:

$$\text{Flood risk} = f\left\{(p,m,w,t)_{\text{source}}, (i,a,c)_{\text{pathways}}, (s,r)_{\text{receptors}}(v,d)_{\text{consequences}}\right\} \quad (7.1)$$

7.2.2 *Flood Risk Assessment*

There are two relevant areas on which flood risk assessment is defined. They are *risk perception and risk weighing*. *Risk perception* is defined by the individual and collective backgrounds of the population facing the risk and those groups who are involved in flood risk management (Miceli et al. 2008; Ludy and Kondolf 2012; Cheikh Lounis et al. 2015).

For instance, a population who have the experience of facing the flood before are more likely to have a different perception of flood risks than those who have not faced it earlier (Grothmann and Reusswig 2006). A straightforward understanding of risk perception is complex, as it is multifaceted.

7.2.3 Flood Risk Reduction

Flood risk reduction is normally practiced through structural and nonstructural measures. In the timeline of risk reduction, they can be defined by *pre-flood, flood event, and post-flood* measures. *Pre-flood* is achieved by prevention, protection, and preparedness before any anticipated flood event by building retention ponds, flood plain zoning, and resilient building construction and creating awareness among people likely to face risk. *Flood event* measure consists of accurate flood forecasting and disseminating flood warning signals to provide information to people at risk. Lastly, *post-flood* measures consist of rebuilding and reconstruction of the damages that occurred after a flood event.

7.2.4 Flood Inundation and Hazard Mapping

Flood inundation is the result of the appearance of floodwater characterized by a specific areal extent, depth, and duration (Bates and De Roo 2000; Bates 2004). This inundation gives rise to flood hazard which is decided based on several factors. It is usually defined as the probability of occurrence of an event of a certain magnitude at a given time and space (Chakraborty et al. 2005). As per Peck et al. (2007) and Karmakar et al. (2010), flood hazard is identified as a probabilistic component, which calls for hydrological analyses and preparation of flood lines. As per Alcantara-Ayala (2002), a hazard is defined as those events capable of incurring damage to the physical and social structure through loss or injuries to human lives, damages to properties, or environmental degradation. A flood hazard map is an important component for appropriate landscape planning as it provides a piece of precise information on the areas prone to different degrees of flood impacts. Such maps can be prepared using various flood methods/models which can be (i) simplified, which can utilize the basin's geomorphology, or (ii) hydrodynamic, which is based on St. Venant's equations for deriving flood hazard areas.

7.2.4.1 Quantification of Flood Hazard

Flood hazard is defined as a function of both flood severity and probability. Flow depth "*d*" and velocity "*f*" are the two main attributes of flood severity, which can be obtained by performing flood inundation modeling. There are several standards that have defined the combination of floodwater depth and velocity into different hazard classes. Most well-known methods are the UK method, Australian method, Austrian method (Fiebiger 1997), the US Bureau of Reclamation method (USBR 1988), and the Swiss method (OFEE 1997). The widely accepted UK and Australian methods consider hazard as a combination of flood depth and velocity. On the contrary, the Austrian method considers the total energy defined as "$d + f^2/2g$," where d is the

Table 7.1 Classification of flood hazard based on the criteria of floodwater depth "*d*" and/or product of floodwater depth and velocity "$d \times f$" in different methods

Flood hazard						
Flood hazard rating	Hazard description	The UK method	Australian method	Austrian method	The US Bureau of Reclamation method	Swiss method
Very Low Hazard	Generally safe for people, vehicles, and buildings	0 to 0.3 m^2/s	0 to 0.3 m^2/s	0 to 3 m	0 to 3	0 to 0.5 m^2/s
Low Hazard	Unsafe for vehicles, children and the elderly	0.3 to 0.7 m^2/s	0.3 to 0.6 m^2/s			
Moderate Hazard	Unsafe for people and vehicles	0.7 to 1.2 m^2/s	0.6 to 1.0 m^2/s			0.5 to 2 m^2/s
High Hazard	Unsafe for vehicles and people. All buildings are vulnerable to structural damage. Some less robust building types vulnerable to failure.	1.2 to 1.6 m^2/s	1.0 to 4.0 m^2/s	>3 m	>3	>2 m^2/s
Very High Hazard	Unsafe for vehicles and people. All building types considered vulnerable to failure	>1.6 m^2/s	>4 m^2/s			

flood water depth, f is the velocity, and g is the gravitational acceleration. The USBR method considers hazard as a combination of depth and velocity. A description of hazard classes and their significance is provided in Table 7.1. Currently, there are very few works on riverine flood hazard mapping that apply both coupled flood modeling and hazard ranking. Figure 7.3 describes the representative past efforts on riverine flood inundation and flood hazard mapping.

7.2.4.2 Geomorphic Approaches

Although several models/software are available for quantifying inundation, their use may be restricted due to several reasons. The limitations are (i) scarcity of extensive data inputs required for precise flood modeling, (ii) fizzling performance of models in large and complex terrains, (iii) high computational cost and time, and (iv) inexpertise in handling model simulations by civic bodies. Recent studies have made use of linear binary classification techniques (Manfreda et al. 2014, 2015; Manfreda and Samela 2019) which are easy to use, computationally inexpensive, and easy compared to the hydrodynamic approach. These classifiers are used to

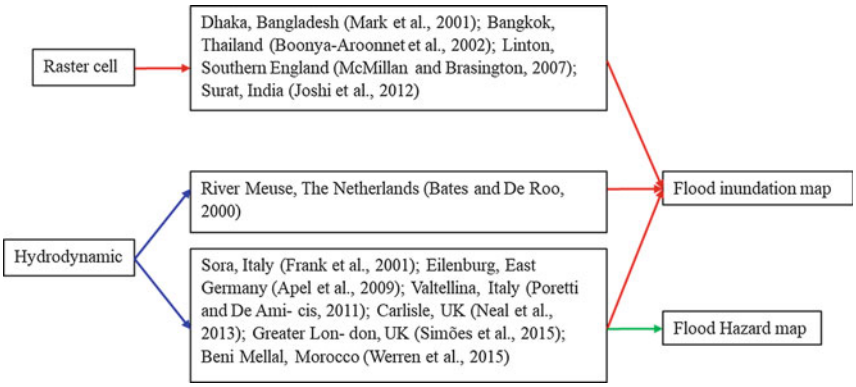

Fig. 7.3 Representative past efforts made on coupled 1D-2D flood inundation/hazard mapping

delineate flood hot-spots (flood-prone areas) based on the information contained in the study bathymetry. Table 7.2 enlists recent efforts made to map flood hazards through geomorphic classifiers.

7.2.5 Flood Vulnerability Mapping

The word "vulnerability" is derived from the Latin word *vulnus*, which means *to wound* (Turner et al. 2003). As per Adger (2006) and Füssel (2007), vulnerability may be expressed as a combination of three components: adaptive capacity, sensitivity, and exposure. Adaptive capacity is the ability of a system to fine-tune to actual or expected climate stresses. Sensitivity is the degree to which a system will respond to alterations, whereas exposure is the extent to which people and assets are exposed to hazards. Figure 7.4 portrays the various spheres of vulnerability theme as described by various researchers.

7.2.5.1 Various Approaches to Flood Vulnerability Assessment

Figure 7.5 illustrates a generic framework for the assessment of flood vulnerability. Once the geospatial data collection for the indicators is completed, statistical operations are performed to obtain an index of vulnerability through aggregation operations. These aggregation operations calculate, display, and validate the indicators of vulnerability, finally to obtain a composite vulnerability index.

Before aggregation, normalization of indicators (adjusting the values measured on different scales to a common scale) is performed. In the last step, suitable aggregation operations are performed using several methods based on the data availability and complexity of the problem statement. Different methods include averaging (Rygel et al. 2006; Karmakar et al. 2010), maximization, Analytic

Table 7.2 Recent efforts made to map flood hazards through geomorphic classifiers

Indicators considered	Case study	DEM considered	Remarks	References
Modified topographic index (TI_m) $TI_m = \log \frac{a_d^n}{\tan(\beta)}$ a_d^n is drained area per unit contour length and tan(β) is local gradient	Arno River Basin, Italy (8830 km^2)	DEM obtained from Arno River Basin Authority (20 m) SRTM DEM (90 m) ASTER DEM (30 m) National elevation data (30 m)	The index is highly sensitive to DEM resolution; however, a resolution of ~100 m is satisfactory for good performance SRTM DEM showed good performance when compared with the other DEMs	Manfreda et al. (2011)
Surface curvature (H) Laplacian of the elevation (ΔH) Contributing area (A) Local slope (S)	Tanaro River Basin, Italy (8000 km^2)	SRTM: DEM–VOID (Void filled)and DEM–CON (Hydrologically conditioned) from HydroSHEDS	The classifiers could identify 93% of flood-prone areas, while validated with the flood inundation map	Degiorgis et al. (2012)
Single features Upslope contributing area, A_s (m^2) Surface curvature ($\nabla^2 H$) Local slope, S Distance from the nearest stream, D (m) Elevation to the nearest stream, H (m) *Composite indices* Modified topographic index (TI_m) Downslope index, (DW_i) Elevation (H) and ratio between the flow distance (D) ln[h_l/H], where h_l is the variable water depth GFI (Geomorphic Flood Index): ln[h_r/H]: hr. is computed as afunction of the contributing area A_r [$h_r - H$]/tan(α_d) and [$h_r - H$]/D	Tiber River Basin, Italy (17,375 km^2)	-do-	Elevation to the nearest stream (H), downslope index (DW_i), and GF_i showed better performance	Manfreda et al. (2014)
			Among the single features, distance from the nearest stream (D) and elevation to the nearest stream (H) performed better, while among composite indices ln[h_l/H] and ln[h_r/H] performed better	
	Bradano River Basin, Italy (2765 km^2)	-do-	Composite indices were found to be less sensitive to the variations in DEM resolution	Manfreda et al. (2015)
	Bulbula river sub- catchment, Ethiopia	-do-	The composite index ln [h_r/H] and elevation difference (H) showed the best performance	Samela et al. (2016)
	Ohio River Basin, USA, (29,000 km^2)	-do-	GFI was found to be the most suitable morphologic classifier, as it exhibited a higher accuracy than the other indices	Samela et al. (2017)

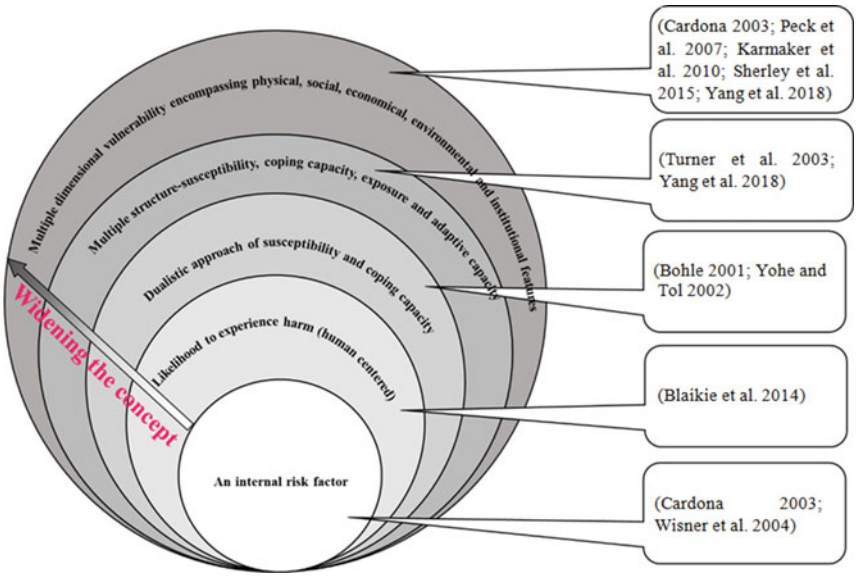

Fig. 7.4 Key spheres of vulnerability. (Birkmann 2005, 2006)

Hierarchy Process (AHP) (Wei et al. 2004), Data Envelopment Analysis (DEA) (Wei et al. 2004; Huang et al. 2011; Sherly et al. 2015b; Mohanty et al. 2020a).

7.2.6 Flood Risk Mapping

Flood risk constitutes flood hazard and vulnerability components (Koks et al. 2015). Assessing flood risk is not straightforward, keeping in mind the complex nature of flood caused due to the impounding precipitation affected by climate change impacts and river basin characteristics. At the same time, there exist numerous knowledge gaps in the conventional flood risk assessments, which most consider the damage to physical well-being in a population (Debortoli et al. 2017). During this approach, the socioeconomic vulnerability studies have produced valuable information, however unable to establish suitable linkages to flood risk. The need of the hour is to consider a compound and marginal assessment of flood hazard and vulnerability to derive the flood risk that directly provides necessary amendments to the flood risk management strategies. Figure 7.6 shows representative efforts on riverine flood risk estimation and mapping which have been addressed for the recent time scales and projected for the future time, considering climate change impacts as well.

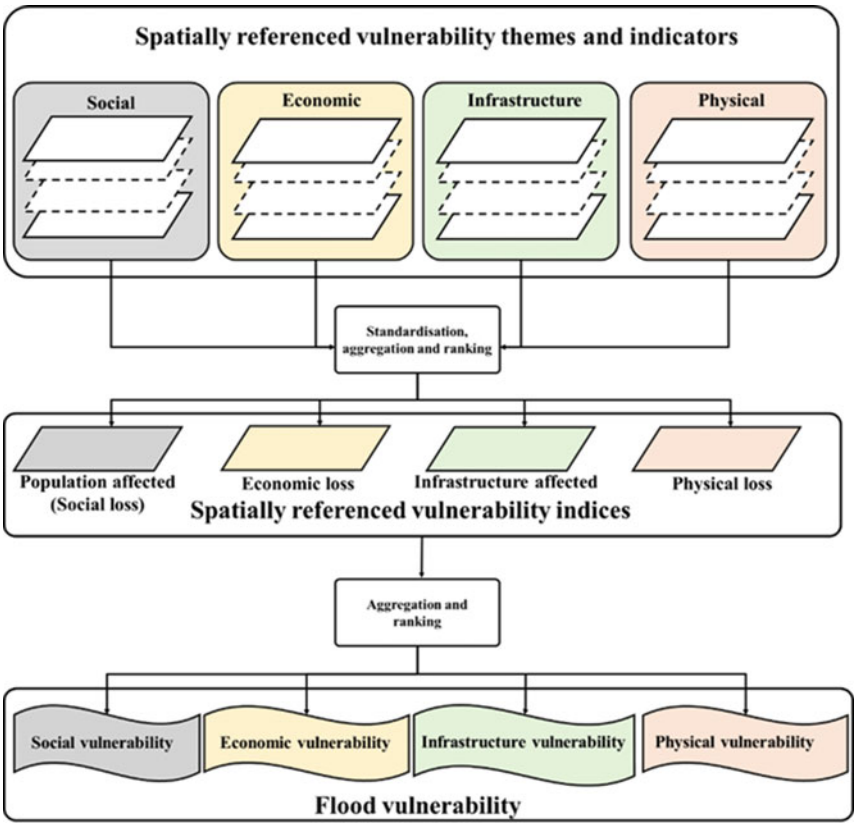

Fig. 7.5 A generic framework for assessment of flood vulnerability

7.2.7 Flood Risk Reduction

The most key aspect of flood risk management is the usage of preparedness measures for minimizing loss before the occurrence of a flood event. These measures are grouped into structural and nonstructural measures.

7.2.7.1 Structural Measures

In structural measures, two alternatives are practiced: (1) the construction of resilient hydraulic structures (defenses) to minimize hazard and (2) ensuring the adaptation of the exposed assets to provide resistance from floods. The crest levels of defenses are set according to design water levels, which are established through statistical analysis with little consideration of potential impacts. In most cases, design water levels just aim for individual flood defenses instead of considering the whole defense

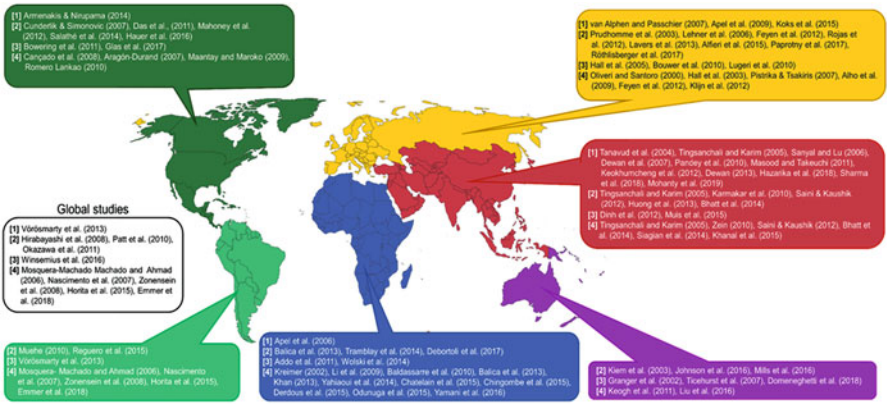

Fig. 7.6 Representative efforts on flood risk mapping across the globe. [**1**] Flood risk considering both hazard and vulnerability components. [**2**] Flood risk considering either hazard or vulnerability component. [**3**] Flood risk with climate change considering both hazard and vulnerability components. [**4**] Flood risk with climate change considering either hazard or vulnerability component

system (Boonya-Aroonnet et al. 2002). The major problem associated with structural measures is concerning the longevity and its associated cost. It usually takes a long time and high investment to build a flood control structure, and when it fails, it fails dramatically with less response time.

7.2.7.2 Nonstructural Measures

Nonstructural measures do not consider huge investments in infrastructures but rather rely on a precise understanding of the flood risk by considering the associated flood hazard and vulnerability components (Kundzewicz 2002; Kang et al. 2009; Bowering et al. 2014). Flood risk awareness forms the base of nonstructural measures. In the event of flooding, the lack of awareness results in communities failing to evacuate, thereby rendering them highly vulnerable. Awareness is high in areas of frequent floods but is often deficient in areas subject to low frequency but high impacts. This can be achieved by proper awareness campaigns and communication channels like posters, newspapers, brochures, televisions, radios, visual clues, training, and demonstrations.

Based on the extensive literature review, it is now well established that several regions in the globe are projected to experience an elevated risk from riverine flooding attributable to concomitant climate change and alterations in socioeconomic dynamics. Under such lines, their lies a major challenge to comprehensively quantify flood risk, which will facilitate in building flood mitigation infrastructures, improving land use/urban planning, and also prioritizing emergency response strategies. The quantification of flood risk is a complex process, not just because it is data-intensive but also involves several sensitive parameters in its formulation. The process becomes more challenging for data scarce regions as they suffer from

considerable data unavailability, e.g., rainfall, discharge, high-resolution topography, etc. The research considers these research gaps and proposes a generic framework to quantify flood risk at the village level (finest administrative scale). The comprehensive framework is demonstrated over data-scarce Jagatsinghpur district in India.

7.3 Case Study of the Mahanadi River Basin in India

This section introduces the case study and demonstrates the proposed framework of flood risk estimation and mapping. The case study is situated in the severely flood-prone Mahanadi river basin in India.

7.3.1 Jagatsinghpur District: The Focal Point Witnessing Severe Flood Impacts in Odisha, India

Jagatsinghpur is located between 19° 58′ N to 20° 23′ N latitude and 86° 3′ E to 86° 45′ E longitude in the downstream of Mahanadi river basin, Odisha, India (Fig. 7.7). Among several other factors, the geographical location and demographic characteristics are considered the two most important reasons for high flood risk according to the District Emergency Operation Centre (DEOC 2016). Considering the fact that the case study is semi-urban, most of the rural villages suffer high risk. This is because a significant proportion of the population depends on agriculture and allied activities as their primary source of income, which is known to face highly vulnerability by floods. Moreover, many people live in their ancestral property for a long time and have left interest in shifting to safer places after a flood strikes (Mishra et al. 2010). The immediate need of the hour is to assemble information from various sources such as meteorological, hydrological, and social domains to quantify flood risks and provide answers to the current flood management situation.

7.3.2 Proposed Framework of Flood Risk Mapping

The flood risk in the case study is quantified for the latest census year 2011 by considering the hazard and socioeconomic vulnerability components. The proposed framework of flood risk mapping is illustrated in Fig. 7.8. This comprehensive framework consists of four building blocks. They are (i) estimation of regionalized design rainfall ($\mathcal{RDR}$), (ii) quantification of flood hazard ($\mathcal{H}$) through hydrodynamic modeling, (iii) analysis of socioeconomic vulnerability analysis ($\mathcal{V}$), and (iv) determination of flood risk through *risk classifier*. A brief description of these steps is outlined in the subsequent sections.

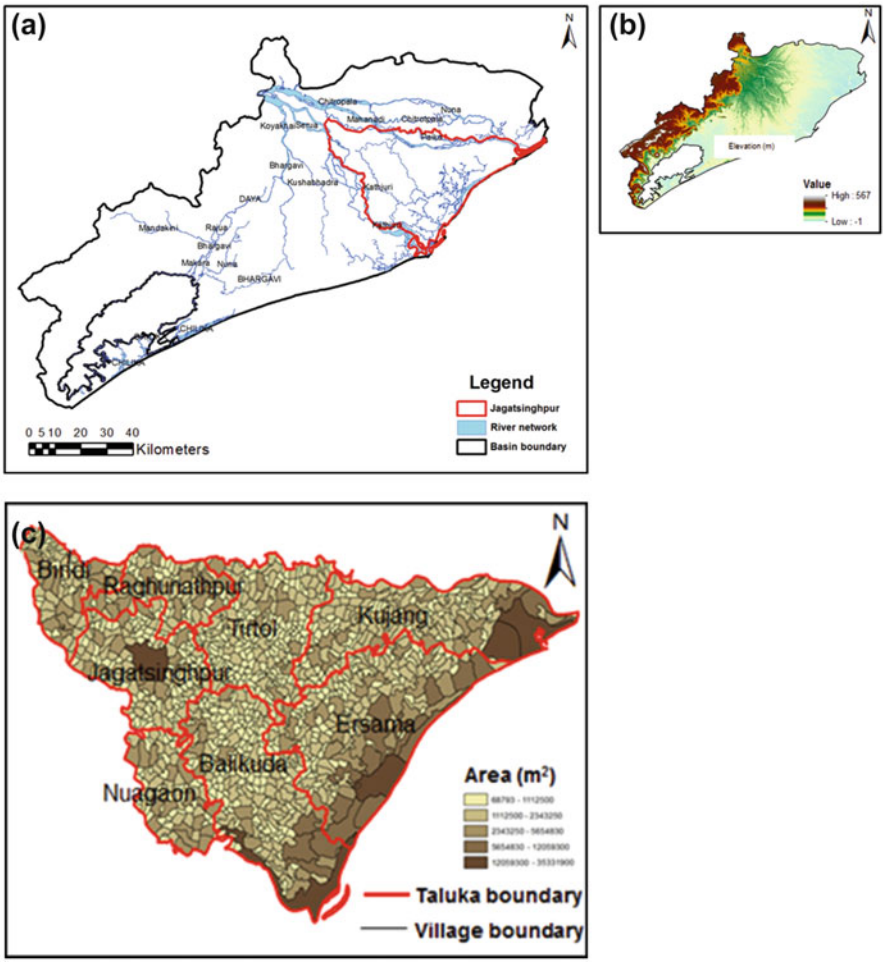

Fig. 7.7 Jagatsinghpur district in Odisha (India): (**a**) river network details; (**b**) description of elevation; (**c**) various administrative blocks and villages

7.3.2.1 Estimation of Regionalized Design Rainfall (*RDR*)

The only long-term hourly rainfall time series operated by the India Meteorological Department (IMD) from 1970 to 2011 located at *Bhubaneswar* (20.2961° N; 85.8245° E), *Paradeep* (20.3166° N, 86.6114° E), and *Puri* (19.8134° N; 85.8315° E) are utilized to form at-site design rainfall time series through a set of multivariate frequency and design temporal pattern analyses. To regionalize the at-site design rainfalls, two new nonlinear optimisation techniques, namely, complete optimisation and combined averaging optimisation, are introduced (Sherly et al. 2015a, b; Mohanty et al. 2018). These robust optimisation schemes are tailor-made to derive the regional bandwidth of the nonparametric kernel function, which has not been addressed in earlier studies.

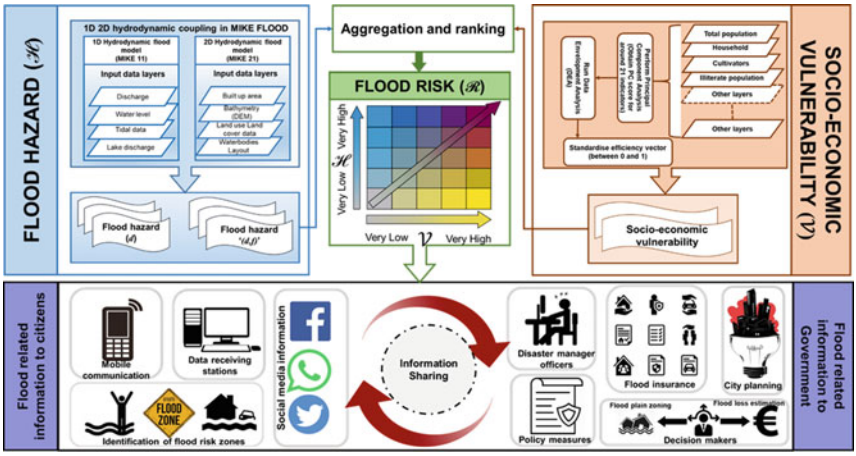

Fig. 7.8 A comprehensive framework for flood risk mapping using flood hazard and socioeconomic vulnerability. (Mohanty et al. 2020a)

7.3.2.2 Quantification of Flood Hazard (H) Through Hydrodynamic Modeling

The flood hazard is quantified with a 1D-2D-coupled MIKE FLOOD. The MIKE FLOOD interface houses MIKE 11 (one-dimensional) and MIKE 21 HD FM (two-dimensional) models, whose outputs are dynamically coupled by establishing appropriate hydraulic linkages (Frank et al. 2001). To represent the bathymetry in MIKE 21 HD FM, LiDAR DEM (horizontal resolution: 2 m × 2 m) is considered for the entire study area. A framework for flood risk mapping is given in Fig. 7.8.

An unstructured triangulated mesh of area <5000 m^2 is generated to account for the optimisation of computation time for the entire domain. The latest available land use and land cover classification map is utilized to represent the roughness values for each land use class. The MIKE 11 model set-up is developed by creating the river channel network and providing details of the channel cross-sections at close intervals of every 100 m along the river channel. The hydraulic inputs in the form of regionalized design rainfall for MIKE 21 HD FM and design discharge and storm tide (Mohanty et al. 2020b) for MIKE 11 are considered as the boundary conditions. The simulated outputs from these individual models are hydraulically combined in MIKE FLOOD by establishing lateral linkages between the river channel banks and adjoining flood plains (Mohanty et al. 2020c). The MIKE FLOOD model provides outputs in the form of flood inundation depth "d" and velocity "f" for each cell. The flood hazard is quantified in terms of "d" and tuple of "(d,f)." The severity of flood hazard is identified by discretizing it into five different classes (Mani et al. 2014) as outlined in Table 7.3.

Table 7.3 Discretization of "*d*" and "(*d*,*f*)" into various hazard categories

Severity of hazard	"*d*" [m]	"(*d*,*f*)" [m^2/s]
Very low	0–0.2	0–0.3
Low	0.2–0.6	0.3–0.7
Medium	0.6–1.5	0.7–1.2
High	1.5–3.5	1.2–1.6
Very high	> 3.5	> 1.6

7.3.2.3 Analysis of Socioeconomic Vulnerability Analysis (*V*)

A suite of 21 socioeconomic indicators is selected from the latest Census of India 2011 data (Census 2011). These indicators are classified into two categories: *cost type* (the larger the value, the larger the vulnerability) and *benefit type* (the larger the quantity, the lesser the vulnerability). The slack-based input-oriented BCC method (Banker et al. 1984) of data envelopment analysis (DEA) is considered for deriving the vulnerability values. Similar to hazard, the socioeconomic vulnerability values are grouped into five different classes.

7.3.2.4 Determination of Flood Risk Through Risk Classifier

This study introduces a bivariate approach for quantifying flood risk through a risk classifier. The classifier has the anatomy of a 5 × 5 choropleth as illustrated in Fig. 7.9. The new concept gives an idea of different levels of flood risk ($\mathcal{R}$) through the identification of the marginal and compound contributions from the hazard ($\mathcal{H}$) and vulnerability ($\mathcal{V}$) components.

7.3.3 Results and Discussion

A large portion of Jagatsinghpur was found to face high and very high $\mathcal{H}$ (Fig. 7.10a). In particular, the N-W and S-W flood plain stretch of Mahanadi and Devi rivers and coastal regions were seen to have several villages facing high and very high $\mathcal{H}$. The $\mathcal{V}$ was scattered, although several villages in the coastal regions were identified as high and very high $\mathcal{V}$ (Fig. 7.10b). The risk map was identified predominantly by $\mathcal{H}-$ and $\mathcal{V}-$ driven risk. The villages facing *very high risk* due to $\mathcal{H}$ or both $\mathcal{H}$ and $\mathcal{V}$ are situated in the N-W (Tirtol, Raghunathpur and Biridi) and the S-E (Ersama block) of Jagatsinghpur District (Fig. 7.10c).

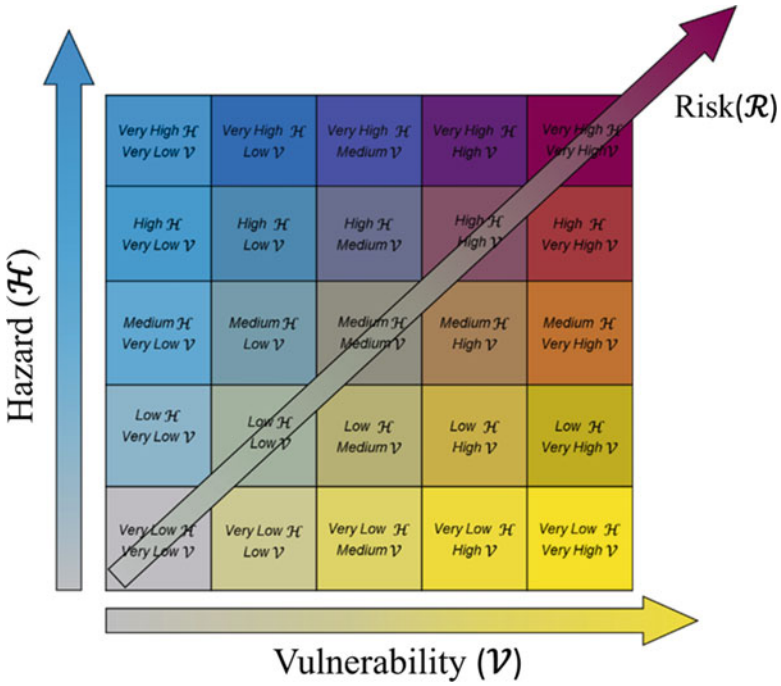

Fig. 7.9 A bivariate choropleth representation of flood risk ($\mathcal{R}$) aggregating flood hazard ($\mathcal{H}$) and socioeconomic vulnerability ($\mathcal{V}$). (Mohanty et al. 2020a)

7.4 Conclusion

Flood risk mapping is the opening step towards flood risk management for any flood-prone region. It paves the path to a comprehensive flood management strategy, as it divides a region into various zones of risk based on the values obtained in the flood risk analysis. Such a map acts as a tool to the public, professionals, and administration for decision-making purposes. This chapter reports the present status and future challenges of flood risk mapping through a comprehensive literature review. In the administration of the generic framework over a case study, the important components of flood hazard and vulnerability were treated keeping in the mind the technical commitments and needs of the society. The flood risk maps were developed using a bivariate concept, showing the gradual increase of both the components and the dependency of either one on risk. The proposed framework was applied in Jagatsinghpur district (Odisha), which has been identified as a severe flood-prone region. The identification of flood risk suggests possible areas of improvement in the current flood risk management plans. Those locations suffering from high risk due to vulnerability alone should be administered by enforcing stringent policies and schemes for the uplifting and spreading awareness on flood damage prevention. The disaster management bodies should focus on nonstructural

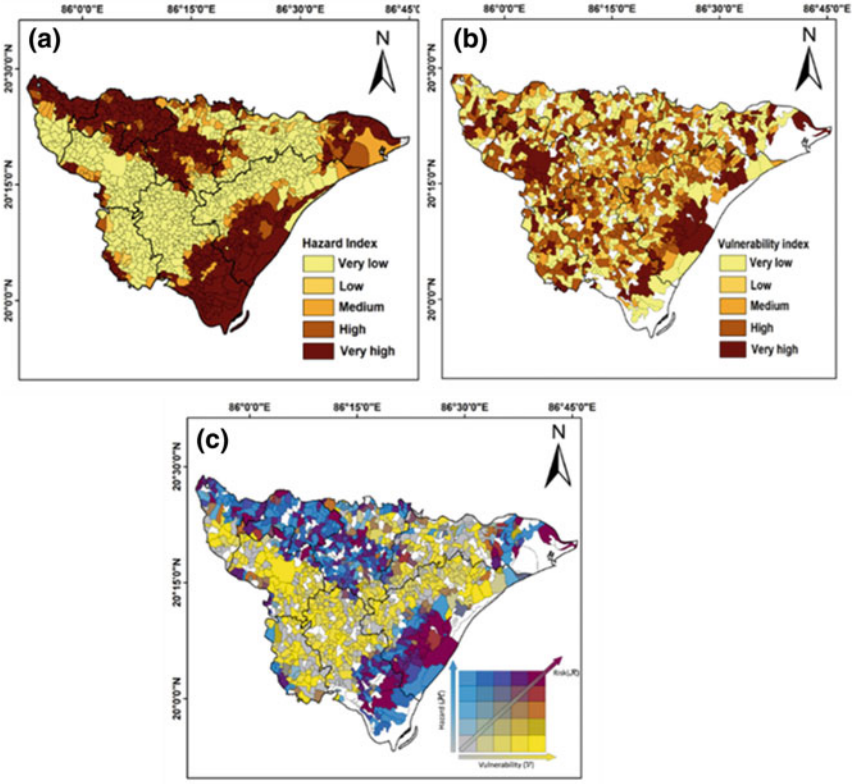

Fig. 7.10 (**a**) Flood hazard map; (**b**) socioeconomic vulnerability map; (**c**) bivariate flood risk map for 2011 for Jagatsinghpur district, Odisha. (Modified from Mohanty et al. 2020a)

measures and develop suitable tools to sensitize the population in combating any form of flood activity. For those regions facing risk from the hazard, improved structural measures and flood zoning practices should be implemented. The flood risk map demands easy access to the public and every end-user. It can be further developed as a cartographic product which can provide important guidelines for sustainable benefits by minimizing flood losses.

Acknowledgments This work is supported by ISRO-IIT(B)-Space Technology Cell (STC) [Project reference numbers: RD/0114-ISROC00-013 (14ISROC009) and RD/0119-ISROC00-001] and partially supported by the Department of Science and Technology (SPLICE-Climate Change Programme), Government of India (Project reference number DST/CCP/CoE/140/2018, Grant Number: 00000000000010013072 (UC ID: 18192442)). The support for computational resources was provided by IIT Bombay.

References

Adger WN (2006) Vulnerability. Glob Environ Chang 16(3):268–281. https://doi.org/10.1016/j.gloenvcha.2006.02.006

Alcantara-Ayala I (2002) Geomorphology, natural hazards, vulnerability and prevention of natural disasters in developing countries. Geomorphology 47:107–124. https://doi.org/10.1016/S0169-555X(02)00083-1

Alfieri L, Burek P, Feyen L et al (2015a) Global warming increases the frequency of river floods in Europe. Hydrol Earth Syst Sci 19(5):2247–2260. https://doi.org/10.5194/hessd-12-1119-2015

Alfieri L, Feyen L, Dottori F et al (2015b) Ensemble flood risk assessment in Europe under high end climate scenarios. Glob Environ Chang 35:199–212. https://doi.org/10.1016/j.gloenvcha.2015.09.004

Apel H, Aronica GT, Kreibich H et al (2009) Flood risk analyses-how detailed do we need to be? Nat Hazards 49:79–98. https://doi.org/10.1007/s11069-008-9277-8

Apel H, Thieken AH, Merz B et al (2004) Flood risk assessment and associated uncertainty. Nat Hazards Earth Syst Sci 4(2):295–308. https://doi.org/10.5194/nhess-4-295-2004

Banker RD, Charnes A, Cooper WW (1984) Some models for estimating technical and scale inefficiencies in data envelopment analysis. Manag Sci 30(9):1078–1092. https://doi.org/10.1287/mnsc.30.9.1078

Bates PD (2004) Remote sensing and flood inundation modelling. Hydrol Process 18(13):2593–2597. https://doi.org/10.1002/hyp.5649

Bates PD, De Roo APJ (2000) A simple raster-based model for flood inundation simulation. J Hydrol 236(1–2):54–77. https://doi.org/10.1016/S0022-1694(00)00278-X

Berghuijs WR, Aalbers EE, Larsen JR et al (2017) Recent changes in extreme floods across multiple continents. Environ Res Lett 12(114035)

Birkmann J (2005) Danger need not spell disaster but how vulnerable are we? Research Brief 1, United Nations University, Tokyo, New York, Bonn, 1-8. Avalailable via United Nations University. https://www.files.ethz.ch/isn/21139/UNU-RB-1-2005-EHS.pdf. Accessed 8 May 2021

Birkmann J (2006) Indicators and criteria for measuring vulnerability: theoretical bases and requirements. In: Birkmann (ed) Measuring vulnerability to natural hazards: towards disaster resilient societies. United Nations University Press, pp 55–77

Blaikie P, Cannon T, Davis I et al (2014) At risk: natural hazards, People's vulnerability and disasters. Routledge. 496p

Bohle HG (2001) Vulnerability and criticality: perspectives from social geography. IHDP Update 2:1–5

Boonya-Aroonnet S, Weesakul S, Mark O (2002) Modelling of urban flooding in Bangkok. In: Proceedings of 9th International Conference on Urban Drainage, Portland, USA

Bowering EA, Peck AM, Simonovic SP (2014) A flood risk assessment to municipal infrastructure due to changing climate part I: methodology. Urban Water J 11(1):20–30. https://doi.org/10.1080/1573062X.2012.758293

Census (2011) Provisional population totals, census of India. Office of the Registrar General and Census Commissioner, India

Chakraborty J, Tobin GA, Montz BE (2005) Population evacuation: assessing spatial variability in geophysical risk and social vulnerability to natural hazards. Nat Hazards Review 6(1):23–33. https://doi.org/10.1061/(ASCE)1527-6988(2005)6:1(23)

Cheikh Lounis G, Chatelain JL, Mimouni O et al (2015) Assessment of flood risk in Kniss Wadi catchment in Urbain Area Algiers—Algeria. In: Lollino G, Arattano M, Rinaldi M et al (eds) Engineering geology for society and territory, vol 3. Springer, Cham. https://doi.org/10.1007/978-3-319-09054-2_94

Debortoli NS, Camarinha PIM, Marengo JA et al (2017) An index of Brazil's vulnerability to expected increases in natural flash flooding and landslide disasters in the context of climate change. Nat Hazards 86(2):557–582. https://doi.org/10.1007/s11069-016-2705-2

Degiorgis M, Gnecco G, Gorni S et al (2012) Classifiers for the detection of flood-prone areas using remote sensed elevation data. J Hydrol s470–471:302–315. https://doi.org/10.1016/j.jhydrol.2012.09.006

DEOC (2016) District disaster management plan Jagatsinghpur. Available via District Emergency Operation Centre

Dottori F, Salamon P, Bianchi A et al (2016) Development and evaluation of a framework for global flood hazard mapping. Adv Water Resour 94:87–102. https://doi.org/10.1016/j.advwatres.2016.05.002

Fiebiger G (1997) Hazard mapping in Austria. J Torrent Avalanche Landslide Rockfall Eng 61(134):1531–1164

Frank E, Ostan A, Coccato M et al (2001) Use of an integrated one dimensional-two dimensional hydraulic modelling approach for flood hazard and risk mapping vol 50. WIT Trans Ecol Environ. https://doi.org/10.2495/RM010091

Füssel H-M (2007) Vulnerability: a generally applicable conceptual framework for climate change research. Glob Environ Chang 17(2):155–167. https://doi.org/10.1016/j.gloenvcha.2006.05.002

Gotham KF, Campanella R, Lauve-Moon K et al (2018) Hazard experience, geophysical vulnerability, and flood risk perceptions in a Post-disaster City, the Case of New Orleans. Risk Anal 38(2):345–356. https://doi.org/10.1111/risa.12830

Grothmann T, Reusswig F (2006) People at risk of flooding: why some residents take precautionary action while others do not. Nat Hazards 38(1–2):101–120. https://doi.org/10.1007/s11069-005-8604-6

Hallegatte S, Green C, Nicholls RJ et al (2013) Future flood losses in major coastal cities. Nat Clim Change 3(9):802. https://doi.org/10.1038/nclimate1979

Huang J, Liu Y, Ma L (2011) Assessment of regional vulnerability to natural hazards in China using a DEA model. Int J Disaster Risk Sci 2:41–48. https://doi.org/10.1007/s13753-011-0010-y

IPCC (2012) Managing the risks of extreme events and disasters to advance climate change adaptation. In: Field CB, Barros V, Stocker TF et al (eds) A special report of working groups I and II of the intergovernmental panel on climate change. Cambridge University Press, Cambridge, UK\New York, NY, 582 p

Jonkman SN (2013) Advanced flood risk analysis required. Nat Clim Change 3(12):1004–1004. https://doi.org/10.1038/nclimate2031

Kang SJ, Lee SJ, Lee KH (2009) A study on the implementation of non-structural measures to reduce urban flood damage. J Asian Archit Build Eng 8(2):385–392. https://doi.org/10.3130/jaabe.8.385

Karmakar S, Simonovic SP, Peck A et al (2010) An information system for risk-vulnerability assessment to flood. J Geogr Inf Syst 2(3):129–146. https://doi.org/10.4236/jgis.2010.23020

Koks EE, Jongman B, Husby TG et al (2015) Combining hazard, exposure and social vulnerability to provide lessons for flood risk management. Environ Sci Pol 47:42–52. https://doi.org/10.1016/J.ENVSCI.2014.10.013

Kron W (2005) Flood Risk=Hazard • Values • Vulnerability. Water Int 30(1):58–68. https://doi.org/10.1080/02508060508691837

Kundzewicz ZW (2002) Non-structural flood protection and sustainability. Water Int 27(1):3–1. https://doi.org/10.1080/02508060208686972

Ludy J, Kondolf GM (2012) Flood risk perception in lands 'protected by 100-year levees. Nat Hazards 61:829–842. https://doi.org/10.1007/s11069-011-0072-6

Manfreda S, Samela C (2019) A digital elevation model based method for a rapid estimation of flood inundation depth. J Flood Risk Manag. https://doi.org/10.1111/jfr3.12541

Manfreda S, Di Leo M, Sole A (2011) Detection of flood-prone areas using digital elevation models. J Hydrol Eng 16(10):781–790. https://doi.org/10.1061/(ASCE)HE.1943-5584.0000367

Manfreda S, Samela C, Gioia A et al (2015) Flood-prone areas assessment using linear binary classifiers based on flood maps obtained from 1D and 2D hydraulic models. Nat Hazards 79:735–754. https://doi.org/10.1007/s11069-015-1869-5

Manfreda S, Samela C, Sole A et al (2014). Flood-prone areas assessment using linear binary classifiers based on morphological indices. Vulnerability, uncertainty, and risk 2002–2011. doi: https://doi.org/10.1061/9780784413609.201

Mani P, Chatterjee C, Kumar R (2014) Flood hazard assessment with multi-parameter approach derived from coupled 1D and 2D hydrodynamic flow model. Nat Hazards 70:1553–1574. https://doi.org/10.1007/s11069-013-0891-8

Miceli R, Sotgiu I, Settanni M (2008) Disaster preparedness and perception of flood risk: a study in an alpine valley in Italy. J Environ Psychol 28(2):164–173. https://doi.org/10.1016/j.jenvp.2007.10.006

Mishra S, Mazumdar S, Suar D (2010) Place attachment and flood preparedness. J Environ Psychol 30(2):187–197

Mohanty MP, Nithya S, Nair AS et al (2020c) Sensitivity of various topographic data in flood management: implications on inundation mapping over large data-scarce regions. J Hydrol. https://doi.org/10.1016/j.jhydrol.2020.125523

Mohanty MP, Sherly MA, Ghosh S et al (2020b) Tide-Rainfall Flood Quotient: An incisive measure of comprehending a region's response to storm-tide and pluvial flooding. Environ Res Lett. https://doi.org/10.1088/1748-9326/ab8092

Mohanty MP, Sherly MA, Karmakar S et al (2018) Regionalized design rainfall estimation: an appraisal of inundation mapping for flood management under data-scarce situations. Water Resour Manag 32:4725–4746. https://doi.org/10.1007/s11269-018-2080-8

Mohanty MP, Vittal H, Yadav V et al (2020a) A new bivariate flood risk classifier for flood management considering hazard and socio-economic dimensions. J Environ Manage 255:109733. https://doi.org/10.1016/j.jenvman.2019.109733

Narayan S, Hanson S, Nicholls R et al (2011) Use of the source- pathway- receptor-consequence model in coastal flood risk assessment. Geophys Res Abstr 13:EGU2011–EG10394

OFEE (1997) Consideration of flood hazards for activities with spatial impact. The Environment in Practice VU-7505-E, Federal Office for the Environment FOEN, Bern

Pall P, Aina T, Stone DA et al (2011) Anthropogenic greenhouse gas contribution to flood risk in England and Wales in autumn 2000. Nature 470(7334):382–385. https://doi.org/10.1038/nature09762

Peck A, Karmakar S, Simonovic SP (2007) Physical, economical, infrastructural and social flood risk-vulnerability analyses in GIS. Water Resources Research Report, The University of Western Ontario, Canada

Rygel L, O'Sullivan D, Yarnal B (2006) A method for constructing a social vulnerability index: an application to hurricane storm surges in a developed country. Mitig Adapt Strat Glob Change 11:741–764. https://doi.org/10.1007/s11027-006-0265-6

Samela C, Manfreda S, De Paola F et al (2016) DEM-based approaches for the delineation of flood-prone areas in an Ungauged Basin in Africa. J Hydrol Eng 21(2):1–10. https://doi.org/10.1061/(ASCE)HE.1943-5584.0001272

Samela C, Troy TJ, Manfreda S (2017) Geomorphic classifiers for flood-prone areas delineation for data-scarce environments. Adv Water Resour 102:13–28. https://doi.org/10.1016/j.advwatres.2017.01.007

Schanze J (2006) Flood risk management- a basic framework. In: Schanze J, Zeman E, Marsalek J (eds) Flood risk management: hazards, vulnerability and mitigation measures. Springer, Dordrecht. https://doi.org/10.1007/978-1-4020-4598-1_1

Schiermeier Q (2011) Increased flood risk linked to global warming. Nature 470(7334):316. https://doi.org/10.1038/470316a

Sherly MA, Karmakar S, Chan T et al (2015a) Design rainfall framework using multivariate parametric-nonparametric approach. J Hydrol Eng 21(1):04015049. https://doi.org/10.1061/(ASCE)HE.1943-5584.0001256

Sherly MA, Karmakar S, Parthasarathy D et al (2015b) Disaster vulnerability mapping for a densely populated coastal urban area: an application to Mumbai, India. Ann Assoc Am Geogr 105(6):1198–1220

Turner BL, Kasperson RE, Matson PA et al (2003) A framework for vulnerability analysis in sustainability science. PNAS 100(14):8074–8079. https://doi.org/10.1073/pnas.1231335100

USBR (1988) Downstream hazard classification guidelines. ACER Technical Memorandum 11, Denver, Colorado

Vousdoukas MI, Mentaschi L, Voukouvalas E et al (2018) Climatic and socioeconomic controls of future coastal flood risk in Europe. Nat Clim Change 8(9):776–780. https://doi.org/10.1038/s41558-018-0260-4

Wei YM, Fan Y, Lu C et al (2004) The assessment of vulnerability to natural disasters in China by using the DEA method. Environ Impact Assess Rev 24(4):427–439

Chapter 8
Trend Analysis of Rainfall: A Case Study of Surat City in Gujarat, Western India

Darshan Mehta, Sahita Waikhom, Vipin Yadav, Zalak Lukhi, Saeid Eslamian, and James N. Furze

Abstract This chapter details a study which was carried out to determine the potential trend of rainfall and assess its significance in Surat city of Gujarat, India. Rainfall is a key characteristic of any watershed and plays a significant role in flood frequency, flood control studies, and water planning and management. In the case study, mean monthly and seasonal rainfall was analyzed to determine its variability in magnitude over the period 1981–2000. Trends in mean monthly precipitation and mean seasonal trends were analyzed using the Mann-Kendall test and Sen's slope estimation for the data period 1981–2000. Analysis of seasonal trends in precipitation showed a negative trend for the months of July, August, September, and October for Surat city. The falling trend holds significance in the southwest monsoon and post-monsoon of the country. Interestingly, seasonal, annual, and pre-monsoon periods showed a rising trend of rainfall for Surat city. Overall, the trend analysis for annual rainfall data shows significant negative trend for Surat city inferring climatic change in the area.

D. Mehta (✉) · S. Waikhom · V. Yadav · Z. Lukhi
Faculty of Civil Engineering, Dr. S. & S. S. Ghandhy Government Engineering College, Surat, India
e-mail: darshanmehta2490@gmail.com; siwgecs@gmail.com; vkygecs@gmail.com; zalaklukhi123@gmail.com

S. Eslamian
Department of Water Engineering, College of Agriculture, Isfahan University of Technology, Isfahan, Iran
e-mail: saeid@iut.ac.ir

J. N. Furze
Royal Geographical Society (with the Institute of British Geographers), London, UK

Laboratory of Biotechnology and Valorization of Natural Resources, Faculty of Sciences-Agadir, Ibn Zohr University, Agadir, Morocco

Control and Systems Engineering Department, University of Technology-Iraq, Baghdad, Iraq
e-mail: james.n.furze@gmail.com; jamesfurze@hotmail.com

J. N. Furze et al. (eds.), *Earth Systems Protection and Sustainability*,
https://doi.org/10.1007/978-3-030-98584-4_8

Key words Mann–Kendall test · Rainfall · Statistical trend analysis · Sen's slope estimator

8.1 Introduction

Rainfall is an essential part of the hydrological cycle, with importance on local, regional, national, and global scales. Precipitation is a climatic parameter that effects both strategical (often seen as discrete triangularly grouped) and functional (continually spread) characteristics of human lifestyle and indeed each member of the ecological system, flora, and fauna. The type, volume, and changeable nature of rain has a strong effect on all natural factors that ultimately effect the life and economy of individuals; the risk and stability of communities are affected by the prevailing water relations and micro change in their locale (WHO 2003; Verma et al. 2016; Darshan and Yadav 2022). Of all water relations, rain has received constant attention from scholars, natural scientists, and meteorologists as despite its irregular and sometimes abrupt intensity, it is of paramount importance, with a huge effect on both terrestrial and atmospheric stability. The amount of rain and its nature is directly attributed to the health and survival of all life forms (Mehta and Yadav 2020; Mehta and Yadav 2021a; Dasgupta 2021).

Highly intense downpours of rain often accompanied by tempestuous winds signify monsoons. Although they are commonly known within climatic systems across the world from Australia to America and Asia to Africa, the Indian southwest monsoon stands out with peculiarities which combine pressure differentials across both land and sea; extremely high winds whirl to generate weather anomalies throughout the year (Huang et al. 2020; Mehta and Yadav 2021b). The boiling or cyclonic patterns of monsoons are both externally and internally forced and are an important component of the Earth's total climate system. Seen from above, monsoonal events pin together the Earth's global atmospheric circulation. Monsoon rainfall is uneven in amount and duration; its spread is consequently erratic (Thenmozhi and Kottiswaran 2016; Zhao 2020).

The capricious nature of monsoon rainfall is coupled with the prevalent society and economical habits of individual monsoon countries, determined by anthropogenic forcing as well as natural and topological elements (Kyung-Ja et al. 2020; Mehta and Yadav 2021c). Our planets both wettest and driest areas are found in India, due to the stochastic patterns of rainfall. The summer monsoon of India stands out in climatic systems and may be thought of as an exclusive weather system, core to the driving of the planetary atmospheric circulation. Consequently, rainfall of India bears spontaneous repercussions of the monsoon and has a high level of unpredictability (Pandit 2016; Panda and Sahu 2019). The deluge of rain over the region is habitually seasonal and is concentrated within 4 months (June to September) of the summer monsoon season affecting western and central India. However, the north-east monsoon season (October to December) has a reflection on the south-eastern part of the country. The monsoon season typically accounts for

90 percent of the annual precipitation of the country (Jagadeesh and Anupama 2014; Kuttippurath et al. 2021; Mehta and Yadav 2021b).

Given the importance of agriculture in India, the monsoon rains have a major impact on production and development of the country. Despite growing industrialization, rain-fed agricultural production provides a key generator for the countries' economy. The southwest monsoon rainfall also drives hydroelectric power generation and drinking water provision and thus directly influences the quality of life of the country (Dunning et al. 2015; Ahammad et al. 2018; Mehta and Yadav 2021a).

Meteorologists use studies of monsoon rainfall for socioeconomic as well as for purely scientific reasons (Pingale et al. 2016). Research on Indian monsoon rainfall has been carried out worldwide including within India to understand its relational facets and dynamic change. Administrative studies are carried out on different areas at national scales, by state, or at the district level. In contrast with rainfall at the national level, scientific studies of natural regions including river basins are very limited (Thomas and Prasannakumar 2016; Somisetty et al. 2022; Darshan and Yadav 2022; Mehta and Yadav 2022). The study of rainfall is highly relevant for water resource management, especially in countries containing neighboring regions of extreme topographical gradients and lower altitudes which may have added risk elements to consider such as landslides or degradation (Pokharel and Hallet 2015; Sharma et al. 2020; Darshan and Yadav 2022).

The objective of the current chapter is to show rainfall characteristics of Surat on the basis of available data. The study has three main objectives: (i) to show the variable pattern of rainfall, (ii) to reveal temporal properties of rainfall, and (iii) to reveal long-term fluctuations in monsoonal rainfall. The remainder of the chapter is structured with Sect. 8.2 describing the study area and data collection, Sect. 8.3 detailing the methodology used for trend analysis, Sect. 8.4 giving the results and making discussion, and Sect. 8.5 concluding the findings of the study.

8.2 Study Area and Data Collection

8.2.1 Study Area

Surat city (21° 30′ N 72° 38′ E) is located in the state of Gujarat, India. The administrative headquarters of the district are based in Surat city, with ten talukas (administrative divisions) and a geospatial area of 7213 km^2. Surat city is surrounded by Bharuch, Narmada in the north, Navsari in the south, Tapi district in the east, and the Gulf of Cambay to the west. It is the second largest city of Gujarat in terms of population. The Tapi river is the major river through Surat city to the Arabian sea, while other four minor rivers, such as Kim, Ambika, Purna, and Midhola rivers, also drain the Surat district. The average annual rainfall of Surat city varies between 1200 and 1400 mm, and it has around 40–45 rainy days during the monsoon period (mid-June to mid-October).

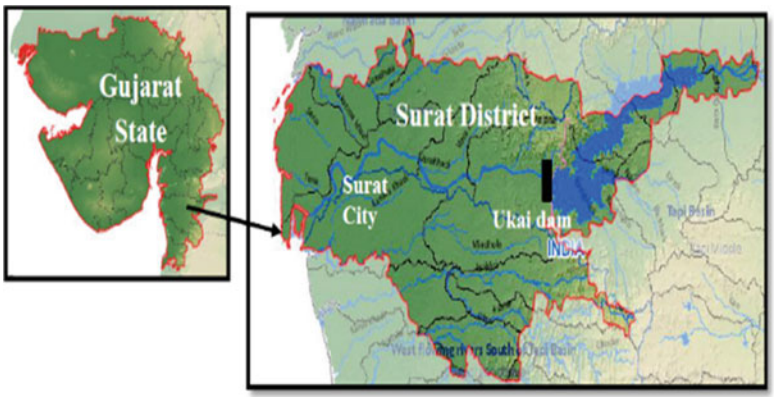

Fig. 8.1 Index map of study area

The soil texture is fine and highly productive; agriculture is the dominant practiced land use, covering in the region of 65% of Surat city. Major crops in Surat city are rice, sugarcane, cotton, wheat, banana, and sorghum. Moreover, the majority of the command area of the Ukai-Kakrapar dam project lies in Surat City. Surat city is a rapidly developing urban center, 106 km downstream of the Ukai dam with an area of about 326.5 km^2 and a population of 4.5 million (Bhat et al. 2013; Smith and Pathak 2018). An index map of the study area is shown in Fig. 8.1.

8.2.2 Data Collection

The monthly precipitation data of Surat city for the period of 20 years (1981–2000) were obtained from the India Meteorological Department (IMD) website portal (http://www.indiawaterportal.org/metdata, accessed May 2021). The data series downloaded was complete and homogenous; no missing data estimation was required. The normality and trend tests were applied on the annual series, which was constructed by summing monthly values, as detailed in the following section.

8.3 Methodology

Trend analysis of hydrometeorological variables of water, energy, and compound data, precipitation, temperature, and streamflow has been keenly used by hydrologists, geologists, and those interested in the historical use of water resources for several decades. The most commonly used method is the nonparametric Mann-Kendall test (Mann 1945; Kendall 1975).

The rainfall data were considered according over the hydrological year (i.e., June–May), in accordance with the India Meteorological Department (IMD)

classification of seasons of India: the southwest monsoon (June–September), post-monsoon (October–December), winter (January–February), and pre-monsoon (March–May). Following Aswad et al. (2020), the detection of trends in rainfall of the study area was made up of the following three main steps:

- Detecting increasing or decreasing trends by Mann-Kendall (nonparametric tests) in the seasonal rainfall data series.
- Estimation of the magnitude (relative importance) of trends using Sen's slope estimator (Sen 1968; Aditya et al. 2021).
- Compiling descriptive statistics: mean, standard deviation (SD), and coefficient of variation (CV) for the monthly, annual, and seasonal rainfall.

8.3.1 *Identifying Trends Using the Mann-Kendall Test in Seasonal Rainfall Data*

The Mann-Kendall test is the most widely used test for trend analysis of hydroclimatic series and is especially useful in ascertaining spatial variation and temporal deviation (Pandit 2016). Trend analysis is carried out here nonparametrically, detecting trends in the time series without prior indication of the trend type. Detected trends may be linear or nonlinear and are found using the following equation:

$$S = \sum_{i=1}^{N-1} \sum_{j=i+1}^{N} \operatorname{sgn}\left(x_j - x_i\right) \tag{8.1}$$

where N is number of data points. Assuming $(xj{-}xi) = \theta$, the value of sgn (θ) is computed using Eq. (8.2).

$$\operatorname{sgn}(\theta) = \begin{cases} 1 & \text{if} \quad \theta > 1 \\ 0 & \text{if} \quad \theta = 1 \\ -1 & \text{if} \quad \theta < 1 \end{cases} \tag{8.2}$$

This statistic represents the number of positive differences less the number of negative differences for all differences considered. For large samples (with a number greater than ten), the test is conducted using a normal distribution with mean calculated and the variance given as follows:

$$\operatorname{Var}(S) = \frac{N(N-1)(2N+5) - \sum_{k=1}^{n} t_k(t_k-1)(2t_k+5)}{18} \tag{8.3}$$

where N is the number of groups with zero difference between compared values and t_k is the number of data points in the k^{th} tied group. The standard normal deviate (z-statistic) is calculated using Eq. (8.4).

$$Z = \begin{cases} \dfrac{S-1}{\sqrt{\text{Var}(S)}} & \text{if} \quad S > 0 \\ 0 & \text{if} \quad S = 0 \\ \dfrac{S+1}{\sqrt{\text{Var}(S)}} & \text{if} \quad S < 0 \end{cases} \tag{8.4}$$

Should the value of Z be within the +/− 1.96, the null hypothesis of there being no trend in the series may not be rejected with 95% confidence. This test is two-tailed and should be correlated by a critical value of the standard normal deviate, $Z\alpha/2$. In the case $Z\alpha/2 \leq Z \leq Z1\text{-}\ \alpha/2$, the null hypothesis H_0 is approved with the use of percentage error.

8.3.2 *Using Sen's Slope Estimator to Provide a Measurement of Trends*

The magnitude of trend in time series may be ascertained using the nonparametric method of Sen's estimator (Sen 1968). The method assumes a linear trend. In the method, all data pairs slopes (T_i) are calculated using Eq. (8.5):

$$\begin{aligned} T_i &= \frac{x_j - x_k}{j-k} \\ &\text{for} \quad i = 1, 2, \ldots\ldots, N \end{aligned} \tag{8.5}$$

where x_j and x_k are data values at time j and k ($j > k$), respectively. The median of N values of T_i gives the Sen's slope estimator (Q). Should the time series have a positive value of Q, an upward trend is relayed, while a negative value shows a downward trend. The calculation is shown in Eq. (8.6):

$$Q_i = \begin{cases} T_{\frac{N+1}{2}} & N \text{ is odd} \\ \dfrac{1}{2}\left(T_{\frac{N}{2}} + T_{\frac{N+2}{2}}\right) & N \text{ is even} \end{cases} \tag{8.6}$$

XLSTAT software was used to complete the above analysis, installed in Microsoft Excel (version 16.0).

8.4 Results and Discussion

8.4.1 Annual and Seasonal Rainfall of Surat

The average annual and seasonal rainfall of the stations within Surat's catchment was computed. The maximum and minimum mean annual rainfall was received and analyzed. The graphical representation of mean annual and seasonal rainfall is shown in Fig. 8.2. The mean rainfall of the stations shows variation from the west to east direction. A major part of the annual rainfall is received during the southwest monsoon period. Upon consideration of rainfall across all months, it is clear that rainfall in Surat is stochastically spread across the time period shown.

Figure 8.2 shows the annual and seasonal rainfall at Surat for the period of 1981–2000. It also shows the variation for different rainfall series respecting the southwest monsoon, post monsoon, winter monsoon, pre-monsoon, and annual monsoon.

Figure 8.3 shows the mean monthly rainfall data of Surat. The graph shows the major rainfall months are June, July, August, and September. The pictorial representation of annual rainfall for Surat is given in Fig. 8.4. The basic statistical analysis of the rainfall series is presented in Table 8.1.

Table 8.1 shows statistical properties of annual and seasonal rainfall, mean, maximum, minimum, standard deviation, Mann-Kendall statistics (S), and variance (S), which are used for Mann-Kendall test and Sen's slope estimator. The statistical properties were used to calculate standard test statistic Z and Sen's slope Q.

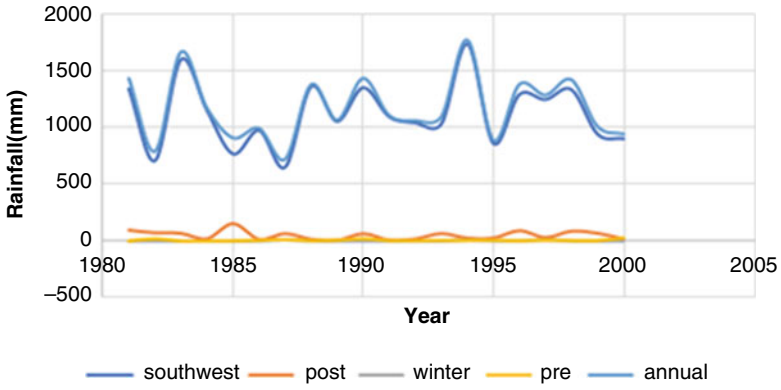

Fig. 8.2 Mean annual and seasonal rainfall (1981–2000) in Surat, India

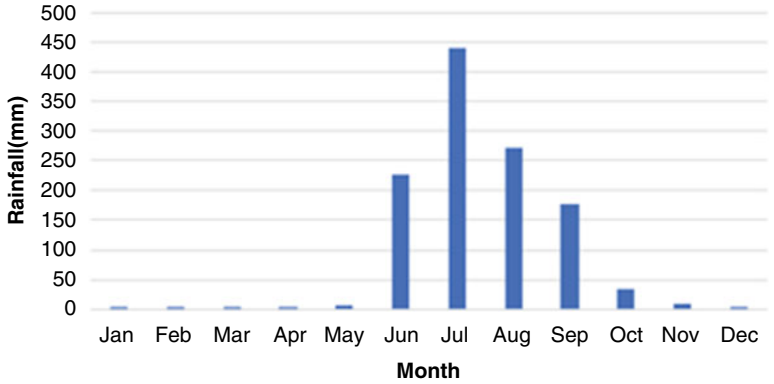

Fig. 8.3 Mean monthly (1981–2000) rainfall data of Surat

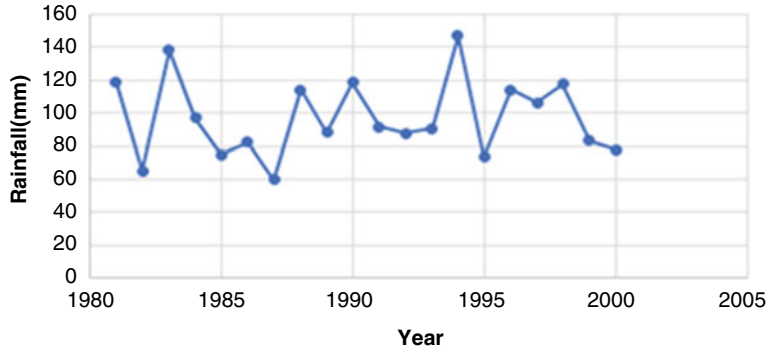

Fig. 8.4 Annual trend (1981–2000) of rainfall for Surat

Table 8.1 Summary of statistical properties of annual and seasonal rainfall in Surat, 1981–2000

Time series (seasonal)	Mean (mm)	Maximum (mm)	Minimum (mm)	Standard deviation	Mann-Kendall statistics (S)	Variance (S)
Annual	1115.43	1732.527	642.020	288.226	2	950
Southwest	45.374	140.341	3.619	35.636	−6	950
Post-monsoon	0.525	3.434	0.000	1.013	−10	950
Winter	6.422	24.947	0.000	6.945	22	884.667
Pre-monsoon	1167.75	1762.165	714.782	284.226	50	950

8.4.2 *Magnitude of Trend of Rainfall in Surat*

The magnitude of the trend in the annual and seasonal rainfall determined using the Mann-Kendall test and Sen's slope estimator for Surat is shown in Tables 8.2 and 8.3.

Table 8.2 shows Mann-Kendall analysis for the annual and seasonal rainfall. A positive trend was observed for annual monsoon, winter monsoon, and pre-monsoon. A negative trend was observed for the greater southwest monsoon and post monsoon.

Table 8.3 shows Sen's slope analysis for the annual and seasonal rainfall. A negative trend was observed for the higher rainfall of the southwest monsoon and post-monsoon. A positive trend was observed for the annual monsoon, winter monsoon, and pre-monsoon. These relationships prove useful in providing firsthand information of rainfall magnitude and change for Surat, India. Further, the general decreasing trend, confirmed here with Mann-Kendall and Sen's estimator gives a statistical breakdown that will confirm least squares regression of the same trend (Pandit 2016). Such data is of use in calculation of matrices for construction of a Laplacian rule structure for climatic systems of India relevant for the structuring and management of sustainability of life (Furze et al. 2017; Mills 2017; Arumugam and Karthik 2017; Praveen et al. 2020).

8.5 Conclusion

Qualitative and quantitative measurements of climate change are essential in order to give us foresight of the abruptly changing conditions that our world increasingly faces, in readiness for adaptations to be made for safeguarding/stability of ecological

Table 8.2 Mann-Kendall analysis for the annual and seasonal rainfall of Surat

Time series	Standard test statistics
Annual	0.032
Southwest	−0.162
Post-monsoon	−0.940
Winter	0.7060
Pre-monsoon	1.622

Table 8.3 Sen's slope analysis for the annual and seasonal rainfall of Surat

Time series	Sen's slope
Annual	0.159
Southwest	−2.474
Post-monsoon	−0.245
Winter	0.000
Pre-monsoon	0.241

systems, agroecological industries, and indeed the resource flow supporting all life forms and their sensitive dynamic among the balance of water and energy on Earth.

The nonparametric Mann-Kendall test and Sen's slope estimator are minimal tests which are sufficient in detection and identification of rainfall patterns for countering water resources issues in the region of Surat, India. The current chapter reveals a downward trend for most months of a year for the period under investigation. As the months of the southwest monsoon (i.e., June–September) have a significant decreasing trend, it can be inferred that the annual rainfall over Surat is decreasing. Given the geographical location and the reflective effect of the southwest monsoon on local extreme topographical areas such as the neighboring Himalayas, the change in distribution and volume of rain adds to the increasingly harsh conditions in India and with respect to global climate circulation, with dire consequences on both human societies and natural ecosystem diversity in India.

References

Aditya F, Gusmayanti E, Sudrajat J (2021) Rainfall trend analysis using Mann-Kendall and Sen's slope estimator test in West Kalimantan. In: 2nd International Conference on Tropical Meteorology and Atmospheric Sciences 23 – 25 March 2021, Jakarta, Indonesia. https://doi.org/10.1088/1755-1315/893/1/012006

Ahammad SJ, Chung ES, Shahid (2018) Parametric assessment of pre-monsoon agricultural water scarcity in Bangladesh. Sustainability 10(3). https://doi.org/10.3390/su10030819

Arumugam P, Karthik SM (2017) Prediction of seasonal rainfall data using fuzzy stochastic modelling. Glob J Pure Appl Math 13(9):6167–6174

Aswad FK, Yousif AA, Ibrahim SA (2020) Trend analysis using Mann-kendall and Sen's slope estimator test for annual and monthly rainfall for Sinjar district, Iraq. JDU 23(2):501–508. https://doi.org/10.26682/csjuod.2020.23.2.41

Bhat GK, Karanth A, Dashora L et al (2013) Addressing flooding in the city of Surat beyond its boundaries. Environ Urban 25(2):429–441. https://doi.org/10.1177/0956247813495002

Darshan M, Yadav SM (2022) Temporal analysis of rainfall and drought characteristics over Jalore District of S-W Rajasthan. Water Pract Technol 17(1):254–267. https://doi.org/10.2166/wpt.2021.114

Dasgupta P (2021) The economics of biodiversity: the Dasgupta review. HM Treasury, London. Available via https://assets.publishing.service.gov.uk/government/uploads/system/uploads/attachment_data/file/882222/The_Economics_of_Biodiversity_The_Dasgupta_Review_Interim_Report.pdf. Accessed 25 Jan 2022

Dunning CM, Turner AG, Brayshaw DJ (2015) The impact of monsoon intraseasonal variability on renewable power generation in India. Environ Res Lett 10. https://doi.org/10.1088/1748-9326/10/6/064002

Furze JN, Zhu Q, Hill J et al (2017) Biological modelling for sustainable ecosystems. In: Mathematical advances towards sustainable environmental systems. Springer, Cham. https://doi.org/10.1007/978-3-319-43901-3_2

Huang X, Zhou T, Turner A et al (2020) The recent decline and recovery of Indian summer monsoon rainfall: relative roles of external forcing and internal variability. J Clim 33(12):5035–5060. https://doi.org/10.1175/JCLI-D-19-0833.1

Jagadeesh P, Anupama C (2014) Statistical and trend analyses of rainfall: a case study of Bharathapuzha River basin, Kerala, India. ISH J Hydraul Eng 20(2):119–132. https://doi.org/10.1080/09715010.2013.843280

Kendall MG (1975) Rank correlation methods, 4th edn. Charles Griffin, London
Kuttippurath J, Murasingh S, Stott PA et al (2021) Observed rainfall changes in the past century (1901–2019) over the wettest place on Earth. Environ Res Lett 16. https://doi.org/10.1088/1748-9326/abcf78
Kyung-Ja H, Byeong-Hee K, Eui-Seok C et al (2020) Major factors of global and regional monsoon rainfall changes: natural versus anthropogenic forcing. Environ Res Lett 15. https://doi.org/10.1088/1748-9326/ab7767
Mann HB (1945) Non parametric tests against trend. Econometrica 13(3):245–225
Mehta D, Yadav SM (2020) Long-term trend analysis of climate variables for arid and semi-arid regions of an Indian State Rajasthan. Int J Hydrol Sci Technol. https://doi.org/10.1504/IJHST.2020.10033400
Mehta D, Yadav SM (2021a) An analysis of rainfall variability and drought over Barmer district of Rajasthan, northwest India. Water Supply 21(5):2505–2517. https://doi.org/10.2166/ws.2021.053
Mehta D, Yadav SM (2021b) Meteorological drought analysis in Pali District of Rajasthan State using standard precipitation index. Int J Hydrol Sci Technol. https://doi.org/10.1504/IJHST.2021.10037751
Mehta D, Yadav SM (2021c) Analysis of long-term rainfall trends in Rajasthan, India. In: Climate change impacts on water resources. Water Science and Technology Library, p 98. https://doi.org/10.1007/978-3-030-64202-0_26
Mehta D, Yadav SM (2022) Long-term trend analysis of climate variables for arid and semi-arid regions of an Indian State Rajasthan. Int J Hydrol Sci Technol 13(2):191–214
Mills TC (2017) Stochastic modeling of rainfall patterns across the United Kingdom. Meteorol Appl 24:580–595. https://doi.org/10.1002/met.1658
Panda A, Sahu N (2019) Trend analysis of seasonal rainfall and temperature pattern in Kalahandi, Bolangir and Koraput districts of Odisha, India. Atmos Sci Lett 20(10). https://doi.org/10.1002/asl.932
Pandit DV (2016) Seasonal rainfall trend analysis. Int J Eng Res Appl 6(7):69–73
Pingale SM, Khare D, Jat MK et al (2016) Trend analysis of climatic variables in an arid and semi-arid region of the Ajmer District, Rajasthan, India. J Water Land Dev 28(1):3–18. https://doi.org/10.1515/jwld-2016-0001
Pokharel AK, Hallet J (2015) Distribution of rainfall intensity during the summer monsoon season over Kathmandu, Nepal. Weather 70(9):257–261. https://doi.org/10.1002/wea.2544
Praveen B, Talukdar S, Shahfahad et al (2020) Analyzing trend and forecasting of rainfall changes in India using non-parametrical and machine learning approaches. Sci Rep 10. https://doi.org/10.1038/s41598-020-67228-7
Sen PK (1968) Estimates of the regression coefficient based on Kendall's Tau. J Am Stat Assoc 63:1379–1389. https://doi.org/10.1080/01621459.1968.10480934
Sharma S, Hamal K, Khadka N et al (2020) Dominant pattern of year-to-year variability of summer precipitation in Nepal during 1987–2015. Theor Appl Climatol 142:1071–1084. https://doi.org/10.1007/s00704-020-03359-1
Smith RM, Pathak P (2018) Urban sustainability in India: green buildings, AMRUT Yojana and smart cities. In: Metropolitan governance in Asia and the Pacific rim. Springer Singapore. https://doi.org/10.1007/978-981-13-0206-0_9
Somisetty A, Pachore A, Remesan R et al (2022) Multi-model assessment of streamflow simulations under climate and anthropogenic changes exemplified in two Indian river basins. Water 14(2). https://doi.org/10.3390/w14020194
Thenmozhi M, Kottiswaran SV (2016) Analysis of rainfall trend using Mann-Kendall test and the Sen's slope estimator in Udumalpet of Tirupur district in Tamil Nadu. Int J Agric Sci Res 6(2):131–138

Thomas J, Prasannakumar V (2016) Temporal analysis of rainfall (1871–2012) and drought characteristics over a tropical monsoon-dominated State (Kerala) of India. J Hydrol 534:266–280. https://doi.org/10.1016/j.jhydrol.2016.01.013

WHO (2003) Climate change and human health risks and responses. World Health Organisation. Available via https://www.who.int/globalchange/publications/climchange.pdf. Accessed 25 Jan 2022

Verma MK, Verma MK, Swain S (2016) Statistical analysis of precipitation over Seonath river basin, Chhattisgarh, India. Int J Appl Eng Res 11(4):2417–2423

Zhao D (2020) Changes in daily and cumulative volumetric rainfall at various intensity levels due to urban surface expansion over China. Tellus A Dyn Meteorol Oceanogr 72(1):1–21. https://doi.org/10.1080/16000870.2020.1745532

Part III
Desertification Risks and Contrasts from Southern Europe and the Philippines

In Thessaly, in recent years, 20000 ha of arable land has been abandoned due to low fertility, loss of top-soil organic matter and soil erosion as a result of tillage and deep plowing. Agricultural practice must accentuate soil quality for ecosystem service value and agroecological production. Figures 1–5 were provided by Dr. Christos Noulas.

In Philippine provinces and on Mindoro, the traditional practices of rice and coconut farming, small livestock and fishing result in strongly bound communities, though the islands are devastated by an increasing frequency of extreme weather and sea-level rise. The people of these islands are innovative, resilient and proud. Figures 6–21 were provided by members of 'Amang' Rodriguez Memorial Medical Centre and resident Filipino farming families.

Fig. 1 Spatial distribution of soil organic matter in agricultural soils in the region of Thessaly, Central Greece in a) 1980, and b) 2015. Map contributions were made by the Hellenic Agricultural Organization, Athens, Greece in 2021

Fig. 2 Hilly landscape of cultivated areas between the villages of Chara and Chalkiades, Thessaly, Greece, 2015

Fig. 3 Gully soil erosion on a cultivated sloping area in Chalkiades, Thessaly, Greece, 2015

Fig. 4 Soil erosion on a hilly landscape between Larissa and Farsala cities, Thessaly, Greece, 2015

Fig. 5 Cotton (*Gossypium* sp.), *Acacia* sp. plantation, aiding reforestation, Skotoussa village, Thessaly, Greece, 2015

Fig. 6 'Silkies'- combined management of chickens cleaning the soil beneath bananas, Bulacan, February 2021

Fig. 7 Rogelio Orfanel – a proud father, grandfather and innovative Filipino environmental farmer observing a frame from a bee box designed to assist 'wild' bee populations, Quezon, April 2014

Fig. 8 Mixed pineapple (*Annanas* sp.) plantation with occasional coconut (*Cocos nucifera* L.) and fig (*Ficus* sp.), staged rotation, benefitting soil and biodiversity, Quezon, April 2014

Fig. 9 Rice (*Oryza sativa*), a Philippine staple, seed sourced from the Department of Agriculture, Mindoro, October 2020

Fig. 10 Combined management practice, the pigs clean and cultivate soil after the rice harvest, Mindoro, May 2020

Fig. 11 Mixed banana (*Musa* sp.) and coconut (*Cocos nucifera* L.) plantation, allowed to overgrow to benefit biodiversity, Mindoro, May 2020

Fig. 12 Carabao (*Bubalus bubalis*) – working cows facilitating functional, diverse farming practice, Mindoro, June 2020

Fig. 13 Carabao (*Bubalus bubalis*) spread across the islands and are trained by the very young, Mindoro, April 2020

Fig. 14 Snake gourds (*Trichosanthes* sp.), Mindoro, April 2020

Fig. 15 Banana (*Musa* sp.) harvesting in preparation for local markets, Mindoro, April 2021

Fig. 16 Lady selecting egg plants (*Solanum* sp.) for the local market, Mindoro, April 2020

Fig. 17 Increased frequency and severity of annual storms cause flooding problems, Mindoro, December 2020

Fig. 18 High winds and rainfall during storms batter the community and its plantations, Mindoro, December 2020

Fig. 19 Fishermen preparing boats for their small daily catch for local sale, Mindoro, July 2020

Fig. 20 Community involvement folding nets after small fishing catch, Mindoro, July 2020

Fig. 21 The lady on her bicycle enjoying her daily delivery of fish, fruit and other produce, Mindoro, August 2020

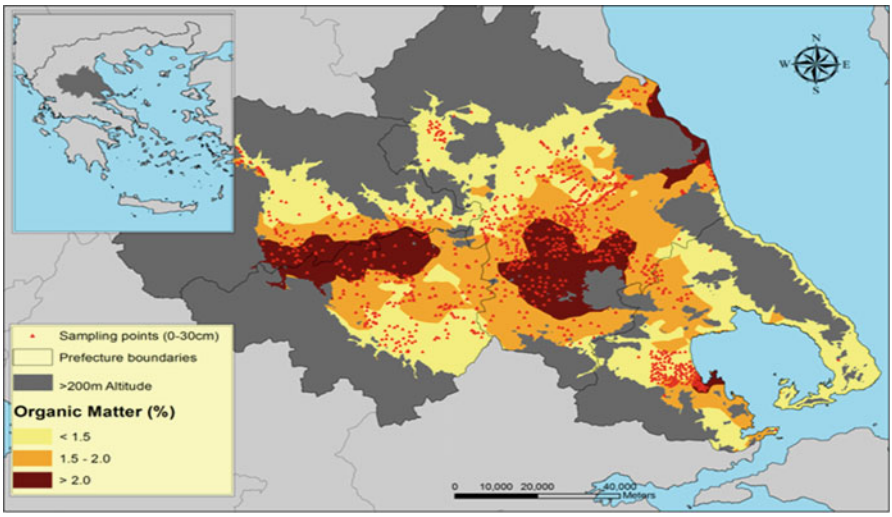
Sampling points (0-30cm)
Prefecture boundaries
>200m Altitude
Organic Matter (%)
< 1.5
1.5 - 2.0
> 2.0
0 10,000 20,000 40,000
Meters
N
W
E
S

Fig. 1a

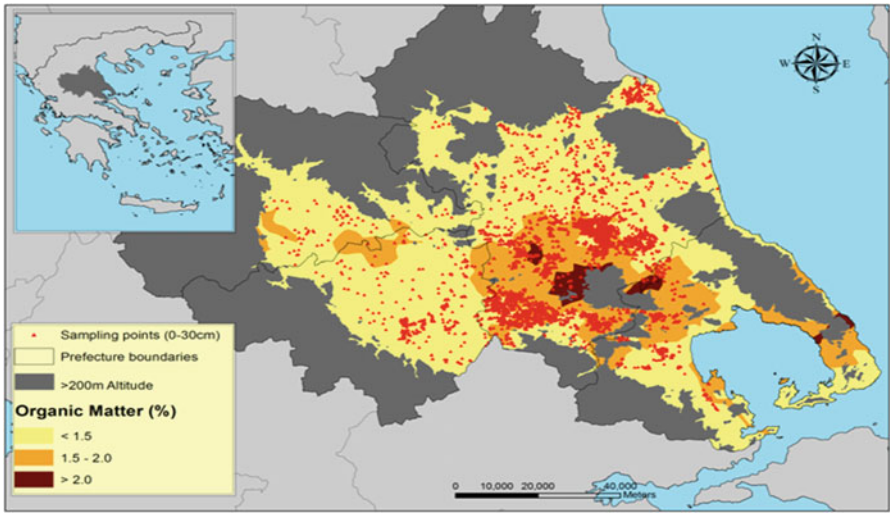
Sampling points (0-30cm)
Prefecture boundaries
>200m Altitude
Organic Matter (%)
< 1.5
1.5 - 2.0
> 2.0
0 10,000 20,000 40,000
Meters
N
W
E
S

Fig. 1b

Fig. 2

Fig. 3

Fig. 4

Fig. 5

Fig. 6

Fig. 7

Fig. 8

Fig. 9

Fig. 10

Fig. 11

Fig. 12

Fig. 13

Fig. 14

Fig. 15

Fig. 16

Fig. 17

Fig. 18

Fig. 19

Fig. 20

Fig. 21

Chapter 9
Risk Assessment Applications: Exposure, Safety, and Security

Mrugesh H. Trivedi, Gautam V. Priyadarshi, Dipa Lalwani, and Saeid Eslamian

Abstract Risk assessment is a term which encompasses the entire process of hazard/risk identification, risk analysis, risk evaluation, and control. The term 'risk' is commonly believed to be associated with industrial operation; however, categorisation of risk reveals common elements, which can be applied to avoid hazards in other areas. Risk in a wider context is related to the probable harmful effects occurring to human health and/or ecological systems as a result of exposure to environmental stressors. The unsustainable use of natural resources creates stress and causes risks to ecology and human health that lead to social issues in surrounding communities, such as low quality of health and unemployment. Although natural events may be responsible for risk, anthropogenic activities are the major basis of risk to the environment and humans. Environmental risks present themselves as the probability of temporary or permanent changes to the atmosphere, hydrosphere, and lithosphere due to human activities that result in the loss of biodiversity, global warming, and climate change. The risk factor can be understood by calculating relative risk, attributable risk, and odds ratio. The risks occur primarily from exposure to factors such as occupational exposure, environmental exposure, biological exposure, and chemical exposure. The magnitude of the impact of risk on humans or wildlife depends on the path of exposure (inhalation, ingestion, and dermal), amount of exposure (dose), and duration of exposure. The severity of overall risk is dependent upon a range of factors and scenarios. Application of risk

M. H. Trivedi (✉) · G. V. Priyadarshi
Department of Earth and Environmental Science, KSKV Kachchh University, Bhuj, Kachchh, India
e-mail: drmrugesh.trivedi@gmail.com; gautamparghi@gmail.com

D. Lalwani
Department of Environmental Science and Technology, Institute of Science and Technology for Advance Studies and Research (ISTAR), Vallabh Vidhyanagar, India
e-mail: lalwani.dipa6@gmail.com

S. Eslamian
Department of Water Engineering, College of Agriculture, Isfahan University of Technology, Isfahan, Iran
e-mail: saeid@iut.ac.ir

J. N. Furze et al. (eds.), *Earth Systems Protection and Sustainability*,
https://doi.org/10.1007/978-3-030-98584-4_9

assessment enables taking care of safety and security in environmental, ecological, and social issues so that the well-being of humans and 'Mother Earth' can be managed. To ensure the safety and security of environmental sustainability, this chapter will focus on environmental contaminants and their risk to human health by projecting five key steps in the process of risk assessment.

Keywords Dose-response · Environmental exposure · Occupational exposure · Risk assessment · Management

9.1 Introduction

Risk is defined as the probability of something going wrong or there may be an unpleasantness that causes injury or loss. Risks revert from specific hazards or threats that occur from any livelihood and affect humans, animals, or the environment (Reynolds and Jennifer 2015). The magnitude of the overall risk is dependent upon various factors such as the potentiality of contaminants to cause damage and the mode and duration of exposure. The overall purpose of risk assessment is to characterise the nature and magnitude of health risks to humans (residents, workers, recreational visitors) and ecological receptors (birds, fish, and wildlife). Thus, risk assessment acts as a safeguarding action from physical, chemical, biological, or other stressors that may be present or anthropogenically introduced to the environment. Risk assessment (RA) is the systematic approach of confronting and expressing uncertainty in predicting the future. RA has been developed as an examination of workplace safety, to determine if adequate safeguards have been taken or more should be done to avert possible harm. To get the environmental clearance for any project, there is a provision to conduct an environmental impact assessment (EIA). Both RA and EIA have similar goals and provide complementary information. The objective is not limited to estimating quantitative risk and the impact on the environment. However, the rationale behind policy-making for conducting EIA and RA is intended to provide reason-based predictions of possible consequences of planned decisions to provide other comfortable alternatives and management plans (Andrews 1990). The United States Environmental Protection Agency (USEPA) divides risk assessment into two categories: (i) human health risk assessment and (ii) ecological risk assessment (USEPA 2019a). As per the USEPA definition, 'the environmental risk is the probability of harmful effects to human health and/or ecological systems due to exposure to that environment'. It is also known as 'ecological risk assessment' (ERA). In the twenty-first century, anthropogenic activities have contaminated all spheres of Mother Nature outside the industrial/research laboratories and commercial areas. Therefore, RA applications should go beyond the boundaries of industry and should cover all three components of sustainability, i.e., social, economic, and ecology. A common man may have some risk from the environmental contamination of the water he drinks, the food he consumes, or the air he used to breathe. The risk that affects humans, animals, or the environment after an accidental exposure or intentional release of a biological agent is known as biological risk. A person, who works directly with biological

materials, faces numerous bio-risks, which also exist for a person who works indirectly with or near infectious agents (Reynolds and Jennifer 2015). The recent example of the coronavirus pandemic (christened by the World Health Organisation as "COVID-19") has further led to a risk of an outburst of pneumonia. It was first detected in Wuhan, Hubei Province, China. The virus has infected almost more than 248,098 out of which more than 10,000 death reported from 182 countries as of 20th March 2020 and continues to expand. The pandemic condition created by COVID-19 has forced us to rethink biosafety and security measures at all possible places to avoid or to reduce the bio-risk. To ensure the safety and security of humans and ecology for environmental sustainability, this chapter will further discuss the risk assessment process with several examples of environmental contaminants and risk assessment applications.

9.2 Risk Assessment Process

Risk assessment is a four-step process that utilises empirical information to assess health effects caused by exposure: The four steps are (1st) hazard identification, (2nd) exposure assessment, (3rd) dose-response assessment, and (4th) risk characterisation. While Carpenter (1995) has shown his consent for the four steps process, he further emphasised that attempts to quantify the risk to human health, economic welfare, and ecosystem from human activities and natural phenomena are incomplete without preparing to mitigate or eliminate unacceptable risks asserting the fifth step of risk management. These steps are illustrated in Fig. 9.1.

The five steps of risk assessment are detailed in subsections of Sect. 9.2.

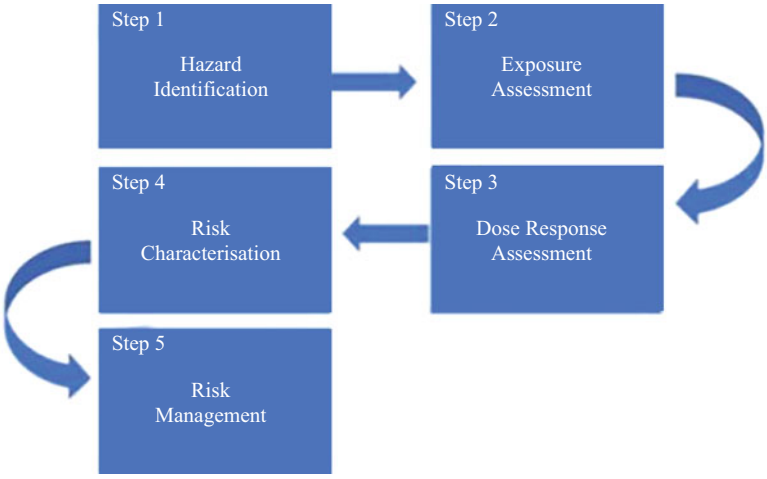

Fig. 9.1 The five steps of the risk assessment process (USEPA 2019b, c; Lohani et al. 1997)

9.2.1 Hazards Identification (Step One)

Hazard identification determines whether environmental exposure of pollutants or contaminants can lead to an increase in the occurrence of certain negative health effects. It lists the possible sources of harm, usually identified by experience elsewhere with certain technologies, materials, or conditions. Exposure to environmental pollutants may cause different adverse effects on human populations such as carcinogenesis, neurotoxicity, cytogenetic damage, and endocrine disruption in addition to developmental, reproductive, and immunological disorders (Tchounwou et al. 2012; Coster and Larebeke 2012). Recent studies reveal that widely used plastic products have contaminated the world with a number of different environmental endocrine-disrupting chemicals (EDCs). EDCs may also lead to deleterious impacts on human blood through the generation of reactive oxygen species (ROS) (Trivedi et al. 2020), in addition to toxicological dysregulation in embryonic reproductive tissue differentiation and development (Rich et al. 2016), which may further lead to gender dysphoria in humans. The EDCs exposure to aquatic animals may cause vitellogenin induction in fish (Thorpe et al. 2001) that may lead to a negative effect on fish breeding and consequently on fish catch. Natural contamination such as the high level of fluoride in drinking water produces neurotoxicity in school children of 12–14 years of age, in addition to known impacts of dental and skeletal fluorosis (Trivedi et al. 2007; Ding et al. 2011; Seraj et al. 2012; Choi et al. 2012; Trivedi et al. 2012; Razdan et al. 2017; Duan et al. 2018). The USEPA (2019b and Damania et al. 2019) have issued threshold guidelines and frequently update the lists of highly toxic chemicals based on new research outcomes. These thresholds indicate the minimum concentration of chemicals involved in causing harm if present at any location in a particular form. In addition to guidelines, environmental indicators provide information on pollution. For example, intensive anthropogenic activities result in the disappearance of foraminifera from the ocean (Bhatt and Trivedi 2018), which is one of the most significant natural indicators of anthropogenically disturbed coast.

Hazard identification is a systematic approach to identify risks and determine their scope, impact, and vulnerability effect in our surroundings. Hazard identification can be more thoroughly understood by the relationship between exposure to any hazardous compounds and the risk of causing adverse consequences (Masters and Ela 2008). That can be identified by using a simple 2 × 2 matrix as given in Table 9.1, where rows divide people by exposure and columns divide them by disease.

Table 9.1 A 2 × 2 matrix for epidemiologic rate comparison

	With disease	Without disease
Exposure	a	b
Non-exposure	c	d

The rows split the populations among those who have been exposed to the risk factor and those who have not. The columns are based on the numbers of people with the disease and without the disease. Relative risk is thus defined as

$$\text{Relative risk} = \frac{a(a+b)}{c(c+d)} \tag{9.1}$$

Here we should note that the numerator is the fraction of those exposed who have the disease and the denominator is the fraction of those not exposed but have the disease. If those two ratios are the same, the probabilities of having the disease would not depend on contact with risk factor. Above 1.0, the higher relative risk shows an association between exposure and risk. The attributable risk is defined as

$$\text{Attributable risk} = \frac{a}{a+b} - \frac{c}{c+d} \tag{9.2}$$

In Table 9.1, the difference between the odds of having the disease with and without exposure is known as attributable risk. Attributable risk with the value of 0.0 shows no relationship between exposure and risk.

The cross product of the entries in the matrix is known as odds ratio.

$$\text{Odds ratio} = \frac{ad}{bc} \tag{9.3}$$

Numbers greater than 1.0 indicate that there is a link between exposure and risk.

An example of hazard identification using the above formula would be an examination of personnel data for employees of a vinyl chloride manufacturing firm revealing that 15 of 200 workers had liver cancer. A control group of persons with smoking histories similar to the exposed employees and who were unlikely to have come into contact with vinyl chloride had 24 people acquire liver cancer and 450 people did not develop liver cancer. To reveal the relationship between exposure and risk, the data may be summarised as shown in Table 9.2.

Solving for each measure yields

$$\text{Relative risk} = \frac{15/(15+185)}{24/(24+450)} = \frac{0.075}{0.05} = 1.5.$$

$$\text{Attributable risk} = \frac{15}{200} - \frac{24}{474} = 0.024$$

Table 9.2 A 2 × 2 matrix for epidemiologic rate comparison

	Liver cancer	Non-cancer worker
Exposure	15	185
Non-exposure (control)	24	450

$$\text{Odds ratio} = \frac{15 \times 450}{185 \times 24} = 1.52$$

In the example, the relative risk and the odds ratio both are above 1.0, so they show that there is a relationship between exposure and risk. For those who were exposed, the risk of cancer has increased by 0.024 (the attributable risk) over that of their cohorts who were not exposed (Masters and Ela 2008). Based on all three measures, we can identify the risk, and further study of risk assessment can give guidance to reduce and manage the risk.

9.2.2 Exposure Assessment (Step Two)

The process of assessing or estimating the size, frequency, and duration of exposure to an environmental agent or stressor is known as an exposure assessment. Contaminant sources, release methods, distribution, and transformation characteristics are all essential considerations in determining exposure. Exposure assessment also includes the determination of any exposure of contaminants through inhalation, ingestion, and dermal in the group of population. There are various ways to identify exposure such as diagnosis of disease including analysis of blood samples, urine samples, saliva, tissue samples, or a swab from nasal or buccal cavity. There are two types of exposure, viz., (i) occupational exposure and (ii) environmental exposure.

9.2.2.1 Occupational Exposure

Occupational exposure can be explained as the exposure to any stressor, either chemical or biological, at a workplace, which might harm the employee/workers. For example, workers in mining or road construction have the risk of accident or mine collapse. Risk identification and analysis for occupational exposure include identifying unfavourable occurrences that result in a hazard, analysing the hazard process of the unfavourable event, and estimating the extent, size, and frequency of detrimental consequences (Paithankar 2011). Due to high-risk procedures, hazardous sectors witness substantial deaths connected to workers and workplaces (Gul and Ak 2018). Hazardous industries are facing serious fatalities related to work, workplaces, and workers because of their high-risk processes (Gul and Ak 2018).

Recent studies revealed that chronic exposure to petrochemical and chemical industry pollutants such as suspended particles, polycyclic aromatic hydrocarbons (PAH), volatile organic compounds (VOCs), SO_x, ozone (O_3), and NO_x are linked with detrimental health effects including reduced lung capacity, increased respiratory illnesses, and increase in rate of mortality. These are particularly found in industrial workers (WHO 2006). Additionally, handling and working on the premises of the above mentioned chemical causes allergies and sever respiratory effects

such as asthma and chronic obstructive pulmonary disease (COPD) (Ramirez et al. 2012).

Apart from the chemical industries, some workers with biological exposure to aquaculture or food production processes may also have a risk of occupational diseases and injuries. Ngajilo and Jeebhay (2019) revealed occupational exposure characterisation for noise and chemicals such as formaldehyde and microorganisms such as *E. coli* bacteria in fish ponds. The occupational diseases related to the aquaculture work included musculoskeletal disorders (MSD), respiratory symptoms and asthma, skin infections, dermatitis and urticarial, and some occupational infections such as leptospirosis. The farmers associated with agricultural activities are also susceptible to the risk of various chemical-based fertilisers and pesticide exposure.

Recently, global studies have shown negative health effects of commonly used agrochemicals in farming. Various diseases ranging from respiratory effects to cancer have been identified among farmers due to exposure to such agrochemicals (Dhananjayan and Ravichandran 2018). Pesticide exposure at work is related to an increased risk of obstructive lung diseases including chronic bronchitis and COPD (Pourhassan et al. 2019). The agrochemical-based industrial occupation has the same types of risk and occupational disease. Therefore, several countries have legislation to conduct risk assessment studies as a part of their EIA for environmental clearance, before starting any industry.

Risks can be identified, and the severity can be measured based on risk assessment analysis. Precautions can be taken to minimise the risk by using risk assessment methods. In most cases, the occupational health-related risk is well managed and given more concern for environmental clearance. The compensation mechanism has encouraged employers to improve the safety of workers at the workplace. The compensation insurance system may reduce occupational accidents and rises the risk-based employer's payment (Shin et al. 2011). In the present era, there are various legislation and guidelines, throughout the world, including the factory act, the mine act, the fire act, the insecticide act, OECD guidelines, and the environmental protection act that provide occupational safety in addition to the well-being of the worker at their workplace.

9.2.2.2 Environmental Exposure

Approximately 25% of global deaths occur due to exposure to environmental pollutants, including those in household and ambient air pollution, ultraviolet radiation, and various chemicals (Pruss-Ustun et al. 2016). According to the United Nations Development Programme (UNDP), every 2 s someone aged between 30 and 70 dies prematurely from non-communicable diseases including cardiovascular and chronic respiratory diseases, diabetes, or cancer. The causes of diseases are often unknown environmental pollution. Every year, seven million people worldwide die as a result of exposure to fine particles in contaminated air (UNDP 2019a). The UNDP has set 17 sustainable development goals in which the 3rd goal focuses on

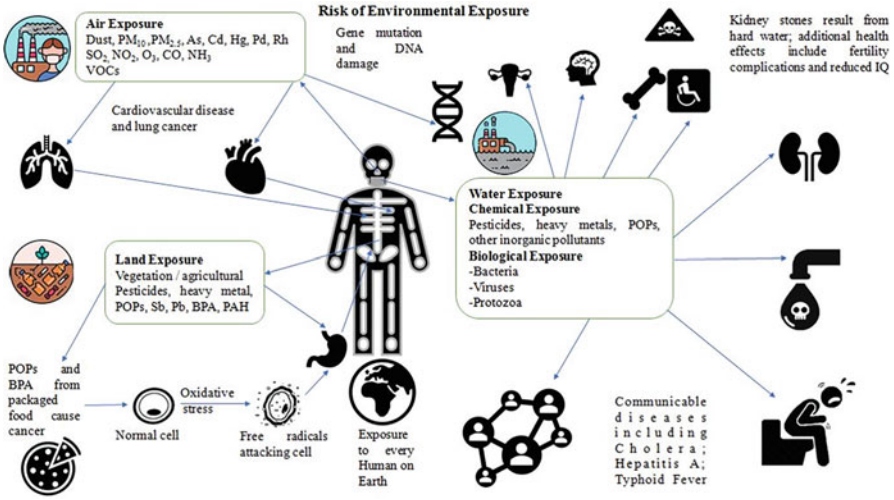

Fig. 9.2 Risk of environmental exposure from the air, water, and land with its health effects

"Good Health and Well-Being." To achieve this, it is essential to have a comprehensive understanding of risk assessment to environmental contaminant exposure. The majority of hazardous chemicals and pollutants and their adverse health effects are summarised in Fig. 9.2.

Due to modern lifestyle and industrialisation, there is a continuous emission of toxic pollutants from various anthropogenic sources; these pollutants have become part of our routine life. Sadly, there is a scarcity of awareness among people towards health risks associated with exposure to environmental pollutants. To understand the same, first, there is a need to understand the intake of pollutants using the universal formula as follows:

$$\text{Intake}\,(I) = \frac{C \times \text{CR} \times \text{EFD}}{(\text{BW} \times \text{AT})} \tag{9.4}$$

where

I = Intake – the amount of the chemical taken [mg (kg body weight)$^{-1}$ × day^{-1}]
C = average concentration of the pollutant over the exposure period, [mg/dm^3 water], [mg/kg soil], [mg/m^3 air]
CR = Contact rate, the quantity of contaminated medium contacted per unit time, [mg soil/day], [m^3 water /day], [m^3 air/day]
EFD = Exposure frequency and duration. It describes how often and how frequently exposure occurs [hours], [days], [years]
BW = Average body weight [kg]
AT = Averaging time, the period of exposure [days]

Environmental exposure may occur in diverse ways, such as inhalation of polluted air, ingestion of contaminated water and food, and exposure to biological pathogens due to unhygienic routine habits. Common environmental exposures to humans are discussed hereafter in brief.

The environmental exposure of pollutants or contaminants occurs through three main pathways: inhalation, ingestion, and dermal exposure (De Miguel et al. 2007). The amount of exposure to the pollutants via their routes can be calculated using different equations, where accurate data of the concentration of the pollutant in the particular matrix is the most important, as the error in the concentration of the pollutants may lead to false-positive or false-negative exposure results. Dose concentration may be calculated by using the following equations:

Inhalation of resuspended particles or toxic gases through mouth and nose from the environment:

$$D_{\text{inhalation}} = \frac{C \times \text{Inh R} \times \text{EF} \times \text{ED}}{\text{BW} \times \text{AT} \times \text{PEF}} \tag{9.5}$$

Direct ingestion of environmental contaminants from the consumption of food and water:

$$D_{\text{ingestion}} = \frac{(C \times \text{Ing R} \times \text{EF} \times \text{ED})}{(\text{BW} \times \text{AT})} \times 10^{-6} \tag{9.6}$$

Dermal absorption of contaminants adhered to exposed skin:

$$D_{\text{dermal}} = \frac{(C \times \text{SA} \times \text{SL} \times \text{ABS} \times \text{EF} \times \text{ED})}{(\text{BW} \times \text{AT})} \times 10^{-6} \tag{9.7}$$

Where:

D = exposed dose in (mg kg^{-1} day^{-1}) through inhalation ($D_{\text{inhalation}}$), ingestion ($D_{\text{ingestion}}$), and dermal (D_{dermal}) contact
C = Concentration of contaminants in mg kg^{-1}
Inh R = Inhalation rate (USEPA 2011)
Ing R = Ingestion rate
EF = Exposure frequency (site-specific)
ED = Exposure duration (site-specific)
BW = Average body weight
AT = Average exposure time
PEF = Particle Emission Factor (USEPA 2014)
SA = Exposed skin area (USEPA 2008)
SL = Skin adherence factor
ABS = Dermal absorption factor

A few examples of environmental pollutant exposures are given in the remainder of this section.

9.2.2.3 Risk Related to Exposure to Polluted Air

As per USEPA (2019d), there are six most common pollutants in the atmosphere, also known as 'criteria pollutants'. These are also considered as a standard of ambient air quality for most of the countries, including airborne particulate matter (PM), carbon monoxide (CO), nitrogen dioxide (NO_2), sulphur dioxide (SO_2), ozone (O_3), and lead (Pb). Evidence from epidemiological studies has demonstrated that both outdoor and indoor air pollution are well-known major problems of public health (Bruce et al. 2000). A recent human study revealed that short-term exposure to traffic-related air pollution (TRAP) alters some extracellular micro-RNAs. TRAP is a dynamic combination of pollutants such as PM_{10}, $PM_{2.5}$, NO, NO_2, CO, CO_2, black carbon, and ultrafine particulate matter. TRAP increased the risk of a variety of illnesses including various forms of cancer, lung, cardiovascular, and neurological disorders, and, more recently, diabetes mellitus (Krauskopf et al. 2019).

9.2.2.4 Particulate Matter (PM) and Gaseous Phase

Particulate matter is classified as PM_{10}, further known as suspended particulate matter (SPM), and $PM_{2.5}$ and respirable particulate matter (RSPM). $PM_{2.5}$ and $PM_{<1.0}$ are of major risk due to their ultrafine size, which can penetrate respiratory systems deeply. Such ultrafine particles are associated with increased mortality and morbidity due to various side effects on humans including cardiovascular disease, respiratory syndrome, COPD, decreased lung function, and premature mortality (Pope et al. 2004; Samoli et al. 2008; Halonen et al. 2009; Guaita et al. 2011; Perez et al. 2012). Liu et al. (2019b) have found that maternal exposure to $PM_{2.5}$ may increase susceptibility to foetal distress. Kim et al. (2017) have found a positive correlation between asthma hospitalisation and the concentration of PM in residential areas. In addition to the fine size, persistent organic chemicals (POPs) attached to the $PM_{<1.0}$ and $PM_{2.5}$ directly penetrate human lungs via inhalation and are also a matter of concern. Recent studies on emerging pollutants give evidence of chemicals attached to particulate matter, being present in the gaseous phase of the atmosphere risking human health (Ge et al. 2017; Guo et al. 2018; Müller et al. 2012; Ruan et al. 2019).

9.2.2.5 Carbon Monoxide (CO)

Carbon monoxide (CO) is a colourless, odourless, tasteless, and fatal gas that is released from incomplete combustion. It is highly toxic when inhaled. The cooking and heating appliances are the sources of CO in our houses due to poorly maintained appliances, clogged flues, vents, or chimneys. Especially in rural areas, wood burners and other solid fuel heating systems are being used that potentially increase the risk of CO poisoning (HES 2019). Cushen et al. (2019) have reported a local area

of a European country (Wales) has experienced an incident of carbon monoxide exposure due to faulty installation of at least 541 wood burners. In developed and developing countries, open burning of municipal waste is practised leading to the emission of CO gas.

9.2.2.6 Nitrogen Oxides (NO_x)

Oxides of nitrogen, a group of nitrogen oxides (NO_x), are highly reactive gases. In the anthropogenic form, they are largely emitted from vehicular emission. NO_x is emitted from natural sources such as lightning and the natural combustion of biomass. The concentration of NO_x is directly related to acid rain, photochemical smog, and ozone in the atmosphere (Liu et al. 2019b). If a high amount of NO_x is inhaled by the human body, it causes damage to lung function and disturbs respiratory systems. Many researchers study the impact of NO_x on human health risks in metro cities where vehicular traffic is highest (Neuberger et al. 2002; Samoli et al. 2007; Boningari and Smirniotis 2016).

9.2.2.7 Sulphur Oxides (SO_x)

Oxides of sulphur, a group of sulphur oxides (SO_x), are also highly reactive gases. The majority of SO_x comes from anthropogenic sources, namely, urban transportation and industrial activity, by the burning of coal (Ielpo et al. 2019). In an Italian epidemiological study related to SO_x exposure, it was revealed that people who reside beside an industrial area have a high risk of adverse health consequences and were suffering from critical situations in terms of short-term health effects and excess mortality (Gianicolo et al. 2016). A researcher from China has found a correlation between exposure to SO_2 and adverse short-term effects on total health with specific cardiovascular disease (CVD) and related hospital admission (Amsalu et al. 2019). Several studies reveal that a high risk of acid rainfall is related to the high atmospheric concentration of SO_x which can deteriorate historically/archaeologically significant monuments such as the Taj Mahal in India.

9.2.2.8 Ozone (O_3)

Ozone is a bluish explosive gas found in the Earth's atmosphere and is considered a major pollutant when present in the troposphere. Ozone is one of the secondary pollutant generated in the atmosphere due to the reaction between two primary pollutants. It is an irritating and toxic pollutant, even at low concentrations. Various VOCs including benzene, ethylbenzene, toluene, and xylene are emitted from vehicular emission and combustion of fossil fuels which is popularly known as BETX. These aromatic compounds play a vital role in photochemical reactions forming peroxyl radicals (RO_2), by reacting with the hydroxyl radicals (OH°) from

ozone molecules (Ceron-Breton et al. 2015). Peroxyl radicals (RO_2) also react with nitric oxide (NO) to form nitrogen dioxide (NO_2). In the presence of sunlight, NO_2 molecules react with various VOCs to generate toxic stratospheric ozone molecules (Geng et al. 2008; Garg and Gupta 2019). Hackney et al. (1975) have experimented and found that a low level of O_3 exposure leads to the development of decreases in pulmonary function.

9.2.2.9 Lead (Pb)

Lead is a well-known highly toxic heavy metal found in nature as well as anthropogenic sources. It can be released directly into the air in the form of particulate matter from vehicular and industrial emissions. Exposure to atmospheric lead occurs mainly through inhalation of dust and aerosol particles containing lead and vapours of paints (Tchounwou et al. 2012). Mrugesh et al. (2011) found the cytotoxic effects of Pb at low concentration on human red blood corpuscle (RBC) under in vitro conditions. The United States has tackled the problem of lead poisoning in children by attempting to eliminate sources of exposure, including gasoline, solder in water pipes, cans, and industrial emissions. Hence, a dramatic reduction was found in the number of children with elevated blood lead levels in the last 20 years (Meyer et al. 2003). Long-term exposure of lead from paint and gasoline is also a positive correlation in violent crime along with the murder rates, which is consistent with findings indicating that children with the higher bone lead often seem to have more impulsive and aggressive behaviour (Nevin 1999). From the 1st January 1996, the US Clean Air Act banned the sale of leaded fuel for use in on-road vehicles. Boskabody et al. (2018) have reviewed and concluded that exposure to lead may increase the likelihood of having a detrimental health effect on respiratory, neurologic, digestive, cardiovascular, and urinary disorders and also explained the mechanism of these effects.

9.2.2.10 Risk Related to Exposure to Polluted Water

Every living creature on the planet requires water to sustain. Only 1% of the water on earth is available for drinking and other daily activities including industrial utility, washing, bathing, and cooking. Following industrialisation, the quality of various water bodies has been deteriorating due to the release of unwanted/foreign chemicals into water bodies. According to UNDP (2019b), 80% of the industrial/municipality wastewater goes into waterways untreatably. In accordance, to get good quality water and for the conservation of natural water bodies, UNDP has set a sustainable development goal (no. 6) as ‘clean water and sanitation’. Polluted water contains toxic and hazardous chemicals, radioactive material, and microorganisms which may harm human health.

9.2.2.11 Microbial Exposure Through Contaminated Water

Microbes grow fast in drinking water; hence, water is a huge source of microbial contamination, including bacteria, viruses, and protozoa. Drinking water is mainly contaminated through poor sanitation and discharge of untreated municipal wastewater. More than 500 waterborne pathogens are found in drinking waters, identified by the USEPA through its candidate contaminant 'CCL 3 Universe' list (USEPA 2019b). Nine out of ten children are dying due to infectious diarrhoea. In most cases, pathogens such as *Rotavirus*, enterotoxigenic *Escherichia coli*, *Campylobacter Jejuni*, *Vibrio cholerae O1*, *Shigella* spp. and possibly *Aeromonas* spp., enteropathogenic *E. coli*, *Aeromonas* spp., *V. cholerae* O139, enterotoxigenic *Bacteroides fragilis*, *Clostridium difficile*, and *Cryptosporidium parvum* are the main culprits of waterborne disease (Ashbolt 2004).

9.2.2.12 Chemical Exposure Through Contaminated Water

Various foreign chemicals flow into the water because of man-made activities and act as contaminants of water. On consumption of such water, the risk of adverse health impact is increased. Water pollutants can be further classified into two types: organic pollutants and inorganic pollutants, viz., VOCs, POPs, pesticides, and heavy metals. Understanding risk in relation to the consumption of contaminated water is discussed based on the origin of the pollutants and its source as per World Health Organisation guidelines (WHO 2011).

9.2.2.13 Industrial Source and Human Dwelling

Mining (extractive industries), manufacturing units, processing industries, sewage (including several contaminants of emerging concern), municipal wastes, fuel leakages, and urban runoff may cause water contamination by changing the physiochemical properties of water. Bungling central effluent treatment plants (CETP) or municipality sewage plants results in a high rate of surface and groundwater contamination. On consumption of contaminated water for extended periods, it either mimics or alters hormonal activities in humans and causes adverse consequences.

9.2.2.14 Agricultural Activities

Excessive use of fertilisers and all classes of pesticides such as cholinesterase inhibitors, organophosphorus compounds, and carbamates is introduced into surface or groundwater through water runoff during monsoon or irrigation practices.

Residues of pesticides on food enter into food webs. The use of vegetables and fruits without proper cleaning may pose the risk of adverse effects on human health.

9.2.2.15 Water Treatment or Material in Drinking Water

Coagulants in piping materials are high in Fe, Mn, Zn, Pd, Cu, and other biological contaminants. The Flint (MI, USA) 2016 water crisis was the major lesson that taught the world the seriousness of increasing health risks related to water contaminants like lead. The contaminants forced governor Rick Snyder to declare an emergency condition in Flint on January 5, 2016. The study conducted by Laidlaw et al. (2016) revealed a meaningful conclusion, i.e., 'In Flint, Michigan, USA, a public health crisis occurred in April 2014 when the water supply was switched from Lake Huron to a more corrosive source from the Flint River, causing lead to leach from water pipes'. On one occasion, former President Barack Obama tweeted, *The mentality is just as corrosive to democracy as that substance that puts lead in your water.* He stated: *It is not enough to just repair the water. We must change the culture of neglect.* He also blamed the Flint water issue on a belief that *less government is the ultimate good*, which he claimed has resulted in disinvestment in low-income communities. Such incidences may increase the risk of exposure of toxic metals to the community.

9.2.2.16 Pesticides Used for Public Health (Other Than Agriculture)

Larvicides such as chlorinated organics, DDT, HCCH, and chlorinated cycloidians are being used to control vectors of diseases that will pose a risk to health and safety of human being. Due to continuous application, microbial resistance develops tolerance against low doses. Such consequences force the application of high doses that lead to public health being increasingly vulnerable.

9.2.2.17 Naturally Occurring Risks

Geogenic sources such as rocks, soil, and sand and eutrophic water bodies (also influenced by sewage inputs and agricultural runoff) including As, Pb, Cu, Fe, Cl^-, F^-, and NO_3^- may contaminate the groundwater and increase consumption related risk.

9.2.2.18 Risk Related to Exposure to Polluted Land

The land is a solid surface, which is not permanently covered by water. The land is a medium, which provides strength and nutrients to grow plants. For thousands of years, humans practised farming to satisfy food requirements. The ever-increasing

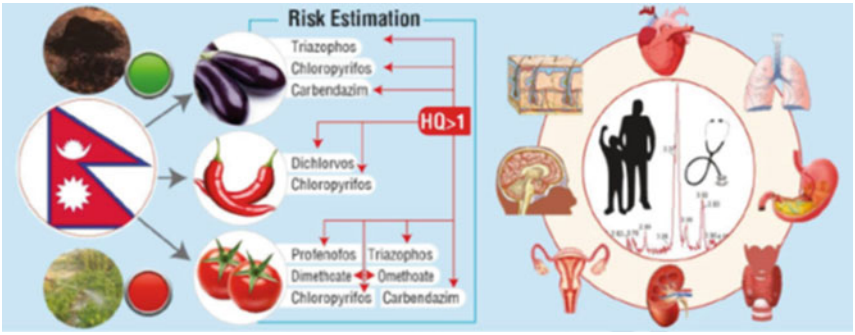

Fig. 9.3 Graphical presentation for risk estimation of pesticides from vegetables (Bhandari et al. 2019)

population generates more pressure on land to increase agriculture yield, which ultimately leads to the increased utilisation of chemical fertilisers and pesticides (Foley 2011). The excessive use of chemical pesticides in developed and developing countries may be hazardous to individuals and the environment. Application of pesticides such as alachlor, atrazine, simazine, and paraquat results in insecticide-resistant in bugs (WRI 1998). Figure 9.3 shows the recent pesticide residue-related risk to human health calculated by Bhandari et al. (2019).

Other than agriculture, mining activities and industrial effluents also cause land degradation with concurrent risk to human health. Most naturally occurring contaminants come from geogenic sources such as weathering and erosion of rocks or mountains, forest fire, and volcanic eruption. The amount of contaminants is lesser than anthropogenic sources. As natural contaminant sources were present from the beginning of life, many life forms may grow by adaptation to the nearby environment, whereas anthropogenic pollutants are added in large quantities over much shorter time scales due to increasing population and industrialisation to compensate for the demands of living beings. Industrialisation activities lead to the extreme use and release of chemicals in the environment which ultimately poses risk to all life forms. Pesticide residue from food, soft drinks, and drinking water poses more risk to human health. The risk from exposure to POPs should be given more attention due to their unique chemical properties, bio-accumulative nature, and relevant toxicity.

9.2.3 Risk Characterisation (Step 3)

Risk characterisation is an important constituent of the risk assessment procedure for both ecological and human health. The purpose of risk characterisation is to interpret the risk calculations based on existing data coming from observations and clarify their meaning for the health of populations. Risk characterisation is an essential element of the risk assessment process that supports decision targeting at the risk

abatement arrangements. Potential health risks can be characterised using hazard quotient (HQ) and hazard index (HI). Data related to the rate of ingestion, rate of inhalation, dermal exposure, exposure frequency, exposure duration, exposed skin area, and skin adherence factor for various age groups are available on USEPA's reports and guidelines (USEPA 2008, 2011). Based on the dose of any contaminants and dose-response relationship, the health effect due to exposure of a particular contaminant can be calculated. The risk of any contaminants can be calculated using a hazard quotient (HQ) and hazard index (HI) following Chabukdhara and Nema (2013):

$$\mathrm{HQ} = \frac{\mathrm{Dose}}{\mathrm{RfD}} \tag{9.8}$$

where

HQ = Hazard quotient
Dose = The concentration of contaminants exposed through inhalation, ingestion, or dermal
RfD = Reference dose (of the daily exposure to human)

There are two types of exposure: (i) acute/short-term and (ii) chronic/long-term exposure

For acute/short-term HQ assessment known as aHQ, the calculation is as follows:

$$\mathrm{aHQ} = \frac{\mathrm{ESTI}}{\mathrm{ARfD}} \times 100\% \tag{9.9}$$

where

ESTI = Estimated short-term intake can be express as the highest level of contaminant × Dose
ARfD = Acute references dose, which can avail from WHO and USEPA database

For chronic/long-term HQ assessment known as cHQ, the calculation is as follows:

$$\mathrm{cHQ} = \frac{\mathrm{EDI}}{\mathrm{ADI}} \times 100\% \tag{9.10}$$

where

EDI = Estimated daily intake that can be expressed as

$$\left(\frac{\text{Mean level of contaminants} \times \text{dose}}{\text{Bodyweight}}\right) \tag{9.11}$$

ADI = Acceptable daily intake (which can be taken from the WHO and USEPA database)

The HQ is used to estimate the potential risk due to an individual contaminant, while HI is a cumulative risk that takes into account multiple contaminants (Posthuma and Suter 2011). The HI is the total sum of the HQs. The HI is based on the cumulative effect of any contaminant with similar mechanisms of adverse health effects. The long-term exposure of contaminants causes the same physiological effects in terms of size and nature in relation to the time of exposure. Therefore, the HI was calculated by adding up the cHQi of contamination of a group and expressed as a hazard index (HI) as follows:

$$\mathrm{HI} = \sum_{i=1}^{n} \mathrm{cHQi} \tag{9.12}$$

An HQ or HI > 1 denotes potential risk to human health, while an HQ or HI $\leq$ 1 indicates no risk.

The above equations can be derived from authentic published literature available on risk assessment studies of specific contaminants such as risk assessment of pesticides, trace metal from the soil, and food contamination; equations have been derived and demonstrated (Darko and Akoto 2008; Chabukdhara and Nema 2013; Akoto et al. 2013; Sun and Chen 2018) for various environmental pollutants or cumulative risk assessment.

9.2.4 Dose-Response Assessment (Step 4)

This step of risk assessment determines the correlation between the dose and the toxic effect among the concerned population. Dose-response can be described as the amount of any contaminant or pollutant that is responsible for a certain adverse health effect. A database of USEPA and WHO may be used for the identification of environmental pollutants regarding health effects and dose-responses. For the dose-response assessment, toxicity databases have been determined and published by different authorities. The most useful are integrated risk information systems (IRIS), risk assessment information system (RAIS), agency for toxic substances and disease registry (ATSDR), and health effects assessment summary tables (HEAST). The use of these databases significantly simplifies the assessment procedure. When no data are available, arduous, time-consuming, and very costly toxicological and epidemiological investigations are needed, which in many cases makes the assessment impossible. Every contaminants has initial symptoms that depend on its dose of exposure. In our daily routine life, there are several products that we use which may contain such chemicals in concentration that may cause adverse health effects. For example, exposure to fluoride at more than 1.5 mg/l concentration may show spotted teeth and a decrease in the IQ level of children. However, dose-response is also dependent largely on an individual's immune system and age.

9.2.5 *Risk Management (Step 5)*

As described in the EPA's risk characterisation handbook, risk management is a process that evaluates how to protect public health from the evaluated risk. Examples of risk management actions include deciding the releasing standards for particular pollutants. Determining the optimum standards for certain contaminants is an example of risk management activity. The national ambient standard along with the permissible limits, acceptable limits for releasing of treated effluent into any waterbody, and set-up of the permission levels for handling, storage, and transport of any hazardous material with its guidelines is also part of risk management. Risk characterisation parameters such as HQ and HI can be used for the management of the risk. At present, no such international standards are available for assessing the risk of environmental exposure (Chartres et al. 2019). Once the international standards have been set for each environmental pollutant, it can be implemented through a proper legislative body of the country. In the absence of standards, published literature might be used to manage the risk. Risk management reduces possible risks, not in terms of environmental safety, and provides economic and social safety. Therefore, the application of risk assessment helps in making the project more sustainable. There are some case studies related to the risk assessment in environmental exposure that will give more insight into the risk assessment application.

9.3 Case Studies Related to the Risk of Environmental Exposure

Various kinds of risks are involved with environmental exposure due to low quality of air, water, and land. Anthropogenic activities pose risk to humans and their environment. Risks of biological agents, toxic chemicals, or radioactive material are commonly found in our habitat. Few landmark case studies in history reveal the significance of studying the risk of environmental exposure from industrial activities that damage the ecological, social, and economical aspects of sustainability. Herein, we describe three case studies related to environmental exposure and its adverse health effects due to contamination of air, water, and land.

9.3.1 *Yellowknife Gold Mine, Canada*

The extraction of resources has the potential of economic benefit but also results in high contamination of the local environment. The gold mines of the Yellowknife, Northwest Territories of Canada, are a classic example. The mine was operational between 1949 and 1999 and released 237,000 tonnes of toxic waste in the form of arsenic trioxide (As_2O_3) dust, and methyl mercury (Houben et al. 2016). The gold

was found in ores of arsenopyrite (FeAsS); consequent roasting was required for conversion of As and S to As_2O_3 and sulphur dioxide (SO_2). These gases were emitted into the environment during the smelting procedure. The toxicity of As is determined by the chemical species and chemical form, rather than the overall amount of As in the environment. For example, arsenobetaine ($(CH_3)_3As^+CH_2COO^-$) is found in marine animals and mushrooms and is less toxic than arsenous acid or arsenite ($As(OH)_3$) (Koch et al. 2000). Ore roasting increases the solubility, toxicity, and bio-accessibility of As by converting sulphide-hosted As to oxide-hosted As. It is more important than the conversion of As as it increases the concentration of dissolved As in groundwater and surface waters. Therefore, it is potentially more toxic due to its high viability. Arsenic trioxide posed a health risk to beings who drank from the tainted water and potentially those that lived near, streams, lakes, and puddles contaminated by falling arsenic dust. Arsenic trioxide dust also settled on local sources of food, especially berries, and vegetables gathered or grown in the Yellowknife area. Various health impacts of arsenic are dose-dependent; arsenic trioxide kills human beings at 70–180 mg. Ingestion of dose levels below the lethal threshold produces a range of health effects that include vomiting, diarrhoea, muscle pain, rashes, parenthesis, and keratosis. Lower exposure over the year can also produce hyperpigmentation (Sandlos and Keeling 2012). Arsenic pollution proved dangerous, even deadly for the Yellowknife's Dene community, in the earliest operating years of the giant mine. Although Yellowknife residents were exposed to arsenic in their water supply, the risk posed to local communities was even greater than the native communities simply due to the proximity of the area they lived in, near the roasting facility, as well as the reliance of people on the polluted snow and lake water for their consumption. The gravity of the situation that the pollution caused can be understood by studying the impacts on animals such as sled dogs, cattle, and chickens dying from drinking arsenic-laden water. Though the Yellowknife gold mine gave a boost to the economy, the pollutants have no boundaries. It increased the risk to the surrounding human health and ecosystem outside the mining area (Jamieson 2014).

9.3.2 Bhopal Gas Disaster, India

Bhopal gas tragedy, the world's deadliest industrial catastrophe, occurred in Union Carbide India Limited (UCIL), Bhopal, India. On the 3rd December 1984, an explosion at the UCIL, a pesticide manufacturing company, released 41 tonnes of methyl iso-cyanate (MIC), a toxic gas that resulted in the death of more than 3000 people, injuring hundreds of thousands more (Koplan et al. 1990). Multitudes of victims in Bhopal were exposed to levels of MIC, with respect to their distance to the plant, and atmospheric factors such as wind velocity and direction; there were more than 500,000 registered survivors of the tragedy (Mishra et al. 2009). According to the Indian council of medical research (ICMR) report, nearly 75% of the deaths occurred within 3 days of the incident. The survivors in the exposed population

continued to be chronically ill with diseases of the respiratory, gastrointestinal, reproductive, musculoskeletal, neurological, and other systems (ICMR 2010). Studies related to the reproductive health effects of the event revealed that many years after the disaster, the females of Bhopal exposed to the MIC suffer from problems of menstrual abnormalities, vaginal discharge, and premature menopause. Investigative research was carried out to assess the effect of MIC exposure in pregnant women, including two groups of women who were and were not exposed in Bhopal gas tragedy. It showed 24.2% spontaneous miscarriages in pregnant women who were exposed to MIC, while the control area showed 5.6% spontaneous miscarriages (Bhandari et al. 1990; ICMR 2010). Six serious accidents in the last 4 years before the 1984 tragedy also occurred in the UCIL, which resulted in the death of workers. However, management authorities failed to take action regarding the analysis of the situation and safety measures (Gupta 2002). The local government of Bhopal failed to act in earlier accidents and ignored the newspaper reports predicting disaster. The abovementioned points revealed that major tragedies could occur in any country irrespective of the level of development. The effect of chemical contamination of Bhopal gas is not restricted to air exposure, but it has caused groundwater contamination of various toxic chemicals. The UK-based Bhopal medical appeal and the Sambhavna clinic of Bhopal said, 'Water contamination is worsening as chemicals leach through soil into the aquifer' (Goodman 2009). The incident affected people beyond the boundary of industries and caused disaster to the entire local community. It may affect their health, culture, wealth, properties, and ultimately the entire socioeconomic environment, important stakes of sustainability.

9.3.3 Lanzhou Region, Yellow River, China

The Yellow River is the 2nd longest river of China and provides water to millions of people; it is highly contaminated at present. On 25th November 2008, a report furnished by The Guardian, a British daily newspaper, claimed that the river has suffered from severe pollution and that one-third of China's Yellow River is unusable for drinking, agricultural, or even industrial use, due to factory discharges and sewage from fast-expanding cities. The report on the state of the environment in China revealed that waste and sewage water discharged into the system in 2006 totalled 4.29 billion tonnes. Industry and manufacturing made up 70% of the discharge into the river, with households accounting for 23% and just over 6% coming from other sources (SoE China 2007). Zhang et al. (2018) and Cheng et al. (2019) have found that the metals in sediments of the Yellow River have high concentrations of Cd and Hg among other heavy metals and the pollution and the ecological risk of Hg and Cd are serious. Six types of alkyl esters of p-hydroxybenzoic acids (parabens) were determined in surface water and sediment from the Yellow River, China. The parabens cause adverse effects on the male reproductive system in rats. Besides, parabens were related to the incidence of breast cancer due to the extensive use of cosmetics containing the toxic class (Oishi 2001;

Darbre et al. 2004; Feng et al. 2019). In 2004, 16 different polycyclic aromatic hydrocarbons (PAHs) were detected with concentrations of 23–370 ng/L soluble and 36–3700 ng/g dry weight in the particulate phase (Yu et al. 2009; Feng et al. 2018). These contaminants are cancer-causing and were released from industrial wastewater and household waste.

9.4 Conclusion

The effect of contaminants is not restricted to occupational workers but also covers the entire communities who are directly or indirectly dependent on any of the ecological services in the proximity of industrial intervention such as water supply by the river, pond, or borewell and agricultural practice. The role and responsibility of risk assessment and its management by all industries should extend up to the community level, not only during construction and operational stages but even after the shutdown. Risk assessment application should be imposed in a way that provides safety and security to environmental, ecological, and economical areas to cover all aspects of sustainability.

References

Akoto O, Andoh H, Darko G et al (2013) Health risk assessment of pesticides residue in maize and cowpea from Ejura, Ghana. Chemosphere 92(1):67–73. https://doi.org/10.1016/j.chemosphere.2013.02.057

Amsalu E, Guo Y, Li H et al (2019) Short-term effect of ambient sulfur dioxide (SO_2) on cause-specific cardiovascular hospital admission in Beijing, China: a time series study. Atmos Environ 208:74–81. https://doi.org/10.1016/j.atmosenv.2019.03.015

Andrews RNL (1990) Environmental impact assessment and risk assessment: learning from each other. In: Wathern P (ed) Environmental impact assessment: theory and practice. Routledge. https://doi.org/10.4324/9780203409978

Ashbolt NJ (2004) Microbial contamination of drinking water and disease outcomes in developing regions. Toxicology 198(1–3):229–238. https://doi.org/10.1016/j.tox.2004.01.030

Bhandari N, Syal A, Kambo I et al (1990) Pregnancy outcome in women exposed to toxic gas at Bhopal. Indian J Med Res 92:28–33

Bhandari G, Zomer P, Atreya K et al (2019) Pesticide residues in Nepalese vegetables and potential health risks. Environ Res 172:511–521. https://doi.org/10.1016/j.envres.2019.03.002

Bhatt K, Trivedi M (2018) Molecular studies on foraminifers: past, present, and future. J Foraminiferal Res 48(3):193–209. https://doi.org/10.2113/gsjfr.48.3.193

Boningari T, Smirniotis P (2016) Impact of nitrogen oxides on the environment and human health: Mn-based materials for the NO x abatement. Curr Opin Chem Eng 13:133–141. https://doi.org/10.1016/j.coche.2016.09.004

Boskabady M, Marefati N, Farkhondeh T et al (2018) The effect of environmental lead exposure on human health and the contribution of inflammatory mechanisms, a review. Environ Int 120:404–420. https://doi.org/10.1016/j.envint.2018.08.013

Bruce N, Perez-Padilla R, Albalak R (2000) Indoor air pollution in developing countries: a major environmental and public health challenge. Bull World Health Organ 78(9):1078–1092

Carpenter R (1995) Risk assessment. Impact Assess 13(2):153–187. https://doi.org/10.1080/07349165.1995.9726088

Ceron-Breton J, Ceron-Breton R, Kahl J et al (2015) Diurnal and seasonal variation of BTEX in the air of Monterrey, Mexico: preliminary study of sources and photochemical ozone pollution. Air Qual Atmos Health 8:469–482

Chabukdhara M, Nema A (2013) Heavy metals assessment in urban soil around industrial clusters in Ghaziabad, India: probabilistic health risk approach. Ecotoxicol Environ Saf 87:57–64. https://doi.org/10.1016/j.ecoenv.2012.08.032

Chartres N, Bero L, Norris S (2019) A review of methods used for hazard identification and risk assessment of environmental hazards. Environ Int 123:231–239. https://doi.org/10.1016/j.envint.2018.11.060

Cheng Q, Zhou W, Zhang J et al (2019) Spatial variations of arsenic and heavy metal pollutants before and after the water-sediment regulation in the wetland sediments of the Yellow River Estuary, China. Mar Pollut Bull 145:138–147. https://doi.org/10.1016/j.marpolbul.2019.05.032

Choi A, Sun G, Zhang Y et al (2012) Developmental fluoride neurotoxicity: a systematic review and meta-analysis. Environ Health Perspect 120(10):1362–1368. https://doi.org/10.1289/ehp.1104912

Coster SD, Larebeke NV (2012) Endocrine-disrupting chemicals: associated disorders and mechanisms of action. J Environ Public Health:1–52. https://doi.org/10.1155/2012/713696

Cushen R, Brunt H, Jones S et al (2019) An unusual incident: carbon monoxide poisoning risk in 540 homes due to faulty wood burner installations. Public Health 173:17–20. https://doi.org/10.1016/j.puhe.2019.05.003

Damania R, Desbureaux S, Rodella A et al (2019) Quality unknown: the invisible water crisis. Washington, DC: World Bank. http://hdl.handle.net/10986/32245

Darbre PD, Aljarrah A, Miller WR et al (2004) Concentrations of parabens in human breast tumours. J Appl Toxicol 24(1):5–13. https://doi.org/10.1002/jat.958

Darko G, Akoto O (2008) Dietary intake of organophosphorus pesticide residues through vegetables from Kumasi, Ghana. Food Chem Toxicol 46(12):3703–3706. https://doi.org/10.1016/j.fct.2008.09.049

De Miguel E, Iribarren I, Chacón E et al (2007) Risk-based evaluation of the exposure of children to trace elements in playgrounds in Madrid (Spain). Chemosphere 66(3):505–513. https://doi.org/10.1016/j.chemosphere.2006.05.065

Dhananjayan V, Ravichandran B (2018) Occupational health risk of farmers exposed to pesticides in agricultural activities. Curr Opin Environ Sci Health 4:31–37. https://doi.org/10.1016/j.coesh.2018.07.005

Ding Y, Gao Y, Sun H et al (2011) The relationships between low levels of urine fluoride on children's intelligence, dental fluorosis in endemic fluorosis areas in Hulunbuir, Inner Mongolia, China. J Hazard Mater 186(2–3):1942–1946. https://doi.org/10.1016/j.jhazmat.2010.12.097

Duan Q, Jiao J, Chen X et al (2018) Association between water fluoride and the level of children's intelligence: a dose–response meta-analysis. Public Health 154:87–97. https://doi.org/10.1016/j.puhe.2017.08.013

Feng J, Hu P, Su X et al (2018) Impact of suspended sediment on the behaviour of polycyclic aromatic hydrocarbons in the Yellow River: spatial distribution, transport and fate. Appl Geochem 98:278–285. https://doi.org/10.1016/j.apgeochem.2018.10.008

Feng J, Zhao J, Xi N et al (2019) Parabens and their metabolite in surface water and sediment from the Yellow River and the Huai River in Henan Province: spatial distribution, seasonal variation and risk assessment. Ecotoxicol Environ Saf 172:480–487. https://doi.org/10.1016/j.ecoenv.2019.01.102

Foley J (2011) A five-step global plan could double food production by 2050 while greatly reducing environmental damage. Sci Am: November:60–66. https://web.mit.edu/12.000/www/m2019/pdfs/Foley_2011_ScientificAmerican.pdf

Garg A, Gupta NC (2019) A comprehensive study on spatio-temporal distribution, health risk assessment and ozone formation potential of BTEX emissions in ambient air of Delhi, India. Sci Total Environ 659:1090–1099. https://doi.org/10.1016/j.scitotenv.2018.12.426

Ge H, Yamazaki E, Yamashita N et al (2017) Particle size specific distribution of perfluoroalkyl substances in atmospheric particulate matter in Asian cities. Environ Sci Process Impacts 19: 549–560. https://doi.org/10.1039/C6EM00564K

Geng F, Tie X, Xu J et al (2008) Characterizations of ozone, NOx, and VOCs measured in Shanghai, China. Atmos Environ 42:6873–6688

Gianicolo EAL, Mangia C, Cervino M (2016) Investigating mortality heterogeneity among neighbourhoods of a highly industrialised Italian city: a meta-regression approach. Int J Public Health 61(7):777–785. https://doi.org/10.1007/s00038-016-0868-y

Goodman S (2009) Poisoned water haunts Bhopal 25 years after chemical accident. Available via Scientific American. https://www.scientificamerican.com/article/groundwater-contamination-india-pesticide-factory/. Accessed 9 Aug 2019

Guaita R, Pichiule M, Mate T et al (2011) Short-term impact of particulate matter ($PM_{2.5}$) on respiratory mortality in Madrid. Int J Environ Health Res 21:260–274. https://doi.org/10.1080/09603123.2010.544033

Gul M, Ak F (2018) A comparative outline for quantifying risk ratings in occupational health and safety risk assessment. J Clean Prod 196:653–664. https://doi.org/10.1016/j.jclepro.2018.06.106

Guo M, Lyu Y, Xu T et al (2018) Particle size distribution and respiratory deposition estimates of airborne perfluoroalkyl acids during the haze period in the megacity of Shanghai. Environ Pollut 234:9–19. https://doi.org/10.1016/j.envpol.2017.10.128

Gupta J (2002) The Bhopal gas tragedy: could it have happened in a developed country? J Loss Prev Process Ind 15(1):1–4. https://doi.org/10.1016/S0950-4230(01)00025-0

Hackney JD, Linn WS, Law DC et al (1975) Experimental studies on human health effects of air pollutants: ii. Two-hour exposure to ozone alone and in combination with other pollutant gases. Arch Environ Health 30(8):385–390. https://doi.org/10.1080/00039896.1975.10666730

Halonen JI, Lanki T, Tuomi TY et al (2009) Particulate air pollution and acute cardiorespiratory hospital admissions and mortality among the elderly. Epidemiology 20:143–153. https://doi.org/10.1097/EDE.0b013e31818c7237

HES (2019) Health, executive safety gas safe register. Carbon monoxide poisoning. What are the symptoms? Available via Health Executive Safety. https://www.gassaferegister.co.uk/help-and-advice/carbon-monoxide-poisoning/. Accessed 30 July 2019

Houben AJ, D'Onofrio R, Kokelj SV et al (2016) Factors affecting elevated arsenic and methyl mercury concentrations in small shield lakes surrounding gold mines near the Yellowknife, NT, (Canada) region. PLoS One 11(4):e0150960. https://doi.org/10.1371/journal.pone.0150960

ICMR (2010) Indian Council of Medical Research report on health effects of the toxic gas leak from the methyl isocyanate plant in Bhopal. Bhopal Gas Disaster Centre & Institute of Pathology, ICMR, New Delhi

Ielpo P, Mangia C, Marra GP et al (2019) Outdoor spatial distribution and indoor levels of NO_2 and SO_2 in a high environmental risk site of the South Italy. Sci Total Environ 648:787–797. https://doi.org/10.1016/j.scitotenv.2018.08.159

Jamieson H (2014) The legacy of arsenic contamination from mining and processing refractory gold ore at Giant Mine, Yellowknife, northwest territories, Canada. Rev Mineral Geochem 79(1): 533–551. https://doi.org/10.2138/rmg.2014.79.12

Kim H, Kim H, Park YH et al (2017) Assessment of temporal variation for the risk of particulate matters on asthma hospitalization. Environ Res 156:542–550. https://doi.org/10.1016/j.envres.2017.04.012

Koch I, Wang L, Ollson C et al (2000) The predominance of inorganic arsenic species in plants from Yellowknife, northwest territories, Canada. Environ Sci Technol 34:22–26. https://doi.org/10.1021/es9906756

Koplan JP, Falk H, Green G (1990) Public health lessons from the Bhopal chemical disaster. J Am Med Assoc 264(21):2795–2796

Krauskopf J, Veldhoven KV, Chadeau-Hyam M et al (2019) Short-term exposure to traffic-related air pollution reveals a compound-specific circulating miRNA profile indicating multiple disease risks. Environ Int 128:193–200. https://doi.org/10.1016/j.envint.2019.04.063

Laidlaw M, Filippelli G, Sadler R et al (2016) Children's blood lead seasonality in Flint, Michigan (USA), and soil-sourced lead hazard risks. Int J Environ Res Public Health 13:358. https://doi.org/10.3390/ijerph13040358

Liu Z, Guan Q, Luo H et al (2019a) Development of land use regression model and health risk assessment for NO_2 in different functional areas: a case study of Xi'an, China. Atmos Environ 213:515–525. https://doi.org/10.1016/j.atmosenv.2019.06.044

Liu H, Liao J, Jiang Y et al (2019b) Maternal exposure to fine particulate matter and the risk of fetal distress. Ecotoxicol Environ Saf 170:253–258. https://doi.org/10.1016/j.ecoenv.2018.11.068

Lohani B, Evans J, Ludwig H et al (1997) Environmental impact assessment for developing countries in Asia. Volume 1 Overview. Asian Development Bank, Manila, p 356

Masters GM, Ela W (2008) Introduction to environmental engineering and science (No. 60457). Prentice Hall, Englewood Cliffs

Meyer PA, McGeehin MA, Falk H (2003) A global approach to childhood lead poisoning prevention. Int J Hyg Environ Health 206(4–5):363–369. https://doi.org/10.1078/1438-4639-00232

Mishra PK, Samarth RM, Pathak N et al (2009) Bhopal gas tragedy: review of clinical and experimental findings after 25 years. Int J Occup Environ Health 22(3):193–202. https://doi.org/10.2478/v10001-009-0028-1

Mrugesh T, Dipa L, Manishika G (2011) Effect of lead on human erythrocytes: an in vitro study. Acta Pol Pharm 68(5):653–656

Müller CE, Gerecke AC, Bogdal C et al (2012) Atmospheric fate of poly-and perfluorinated alkyl substances (PFASs): I. Day–night patterns of air concentrations in summer in Zurich, Switzerland. Environ Pollut 169:196–203. https://doi.org/10.1016/j.envpol.2012.04.010

Neuberger M, Moshammer H, Kundi M (2002) Declining ambient air pollution and lung function improvement in Austrian children. Atmos Environ 36:1733–1736. https://doi.org/10.1016/S1352-2310(02)00179-6

Nevin R (1999) How lead exposure relates to temporal changes in IQ, violent crime, and unwed pregnancy. Environ Res 83(1):1–22. https://doi.org/10.1006/enrs.1999.4045

Ngajilo D, Jeebhay MF (2019) Occupational injuries and diseases in aquaculture – a review of literature. Aquaculture 507:40–55. https://doi.org/10.1016/j.aquaculture.2019.03.053

Oishi S (2001) Effects of butylparaben on the male reproductive system in rats. Toxicol Ind Health 17(1):31–39. https://doi.org/10.1191/0748233701th093oa

Paithankar A (2011) Hazard identification and risk analysis in mining industry. Department of Mining Engineering National Institute of Technology Rourkela

Perez L, Tobías A, Querol X et al (2012) Saharan dust, particulate matter and cause-specific mortality: a case-crossover study in Barcelona (Spain). Environ Int 48:150–155. https://doi.org/10.1016/j.envint.2012.07.001

Pope CA, Burnett RT, Thurston GD et al (2004) Cardiovascular mortality and long-term exposure to particulate air pollution epidemiological evidence of general zathophysiological pathways of disease. Circulation 109(1):71–77. https://doi.org/10.1161/01.CIR.0000108927.80044.7F

Posthuma L, Suter G (2011) Ecological risk assessment of diffuse and local soil contamination using species sensitivity distributions. In: Dealing with contaminated sites. Springer, Dordrecht

Pourhassan B, Meysamie A, Alizadeh S et al (2019) Risk of obstructive pulmonary diseases and occupational exposure to pesticides: a systematic review and meta-analysis. Public Health 174:31–41. https://doi.org/10.1016/j.puhe.2019.05.024

Pruss-Ustun A, Wolf J, Corvalán C et al (2016) Preventing disease through healthy environments: a global assessment of the burden of disease from environmental risks. World Health Organisation, Geneva

Ramirez N, Cuadras A, Rovira E et al (2012) Chronic risk assessment of exposure to volatile organic compounds in the atmosphere near the largest Mediterranean industrial site. Environ Int 39(1):200–209

Razdan P, Patthi B, Kumar JK et al (2017) Effect of fluoride concentration in drinking water on intelligence quotient of 12–14-year-old children in Mathura district: a cross-sectional study. J Int Soc Prev Community Dent 7(5):252–258. https://doi.org/10.4103/jispcd.JISPCD_201_17

Reynolds M, Jennifer G (eds) (2015) Laboratory bio-risk management biosafety and biosecurity. CRC Press Inc, Boca Raton

Rich AL, Phipps LM, Tiwari S et al (2016) The increasing prevalence in intersex variation from toxicological dysregulation in fetal reproductive tissue differentiation and development by endocrine-disrupting chemicals. Environ Health Insights 8(10):163–171. https://doi.org/10.4137/EHI.S39825

Ruan Y, Lalwani D, Kwok K et al (2019) Assessing exposure to legacy and emerging per- and polyfluoroalkyl substances via hair – the first nationwide survey in India. Chemosphere 229: 366–373. https://doi.org/10.1016/j.chemosphere.2019.04.195

Samoli E, Aga E, Touloumi G (2007) Short-term effects of nitrogen dioxide on mortality: an analysis within the APHEA project. Environ Health Perspect 115:1578–1583. https://doi.org/10.1183/09031936.06.00143905

Samoli E, Peng R, Ramsay T et al (2008) Acute effects of ambient particulate matter on mortality in Europe and North America: results from the APHENA study. Environ Health Perspect 116(11): 1480–1486. https://doi.org/10.1289/ehp.11345

Sandlos J, Keeling A (2012) Giant mine: historical summary. Memorial University August 8, 2012. Available via Memorial University Research Repository. https://research.library.mun.ca/638/. Accessed 6 May 2021

Seraj B, Shahrabi M, Shadfar M et al (2012) Effect of high water fluoride concentration on the intellectual development of children in Makoo/Iran. Int J Dent 9(3):221–229

Shin I, Oh JB, Yi HK (2011) Workers' compensation insurance and occupational injuries. Saf Health Work 2(2):148–157. https://doi.org/10.5491/SHAW.2011.2.2.148

SoE (2007) Report on the state of the environment in China. Ministry of Environmental Protection, The People's Republic of China. Available via http://english.mee.gov.cn/Resources/Reports/soe/soe2007/201605/P020160531580295293022.pdf. Accessed 6 May 2021

Sun Z, Chen J (2018) Risk assessment of potentially toxic elements (PTEs) pollution at a rural industrial wasteland in an abandoned metallurgy factory in North China. Int J Environ Res Public Health 15(1):85. https://doi.org/10.3390/ijerph15010085

Tchounwou PB, Yedjou CG, Patlolla AK et al (2012) Heavy metal toxicity and the environment. In: Luch A (ed) Molecular, clinical and environmental toxicology. Experientia Supplementum, vol 101. Springer, Basel. https://doi.org/10.1007/978-3-7643-8340-4_6

Thorpe KL, Hutchinson TH, Hetheridge MJ et al (2001) Assessing the biological potency of binary mixtures of environmental estrogens using vitellogenin induction in juvenile rainbow trout (*Oncorhynchus mykiss*). Environ Sci Technol 35(12):2476–2481. https://doi.org/10.1021/es001767u

Trivedi M, Verma R, Chinoy N et al (2007) Effect of high fluoride water on intelligence of school children in India. Fluoride 40(3):178–183

Trivedi M, Sangai NP, Patel RS et al (2012) Assessment of groundwater quality with special reference to fluoride and its impact on IQ of schoolchildren in six villages of the Mundra region, Kachchh, Gujarat, India. Fluoride 45(4):377–383

Trivedi M, Vaidya D, Patel C et al (2020) In silico and in vitro studies to elucidate the role of 1HYN and 1QKI activity in BPA induced toxicity and its amelioration by Gallic acid. Chemosphere 241:125076. https://doi.org/10.1016/j.chemosphere.2019.125076

UNDP (2019a) Goal 3: good health and well-being. Facts and figures. https://www.undp.org/content/undp/en/home/sustainable-development-goals/goal-3-good-health-and-well-being.html. Accessed 30 July 2019

UNDP (2019b) Goal 6: clean water and sanitation. Facts and figures. https://www.undp.org/content/undp/en/home/sustainable-development-goals/goal-6-clean-water-and-sanitation.html. Accessed 1 Aug 2019

USEPA (2008) Child-specific exposure factors handbook. National Center for Environmental Assessment Office of Research and Development, Washington, DC; EPA/600/R-06/096F. 20460

USEPA (2011) Exposure factors handbook: 2011 edition. National Center for Environmental Assessment, Washington, DC. EPA/600/R-09/052F

USEPA (2014) Human health evaluation manual, supplemental guidance: update of standard default exposure factors. OSWER Directive 9200.1-120. Office of Solid Waste and Emergency Response. US Environmental Protection Agency, Washington, DC. Available via EPA. https://www.epa.gov/sites/production/files/2015-11/documents/oswer_directive_9200.1-120_exposurefactors_corrected2.pdf

USEPA (2019a) About risk assessment. Available via EPA. https://www.epa.gov/risk/about-risk-assessment#whatisrisk. Accessed 26 July 2019

USEPA (2019b) CCL 3 Universe list. Available via EPA. http://www.epa.gov/safewater/ccl/pdfs/report_ccl3_microbes_universe.pdf. Accessed 1 Aug 2019. Accessed 6 May 2021

USEPA (2019c) Conducting a human health risk assessment. Available via EPA. https://www.epa.gov/risk/conducting-human-health-risk-assessment. Accessed 26 July 2019

USEPA (2019d) Criteria air pollutants. Available via EPA. https://www.epa.gov/criteria-air-pollutants. Accessed 26 July 2019

WHO (2006) Air quality guidelines of WHO for particulate matter, ozone, nitrogen dioxide and sulfur dioxide, Global update 2005: WHO/SDE/PHE/OEH/06.02. World Health Organization. Available via WHO. http://whqlibdoc.who.int/hq/2006/WHO_SDE_PHE_OEH_06.02_eng.pdf. Accessed 6 May 2021

WHO (2011) WHO guideline for drinking water quality, 4th edn. World Health Organization, Geneva

WRI (1998) World Resources Institute – world resources, 1998/1999. Oxford University Press, UK

Yu Y, Xu J, Wang P et al (2009) Sediment-porewater partition of polycyclic aromatic hydrocarbons (PAHs) from Lanzhou Reach of Yellow River, China. J Hazard Mater 165(1–3):494–500. https://doi.org/10.1016/j.jhazmat.2008.10.042

Zhang P, Qin C, Hong X et al (2018) Risk assessment and source analysis of soil heavy metal pollution from lower reaches of Yellow River irrigation in China. Sci Total Environ 633:1136–1147. https://doi.org/10.1016/j.scitotenv.2018.03.228

Chapter 10
Application and Control of Quadrotors

Safanah M. Raafat, Firas A. Raheem, Ahmed A. Alawsi, and Zainab S. Mahmood

Abstract A quadrotor is a multirotor helicopter, boosted by four rotors. In contrast to fixed-wing aircraft, quadrotors are categorized as rotorcraft, since their lift is produced by a set of rotors. The usage of quadrotors has increased in recent years in civilian and military operations. They are adaptable during vertical takeoff and landing and have stability when hovering. Additionally, quadrotors have low power consumption and are unobtrusive.

The many important applications of quadrotors include delivery and monitoring. A quadrotor can fly in an autonomous and non-autonomous manner with use of methods using the proportional integral derivative (PID) and linear quadratic regulator (LQR), sliding mode control, and fuzzy control. Such methods stabilize the quadrotor through flights. The aim of most controllers is to eliminate the error which is the difference between a measured value (measured states by sensors) and a desired set-point (desired states). The "error" can be minimized by adjusting the control inputs and the speed of the motors, in an iterative manner. This chapter illustrates key applications, and further the modeling and control of quadrotors is described in brief. Two cases of studies are presented, the first of which deals with the design of PID control for precise positioning of delivery quadrotors, and the second entails the design of multiple model adaptive control (MMAC) of the quadrotor.

Key words Quadrotor · Multirotor · Delivery · Power consumption · PID · MMAC

S. M. Raafat (✉)
Automation and Robotics Research Unit, Control and Systems Engineering Department, University of Technology-Iraq, Baghdad, Iraq
e-mail: 60154@uotechnology.edu.iq

F. A. Raheem · Z. S. Mahmood
Control and Systems Engineering Department, University of Technology-Iraq, Baghdad, Iraq
e-mail: 60124@uotechnology.edu.iq; zainabalsafar299@gmail.com

A. A. Alawsi
College of Science, Physics Department, University of Wasit, Wasit, Iraq
e-mail: aalawsi@uowasit.edu.iq

J. N. Furze et al. (eds.), *Earth Systems Protection and Sustainability*,
https://doi.org/10.1007/978-3-030-98584-4_10

10.1 Introduction

The study of micro unmanned air vehicles (UAVs) through developing technologies enables expansive application. UAVs are useful in a wide array of operations and have gained importance. UAVs are aircraft which may be flown without a pilot (Newcome 2004).

Modern rotorcraft UAVs have many benefits compared to old-styled crafts, including improved maneuverability, an ability to fly above objectives, and capacity to take off and land in limited space in comparison to fixed-wing crafts. Quadrotors belong to the class of rotorcrafts and are recognized by their simple structure, ease of maintenance, and unsophisticated dynamics in comparison to those of helicopters (Schmidt 2011).

Quadcopters operate in two flight modes: autonomous and non-autonomous. Non-autonomous flights are controlled by the user through a radio device (control joystick) as shown in Fig. 10.1.

In autonomous flight, the quadcopter flies and controls itself, carrying out required missions without user interference. Quadcopters operate with a global positioning system (GPS) sensor to ascertain their linear position in relation to other sensors and achieve a stable and balanced flight. The GPS sensor connects with GPS satellite systems as shown in Fig. 10.2 and uses information provided for operation (Grisso et al. 2009; Rahemi et al. 2014; Ziaul 2016).

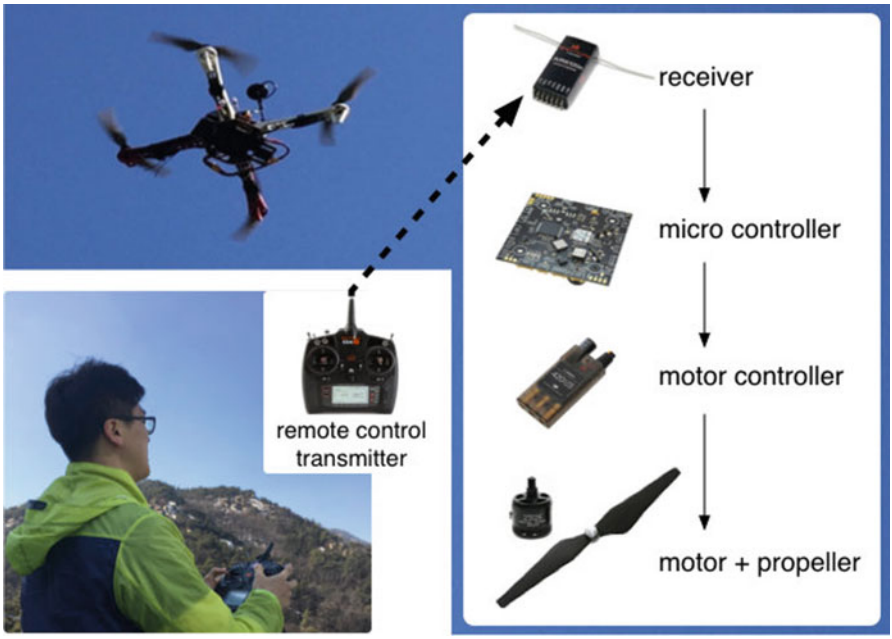

Fig. 10.1 Joystick control of a quadcopter through non-autonomous flight (Jung et al. 2018)

Fig. 10.2 Quadcopters control themselves in autonomous flight using a Global Positioning System (GPS)

In the literature, the many types of control methods applied in autonomous or non-autonomous modes include PID (Ferry 2017), LQR (Purnawan et al. 2017), sliding mode (Tripathi et al. 2016; Thomas 2010), fuzzy control (Sattar and Ismail 2017), image recognition (Luo et al. 2016), and adaptive control (Minh et al. 2014), stabilizing and improving their flight performance.

The remaining parts of this chapter are structured as follows: Sect. 10.2 details applications of quadrotor UAVs; Sect. 10.3 presents the modeling of a (six degrees of freedom) quadrotor; Sect. 10.4 discusses quadrotor control; and Sect. 10.5 features two case studies of quadrotor control, the first case demonstrates the design of a PID controller for delivery quadrotor systems and the second shows the design of a Multiple Model Adaptive Control (MMAC) based on three Kalman fiters (KFs). Conclusions and prospective future directions are covered in Sect. 10.6.

10.2 Applications of Quadrotors

Common quadrotor applications (Air Drone Craze, Drone Deals 2019) are detailed in this section.

10.2.1 Journalism, Filming, and Aerial Photography

Quadcopters are increasingly popular in photography of sport events, competitions, and cinematography owed to their maneuverability, takeoff, and vertical landing, as

well as hovering. Drones have recently started to be used in the direct broadcasting of satellite channels by linking live broadcast cameras to Earth stations, which in turn are transmitted through the satellite channel.

10.2.2 Shipping/Delivery

One of the most important properties of quadrotors is their ability to be operated autonomously through a range of techniques. Avoiding traffic and jammed roads, UAVs are used to deliver small parcels, letters, medicines, and even pizzas over short distances.

10.2.3 Disaster Management, Search, and Rescue/Healthcare

The task of rescuing people exposed to hazards or perilous circumstances at night and in difficult terrain is a race against time. Equipped with thermal cameras, quadcopters can be used to locate people and rapidly assess situations.

10.2.4 Geographic Mapping

The ability of the quadcopter to reach/overview uneven terrain enables its use in the collection of accurate information with high-precision cameras for geographic mapping.

10.2.5 Structural Safety Inspections

The quadcopter is used by various sectors to provide accurate assessment, such as in checking building structures, electric power lines, and crude oil pipelines. Increased visual clarity and thermal, water, and gaseous sensors allow identification of potential future problems, in order that one may take appropriate measures to prevent them from happening.

10.2.6 Precision Agriculture

Quadcopters help farmers to closely monitor agricultural fields, enabling them to improve management and increase production. Quadcopters are additionally used in

spraying pesticides, covering vast areas in a fast and consistent manner, with improved coverage while losses of pesticides are reduced.

10.2.7 Wildlife Monitoring/Poaching

The quadcopter assists security services charged with protection of remote, wild areas by detecting hunters trapping rare animals, often useful where extinction is a very present threat. They may also be used to detect the positions of sick animals more quickly allowing necessary actions to be carried out to help and preserve them.

10.2.8 Law-Enforcement and Border Patrol

The quadcopter assists the police and security services in law enforcement operations, especially in preventing the smuggling of drugs and prohibited substances by monitoring external and internal borders of countries.

10.2.9 Construction Sites

Quadcopters help to provide three-dimensional vision of construction stages, thus enabling engineers to detect errors early for process and increased safety of projects.

10.2.10 Entertainment

Plenty of hobbyists are picking up quadrotors to play around with, both in remote flight and by programming quadrotor AI (artificial-intelligence). As such quadrotors can be used in many ways to capture videos and photographs.

10.2.11 Military and Law Enforcement

The quadcopter is used extensively in military fields today to carry out multiple tasks including reconnaissance and surveillance of enemy sites (Armed Quadrotors Are Coming 2014). For example, a small UAV may be used in provision of visual surveillance of a drug trafficker's compound deep in the jungle (Dhanalakshmi et al. 2015).

10.3 Modeling of Quadrotors

Generally, a quadcopter is characterized by four independently controllable actuators (motors) assembled in a cross configuration as shown in Fig. 10.3. The actuators are two clockwise (CW) and two counterclockwise (CCW), so the affected rotational torque on the body around the Z axis of the quadcopter is cancelled during the hovering state (Allen 2014; Quadcopter 2017; Fernando et al. 2013). The figure shows two basic coordinate frames called inertial frames, being a fixed earth frame and body frame. The two frames are used to identify the quadrotor's locations and attitude in order that translation and rotation matrices can be applied to transfer the vehicle from one coordinate frame to another (Fernando et al. 2013; Alaiwi and Mutlu 2018).

In this section, the performance of unmanned rotorcraft is demonstrated using a six degree of freedom (6-DoF) prototype model. The quadrotor includes four propellers responsible for lift force. Propellers are driven by four motors that are fixed onto a frame with a plus shape structure. Dynamic modeling is usually developed using the Newton Euler Formula, where the drive force and produced torque are regarded as the main quadrotor control elements (Magnussen and Skjonhaug 2011).

Quadrotor control is taken into consideration as a multivariable and as a substitute nonlinear system due to its dynamics, having sturdy coupling among translation and angular motion, and suffers from external disturbances related to flight surroundings and the effect of huge payload variability. These factors demand a robust control design. The control goal is to allow for sudden changes and rewards an ability of

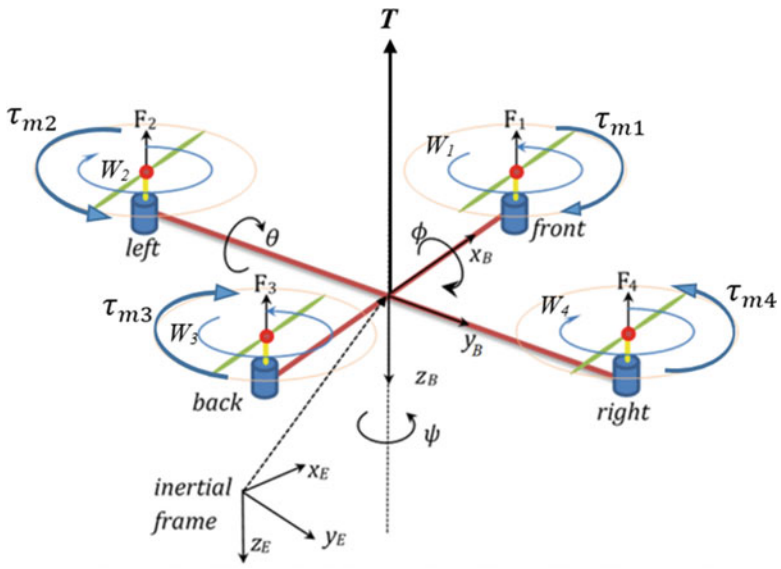

Fig. 10.3 The inertial and body frames of a quadrotor

discovering improved tracking performance in contrast to any modeling error and uncertainty.

The quadrotor has a linear position $\xi = (x, y, z)$ and the attitude (angular position) defined by Euler angles $H =$ (roll (ϕ), pitch (θ), yaw (ψ)) with respect to the inertial frame. The Euler angles determine the rotation of the quadrotor around each axis (x, y, and z axis, respectively). The roll angle determines rotation around the x-axis, while the pitch angle determines rotation around the y axis and the yaw angle determines rotation around the z-axis. The angular velocity in the body frame $\boldsymbol{V} = [p, q, r]$ can be related to the Euler angles velocities $(\dot{x}, \dot{y}, \dot{z})$ in the same frame by the following relation:

$$V = W_H \dot{\theta}$$
$$\begin{bmatrix} p \\ q \\ r \end{bmatrix} = \begin{bmatrix} 1 & 0 & -s_\theta \\ 0 & c_\phi & c_\theta s_\phi \\ 0 & -s_\phi & c_\theta s_\phi \end{bmatrix} \begin{bmatrix} \dot{\phi} \\ \dot{\theta} \\ \dot{\psi} \end{bmatrix} \tag{10.1}$$

where $c_\phi =$ cos (ϕ), $s_\phi =$ sin (ϕ), $c_\theta =$ cos (θ), $s_\theta =$ sin (θ), and W_H is the transformation matrix for angular velocities from the inertial frame to the body frame. Conversely, a rotation matrix (R) can be used to transform the linear velocity $(\boldsymbol{\eta} = [u\ v\ w])$ from the body frame to the inertial frame. The matrix R has an orthogonal property, so $R^T = R^{-1}$ (Castillo–Zamora et al. 2018; Bouzgou et al. 2017; Gordon et al. 2016).

$$R = \begin{bmatrix} c_\psi c_\theta & c_\psi s_\theta s_\phi - s_\psi c_\phi & c_\psi s_\theta c_\phi + s_\psi s_\phi \\ s_\psi c_\theta & s_\psi s_\theta s_\phi + c_\psi c_\phi & s_\psi s_\theta c_\phi - c_\psi s_\phi \\ -s_\theta & c_\theta s_\phi & c_\theta c_\phi \end{bmatrix} \tag{10.2}$$

The quadrotor has four motors which are used to provide it with the required thrust force (T), moving in the direction of the body z-axis. These are calculated via (10.3) and (10.4) as

$$T = \sum_{i=1}^{4} T_i = k\left(w_1^2 + w_2^2 + w_3^2 + w_4^2\right) \tag{10.3}$$
$$T_i = f_i = k w_i^2 \tag{10.4}$$

where T_i is the thrust force generated by the ith motor, k is the thrust factor, and w_i is the angular velocity of the ith motor. The motors provide the quadcopter with required torques τ_ϕ, τ_θ, and τ_ψ in the direction corresponding to the body frame (Alaiwi and Mutlu 2018; Bouzgou et al. 2017). This is further expanded in (10.5) as follows:

$$\tau_B = \begin{bmatrix} \tau_\phi \\ \tau_\theta \\ \tau_\psi \end{bmatrix} = \begin{bmatrix} lk\left(-w_2^2 + w_4^2\right) \\ lk\left(-w_1^2 + w_3^2\right) \\ k\left(w_2^2 + w_4^2 - w_1^2 - w_3^2\right) \end{bmatrix} = \begin{bmatrix} lU_2 \\ lU_3 \\ U_4 \end{bmatrix} \tag{10.5}$$

where l is the distance from the centre of the motor to the center of mass of the quadrotor; U_2, U_3, and U_4 are input forces to the quadrotor generated by motors. These forces can be calculated as

$$U_2 = f_2 - f_4 = k\left(-w_2^2 + w_4^2\right) \tag{10.6}$$

$$U_3 = f_1 - f_3 = k\left(-w_1^2 + w_3^2\right) \tag{10.7}$$

$$U_4 = f_2 + f_4 - f_1 - f_3 = k\left(w_2^2 + w_4^2 - w_1^2 - w_3^2\right) \tag{10.8}$$

Each motor generates an extra torque τ_{m_i} around its rotor axis which can be calculated by

$$\tau_{\mathrm{m}_i} = dw_i^2 + I_{\mathrm{m}}\dot{w}_i \tag{10.9}$$

where d, $\dot{w}_i$, and I_{m} represent the drag factor, the angular acceleration of the ith motor, and the inertia moment retrospectively. Generally, $\dot{w}_i$ is very small and can be omitted, leading to (10.10)

$$\tau_{m_i} = dw_i^2 \tag{10.10}$$

The quadrotor is assumed to be symmetric, so its inertia matrix I is diagonal with $I_{xx} = I_{yy}$. The inertia matrix of quadcopter around three axes can be represented as

$$I = \begin{bmatrix} I_{xx} & 0 & 0 \\ 0 & I_{yy} & 0 \\ 0 & 0 & I_{zz} \end{bmatrix} \tag{10.11}$$

The linear acceleration $(\ddot{x}, \ddot{y}, \ddot{z})$ and angular acceleration $\left(\ddot{\phi}, \ddot{\theta}, \ddot{\psi}\right)$ equations are used to represent the dynamic motion equations of the quadrotor. These functions can be derived by Euler-Lagrange equations of motion and Eqs. (10.1, 10.2, 10.3, 10.4, 10.5, 10.6, 10.7, 10.8, 10.9, 10.10, and 10.11) shown above.

The Lagrange equation variable L is key in derivation of linear and angular acceleration equations. The Lagrange equation represents the algebraic sum of translational (E_{trans}), rotational (E_{rot}), and potential (E_{pot}) energies. It can be defined as (Alaiwi and Mutlu 2018)

$$\mathrm{L}(o, \dot{p}) = E_{trans} + E_{rot} + E_{pot} = \frac{m}{2}\dot{\xi}^T\ddot{\xi} + \frac{1}{2}v^T I v - mgz \tag{10.12}$$

where $o = \begin{bmatrix} \xi \\ H \end{bmatrix} = [x, y, z, \phi, \theta, \psi\,]^T$.

Quadcopters are exposed to external forces such as wind that affect the copter's torques. The relationship between external forces and torques can be represented by the following:

$$\begin{bmatrix} f \\ \tau \end{bmatrix} = \frac{d}{dt}\left(\frac{\partial \mathrm{L}}{\partial \dot{o}}\right) - \frac{\partial \mathrm{L}}{\partial o} \tag{10.13}$$

Linear and angular components are not independent so should be studied separately. Therefore, the linear Euler-Lagrange equations are

$$f = RT^B = m\,\ddot{\xi} + mg\begin{bmatrix} 0 \\ 0 \\ 1 \end{bmatrix} \tag{10.14}$$

where T^B is the thrust force vector in the direction of body axis and $T^B = [0 \;\; 0 \;\; T]^T$. Therefore,

$$\ddot{\xi} = \frac{R}{m}\begin{bmatrix} 0 \\ 0 \\ T \end{bmatrix} - g\begin{bmatrix} 0 \\ 0 \\ 1 \end{bmatrix} \tag{10.15}$$

Equation (10.2) is substituted in Eq. (10.15) to get the following:

$$\begin{bmatrix} \ddot{x} \\ \ddot{y} \\ \ddot{z} \end{bmatrix} = \frac{T}{m}\begin{bmatrix} c_\psi s_\theta c_\phi + s_\psi s_\phi \\ s_\psi s_\theta c_\phi - c_\psi s_\phi \\ c_\theta c_\phi \end{bmatrix} - g\begin{bmatrix} 0 \\ 0 \\ 1 \end{bmatrix} \tag{10.16}$$

As we mentioned earlier, the symbol T represents the thrust force generated by motors. We will replace it with U_1 to format all symbols that represent the forces generated by quadcopter's motors.

$$\left.\begin{aligned} \ddot{x} &= \frac{U1}{m}\left(c_\psi s_\theta c_\phi + s_\psi s_\phi\right) \\ \ddot{y} &= \frac{U1}{m}\left(s_\psi s_\theta c_\phi - c_\psi s_\phi\right. \\ \ddot{z} &= \frac{U1}{m} c_\theta c_\phi - g \end{aligned}\right\} \tag{10.17}$$

where m represents the mass of the quadrotor.

The relations between angular velocity of motors w_i and generated forces U_1, U_2, U_3, and U_4 by motors can be presented in a matrix form (Armah et al. 2016; Herrera and Gómez 2015).

$$\begin{bmatrix} w_1^2 \\ w_2^2 \\ w_3^2 \\ w_4^2 \end{bmatrix} = \begin{bmatrix} \frac{1}{4k} & 0 & \frac{-1}{2k} & \frac{-1}{4d} \\ \frac{1}{4k} & \frac{-1}{2k} & 0 & \frac{1}{4d} \\ \frac{1}{4k} & 0 & \frac{1}{2k} & \frac{-1}{4d} \\ \frac{1}{4k} & \frac{1}{2k} & 0 & \frac{1}{4d} \end{bmatrix} \begin{bmatrix} U_1 \\ U_2 \\ U_3 \\ U_4 \end{bmatrix} \tag{10.18}$$

The angular Euler-Lagrange equations can be defined as follows:

$$\tau_B = J\ddot{H} + C(H, \dot{H})\dot{H} \tag{10.19}$$

where J is the Jacobian matrix transform from V to $\dot{H}$ and can defined as follows:

$$\begin{aligned} J &= W_H^T I W_H \\ &= \begin{bmatrix} I_{xx} & 0 & -I_{xx}s_\theta \\ 0 & I_{yy}c_\phi^2 + I_{zz}s_\phi^2 & (I_{yy} - I_{zz})c_\phi s_\phi c_\theta \\ -I_{xx}s_\theta & (I_{yy} - I_{zz})c_\phi s_\phi c_\theta & I_{xx}s_\theta^2 + I_{yy}s_\phi^2 c_\theta^2 + I_{zz}c_\phi^2 c_\theta^2 \end{bmatrix} \end{aligned} \tag{10.20}$$

where the c matrix is the Coriolis term containing the gyroscope and centripetal terms (Herrera and Gómez 2015).

Now, Eq. (10.19) can be used to derive angular acceleration equations to get

$$\ddot{H} = J^{-1}(\tau_B - C(H, \dot{H})\dot{H}) \tag{10.21}$$

Then, calculate the inverse of J and substitute it in Eq. (10.21) to get the following angular acceleration equations of the quadcopter:

$$\left.\begin{aligned} \ddot{\phi} &= \frac{I_y - I_z}{I_x}\dot{\theta}\dot{\psi} - \frac{J_r}{I_x}W_r\dot{\theta} + \frac{U_2}{I_x} \\ \ddot{\theta} &= \frac{I_z - I_x}{I_y}\dot{\phi}\dot{\psi} - \frac{J_r}{I_y}W_r\dot{\phi} + \frac{U_3}{I_y} \\ \ddot{\psi} &= \frac{I_x - I_y}{I_z}\dot{\theta}\dot{\phi} + \frac{U_4}{I_z} \end{aligned}\right\} \tag{10.22}$$

where W_r is the algebraic sum of the angular speeds of motors:

$$W_r = -w_1 + w_2 - w_3 + w_4 \tag{10.23}$$

J_r is the inertia of the motor and is a very small value and often can be omitted so Eq. (10.22) and (10.24):

$$\left.\begin{aligned}\ddot{\phi} &= \frac{I_y - I_z}{I_x}\dot{\theta}\dot{\psi} + \frac{U_2}{I_x}\\ \ddot{\theta} &= \frac{I_z - I_x}{I_y}\dot{\phi}\dot{\psi} + \frac{U_3}{I_y}\\ \ddot{\psi} &= \frac{I_x - I_y}{I_z}\dot{\theta}\dot{\phi} + \frac{U_4}{I_z}\end{aligned}\right\} \tag{10.24}$$

Equations (10.17) and (10.24) represent linear and angular motions of quadrotors. The mathematical model can be implemented in MATLAB/Simulink or another environment to perform the tests in multiple scenarios and additional purposes by researchers to achieve optimal performance (Armah et al. 2016).

Linear and angular velocity states can be calculated by integrating Eqs. (10.17) and (10.24), respectively; in turn, linear and angular position states can be calculated by double integration of Eqs. (10.17) and (10.24). The 12 states $\left(x, \dot{x}, y, \dot{y}, z, \dot{z}, \phi, \dot{\phi}, \theta, \dot{\theta}, \psi, \dot{\psi}\right)$ are the required states for the control of the quadrotor. Some of these states can be measured by sensors, while others can be estimated by special "observers" such as KFs or extended Kalman filters (EKFs).

10.4 Control of Quadrotors

Every type of aircraft has actuators that are used to generate linear and angular forces which enable movement in different ways to achieve the desired position. As mentioned earlier, quadrotors use four motors (actuators) to generate forces but are unable to achieve desired positions without the use of control systems which generate appropriate control signals.

A flight controller is essentially a circuit board with sensors that relays variation in coordinates of the quadrotor. It may receive user commands and controls the rotor's motors so as to retain the sought after position.

Most control systems reduce the error ratio between desired and sensor-measured signals to generate appropriate control signals for motors, until the quadrotor reaches the desired location where the error signal will be zero. Quadrotors require a highly nonlinear multivariable system that has strong coupling between translation and angular motion and hence are highly sensitive to external disturbances. Moreover, large payload variation may have noticeable effects. Accordingly, robust controller is needed to deal with sudden changes as well as provision of tracking performance in the presence of modeling error and uncertainties. The most commonly used types of controllers are as follows:

Proportional Integral Derivative (PID) Controllers

Different types of PID controllers are usually designed to reach a desired position. However, tuning methods are required to obtain suitable controller settings; for this purpose, Bouabdallah et al. (2004), Pounds et al. (2010), and Argentim et al. (2013) utilized integral time absolute error (ITAE) criteria. In Abbasi et al. (2013), a fuzzy

self-tuned PID controller was proposed. Bergkvist (2013) implemented a PID controller for real-time "Android" operating systems. Sadeghzadeh et al. (2014) implemented single PID and gain scheduling-PID. Kader et al. (2014) proposed PID and compared it with fuzzy controllers for attitude and altitude signals. It is simple to design a PID; it provides good performance and requires minimal control effort. Wang et al. (2016) provided a robust cascade PID controller that alleviates disturbances, and Ferry (2017) designed a PID.

Optimal and Adaptive Controllers
Linear quadratic (LQ) control was applied by Bouabdallah et al. (2004), and a classic linear quadratic regulator (LQR) controller was utilized by Argentim et al. (2013); Araar and Aouf (2014) designed an LQ-servo controller that provides improved performance and attains robust trajectory design even in presence of gusts of wind. Moness and Bakr (2015) and Purnawan et al. (2017) introduced a further LQR controller design for quadrotors.

Adaptive Control
Adaptive control is an advanced control technique to maintain a desired level of control system performance, when the parameters of the plant dynamic model are unknown and/or change in time (Minh et al. 2014).

Nonlinear and Intelligent Controllers
Dikmen et al. (2009) applied different types of nonlinear controllers for quadrotor control systems including inverse dynamic control, feedback linearization control, and sliding mode control. Sliding mode (Thomas 2010; Balasubramanian and Vasantharaj 2013) applied computed torque control mechanism to nonlinear dynamics of a quadrotor with consideration of disturbance; in the latter, improved robustness is gained in the presence of small changes in the payload as compared to other techniques. Yacine et al. (2015) used a combination of a fuzzy logic control (FLC) and a sliding mode control (SMC) in order to improve performance of quadrotors. Sliding mode has been further advanced (Tripathi et al. 2016; Abdullah and Sabar 2015) establishing a fuzzy controller to regulate the height, roll, pitch, and yaw of the quadrotor using a genetic algorithm (GA). In addition, fuzzy control has been applied by Sattar and Ismail (2017).

10.5 Case Studies

10.5.1 Precise Positioning for Delivery Quadrotor

In this case study, the PID control algorithm will be applied to control the position of a quadrotor system. The block diagram used to calculate the PID is shown in Fig. 10.4. The PID is the part of the flight control software that receives the data from sensors and determines the necessary speed of the quadrotor's motor. There are three parameters in a PID controller, the *P*, *I*, and *D* terms (Liang 2018):

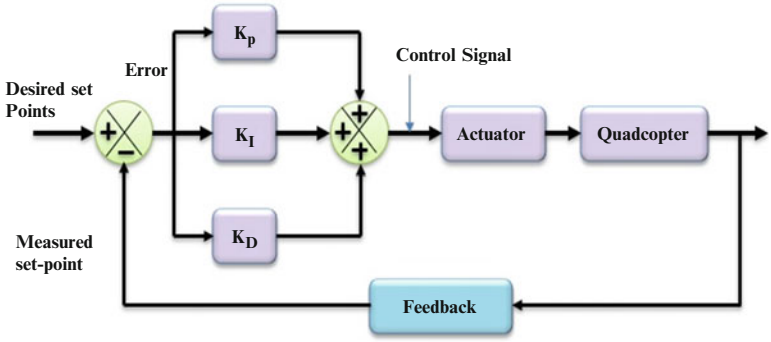

Fig. 10.4 Block diagram of quadcopter control by PID control

- "*P*" tends to reduce the present error.
- "*D*" is a prediction of future errors – it helps to accelerate approaching a set-point and counteracts P when it is getting close to minimize overshoot.
- "*I*" is the accumulation of past errors; it works on reducing the steady-state error by managing the forces that happen over time; for example, if a quad constantly drifts away from a set-point due to wind, it will spool motors up to counteract it.

The general formula of a PID controller (Fernando et al. 2013; Kotarski et al. 2016) can be written as

$$PID(e) = k_{\mathrm{p}} e(t) + k_{\mathrm{I}} \int_0^t e(\tau) d\tau + k_{\mathrm{D}} \frac{d}{dt} \mathrm{state} \tag{10.25}$$

where $e(t) =$ desired state$(t) -$ measured state(t), k_{p}, k_{I}, and k_{D} are the proportional, integral, and derivative gains, respectively.

Altitude Control

Appropriate thrust force, U_1, is required to achieve the desired altitude and can be calculated by

$$U_1 = k_{p_z} e_z + k_{I_z} \int e_z + k_{D_z} \frac{d}{dt} e_z + mg \tag{10.26}$$

where k_{p_z}, k_{I_z}, and k_{D_z} are the altitude PID gains controller; e_z is the altitude error $e_z = z_{\mathrm{des}} - z_{\mathrm{meas}}$, z_{des} and z_{meas} are desired and measured altitude, respectively; and g is the Earth gravity.

The roll control, pitch control, and yaw control Eqs. (10.27–10.29) are used to determine appropriate torques to achieve the desired attitude.

Roll Control

The following equation is used to determine appropriate torque (U_2) to rotate a quadrotor around the x-axis:

$$U_2 = k_{p_\phi} e_\phi + k_{I_\phi} \int e_\phi + k_{D_\phi} \frac{d}{dt} e_\phi \tag{10.27}$$

where k_{p_ϕ}, k_{I_ϕ}, and k_{D_ϕ} are the roll angle PID gains controller; e_ϕ is the roll angle error; $e_\phi = \phi_{\text{des}} - \phi_{\text{meas}}$; ϕ_{des} and ϕ_{meas} are the desired and measured roll angle, respectively.

Pitch Control

The torque (U_3) is required to rotate a quadrotor around the y-axis and can be calculated by

$$U_3 = k_{p_\theta} e_\theta + k_{I_\theta} \int e_\theta + k_{D_\theta} \frac{d}{dt} e_\theta \tag{10.28}$$

where k_{p_θ}, k_{I_θ}, and k_{D_θ} are the pitch angle PID gains controller; e_θ is the pitch angle error $e_\theta = \theta_{\text{des}} - \theta_{\text{meas}}$; θ_{des} and θ_{meas} are the desired and measured pitch angle, respectively.

Yaw Control

The torque (U_4) is needed to rotate a quadrotor around z-axis and can be properly calculated by

$$U_4 = k_{p_\psi} e_\psi + k_{I_\psi} \int e_\psi + k_{D_\psi} \frac{d}{dt} e_\psi \tag{10.29}$$

where k_{p_ψ}, k_{I_ψ}, and k_{D_ψ} are yaw angle PID gains controller; e_ψ is yaw angle error $e_\psi = \psi_{\text{des}} - \psi_{\text{meas}}$; ψ_{des} and ψ_{meas} are desired and measured yaw angle, respectively.

The current quadrotor model has six DOF and only four actuators (motors), so direct control of all DOF is complex. Meanwhile, the control Eqs. (10.26–10.29) are used to directly control four of the DOF (z, ϕ, θ, ψ). The roll and pitch angles move the quadrotor towards the desired x and y location. Consequently, the desired x and y will be used first to calculate the desired roll and pitch angles in order to control x and y positions indirectly. Meanwhile, the equations that are used to calculate desired roll and pitch angles are obtained in terms of desired x and y as Shahid et al. (2016):

$$\phi_d = \tan^{-1}\left(\frac{U_y \cos\theta_d}{g - U1}\right) \tag{10.30}$$

and

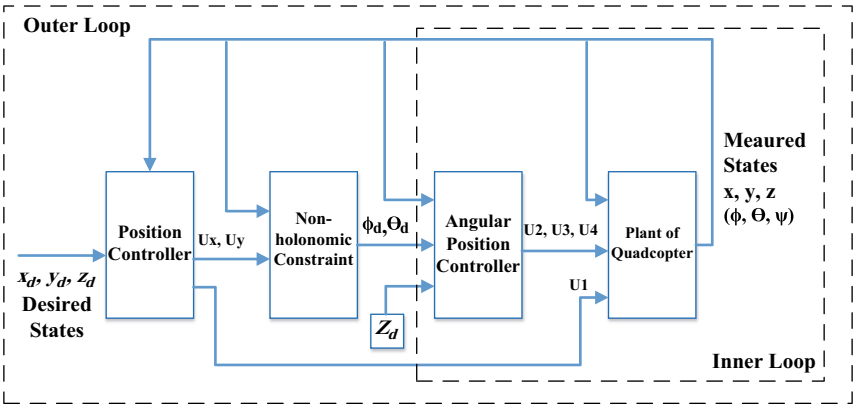

Fig. 10.5 Control block diagram of quadrotor

$$\theta_d = \tan^{-1}\left(\frac{U_x}{U1 - g}\right) \tag{10.31}$$

where U_x and U_y are calculated as follows:

$$U_x = k_{p_x} e_x + k_{I_x} \int e_x + k_{D_x} \frac{d}{dt} e_x \tag{10.32}$$

$$U_y = k_{p_y} e_y + k_{I_y} \int e_y + k_{D_y} \frac{d}{dt} e_y \tag{10.33}$$

where $e_x = x_{\text{des}} - x_{\text{meas}}$ is the error position in the direction of x-axis, x_{des} and x_{meas} are desired and measured position in the direction of x-axis, respectively. Further, $e_y = y_{\text{des}} - y_{\text{meas}}$ is the error position in the direction of y-axis, y_{des} and y_{meas} are the desired and measured position in the direction of the y-axis, respectively.

There are two main control loops: *inner* and *outer*. The outer loop is used to calculate U_1, U_x, U_y, ϕ_d, and θ_d. The inner loop is used to calculate the desired control signals U_2, U_3, and U_4. Figure 10.5 shows the overall control block diagram of quadrotor. Control signals U_1, U_2, U_3, and U_4 are feed to the Electronic Speed Control (ESC) devices to generate appropriate electrical signal used to control the speed of each motor. The block diagram in Fig. 10.5 has been implemented by the technical computing platform Matlab. Figure 10.6a–e shows the simulation response of the states X, Y, Z, φ, and θ of the quadrotor under a PID controller for fixed position ($x = 20$, $y = 15$, $z = 10$, and $\psi = 0$).

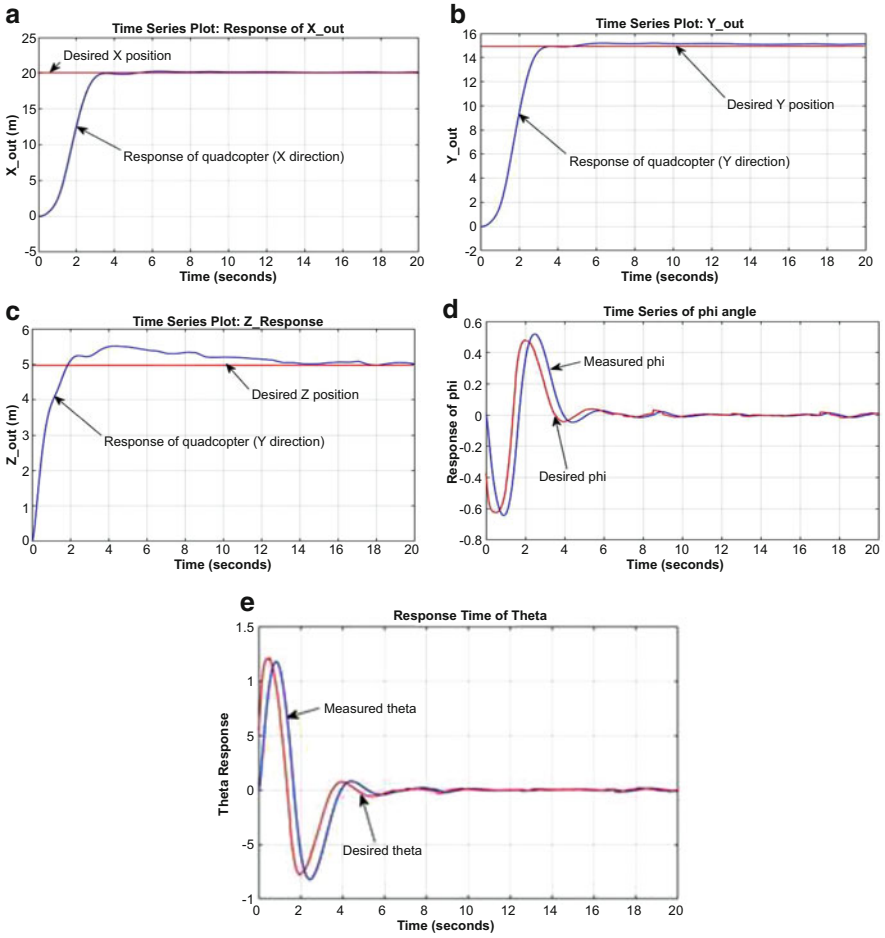

Fig. 10.6 State simulation time response of quadrotor: (**a**) X-out response; (**b**) Y-out response; (**c**) Z response; (**d**) φ response; (**e**) θ response

10.5.2 Adaptive Positioning of Quadrotor

Multiple model adaptive control (MMAC) is a state feedback controller. This adaptive control implants its construction in a bank of filters as Kalman filters (KFs). For the quadrotor, each KF is intended for an explicit value of payload variation. Then, accordingly, a set of LQ-servo state feedback controllers are designed for tracking reference trajectories. The integral term of the LQ-Servo can effectively eliminate the tracking error.

MMAC is applied here to meet stability and performance requirements in two situations: additive payload, which leads to performance degradation or instability, and fluctuating of the operating point. The appropriate control signal is correlated

with the highest weighting signal in order to provide the required control action. The assigned weighting signals rely on two important elements: the residual and covariance matrices of the KFs. Note that each KF is designed for a model that corresponds to the known value of the uncertain parameter (Hassani et al. 2011; Hassani et al. 2009).

The MMAC comprises of (i) N weighting signal, P_N, that generated from a dynamic weighting signal generator and (ii) a bank of N continuous-time estimator, KF_N. Each estimator is intended for one of the selected adopted models. Each of these carefully chosen models belongs to the original set of the plant's model (Fekri et al. 2006).

The uncertain parameters' vector signifies the uncertainty in linear state model of the quadrotor dynamic system. These parameters tolerate the matrices that define the structure of the linear model. For flexible illustration, it is presumed that the uncertain parameter (a) can take only one value for each run.

The dynamic weights characterize the finest deduction of model that is most likely to be accurate. These weights are supposed be the characterized issue in multiple model algorithms, and they are usually evaluated online. The dynamic weighting is initially set to $1/N$ and fulfils the following condition:

$$(P_i(t)) \in (0, 1) \;\; \text{For } i = 1 \ldots N \tag{10.34}$$

The dynamic weights are produced by dynamic weighting signal generator (DWSG) which is denoted by the following differential equation:

$$\dot{P}_i(t) = -\mu \left(1 - \frac{\beta_i(t)\, e^{-w_i(t)}}{\sum_{j=1}^{N} P_j(t)\, \beta_j(t)\, e^{-w_j(t)}} \right) P_i(t) \tag{10.35}$$

where μ is a positive constant theoretically equals to one and the function $\beta_i(t)$ is denoted by

$$\beta_i(t) = \frac{1}{\sqrt{\mathbf{det} \boldsymbol{S_i}(\boldsymbol{t})}} \tag{10.36}$$

and $w_i(t)$ is an error measuring function between the measurement states of the quadrotor and the estimated measurable states of each local estimator. It can be evaluated as follows:

$$\boldsymbol{w_i}(t) = \frac{\mathbf{1}}{\mathbf{2}} \| \boldsymbol{z}(t) - \widehat{\boldsymbol{y}}_{\boldsymbol{i}}(t) \|_{\mathbf{2}}\, \boldsymbol{S_i^{-1}}(t) \tag{10.37}$$

$$\boldsymbol{S_i} = \boldsymbol{C}\, \boldsymbol{s_i}\, \boldsymbol{C^T} + \boldsymbol{R_i} \tag{10.38}$$

where $\boldsymbol{s_i}(t)$ is a uniformly positive definite weighting matrix, described by

$$\|\boldsymbol{x}\|_2 \boldsymbol{S} = \left(\boldsymbol{x}^{\boldsymbol{T}} \boldsymbol{S} \boldsymbol{x}\right)^{(1/2)} \tag{10.39}$$

Each control signal is obtained from the product of the state estimation $KF\ \widehat{x}_k(t|t), k = 1, 2, 3, \ldots N$ and the gain supplied by an optimal linear quadratic control, G_k, as

$$u_k(t) = -G_k\ \widehat{x}_k(t|t), k = 1, 2, 3, \ldots\ldots N \tag{10.40}$$

The "global" control signal, which enters both the quadrotor system and the banks of KFs, is calculated by the probabilistic weighting of each local control signal (Hassani et al. 2009). Consequently, the mixing of state estimation and generated feedback control can be clearly noticed. Therefore, any estimation errors of the state will directly affect the local control signals. Accordingly, in the MMAC design, the identification system and the control system are not separated (Fekri et al. 2007).

The employed MMAC with three KFs is shown in Fig. 10.7. The (a) value equals 0, 0.3, and 0.8 kg for KF number 1, 2, and 3, respectively. The three KFs are run in parallel when the parameter (a) is allocated to the reference model. The three KFs are initialized with $x_o = [2\ 0\ 3\ 0\ -\ 10\ 0\ 0.2\ 0.3\ 0\ 0.05]^T$ values with the initial weighting signal uniformly distributed $Po = 1/3$ (Raafat and Mahmoud 2018). Figure 10.8 shows the progress with time for the conditional probabilities for the three KFs. The quadrotor system tracks the desired references in about 5 s. This demonstrates the capability of the MMAC of reasonably fast convergence.

Figure 10.9 shows the closed loop responses of MMAC using three KFs, where the model and filters start at the same initial point. Figure 10.9a shows the response of the linear position (x) by using MMAC, where (curve 1) represents the actual response from the model, the estimated signal is represented in (curve 2), and the reference signal is explained in (curve 3). Figure 10.9(a–e) also shows the tracking for y, z, roll, pitch, and yaw, respectively. In Fig. 10.9, the linear and angular positions track the references, and the adaptation of this algorithm can be seen clearly where the actual response follows the true value by adjusting its parameter (a). Accordingly, Fig. 10.10 demonstrates the performance of the MMAC controlled system to follow the applied references. That reflects the capability of the controller to select the correct control signal. The root mean square error (RMSE) is used as a performance index.

Figure 10.11 demonstrates the capability of tracking with initial conditions of the reference model which are different from those of filters which have a value of $x = [5\ 0\ 6\ 0\ -\ 5\ 0.1\ 0\ 0.3\ 0.9\ 0]$. The four motors in our example provide plenty of power for the rotors to climb rapidly. Each motor is designed for 'aeroplanes' weighing (280–400 g). For additive payload, we use a large motor that provides more thrust with the same size of propellers. These motors have larger output wattage which usually handles bigger loads sufficiently.

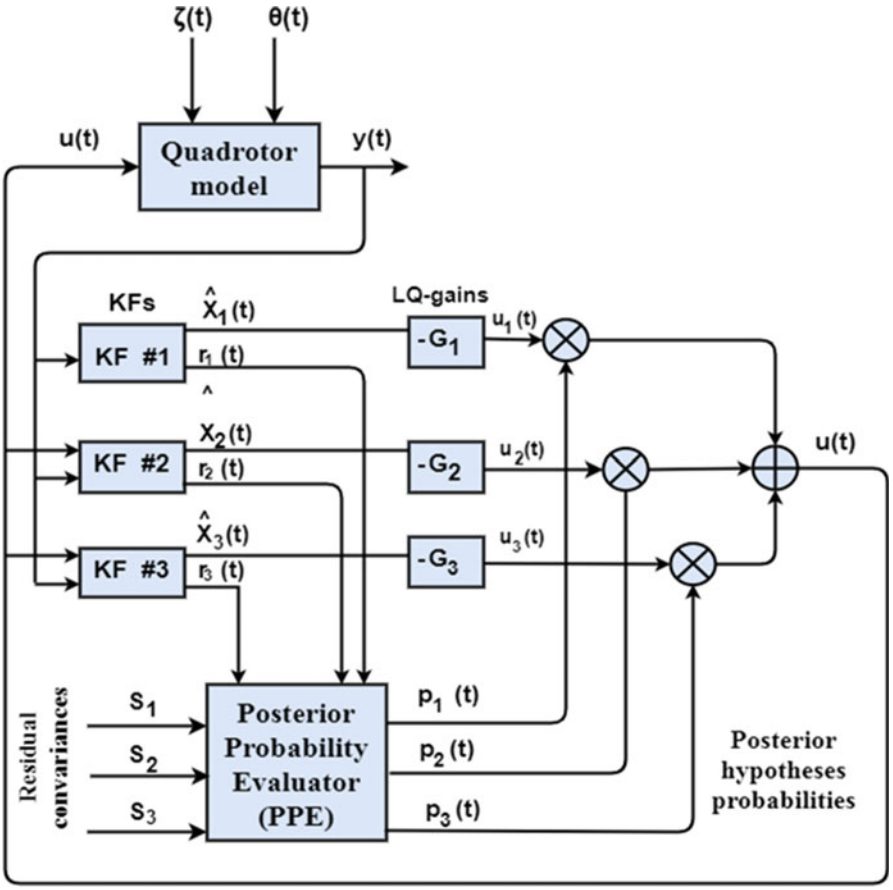

Fig. 10.7 Block diagram of MMAC

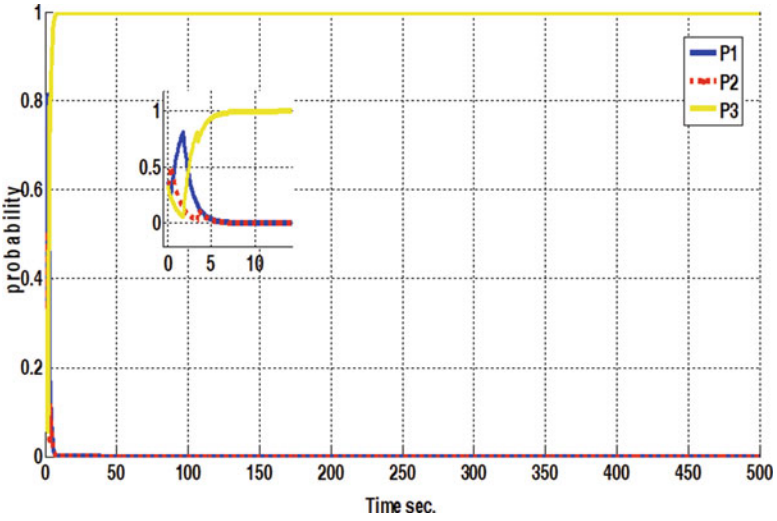

Fig. 10.8 Time histories for probability when the uncertainty in mass of a reference model is $0.8Kg$

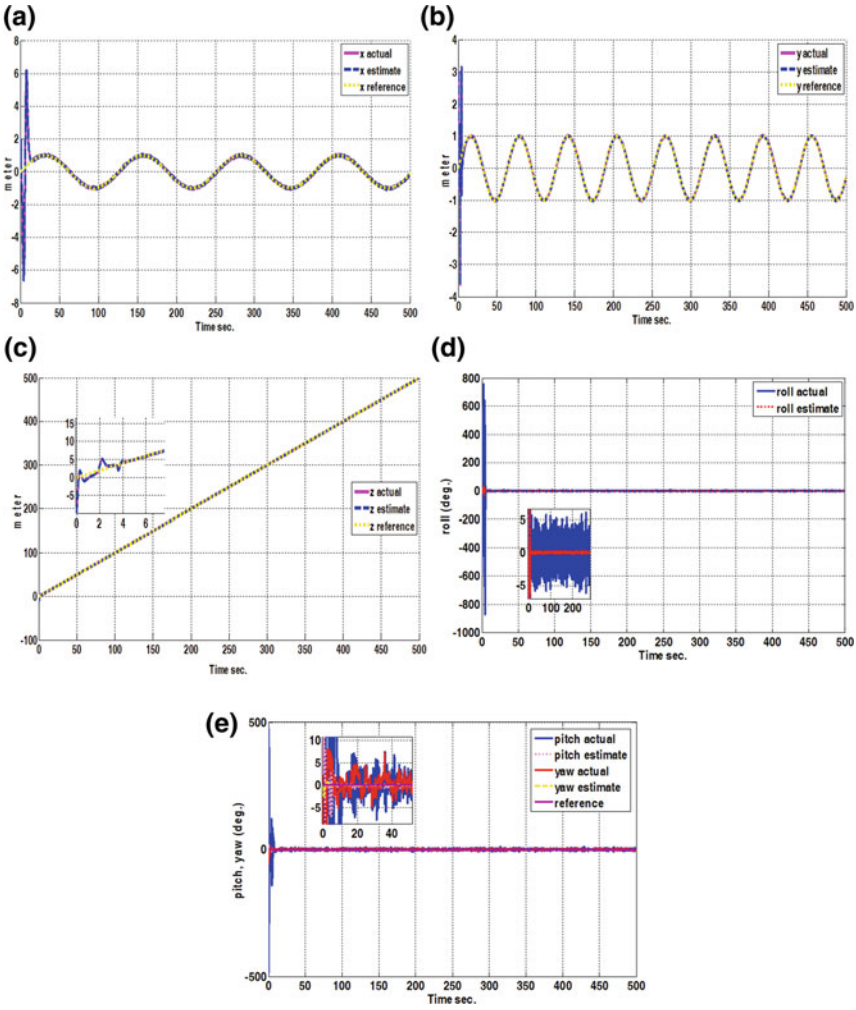

Fig. 10.9 A closed loop response of the reference model for (**a**) the linear position *x*; (**b**) the linear position *y*; (**c**) the linear position *z*; (**d**) the angular position roll; (**e**) the angular positions pitch and yaw

10.6 Conclusion and Future Applications

Different types of quadrotors are increasingly used for different applications. The type and application affects the design of the required controller. A high level of safety and reliability need to be assured for social and airspace applications. Accurate measurements are necessary for robust behavior of quadrotors. In order to achieve observability of all the states, it is necessary to use estimators of KFs or EKFs.

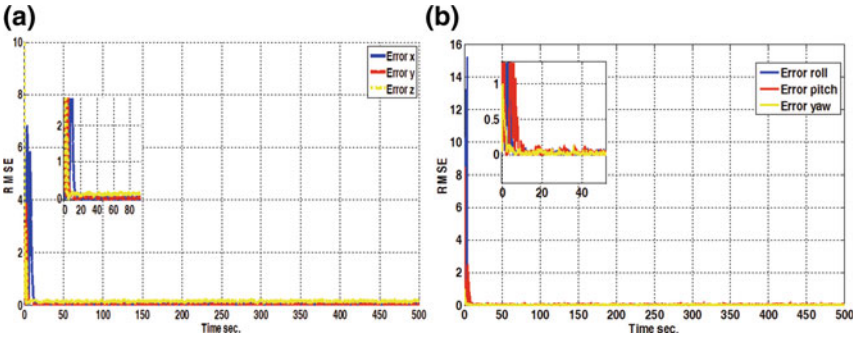

Fig. 10.10 RMSE of tracking design when the mass uncertainty at reference model = 0.8 kg for: (**a**) The linear position, (**b**) the angular position

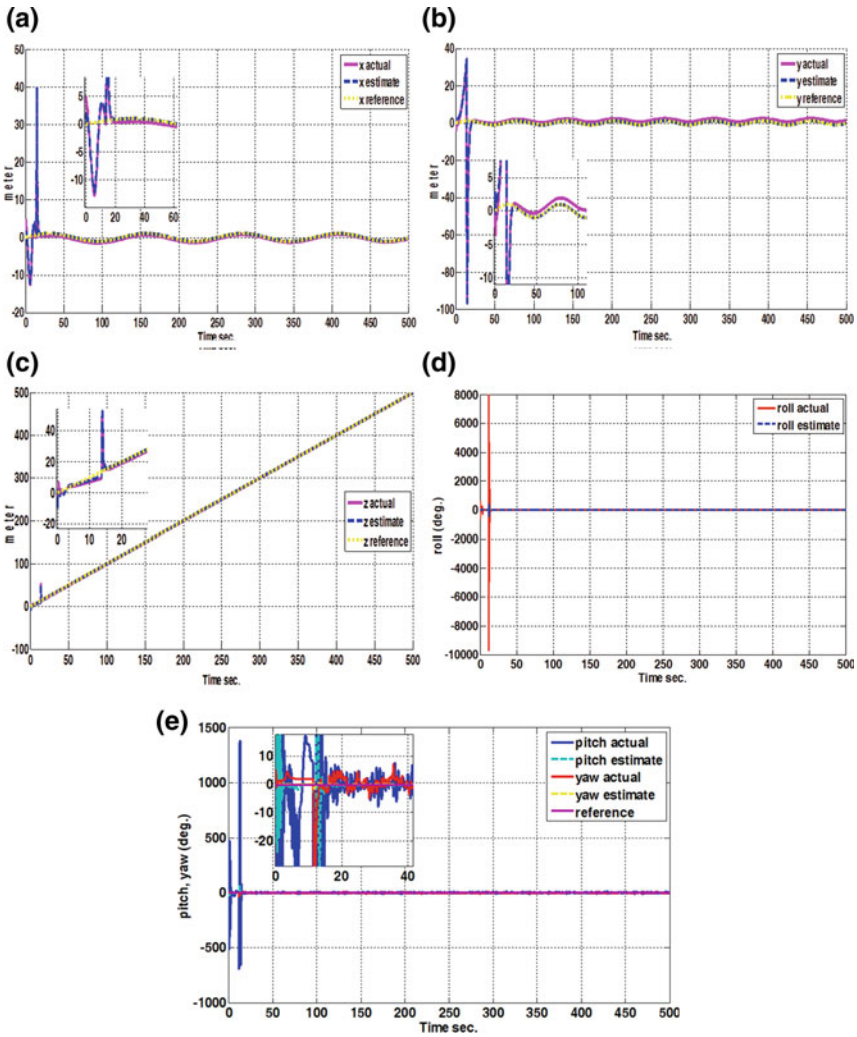

Fig. 10.11 A closed loop response of quadrotor controlled system using MMAC, with Kalman filters (KFs) starting at different initial points from that of the reference model: (**a**) the linear position x; (**b**) the linear position y; (**c**) the linear position z; (**d**) the angular position roll; (**e**) the angular position pitch and yaw

Quadrotor has been increasingly used for delivery owed to the low cost, efficiency, and speed of parcel carriage; it overcomes the flow, congestion of roads, and traffic lights. Another important point is the reduction of the pollution of the environment; no combustible fuel is used, and power is supplied via a rechargeable battery. Quadrotors are unobtrusive and may reach rugged areas where cars or other forms of carriage cannot.

In this chapter, two cases of designing a controller for quadrotors have been described. The first presents the development of a PID controller to solve impulse input signal and prevent the system from saturation as well, as well as operating with minimal power under a simple and efficient algorithm. The second case presents the design of MMAC, in which the reference position is effectively tracked. The robustness of the adaptive controller is demonstrated when different initial positions are used from the true initial condition of the quadrotor. The performance of the adaptive control has been evaluated using the RMSE index, demonstrating its robust potential application in resource flow, as part of efficient systematic management of the needs of increasing, potentially remote/variable demographic populations.

References

Abbasi E, Mahjoob M, Yazdanpanah R (2013) Controlling of quadrotor UAV using a fuzzy system for tuning the PID gains in hovering mode. In: 10th Int Conf Adv Computer Entertain Tech, pp 1–6

Abdullah F, Sabar RA (2015) Design and implementation of autopilot system for quadcopter. Int J Sci Eng Comput Technol 5(6):190–199

Air Drone Craze, Drone Deals + Information + Resources (2019). Accessed 2019. https://airdronecraze.com/drones-action-top-12-non-military-uses/

Alaiwi Y, Mutlu A (2018) Modelling, simulation, and implementation of autonomous unmanned quadrotor. Mach Technol Mater 12(8):320–325

Allen C (2014) How a quadcopter works. University of Alaska. Available via http://ffden2.phys.uaf.edu/webproj/212_spring_2014/Clay_Allen/clay_allen/works.html. Accessed 27 Oct 2020

Araar O, Aouf N (2014) Full linear control of a quadrotor UAV, LQ vs H_∞. In: IEEE, UKACC International Conference on Control (CONTROL). pp 133–138. https://doi.org/10.1109/CONTROL.2014.6915128

Argentim LM, Rezende WC, Santos PE et al (2013) PID, LQR and LQR-PID on a quadcopter platform. In: IEEE, International Conference on Informatics, Electronics & Vision (ICIEV). pp 1–6. https://doi.org/10.1109/ICIEV.2013.6572698

Armah S, Yi Sun, Choi W et al (2016) Feedback control of quad-rotors with a Matlab-based simulator. Am J Appl Sci 13(6):779–793. https://doi.org/10.3844/ajassp.2016.779.793

Armed Quadrotors Are Coming (2014) Hearst Magazine Media, Popular Mechanics. https://www.popularmechanics.com/military/a7926/armed-quadrotors-are-coming-10720086/. Accessed 27 Oct 2020

Balasubramanian E, Vasantharaj R (2013) Dynamic modeling and control of quad rotor. Int J Eng Technol 5(1):63–69

Bergkvist H (2013) Quadcopter control using android based sensing. M.Sc. Thesis, Department of Automatic Control, University of Lund

Bouabdallah S, Noth A, Siegwart R (2004) PID vs LQ control techniques applied to an indoor micro quadrotor. In: IEEE/RSJ, International Conference on Intelligent Robots and Systems (IROS), vol 3. pp 2451–2456

Bouzgou K, Bestaoui Y, Benchikh L et al (2017) Dynamic modeling, simulation and PID controller of unmanned aerial vehicle UAV. In: The Seventh International Conference on Innovative Computing, Technology. https://doi.org/10.1109/INTECH.2017.8102445

Castillo–Zamora JJ, Camarillo–Gomez KA, Perez–Soto GI et al (2018) Comparison of PD, PID and sliding-mode position controllers for V–tail quadcopter stability. IEEE Access 6:38086–38096

Dhanalakshmi KS, Karthika S, Saravanakumar P et al (2015) Implementation of highly automated UAV with GPS for product delivery using Labview. Int J Adv Electron Comput Sci 2(11): 39–42

Dikmen IC, Arisoy A,Temeltas H (2009) Attitude control of a quadrotor. In: IEEE, 4th international conference on recent advances in space technologies. RAST'09, pp 722–727

Fekri S, Athans M, Pascoal A (2006) Issues, progress and new results in robust adaptive control. Int J Adapt Control Signal Process 20(10):519–579. https://doi.org/10.1002/acs.912

Fekri S, Athans M, Pascoal A (2007) Robust multiple model adaptive control (RMMAC): a case study. Int J Adapt Control Signal Process 21(1):1–30. https://doi.org/10.1002/acs.944

Fernando HCTE, De Silva ATA, De Zoysa MDC et al (2013) Modelling, simulation and implementation of a quadrotor UAV. In: IEEE 8th international conference on industrial and information systems, ICIIS, Sri Lanka. https://doi.org/10.1109/ICIInfS.2013.6731982

Ferry N (2017) Quadcopter plant model and control system development with MATLAB/Simulink implementation. M.Sc. Thesis. Rochester Institute of Technology, Rochester

Gordon O, Ondoma O, Oliver O, Onyebuchi N (2016) Quadcopter design for payload delivery. J Comput Commun 04(10):1–12

Grisso R, Alley M, Conrad H (2009) Precision farming tools: global positioning system (GPS). Communications and Marketing. College of Agriculture and Life Sciences Virginia Polytechnic Institute and State University, pp 442–503

Hassani V, Aguiar AP, Pascoal AM et al (2009) Further results on plant parameter identification using continuous-time multiple-model adaptive estimators. In: 48th IEEE Conference on Decision and Control, held jointly with the 28th Chinese Control Conference [CDC/CCC]. pp 7261–7266. Available via https://web.fe.up.pt/~apra/publications/cdc2009-MMAE.pdf. Accessed 15 Dec 2021

Hassani V, Hespanha JP, Athans M et al (2011) Stability analysis of robust multiple model adaptive control. IFAC Proceed 44(1):350–355. Available via https://folk.ntnu.no/skoge/prost/proceedings/ifac11-proceedings/data/html/papers/1194.pdf. Accessed 15 Dec 2021

Herrera M, Gómez AP (2015) Sliding mode control: an approach to control a quadrotor. 2015 Asia-Pacific Conference on Computer Aided System Engineering, pp 314–319

Jung HC, Kyoohyung H, Seong-Min H, Hyoun JK (2018) Toward a Secure Drone System: Flying With Real-Time Homomorphic Authenticated Encryption. IEEE Access, Special Section on Security Analytics and Intelligence for cyber Physical System 6:2425–2439

Kader SA, EL Henawy AE, Oda AN (2014) Quadcopter system modeling and autopilot synthesis. Int J Eng Res Technol. https://doi.org/10.17577/IJERTV3IS110007

Kotarski D, Benić Z, Krznar M (2016) Control design for unmanned aerial vehicles with four rotors. Interdiscip Descr Complex Syst 14(2):236–245. https://doi.org/10.7906/indecs.14.2.12

Luo H, Niu Y, Liang Z et al (2016) Quadcopter autonomous control system based on image recognition. In: 12th World Congress on Intelligent Control and Automation [WCICA], Guilin, China, 12–15 June 2016

Magnussen Ø, Skjønhaug KE (2011) Modeling, design and experimental study for a quadcopter system construction. M.Sc. Thesis. Department of Engineering. Faculty of Technology and Science. University of Agder

Minh QH, Weihua Z, Lihua X (2014) L1 Adaptive control for quadrotor: design and implementation. In: International Conference on Control, Automation, Robotics and Vision Marina Bay Sands. Singapore

Moness M, Bakr M (2015) Development and analysis of linear model representations of the quadrotor system. In: 16th International Conference on Aerospace Sciences & Aviation Technology. https://doi.org/10.21608/ASAT.2015.22894

Newcome LR (2004) Unmanned Aviation: A Brief History of Unmanned Aerial Vehicles. American Institute of Aeronautics and Astronautics, Inc., 1st ed. Reston, VA: American Institute of Aeronautics and Astronautics

Oscar Liang (2018) Quadcopter PID explained. Tutorial, 8 February. https://oscarliang.com/quadcopter-pid-explained-tuning/. Accessed 28 Oct 2020

Pounds R, Mahony R, Corke P (2010) Modelling and control of a large quadrotor robot. Control Eng Pract 18(7):691–699. https://doi.org/10.1016/j.conengprac.2010.02.008

Purnawan H, Mardlijah, Purwanto EB (2017) Design of linear quadratic regulator [LQR] control system for flight stability of LSU-05. IOP Conf Ser. J Phys Conf Ser 890:012056. https://doi.org/10.1088/1742-6596/890/1/012056

Quadcopter (2017) What is a GPS quadcopter. Available via http://quad.phillycreative.com/category/articles/. Accessed 29 Oct 2020

Raafat SM, Mahmoud ZS (2018) Robust multiple model adaptive control for dynamic positioning of quadrotor helicopter system. Eng Technol J 36(12):1249–1259. https://doi.org/10.30684/etj.36.12A.6

Rahemi N, Mosavi MR, Abedi AA et al (2014) Accurate solution of navigation equations in GPS receivers for very high velocities using pseudo range measurements. Adv Aerosp Eng. https://doi.org/10.1155/2014/435891

Sadeghzadeh I, Abdolhosseini M, Zhang Y (2014) Payload drop application using an unmanned quadrotor helicopter based on gain-scheduled PID and model predictive control. Unmanned Syst 2(1):39–52. https://doi.org/10.1142/S2301385014500034

Sattar MA, Ismail A (2017) Modeling and fuzzy logic control of a quadrotor UAV. Int Res J Eng Technol 4(08):1–5

Schmidt MD (2011) Simulation and control of a quadrotor unmanned aerial vehicle. M.Sc. Thesis. University of Kentucky, USA

Shahid F, Kadri MB, Jumani NA et al (2016) Dynamical modeling and control of quadrotor. Trans Mach Des 4(2):50–63. Available via https://www.dline.info/tmd/v4n2.php. Accessed 15 Dec 2021

Thomas R (2010) Sliding mode controller for a quadrotor. M.Sc. Thesis, B. Engineering. Anna University, India

Tripathi VK, Behera L, Verma N (2016) Design of sliding mode and back stepping controllers for a quadcopter. In: IEEE 39th National Systems Conference [NSC]

Wang Z, Man Z, Cao J et al (2016) Dynamics modeling and linear control of quadcopter. In: IEEE, International Conference on Advanced Mechatronic Systems (ICAMechS). https://doi.org/10.1109/ICAMECHS.2016.7813499

Yacine D, Madjid K, Aimad A (2015) Fully decentralized fuzzy sliding mode control with chattering elimination for a quadrotor attitude. In: IEEE, 4th International Conference on Electrical Engineering, 1–6 Oct 2016

Ziaul H (2016) Basic Concept of GPS and Its Applications. IOSR Journal of Humanities and Social Science (IOSR-JHSS) 21(3)II:31–37

Chapter 11
Sustainable Wind Turbine Systems Based on On-line Fault Estimation and Fault Tolerant Control

Asaad A. Kraidi, Ruaa H. Ahmed, Ali S. Hadi, and Montadher S. Shaker

Abstract In many countries, wind turbine systems are the dominant source of green energy. Developers of such projects aim to increase the percentage of wind power over other non-renewable resources and consequently reduce downtime duration and maintenance cost. To meet requirements, the use of robust control and fault diagnosis methods has become a promising approach to ensure sustainability and to enhance the conversion efficiency of such systems. This chapter investigates the use of online fault estimation (FE) and fault-tolerant control (FTC) methods to realize the sustainable operation of wind turbine systems. The use of FE/FTC attains sustainability by eliminating unscheduled maintenance and reducing downtime durations. The work then presents the design of an integrated FE/FTC strategy to tackle parametric and sensor faults in blade pitching systems. This chapter utilizes the proportional-proportional-integral-observer (PPIO) to estimate sensor faults. Further, the decoupling ability of sliding mode control (SMC) is recalled to tolerate uncertainty in the blade pitching system. An integrated FE/FTC design combining the PPIO and the SMC is presented to assure turbine sustainability against parameter uncertainty and sensor faults. This chapter uses the linear matrix inequality (LMI) and the Lyapunov approach to set stability conditions. Finally, a simulation of a 5 MW benchmark model shows the effectiveness of integrating FE/FTC.

Keywords Fault-tolerant control · Robust · Fault estimation · Wind turbine · Sliding mode · Augmented state observer

11.1 Introduction

The last decades have witnessed an increasing growth in the contribution of renewable energy over fossil fuel energy resources. However, installation and maintenance costs are the main challenges in the green energy sector (Karimi 2018; Luo et al.

A. A. Kraidi · R. H. Ahmed · A. S. Hadi · M. S. Shaker (✉)
Electrical Engineering Department, University of Technology-Iraq, Baghdad, Iraq
e-mail: asaadabdlbari@gmail.com; 316523@student.uotechnology.edu.iq; ali_saad573@yahoo.com; montadher.s.shaker@uotechnology.edu.iq

J. N. Furze et al. (eds.), *Earth Systems Protection and Sustainability*,
https://doi.org/10.1007/978-3-030-98584-4_11

2014). Recent publications have introduced several methods to tackle these challenges (Bergami and Poulsen 2015; Dunne and Pao 2016; Lio 2018; Wang et al. 2014). For instance, research in controlling wind turbines has led to enhancing the conversion efficiency of wind energy to electrical energy. In this regard, fault-tolerant control (FTC) methods have led to a significant reduction of plant downtime through avoiding unscheduled maintenance (Lan et al. 2018; Lio 2018; Schulte and Gauterin 2016; Simani 2015a; Simani 2015b).

Badihi et al. (2014) combines a model-based fault estimation (FE) observer and a PI fuzzy controller to guarantee closed-loop control robustness to sensor faults. Sami and Patton (2012c) and Shaker and Patton (2014a) proposed an active sensor FTC using the Takagi-Sugeno (TS) fuzzy multiple-model approach for 5 MW wind turbines. In the latter, estimation and compensation of generator and rotor sensor faults were achieved. FE and FTC methods for systems with model uncertainty and disturbance have attracted several researchers. Schulte and Gauterin (2015) used the TS sliding mode observer to attain robust actuator fault estimation for uncertain wind turbine systems. Additionally, the robustness of sliding mode controllers (SMC) has motivated several researchers to operate wind turbine systems (Azizi et al. 2019). An SMC is used by Benbouzid et al. (2014) to maintain optimal conversion efficiency by tolerating scale fault in generator subsystem. Further, Lan et al. (2018) have developed a sliding mode observer-based FTC tolerating blade pitch actuator faults.

An approach combining virtual sensor/actuator with set membership is proposed by Rotondo et al. (2012) to achieve active FTC for wind turbine system. However, the proposal does not consider the case of simultaneous actuator and sensor faults. Further, the parametric defect in blade pitching system influences the performance of the developed FTC strategy. Various studies have attempted fixing the estimation of fault in blade pitching system. In this regard, it is worth remarking that the interval observer in Blesa et al. (2014) was unable to tackle the limitation of Rotondo et al. (2012). Simani and Castaldi (2012) proposed adaptive PI controllers with an online estimation module for the full load region. The PI method cannot tolerate the faults of the blade pitch system (Odgaard and Stoustrup 2014). Results have examined the usefulness of TS-based model inverse control for wind turbines (Simani and Castaldi 2013). However, the controller has tackled model uncertainty without considering the effects of actuator and sensor faults.

Authors (Sami and Patton 2012a; Shaker and Patton 2014a) have suggested the TS fuzzy approach to model and design an FTC for a wind turbine in the partial load region. Considering one operation region, the actuator and sensor faults in the full load region influence the FTC response. The above literature highlights the reason for the recent interest in tolerating simultaneous actuator and sensor faults (Han et al. 2016; Li and Zhu 2016; Shaker 2019).

The main contributions of this chapter are (i) the proposal of FTC architecture for simultaneous system and sensor faults in blade pitching systems in full range of operation and (ii) setting the nominal reference pitch controller against generator speed sensor fault via the use of a robust proportional-proportional-integral-observer (PPIO)-based sensor fault estimation/compensation methodology.

11.2 Wind Turbine Projects: Current Situation and Challenges

Renewable energy projects have shown significant growth as an alternative to fossil fuels and nuclear systems. The aim of deploying renewable projects is to transfer various nonrenewable energy supply systems into one based on renewables. The interest in such projects aims to reduce global carbon emission, secure energy production, and increase access to electricity worldwide. In recent years, the expenses for renewable projects were higher than for conventional energy sources (Fig. 11.1). Nowadays, renewable power dominates other power sources worldwide and contributes 30% of the global power capacity (REN21 2019).

Wind power is the leading form of renewables. Compared with conventional power plants, wind projects have been approved as the most cost-competitive form of renewables. The average price of wind power in the USA has dropped to 2 cents per kilowatt-h in 2017 compared with 7 cents per kilowatt-h in 2009. Hence, the global gigawatt of wind power shows an annual increase worldwide as a mean of diversification of national energy sources, creates new jobs, and reduces carbon emissions, thus stabilizing the cost of electricity against price and supply disruptions.

The World Wind Energy Association (WWEA 2019) site, https://wwindea.org/information-2/information/ (accessed 21 May 2021), highlights the growth in wind power generation. The overall capacity of all wind turbines installed worldwide reached 597 gigawatt in 2018. In Table 11.1, about 9.1% growth was achieved by addition of 50 gigawatts. All wind turbines installed by the end of 2018 cover 6% of the overall electricity demand. Furthermore, the continuous increase in wind power installation will play an essential role in the global energy transition towards

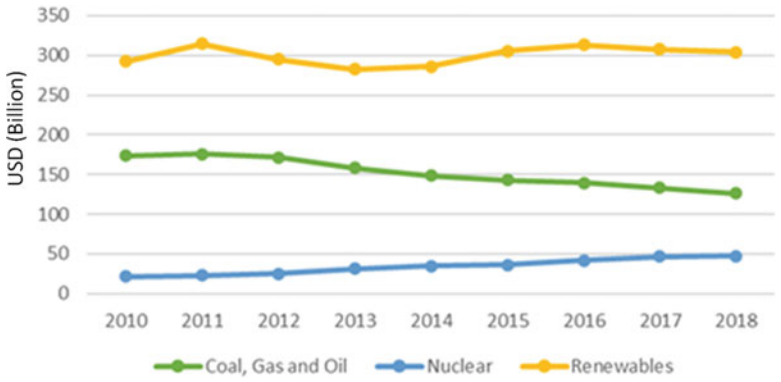

Fig. 11.1 World energy investment 2019 (IEA 2019)

Table 11.1 Total installed capacity by the end of 2018 (WWEA 2019)

Year	2018	2017	2016	2015
Wind power capacity worldwide (Megawatt)	596,556	546,388	486,939	435,284

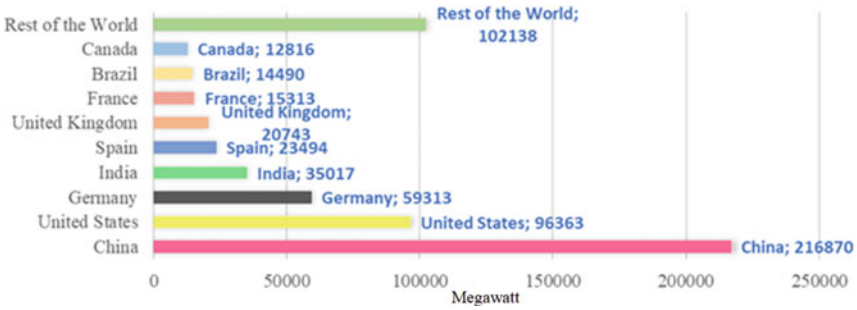

Fig. 11.2 Shares of total installed wind power capacity in megawatt (by the end of 2018)

renewables. Nowadays, 91 countries worldwide take part in total wind energy production. Figure 11.2 shows the leading countries developing wind turbine projects.

The new wind energy investments focus on large-scale multi-megawatt onshore/offshore wind farm projects. Installation of these farms worldwide has made wind power more cost-competitive than the conventional power generation. Although onshore wind farms are the cheapest, the stochastic nature of wind as well as population resistance to onshore sites has lessened deployment. Interest in offshore wind farm projects has been recognized worldwide. Offshore sites offer faster and steadier wind speeds and thus permit more wind energy. Thus, the industry has exploited offshore sites to build large-scale wind farms and install large turbine size thereby offering large wind power capacity. However, installation, operation, and maintenance (IOM) cost of offshore projects are higher than for onshore and vary depending on the site, water depth and distance to shore, and wind variation. IOM consumes around 25–30% of the life span costs of projects (Shafiee and Dinmohammadi 2014). Further, maintenance in projects is expensive and incorporates safety-critical work. Figure 11.3 shows the number of recorded accidents in wind turbine projects up to 2018. This chart confirms that as more turbines are built, more accidents occur (Forum 2019).

Wind power projects need to operate sustainably and minimize the IOM cost. To fulfill needs, turbine downtime may be reduced, harvesting more wind energy. The benefit enhances the cost-competitiveness of wind power above conventional fossil fuel and nuclear power. Fault diagnosis (FD) and FTC strategies sustain operation of wind turbines. Research in FD and control strategies has been led by “kk-electronic” and “MathWorks” in 2009. Since which, an emerging research trend in FD and FTC has been established to ensure reliable and sustainable wind turbine systems. This chapter focuses on employing model-based FD and FTC methods for sustainable operation of wind turbines.

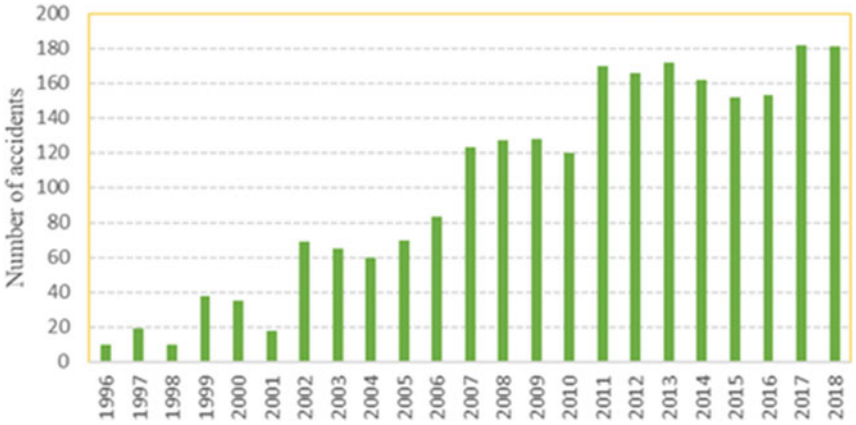

Fig. 11.3 Numbers of recorded accidents (Forum 2019)

11.3 Wind Turbine Model, Operation, and Control

Wind turbine systems convert wind energy into mechanical energy to drive an electrical generator. The working principle of such systems has been extensively explained (Bianchi et al. 2007; Carriveau 2011; Hansen 2015; Shaker and Patton 2014b).

As given in (11.1), three variables affect the amount of power captured by the rotor: the effective wind speed (v_{EWS}), the blade pitch angles (β), and the rotor speed (ω_r):

$$P_{\text{cap}} = \frac{1}{2}\rho\pi R^3 C_p(\lambda,\beta)v_{\text{EWS}}^3 \tag{11.1}$$

where ρ, R, and C_p are air density, rotor radius, and power coefficient, respectively. C_p depends on the blade pitch angle (β) and the tip speed ratio (λ) (TSR). The λ is given by

$$\lambda = \frac{\omega_r R}{v_{\text{EWS}}} \tag{11.2}$$

In an ideal case, the TSR should be kept optimal by controlling the rotor speed and blade pitch angle. Sustaining optimality of TSR ensures maximum wind energy conversion efficiency. In this regard, one should note the following:

- Each turbine has its own optimal TSR value, determined by the manufacturer.
- In low wind speed, setting the pitch angle at a value ($\beta = 0$) ensures harvesting maximum wind energy, while the generator torque control is used to track the optimal rotor speed. The generator will load the aerodynamic subsystem leading to deceleration or release of rotor rotation. Precise tracking of the optimal speed

will oscillate the output power and load the drive train shafts though reduce its lifetime.
– In high wind speeds, the pitch angle maybe controlled to prevent the turbine from surpassing the rated power. Further, inertia of large-scale wind turbines limits the rate of blade rotation. Generator torque control technique is used in this range to improve regulation.

Since wind turbines are driven by a natural force, the operation range may be divided into four regions depending on wind speed. In region one, the wind speed is not adequate to overcome the wind turbine inertia, and hence there is no rotation and no electrical power generation. Region two covers the range between the cut-in and the rated wind speed; wind force is adequate to drive the turbine and initiate rotation; the objective is to maintain the harvested power from the available wind at the optimal value. In region three, there is a high enough wind speed to achieve rotational speed equal or above the rated speed, and below the cut-out speed, an objective is to achieve rated electrical power using regulation. Region four corresponds to the case when the wind speed is above the upper predefined limit.

It is important to ensure reliable operation of wind turbine systems due to their great contribution electrical power, as stated in Sect. 11.2. However, faults and failures decrease system sustainability leading to higher IOM costs (Artigao et al. 2018; Liu et al. 2019; Ozturk et al. 2018). Figure 11.4 shows failures in different parts of the wind turbine system (Ozturk et al. 2018).

It should be clear by now that the stochastic nature of wind, the probability of different types of faults, and the nonlinearly of the aerodynamic subsystem should be considered by the controller designer to meet required control objectives. Consequently, there is increased interest in robust control, fault diagnosis, and fault-tolerant control of wind turbines. Recent studies have attended to development of control strategies to relax these challenges (Corradini et al. 2017; Jabbari Asl and Yoon 2016; Kinnaert and Rakoto 2016; Liu et al. 2017; Miguel et al. 2017; Yang and Chai 2016). In context, the use of FTC and FD methods offers significant reduction of plant downtime and avoids unscheduled maintenance costs (Lan et al. 2018; Liu et al. 2017; Sami and Patton 2012c; Shaker and Kraidi 2017; Shaker and Patton 2014a; Shaker and Patton 2014b). Most proposed designs tolerate either sensor or actuator faults; the real challenge is to develop an FTC design strategy which tolerates simultaneous system and sensor faults.

11.4 Wind Turbine Nominal Control: FTC

Wind turbine operation is governed by two distinct regions, namely, partial and full load regions. Maximizing the amount of power harvested from wind is the control objective at low wind speed. Conversely, regulating the generated electrical power to its rated value is the objective at high wind speed (Carriveau 2011; Hansen 2015; Luo et al. 2014). Whenever wind speed is below the rated value, the reference

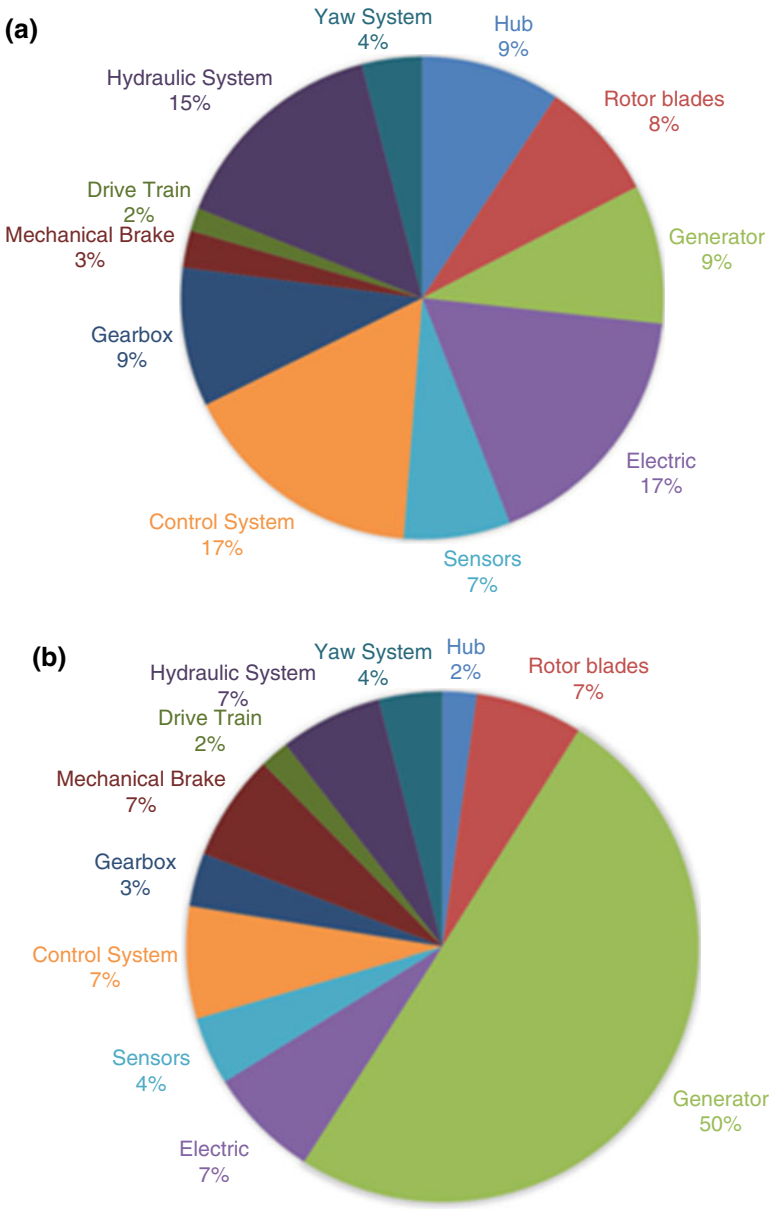

Fig. 11.4 Wind turbines for geared drive 500 kW: (**a**) percentage of annual failure rate; (**b**) downtime per failure

controller maintains turbine operation via the optimal tip speed ratio. Above the rated wind speed, controllers produce the reference pitch angle required to regulate the output power constant at its rated value. Further, inner controllers are designed to ensure robust tracking performance of the reference signals that are produced by the reference controller.

From the viewpoint of system reliability, faults potentially affect any subsystem of wind turbines, and hence the objective of robust control is to tolerate consequent effects to sustain nominal closed-loop performance (Odgaard et al. 2013; Odgaard and Johnson 2013). This work concerns the blade pitch actuator system since it has a high failure rate (Ozturk et al. 2018). The hydraulic pitch system consists of three identical pitch actuators. Such actuators are modeled in state space relating the measured pitch angle and its reference, written as

$$\left.\begin{aligned} \dot{x}_p &= A_p x_p + B_p \beta_r + D_p \varphi_p\left(x_p, \beta_r\right) \\ y_p &= C_p x_p \end{aligned}\right\} \tag{11.3}$$

where $\dot{x}_p = \begin{bmatrix} \beta \\ \dot{\beta} \end{bmatrix}, A_p = \begin{bmatrix} 0 & 1 \\ -\omega_n^2 & -2\zeta\omega_n \end{bmatrix}, B_p = \begin{bmatrix} 0 \\ \omega_n^2 \end{bmatrix}, D_p = \begin{bmatrix} 0 \\ 1 \end{bmatrix}, C_p = [1 \;\; 0]$, and $\varphi_p(x_p, \beta_r)$ represents system fault or actuator fault, ζ is the damping ratio, and ω_n is the natural undamped frequency. The nominal values of the parameters are $\zeta = 0{:}6$ and $\omega_n = 11{:}11$ rad = s.

Remark One

- In the blade pitch scale and stuck sensor fault scenarios, the inner-loop blade pitch controller alleviates the difference between the β_r and the faulty measured β and causes improper blade orientation (see Fig. 11.5). Clearly, this situation induces structural loads of the wind turbine system due to the unevenness in the wind force on the rotor area.
- The system fault of pitch actuators is attributed to the drop of oil pressure or the increase in air content of the pitch actuator. This fault will directly affect the tracking performance of the pitch system.

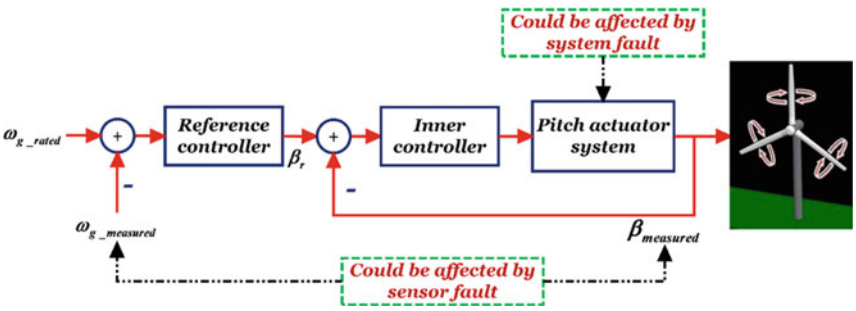

Fig. 11.5 Possible faults that affect blade pitch system

– Variations in the nominal values of the parameters ζ and ω_n may represent a drop of oil pressure fault or increase in air content fault (Corradini et al. 2017; Odgaard and Stoustrup 2015; Shaker and Kraidi 2017). Thus, the model parameters of (11.3) have the following generalized form:

$$\omega_n^2 = \omega_{no}^2 + \Delta\left(\omega_{nf}^2 - \omega_{no}^2\right) \text{ and } \zeta\omega_n = \zeta_o\omega_{no} + +\Delta\left(\zeta_f\omega_{nf} - \zeta_o\omega_{no}\right) \tag{11.4}$$

where $\Delta \in [0\ 1]$ is the fault severity parameter, $\Delta = 0$ and $\Delta = 1$ corresponds to fault free and complete faulty system, respectively. The parameters $\zeta_o\omega_{no}$, $\zeta\omega_n$, and $\zeta_f\omega_{nf}$ refer to nominal, generalized, and faulty model parameters. Hence, the parameters of (11.3) become

$$A_p = \begin{bmatrix} 0 & 1 \\ -\omega_{no}^2 & -2\zeta\omega_{no} \end{bmatrix}, B_p = \begin{bmatrix} 0 \\ \omega_{no}^2 \end{bmatrix}, D_p = \begin{bmatrix} 0 \\ 1 \end{bmatrix}, C_p = [1 \quad 0] \tag{11.5}$$

$$\varphi_p\left(\mathrm{x}_p, \beta_r\right) = \Delta\left(2\zeta_o\omega_{no} - 2\zeta_f\omega_{nf}\right)\dot{\beta} + \Delta\left(\omega_{no}^2 - \omega_{nf}^2\right)\beta - \Delta\left(\omega_{no}^2 - \omega_{nf}^2\right)\beta_r$$

Assumption One
The function $\varphi_p(x_p, \beta_r)$ satisfies the condition $\varphi_p(x_p, \beta_r) \leq \vartheta$, where ϑ represents the known upper bound of $\varphi_p(x_p, \beta_r)$. This assumption is acceptable in practical terms since x_p and β_r are bounded.

It is important to maintain the nominal closed-loop performance of the pitch system without changes being imposed in both faulty and fault-free operating conditions. Figure 11.5 shows the faults that directly affect the pitch system are the generator speed sensor fault, the pitch angle sensor fault, and the pitch actuator system fault.

Employing the inherent robustness of incremental sliding mode controllers (ISMC) against matched uncertainty and the fault estimation capability of PPIO develops FTC of the pitch actuator system against the simultaneous system and sensor faults (see Fig. 11.6). The ISMC is used as passive FTC to maintain the nominal closed-loop performance of the pitch actuator system during parametric pitch actuator fault; two PPIOs are used to provide online estimation and compensation of the faults of generator speed sensor and pitch position sensor from the inputs of reference and inner controllers.

11.5 Sliding Mode Controller (SMC) Design

The use of robust SMCs against matched disturbances has been widely approved. Robustness affects SMC as the dominant candidate for passive fault-tolerant controller design against actuator and system faults. To attain the robustness of SMC,

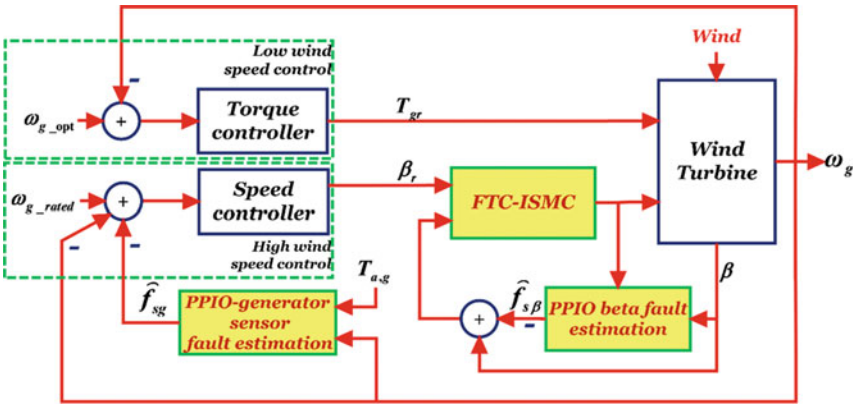

Fig. 11.6 The proposed control structure

the sliding motion must occur within a finite time – the reaching time (t_{reach}). Additionally, the states should remain within the sliding vicinity for all time greater than the reaching time ($t > t_{\text{reach}}$). Basically, the SMC law has a linear control term and a discontinuous term (Shtessel et al. 2014). While the linear control term enables the reachability condition, the discontinuous control term ensures the sliding condition.

Remark Two

- While the generator speed sensor faults force the reference controller to produce incorrect reference pitch angle (β_r), the inner controller is directly affected by the pitch position sensor faults. The consequence is that the overall system performance deviates from the rated operating conditions.
- The sliding mode controller is considered as a passive fault-tolerant controller responsible for tolerating the effects of parametric pitch system faults, thereby ensuring acceptable reference tracking of the pitching system.

The objective of the controller is to stabilize the error $e = \beta - \beta_r$ regardless of the effect of parametric pitch system faults. The error dynamic of the pitch actuator system combined with the supplementary controller is given as

$$\left.\begin{aligned} \dot{e} &= \dot{\beta} - \dot{\beta}_r \\ \ddot{e} &= -2\varsigma w_{no}\dot{\beta} - w_{no}^2\beta - \ddot{\beta}_r + w_{no}^2\beta_r + w_{no}^2 u_{\text{ftc}}^{\text{smc}} + \psi_p\left(x_p, \beta_r\right) \end{aligned}\right\} \tag{11.6}$$

Initially, a sliding surface capable of achieving control objectives whenever the system attains this surface is to be designed. In this concern, Wang et al. (2015) and Shaker and Kraidi (2019) solved the pitch actuator system of (11.3) by proposition of the following integral surface shown in Eq. (11.7):

$$S = \dot{e} + k_1 e + k_2 \int e \, \mathrm{dt} \tag{11.7}$$

where the tuning variables k_1 and k_2 are used to set the performance of the pitch system during the sliding phase. This begets the further setting of a control action that satisfies the reachability condition and the sliding condition. To achieve this, the control signal must satisfy the following inequality:

$$S\dot{S} \leq -\varepsilon |S| \tag{11.8}$$

where ε is a positive constant. Using (11.6) gives the following expression for $\dot{S}$:

$$\begin{aligned} \dot{S} &= \ddot{e} + k_1 \dot{e} + k_2 e \\ &= -2\zeta\omega_{no}\dot{\beta} - \omega_{no}^2\beta - \ddot{\beta}_r + \omega_{no}^2\beta_r + \omega_{no}^2 u_{\mathrm{ftc}}^{\mathrm{smc}} + \psi_p(xp, \beta_r) + k_1\dot{e} + k_2 e \end{aligned} \tag{11.9}$$

Once the system reaches the sliding region ($S = \dot{S} = 0$), the equivalent control signal becomes

$$u_{\mathrm{eq}} = \frac{1}{\omega_{no}^2}\left[2\zeta\omega_{no}\dot{\beta} + \omega_{no}^2\beta + \ddot{\beta}_r - \omega_{no}^2\beta_r - \psi_p\left(x_p, \beta_r\right) - k_1\dot{e} - k_2 e \right. \tag{11.10}$$

A more practical expression for the equivalent control (11.10) is

$$u_{\mathrm{eq}} = \frac{1}{\omega_{no}^2}\left[2\zeta\omega_{no}\dot{\beta} + \omega_{no}^2\beta + \ddot{\beta}_r - \omega_{no}^2\beta_r - \psi_p\left(x_p, \beta_r\right) - k_1\dot{e} - k_2 e - \eta\,\mathrm{sgn}\ (S)\right. \tag{11.11}$$

where $\eta = \varphi + \varepsilon$. By substituting (11.10) into (11.9), one can obtain

$$\dot{S} = \psi_{\mathrm{p}}\left(x_{\mathrm{p}}, \beta_{\mathrm{r}}\right) - (\varphi + \varepsilon)\,\mathrm{sgn}\ (S) \tag{11.12}$$

Multiplying both sides of (11.12) by (S) gives reachability condition as for region four of Sect. 11.2. Therefore, regardless of the effects of low-pressure faults or increase in air content fault, the SMC ensures accurate tracking of the reference pitch angle.

Remark Three
Although the controller in (11.11) provides robust closed-loop tracking performance against parametric system faults, the sensor fault directly affects the sliding surface in (11.7) and hence cannot be tolerated using the controller (11.11). Additionally, the terms that contain unmeasurable signals can be considered as matched uncertainty.

The robustness of the SMC is remarked upon for various faults in the remainder of this section.

11.5.1 The Effect of System Fault $\psi_p(x_p, \beta_r)$

With reference to (11.6), this fault affects the system in the direction of the input channel (11.7). Hence, with an appropriate choice of the discontinuous control component gain ($\varphi + \varepsilon$), the system reaches the sliding surface at finite time (t_r) and remains within the sliding manifold for all time ($t < t_r$). While sliding, the tracking error dynamics will be governed by the design parameters (k_1, k_2) of the second-order homogeneous equation $\left(S = 0 = \dot{e} + k_1 e + k_2 \int e dt\right)$. The non-homogeneous part $\left(\text{i.e., } -\dot{f}_\beta - k_1 f_\beta - k_2 \int f_\beta dt\right)$ corresponds to a forcing term that prevents the SMC from achieving the objective ($e = 0$).

11.5.2 The Effect of the Generator Speed Sensor $\omega_{gf} = \omega_g + f_g$ (Where ω_{gf} Is the Faulty Measurement and f_s Is the Additive Sensor Fault)

Figure 11.6 illustrates that this fault directly affects the reference controller (i.e., the outer loop controller) and thereby generates incorrect reference pitch angle β_{rf} which can be written as $\beta_{rf} = \beta_r + f_r$, where f_r represents additive fault signal. Therefore, while sliding, the tracking error dynamics will be governed by the second-order non-homogeneous equation $\left(S = 0 = \dot{e} + k_1 e + k_2 e + k_2 \int e \, dt + \dot{f}_r \quad + k_1 f_r + k_2 \int f_r dt\right)$. The non-homogeneous part (i.e., $\dot{f}_r + k_1 f_r + k_2 \int f_r dt$) corresponds to a forcing term that prevents the SMC from achieving the objective ($e = 0$).

Consequently, the controller in (11.11) provides robust closed-loop tracking performance against parametric system fault; the sensor fault directly affects the sliding surface in (11.7) and hence cannot be tolerated using the controller in (11.11). Therefore, a combination of SMC with PPIO-based sensor fault estimation/compensation has been proposed in this chapter (see Fig. 11.6) to enhance the overall robustness of the closed-loop system against simultaneous system and sensor faults.

11.6 PPIO-Based Generator Speed Sensor Fault Estimation

This section presents the proposed FTC approach to correct a faulty generator speed sensor reading. A proportional-proportional-integral augmented fault estimation observer is proposed to provide accurate estimations of various sensor fault scenarios. The model of the drive train system affected by generator speed sensor fault is given as

$$\left.\begin{aligned} \dot{x} &= Ax + BT_{a,g} + D\psi_D \\ y &= Cx + D_s f_s \end{aligned}\right\} \tag{11.13}$$

$$\dot{x} = \begin{bmatrix} \dot{\omega}_r \\ \dot{\omega}_g \\ \dot{\theta}_\delta \end{bmatrix}, A = \begin{bmatrix} a_{11} & a_{12} & a_{13} \\ a_{21} & a_{22} & a_{23} \\ a_{31} & a_{32} & a_{33} \end{bmatrix}, B = \begin{bmatrix} b_{11} & 0 \\ 0 & b_{22} \\ 0 & 0 \end{bmatrix}, D = \begin{bmatrix} 1 \\ 1 \\ 0 \end{bmatrix},$$

$$T_{a,g} = \begin{bmatrix} T_a \\ T_g \end{bmatrix}, C = [0 \quad 1 \quad 0], D_s = [0 \quad 1 \quad 0]^T$$

$$a_{11} = \frac{-(B_{dt} + B_r)}{J_r}, a_{12} = \frac{B_{dt}}{n_g J_r}, a_{13} = \frac{-K_{dt}}{J_r}, a_{21} = \frac{B_{dt}}{n_g J_g},$$

$$a_{22} = \frac{-\left(B_{dt} + n_g B_g\right)}{n_g^2 J_g}, a_{23} = \frac{K_{dt}}{n_g J_g}, a_{31} = 1, a_{32} = \frac{-1}{n_g}, a_{33} = 0, b_{11} = \frac{1}{J_r}, b_{22} = \frac{-1}{J_g},$$

where J_r, B_r, J_g, ω_g, T_g, B_g, n_g, K_{dt}, B_{dt}, θ_Δ, T_a, and f_s are the rotor inertia, the rotor external damping, the generator inertia, the generator speed, the generator torque, generator, external damping, the gearbox ratio, the torsion stiffness, the torsion damping coefficient, the torsion angle, represents bounded uncertainty, and the aerodynamic torque and f_s is the sensor fault.

Remark Four
The aerodynamic and generator torques of (11.11) are not directly measured. Instead, these two input signals are obtained via soft sensors (Sloth et al. 2011). In (11.11), the term ψ_D represents the expected error between the actual and the soft sensed $T_{a,\ g}$. Consequently, the PPIO should guarantee robust fault estimation regardless of the effect of ψ_D.

To estimate sensor fault using an extended state observer framework (Klinkhieo 2009), an augmented system accumulates the model in (11.13), and an output filter (11.14) is developed in (11.15) (Sami and Patton 2012b).

$$\dot{x_s} = -A_s x_s + A_s C_x + A_s D_s f_s \tag{11.14}$$

$$\dot{x} = \overline{A}\overline{x} + \overline{B}T_{a,g} + D_{\psi D} + \overline{D}_s f_s, \overline{y} = \overline{C}\overline{x} \tag{11.15}$$

$$A_s = \begin{bmatrix} A & 0 \\ A_s C & -A_s \end{bmatrix}, \overline{B} = \begin{bmatrix} B \\ 0 \end{bmatrix}, \overline{D} = \begin{bmatrix} D \\ 0 \end{bmatrix}, \overline{D}_s = \begin{bmatrix} 0 \\ D_s A_s \end{bmatrix}, \overline{C}_s = [0 \quad I_1]$$

where $-A_s \in R^{l\ *\ l}$ is a stable filter matrix. As illustrated in remark three, the proposed control strategy employs compensation of the sensor faults affecting the system. The PPIO for the system (11.15) is given as

$$\left.\begin{aligned}\dot{\widehat{x}} &= \overline{A}\widehat{x} + \overline{B}T_{a,g} + \overline{D}_s\widehat{f}_s + L\overline{C}e_x \\ \widehat{y} &= \overline{C}\widehat{x} \\ \dot{\widehat{f}}_s &= \rho\left[K_1\overline{C}\dot{e}_x + K_2\overline{C}e_x\right]\end{aligned}\right\} \tag{11.16}$$

where $\widehat{x}$ and $\widehat{y}$ and $e_y = \overline{y} - \widehat{y} = \overline{C}e_x$ are the estimated state, estimated output, and output estimation error, respectively, and K_1 and K_2 are the proportional and integral gains, respectively, and are a symmetric positive definite matrix. Subtracting the observer in (11.16) from the system (11.15), the state estimation error will be defined as

$$\left.\begin{aligned}\dot{e}_x &= \left(\overline{A} - L\overline{C}\right)e_x + \overline{D}_s e_{fs} + \overline{D}_{\psi D} \\ e_y &= \overline{C}e_x\end{aligned}\right\} \tag{11.17}$$

where $e_{fs} = f_s - \widehat{f}_s$. Using (11.13), the e_{fs} dynamics will become

$$\left.\begin{aligned}\dot{e}_{fs} &= \dot{f}_s - \dot{\widehat{f}}_s \\ \dot{e}_{fs} &= \dot{f}_s - \rho K_1\overline{CA}e_x + \rho K_1\overline{C}L\overline{C}e_x - \rho K_2\overline{C}e_x - \rho K_1\overline{CD}_s e_{fs} - \rho K_1\overline{CD}_{s\psi D}\end{aligned}\right\} \tag{11.18}$$

By combining (11.17) and (11.18), the augmented error dynamics can be assembled as in (11.19)

$$\dot{\widetilde{e}}_a = \widetilde{A}\widetilde{e}_a + \check{N}\,\widetilde{z} \tag{11.19}$$

$$\widetilde{A}_s = \begin{bmatrix}\overline{A} - L\overline{C} & \overline{D}_s \\ \rho K_1\overline{CA} + \rho K_1\overline{C}L\overline{C} - \rho K_2\overline{C} & -\rho K_1\overline{CD}_s\end{bmatrix}, \widetilde{e}_a = \begin{bmatrix}e_x \\ e_{fs}\end{bmatrix}, \widetilde{N}_a = \begin{bmatrix}\overline{D} & 0 \\ -\rho K_1\overline{CD} & I\end{bmatrix}, \widetilde{z} = \begin{bmatrix}\psi(D) \\ \dot{f}_s\end{bmatrix}$$

Now, the goals are to compute the gains L, K_2, and K_3 as well as attenuate the effects of the input $\widetilde{z}$ on the estimation error via minimizing the L_2 norm, which should stay below a desired level.

Remark Five

Based on the available information of $\overline{D}$ and $\overline{D}_s$, the following theorem guarantees an attenuation of disturbance effects $\widetilde{z}$ on fault estimation signal via L_2 norm minimization.

Theorem 1 The $\dot{\widetilde{e}}_a$ in (11.19) is stable, and the performance is guaranteed with an attenuation level if there exists a symmetric positive definite matrices P_1, ρ^{-1}, and G; matrices H, K_1, and K_2; and a scalar μ satisfying the following LMI constraint,

provided that the signals $(\psi_D, \dot{f}_s)$ are bounded, rank $\overline{CD}_s$, and the pair $(\overline{A}, \overline{C})$ is observable:

Minimize $\overline{\gamma}$ such that

$$\begin{bmatrix} \varphi_{11} & \varphi_{12} & \varphi_{13} & 0 & 0 & \varphi_{16} & 0 \\ * & \varphi_{22} & \varphi_{23} & \rho^{-1} & \varphi_{25} & 0 & 0 \\ * & * & -\gamma I & 0 & 0 & 0 & 0 \\ * & * & * & -\gamma I & 0 & 0 & 0 \\ * & * & * & * & -G^{-1} & 0 & 0 \\ * & * & * & * & * & -2\mu P_1 & \mu I \\ * & * & * & * & * & * & G^{-1} \end{bmatrix} < 0 \tag{11.20}$$

$$\begin{aligned} \varphi_{11} &= P_1\overline{A} + \left(P_1\overline{A}\right)^T - H\overline{C} - \left(H\overline{C}\right)^T + \omega_1, \varphi_{12} \\ &= P_1\overline{D}_s + \left(K_1\overline{CA}\right)^T - \left(K_2C\overline{A}\right)^T, \varphi_{13} = P_1\overline{D}_s, \varphi_{16} = \left(H\overline{C}\right)^T, \varphi_{22} \\ &= -\rho K_1\overline{CD}_s - \left(\rho K_1\overline{CD}_s\right)^T + \omega_2, \varphi_{23} = -K_1\overline{CD}, \varphi_{25} = K_1\overline{C}, L = P_1^{-1}H, \gamma \\ &= \sqrt{\overline{\gamma}}, \end{aligned}$$

where ω_1 and ω_2 are weighting matrices.

Proof The PPIO-based sensor fault estimation presented in (11.16) and Theorem 1 represents extension to the PPIO-based actuator fault estimation presented in Shaker (2015); hence the proof is omitted here.

Remark Six
Using (11.3) and the design procedure presented in Sect. 11.3, it is easy to design PPIO for pitch position sensor fault estimation.

11.7 Simulation Results

This section investigates the response of the benchmark model given in Odgaard et al. (2009) and Odgaard and Stoustrup (2015) to verify the usefulness of the proposed hybrid control strategy in Fig. 11.7. Determining the gain η of (11.11) is an essential step to achieve sliding motion governed by the second-order sliding dynamics:

$$\ddot{e} + k_1\dot{e} + k_2 e = 0 \tag{11.21}$$

Clearly, the performance parameters during sliding phase, governed by k_1 and k_2, are nominated to maintain the nominal values of the pitch actuator system parameters (i.e., ζ and ω_n) as closely as possible.

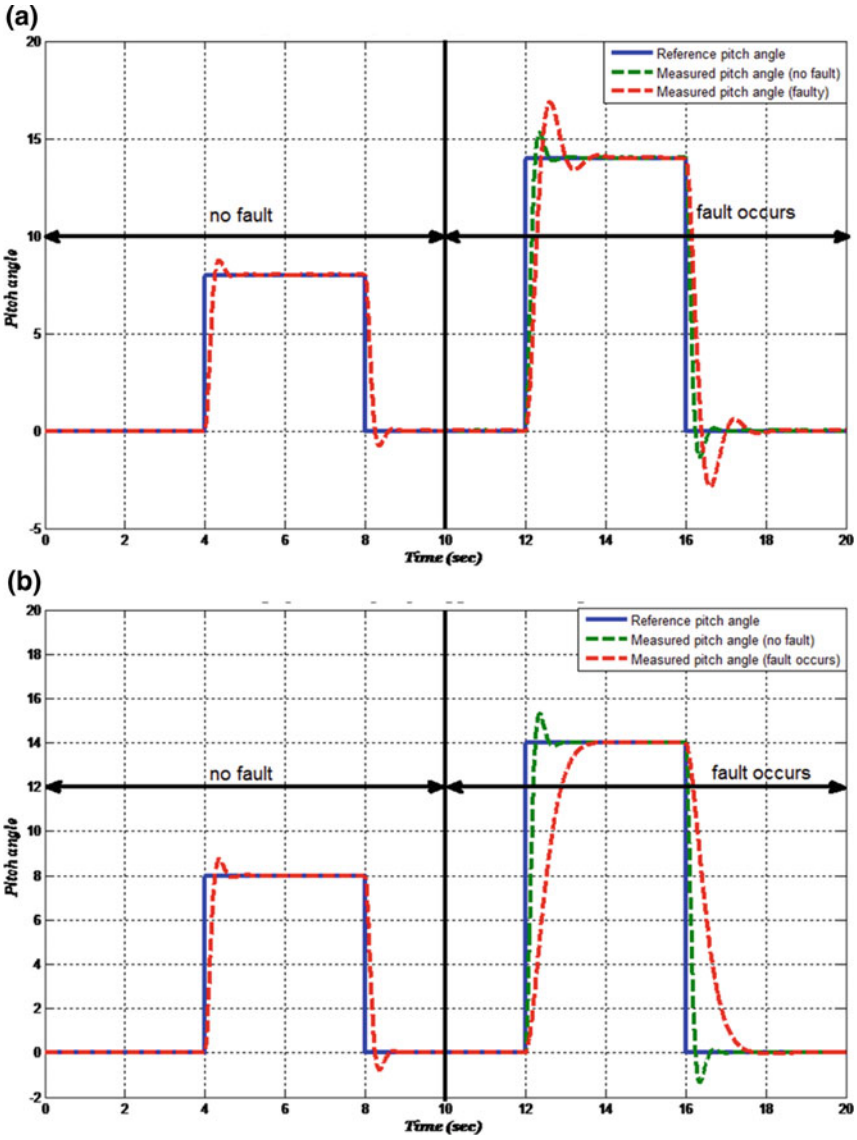

Fig. 11.7 The tracking performance of pitch actuator system: (**a**) $\zeta = 0{:}25$, $\omega_n = 5{:}73$ rad/s; (**b**) $\zeta = 0{:}9$, $\omega_n = 3{:}42$ rad/s

Remark Seven
The sliding surface parameters (k_1, k_2) should be chosen such that the error dynamics remain within specific bound on transient responses such as the settling time (T_s) and the peak time (T_p):

$$T_p^2 = \left[\frac{\pi^2}{\omega_n^2\left(1-\zeta^2\right)} = \frac{\pi^2}{k_2\left(1-\zeta^2\right)}\right], T_s = \left[\frac{4}{\zeta\omega} = \frac{8}{k_1}\right] \tag{11.22}$$

Additionally, the design parameter $\eta = 50$ is selected to satisfy the reachability condition.

11.7.1 The Performance of ISMC as a Passive FTC Against Pitch Actuator System Fault

For two sets of faulty system parameters, Fig. 11.7 shows the response of the fault free and faulty pitch actuator to a multilevel reference pitch angle.

The function of ISMC is to steer the faulty system to track the nominal desired response. Figure 11.8 shows the effectiveness of the proposed ISMC. The advantage of the proposal is that once the ISMC is designed, there is no need to readjust controller parameters during faults.

Additionally, the ISMC tolerates system faults without needing for fault diagnosis block. Hence, using such controller will result in a simple structure that makes the ISMC a proper candidate for reliable pitch control.

11.7.2 The Performance of Integrated ISMC and PPIO Against Simultaneous System and Generator Speed Sensor Faults

Regarding Fig. 11.5, the reference controller is directly affected by the generator speed sensor fault. The consequence is that this controller will produce incorrect β_r. The ISMC has unable to tolerate the effects of this scenario since it directly affects the sliding surface. Such scenarios have stimulated the integration of ISMC with PPIO. In the integrated system, the PPIO is responsible for providing online sensor fault estimation. Then, the estimated signals compensate for the faulty readings that feed the input of the reference controller. Thus, the integrated ISMC and PPIO is capable of tolerating simultaneous system and sensor faults. Now, solving the LMI constraints of the PPIO in inequality (11.20) gives the following values: $\rho = 0.1, A_s = 10, \gamma = 0.0198$, $K_1 = 0.6451$, $K_2 = 5969$, $L = [0.00003 - 0.0585\ 0.0000021.5068]^T$. Figure 11.9 shows the tracking performance of the ISMC when

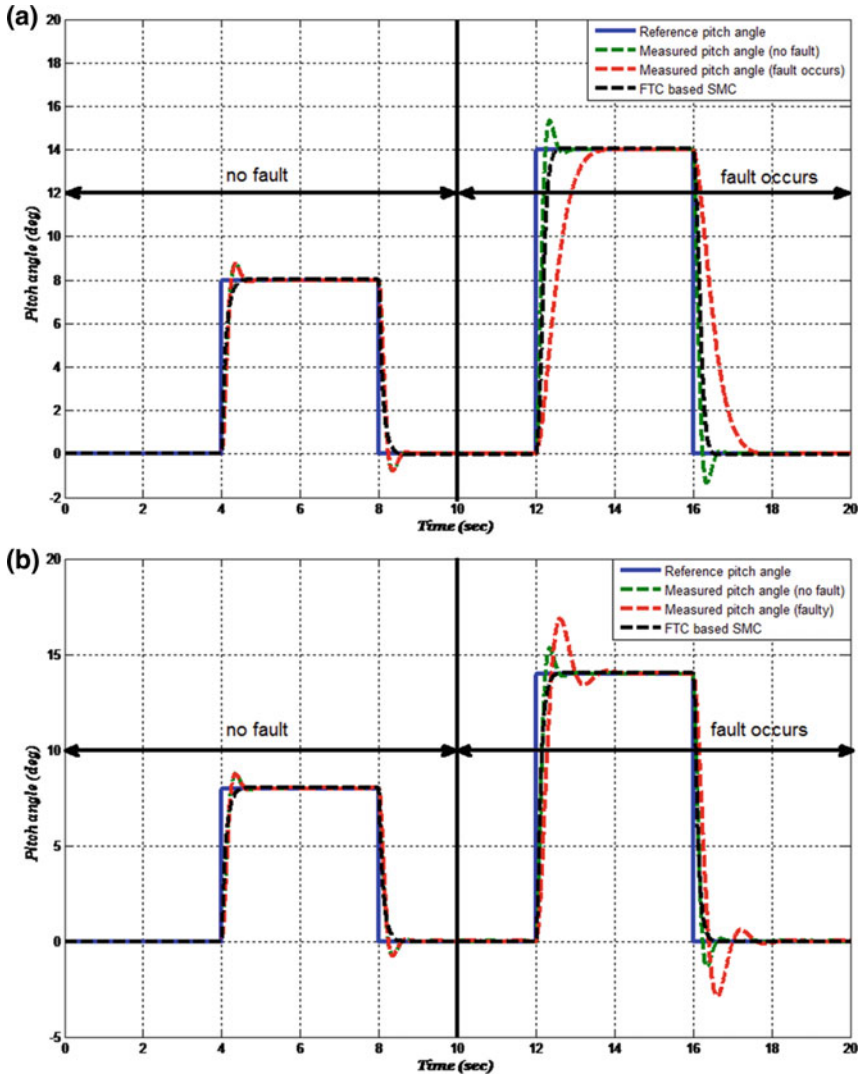

Fig. 11.8 The ISMC performance of pitch actuator system: (**a**) $\zeta = 0{:}25$, $\omega_n = 5{:}73$ rad/s; (**b**) $\zeta = 0{:}9$, $\omega_n = 5{:}73$ rad/s

$1.5\beta_r$ scale fault affects the input of the inner controller. Such a scenario occurs when the reference controller receives faulty generator speed measurement. Hence, while sliding, the error signal becomes $e = 0 = \beta - 1.5\beta_r$, and hence the actual pitch position is $\beta = 1.5\beta_r$.

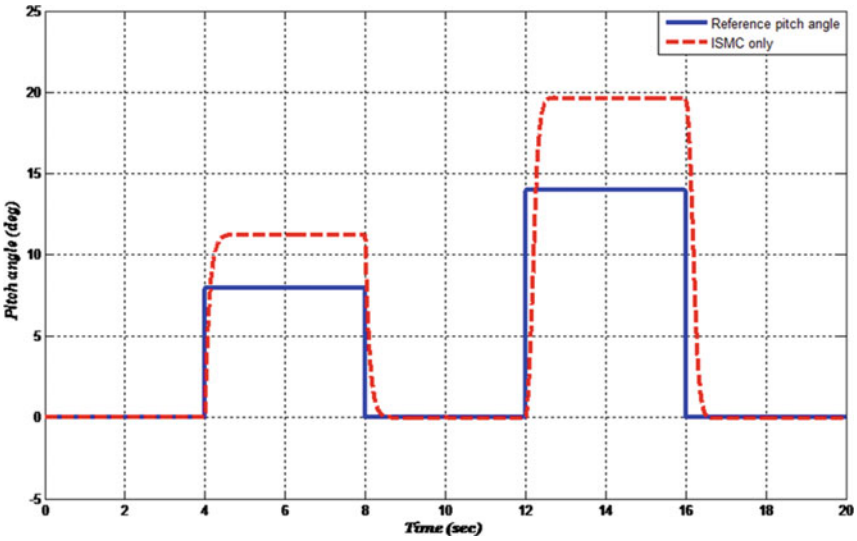

Fig. 11.9 ISMC performance against simultaneous system fault $\zeta = 0{:}25$, $\omega_n = 5{:}73$ rad/s and faulty ω_g

11.7.3 The Performance of Integrated ISMC and PPIO Against Simultaneous System and Pitch Angle Sensor Fault

In this scenario, the ISMC-based inner controller minimizes the error $e = (\beta + f_s) - \beta_r$, and hence, when $e = (\beta + f_s) - \beta_r = 0$, the actual pitch position becomes $\beta = \beta_r - f_s$. Figure 11.10 demonstrates the performance of the proposed integrated ISMC and PPIO. It should be noted that the sensor fault ($D_s f_s = 0.5\beta$) has been tolerated using an estimation and compensation approach to FTC.

Remark Eight
In this subsection, for comparison purposes, the fault tolerance capability of the proposal (Sami and Patton 2012a) has been tested against actuator system fault and sensor fault. Figures 11.11 and 11.12 show inability (Sami and Patton 2012a) to tolerate these faults as also stated in 11.1.

The effectiveness of the proposal has been verified by realistic faults and wind data of the 5 MW wind turbine FTC benchmark model. Figure 11.13 demonstrates the effects of parametric fault as well as the tolerance capability of the ISMC. Figure 11.14 shows the nominal generator speed and faulty generator speed measurement. In Fig. 11.15, the PPIO has been used to estimate generator speed sensor fault. Moreover, the advantages of using the combining ISMC and PPIO to tolerate simultaneous system and generator speed sensor faults have been demonstrated in Fig. 11.16. Finally, in Fig. 11.17, the PPIO has been exploited to estimate stuck

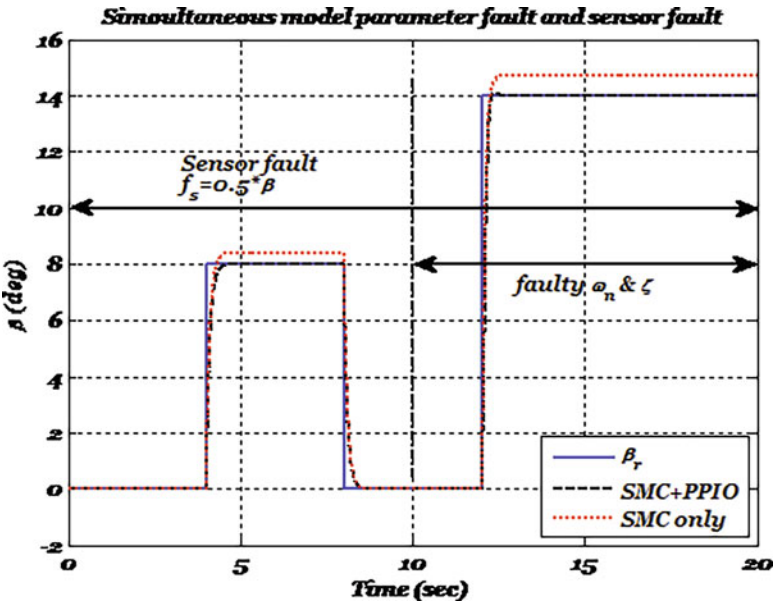

Fig. 11.10 The integrated SMC and PPIO for simultaneous actuator system fault $\zeta = 0.25$, $\omega_n = 5.73$ rad/s and sensor fault $f_s = 0.5\beta$

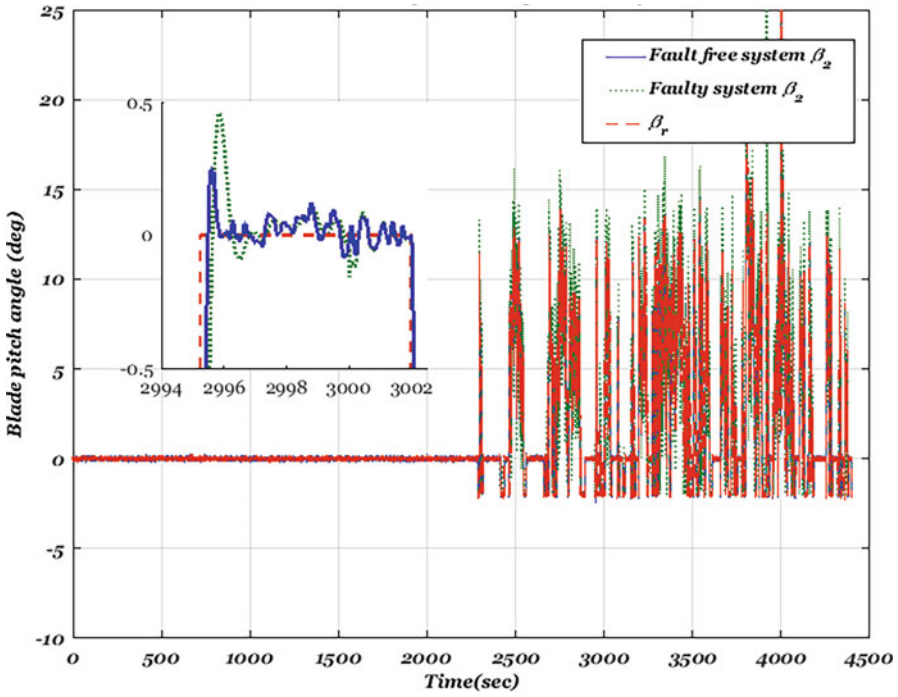

Fig. 11.11 The performance of Sami and Patton (2012a) against pitch system fault

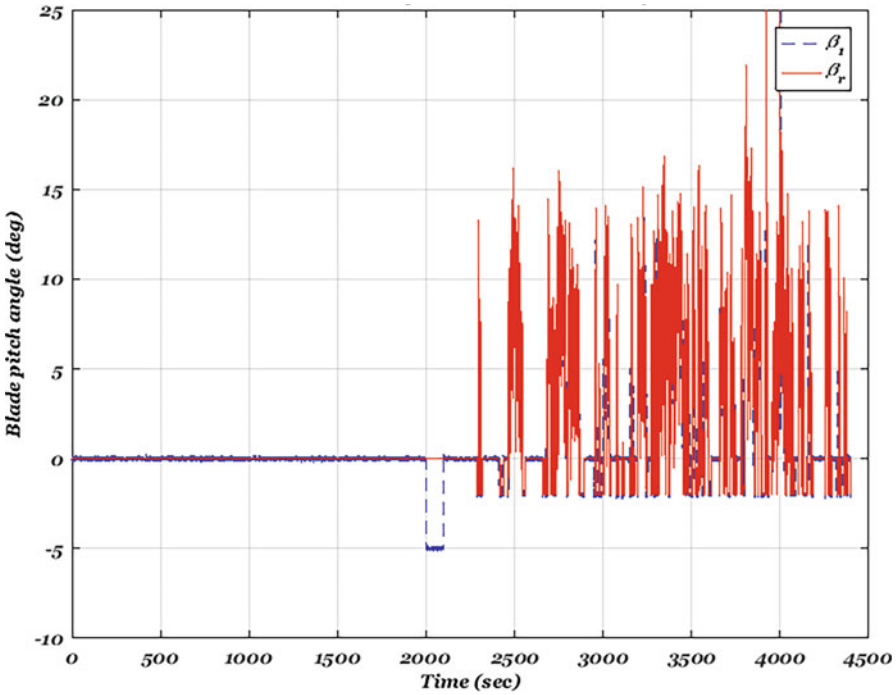

Fig. 11.12 The performance of Sami and Patton (2012a) against pitch sensor fault

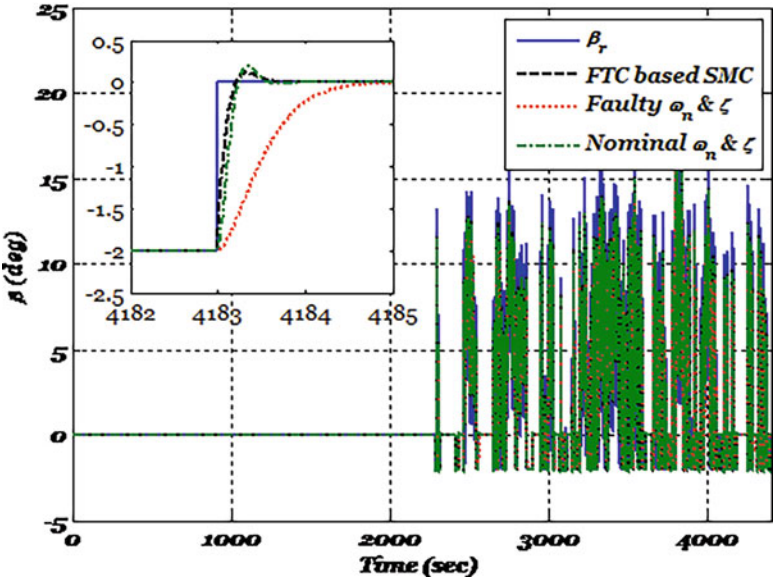

Fig. 11.13 The tracking performance of the ISMC for faulty pitch actuator system $\zeta = 0.9$, $\omega_n = 3.42$ rad/s using realistic wind data

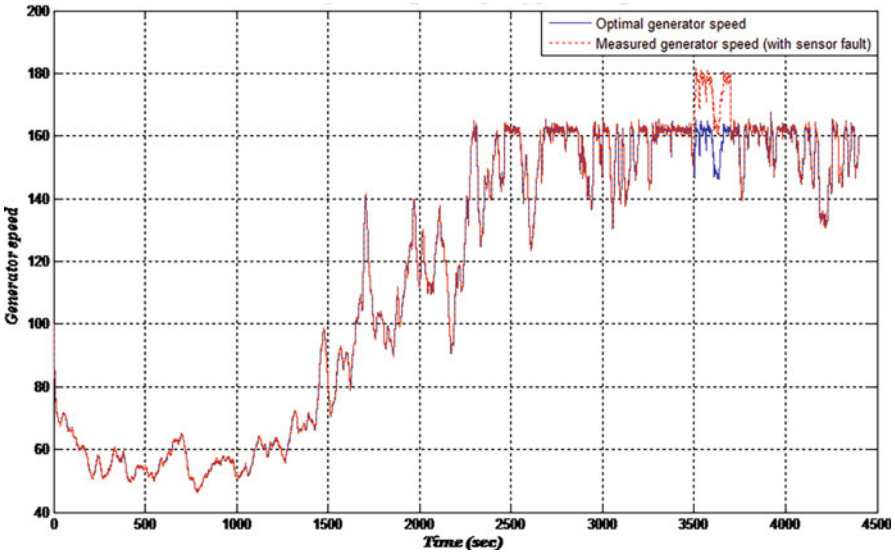

Fig. 11.14 Nominal speed and faulty speed sensor

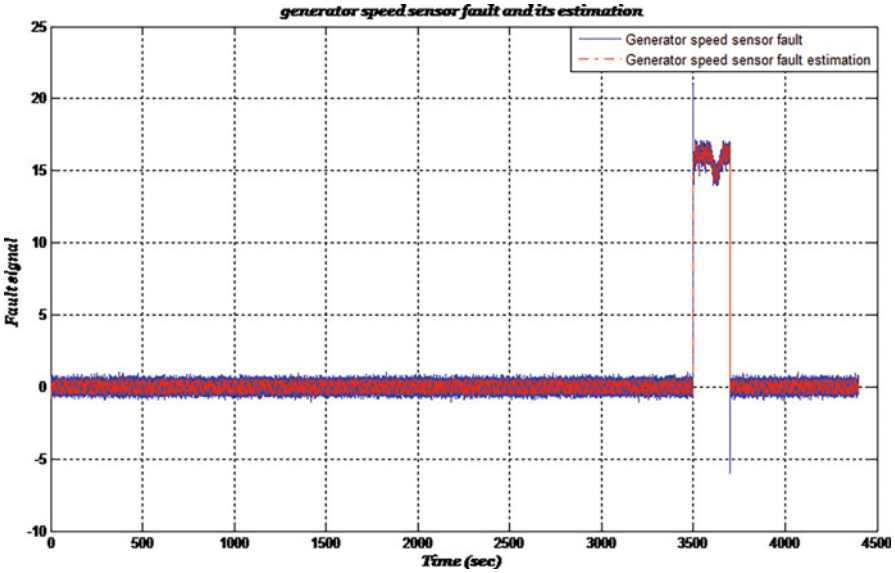

Fig. 11.15 **S**peed sensor fault and its estimation using PPIO

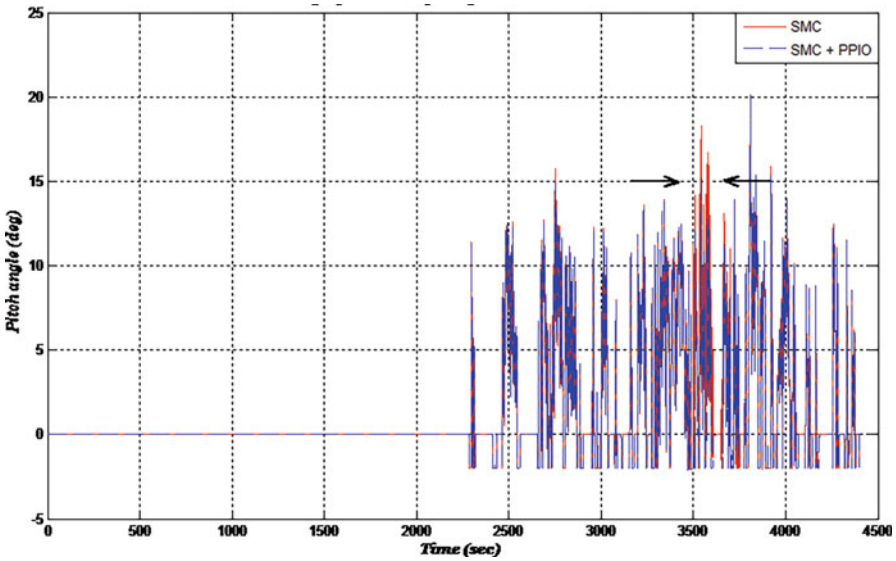

Fig. 11.16 The performance of integrated ISMC+PPIO

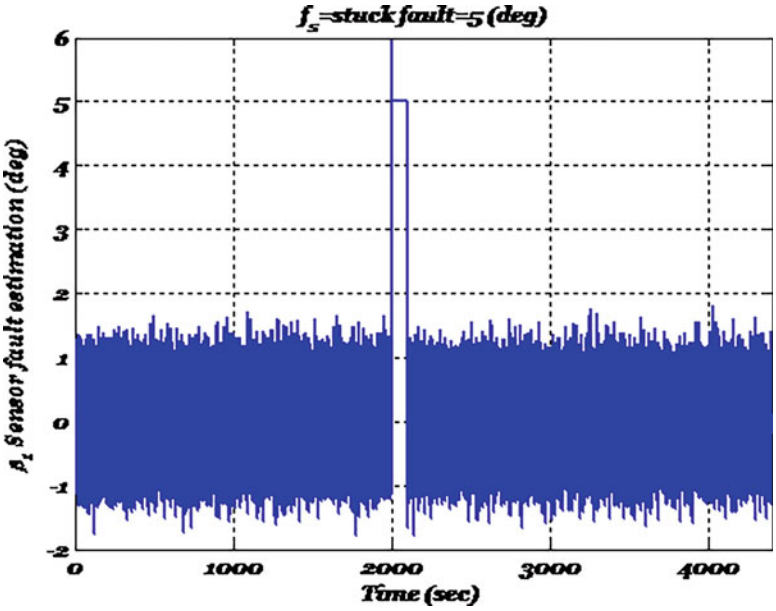

Fig. 11.17 Blade stuck fault estimation using PPIO

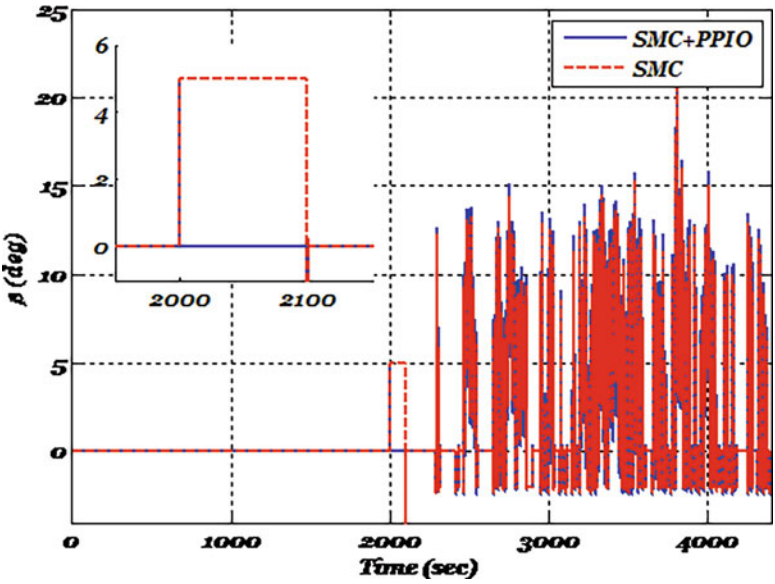

Fig. 11.18 The performance of integrated SMC + PPIO against simultaneous actuator system fault $\zeta = 0.25$, $\omega_n = 5.73$ rad/s and blade-1 stuck sensor fault

sensor fault of blade-1. Besides, the advantages of combining ISMC and PPIO to tolerate simultaneous system and pitch position sensor faults have been demonstrated in Fig. 11.18.

11.8 Conclusions

This chapter proposes an integrated PPIO and ISMC design methodology to solve the robustness problem of control systems affected by simultaneous system and sensor faults. The ISMC has been employed to passively tolerate system faults; two PPIOs have been used to estimate and compensate the effects of sensor faults. The effectiveness of the proposal has been presented using a 5 MW wind turbine benchmark model in which the pitch system is affected by system and sensor faults. Based on simulation results, the ISMC can inherently tolerate faults that achieve the matching condition without the need for a fault diagnosis system. However, sensor faults have direct effects on the sliding variable, and hence the ISMC signal steers the system to follow incorrect measurements. The observer-based fault estimation/compensation approach to FTC shows powerful capability to tolerate sensor faults of control systems. Therefore, combining ISMC with PPIO presents robust closed-loop tracking performance against simultaneous system and sensor faults. Finally, for

further improvement, minimizing structural loads induced by wind force and/or faults is an interesting objective for fault-tolerant individual pitch control. Moreover, model uncertainty due to system aging and blade deformation and the uncertainty in the measured wind speed represent real challenges to wind turbine control problems. Robust estimation of these variables ensures good system performance and hence integrity in wind renewable energy ensuring sustainability value in energy mixes.

References

Artigao E, Martín-Martínez S, Honrubia-Escribano A et al (2018) Wind turbine reliability: a comprehensive review towards effective condition monitoring development. Appl Energy 228:1569–1583. https://doi.org/10.1016/j.apenergy.2018.07.037

Azizi A, Nourisola H, Shoja-Majidabad S (2019) Fault tolerant control of wind turbines with an adaptive output feedback sliding mode controller. Renew Energy 135:55–65. https://doi.org/10.1016/j.renene.2018.11.106

Badihi H, Zhang Y, Hong H (2014) Fuzzy gain-scheduled active fault-tolerant control of a wind turbine. J Frankl Inst 351(7):3677–3706. https://doi.org/10.1016/j.jfranklin.2013.05.007

Benbouzid M, Beltran B, Amirat Y et al (2014) Second-order sliding mode control for DFIG-based wind turbines fault ride-through capability enhancement. ISA Trans 53(3):827–833. https://doi.org/10.1016/j.isatra.2014.01.006

Bergami L, Poulsen NK (2015) A smart rotor configuration with linear quadratic control of adaptive trailing edge flaps for active load alleviation. Wind Energy 18(4):625–641. https://doi.org/10.1002/we.1716

Bianchi DF, De Battista H, Mantz JR (2007) Wind turbine control systems: principles, modelling and gain scheduling design. Springer-Verlag

Blesa J, Rotondo D, Puig V et al (2014) FDI and FTC of wind turbines using the interval observer approach and virtual actuators/sensors. Control Eng Pract 24:138–155. https://doi.org/10.1016/j.conengprac.2013.11.018

Carriveau R (2011) Fundamental and advanced topics in wind power. InTech

Corradini ML, Ippoliti G, Orlando G (2017) An observer-based blade-pitch controller of wind turbines in high wind speeds. Control Eng Pract 58:186–192. https://doi.org/10.1016/j.conengprac.2016.10.011

Dunne F, Pao LY (2016) Optimal blade pitch control with realistic preview wind measurements. Wind Energy 19(12):2153–2169

Forum WI (2019) Available via http://www.caithnesswindfarms.co.uk/. Accessed 15 Jul 2019

Han J, Zhang H, Wang Y et al (2016) Robust state/fault estimation and fault tolerant control for T–S fuzzy systems with sensor and actuator faults. J Frankl Inst 353(2):615–641. https://doi.org/10.1016/j.jfranklin.2015.12.009

Hansen MO (2015) Aerodynamics of wind turbines. Routledge

IEA (2019) The international energy agency. Available via https://www.iea.org/wei2019/data/. Accessed 30 Jul 2019

Jabbari Asl H, Yoon J (2016) Power capture optimization of variable-speed wind turbines using an output feedback controller. Renew Energy 86:517–525. https://doi.org/10.1016/j.renene.2015.08.040

Karimi HR (2018) Structural control and fault detection of wind turbine systems. United Kingdom Institution of Engineering and Technology

Kinnaert M, Rakoto L (2016) Model-based fault diagnosis for wind turbines? Can it work in practice? In: 2016 3rd Conference on Control and Fault-Tolerant Systems (SysTol) 2016 Sept 7. IEEE, pp 730–734

Klinkhieo S (2009) On-line estimation approaches to fault-tolerant control of uncertain systems. Ph. D. Thesis, The University of Hull

Lan J, Patton RJ, Zhu X (2018) Fault-tolerant wind turbine pitch control using adaptive sliding mode estimation. Renew Energy 116:219–231. https://doi.org/10.1016/j.renene.2016.12.005

Li X, Zhu F (2016) Simultaneous actuator and sensor fault estimation for descriptor LPV system based on H∞ reduced-order observer. Optim Control Appl Methods 37(6):1122–1138. https://doi.org/10.1002/oca.2226

Lio WH (2018) Blade-pitch control for wind turbine load reductions. Springer, Cham

Liu X, Gao Z, Chen M (2017) Takagi-Sugeno fuzzy model based fault estimation and signal compensation with application to wind turbines. IEEE Trans Ind Electron 64(7):5678–5689. https://doi.org/10.1109/TIE.2017.2677327

Liu Z, Zhang L, Carrasco JJRE (2019) Vibration analysis for large-scale wind turbine blade bearing fault detection with an empirical wavelet thresholding method. Renew Energy 146:99–110. https://doi.org/10.1016/j.renene.2019.06.094

Luo N, Vidal Y, Acho L (2014) Wind turbine control and monitoring. Springer

Miguel AJ, Mohammed A-HB, Agustín J (2017) Wind turbine multivariable optimal control based on incremental state model. Asian J Control 20(6):2075–2087. https://doi.org/10.1002/asjc.1720

Odgaard PF, Johnson KE (2013) Wind turbine fault detection and fault tolerant control-an enhanced benchmark challenge. In: American control conference (ACC). IEEE, pp 4447–4452. https://doi.org/10.1109/CCA.2014.6981514

Odgaard PF, Stoustrup J (2014) An evaluation of fault tolerant wind turbine control schemes applied to a benchmark model. In: IEEE conference on control applications (CCA), 8–10 Oct. IEEE, pp 1366–1371

Odgaard PF, Stoustrup J (2015) A benchmark evaluation of fault tolerant wind turbine control concepts. IEEE Trans Control Syst Technol 23(3):1221–1228. https://doi.org/10.1109/TCST.2014.2361291

Odgaard PF, Stoustrup J, Kinnaert M (2009) Fault tolerant control of wind turbines: a benchmark model. 7th IFAC Symposium on fault detection, supervision and safety of technical processes Safeprocess, Barcelona

Odgaard PF, Stoustrup J, Kinnaert M (2013) Fault-tolerant control of wind turbines: a benchmark model. IEEE Trans Control Syst Technol 21(4):1168–1182. https://doi.org/10.1109/TCST.2013.2259235

Ozturk S, Fthenakis V, Faulstich SJE (2018) Failure modes, effects and criticality analysis for wind turbines considering climatic regions and comparing geared and direct drive wind turbines. Energies 11(9):2317. https://doi.org/10.3390/en11092317

REN21 (2019) Renewables now [Online]. Available via https://www.ren21.net/gsr-2019/. Accessed 30 Jul 2019

Rotondo D, Nejjari F, Puig V et al (2012) Fault tolerant control of the wind turbine benchmark using virtual sensors/actuators. IFAC Proc Volumes 45(20):114–119

Sami M, Patton RJ (2012a) Published. An FTC approach to wind turbine power maximisation via T-S fuzzy modelling and control. 8th IFAC symposium on fault detection, supervision and safety of technical processes, Mexico City, Mexico, 29–31 Aug 2012

Sami M, Patton RJ (2012b) Global wind turbine FTC via T-S fuzzy modelling and control. 8th IFAC symposium on fault detection, supervision and safety of technical processes. Mexico City, Mexico, 19–31 Aug 2012

Sami M, Patton RJ (2012c) Wind turbine sensor fault tolerant control via a multiple-model approach. UKACC International Conference on Control. Cardiff, 2012

Schulte H, Gauterin E (2015) Fault-tolerant control of wind turbines with hydrostatic transmission using Takagi–Sugeno and sliding mode techniques. Annu Rev Control 40:82–92. https://doi.org/10.1016/j.arcontrol.2015.08.003

Schulte H, Gauterin E (2016) Two-layer observer-based FDI with application to NREL 5 MW wind turbine model. In: 2016 3rd Conference on Control and Fault-Tolerant Systems (SysTol). IEEE, pp 275–280

Shafiee M, Dinmohammadi FJE (2014) An FMEA-based risk assessment approach for wind turbine systems: a comparative study of onshore and offshore. Energies 7(2):619–642. https://doi.org/10.3390/en7020619

Shaker MS (2015) A robust adaptive observer-based time varying fault estimation. Amirkabir Aut J Model Identif Simul Control 47(2):11–19. https://doi.org/10.22060/MISCJ.2015.566

Shaker MS (2019) Hybrid approach to design Takagi–Sugeno observer-based FTC for non-linear systems affected by simultaneous time varying actuator and sensor faults. IET Control Theory Appl 13(5):632–641. https://doi.org/10.1049/iet-cta.2018.5919

Shaker MS, Kraidi AA (2017) Robust fault-tolerant control of wind turbine systems against actuator and sensor faults. Arab J Sci Eng 42(7):3055–3063. https://doi.org/10.1007/s13369-017-2525-z

Shaker MS, Kraidi AA (2019) Robust observer-based DC-DC converter control. J King Saud Univ Eng Sci 31(3):238–244

Shaker MS, Patton RJ (2014a) Active sensor fault tolerant output feedback tracking control for wind turbine systems via T–S model. Eng Appl Artif Intell 34:1–12. https://doi.org/10.1016/j.engappai.2014.04.005

Shaker MS, Patton RJ (2014b) A fault tolerant control approach to sustainable offshore wind turbines. In: Luo N, Vidal Y, Acho L (eds) Wind turbine control and monitoring. Springer

Shtessel Y, Christopher E, Leonid F et al (2014) Sliding mode control and observation. Springer

Simani S (2015a) Advanced issues of wind turbine modelling and control. J Phys Conf Ser 659(1):012001. https://doi.org/10.1088/1742-6596/659/1/012001

Simani S (2015b) Overview of modelling and advanced control strategies for wind turbine systems. Energies 8(12):13395–13418. https://doi.org/10.3390/en81212374

Simani S, Castaldi P (2012) Adaptive fault–tolerant control design approach for a wind turbine benchmark. IFAC Proc Volumes 45(20):319–324. https://doi.org/10.3182/20120829-3-MX-2028.00066

Simani S, Castaldi P (2013) Data-driven and adaptive control applications to a wind turbine benchmark model. Control Eng Pract 21(12):1678–1693. https://doi.org/10.1016/j.conengprac.2013.08.009

Sloth C, Esbensen T, Stoustrup J (2011) Robust and fault-tolerant linear parameter-varying control of wind turbines. Mechatronics 21(4):645–659. https://doi.org/10.1016/j.mechatronics.2011.02.001

Wang N, Johnson KE, Wright AD et al (2014) Lidar-assisted wind turbine feedforward torque controller design below rated. In: American control conference, 2014. IEEE, pp 3728–3733. https://doi.org/10.1109/ACC.2014.6859039

Wang J, Li S, Yang J et al (2015) Extended state observer-based sliding mode control for PWM-based DC–DC buck power converter systems with mismatched disturbances. IET Control Theory Appl 9(4):579–586. https://doi.org/10.1049/iet-cta.2014.0220

WWEA (2019) World wind energy association [Online]. Available via https://wwindea.org/information-2/information/. Accessed 30 Jul 2019

Yang Z, Chai Y (2016) A survey of fault diagnosis for onshore grid-connected converter in wind energy conversion systems. Renewable Sustainable Energy Rev 66:345–359. https://doi.org/10.1016/j.rser.2016.08.006

Chapter 12
Deep Learning and Its Environmental Applications

Ahmed R. Nasser and Ali M. Mahmood

Abstract The rapid development of technologies brings a new set of challenges and difficulties in scientific studies and research in different fields. These challenges arose due to the considerable increment in the amount of data produced and the complexity of mathematical problems. Consequently, machine learning (ML) approaches, particularly deep learning (DL), receive enormous attention from academia recently. DL is a subfield of ML, which is intended to solve high complexity problems and address complex mathematical models accurately. This chapter explores DL algorithms from viewpoints including mathematical theories description of DL algorithms, the advantages of DL with its challenges, the present state of the art of DL applications, and future fields of knowledge, particularly solving complex problems of environmental systems. The focus is on three key issues including earthquake prediction, weather forecasting, and environment protection and sustainability. The reader of this chapter can gain comprehensive knowledge regarding DL with potential research issues and challenges to be solved in environmental systems.

Key words Machine learning · Deep learning · Environmental systems applications · Sustainability

12.1 Introduction

We introduce artificial intelligence and embellish its main subfields of machine learning and deep learning.

A. R. Nasser (✉) · A. M. Mahmood
Control and Systems Engineering Department, University of Technology-Iraq, Baghdad, Iraq
e-mail: ahmed.r.nasser@uotechnology.edu.iq; Ali.M.Mahmood@uotechnology.edu.iq

J. N. Furze et al. (eds.), *Earth Systems Protection and Sustainability*,
https://doi.org/10.1007/978-3-030-98584-4_12

12.1.1 Artificial Intelligence

Artificial intelligence (AI) can be defined as the science of creating intelligent machines (McCarthy et al. 1959). AI is a general name for technologies that make any guess or decision process. Contrary to the general view, AI can be an algorithm that works with or without a deep learning process. Up until the emergence of machine learning algorithms, AI studies were based on a structure that was described as "hard-coded," where all logical and mathematical operations were coded by the developer. The first AI chess game was simply an artificial intelligence algorithm, solely learning without the help of human knowledge via solving complex, multistep problems. This type of AI is called symbolic artificial intelligence (Hernández-Orallo 2017). Studies in the science of AI date back to the 1950s. Later, AI involved different subfields such as machine learning and deep learning as shown in Fig. 12.1, which illustrates the correlation of AI and its subdivisions (Goodfellow et al. 2016).

12.1.2 Machine Learning

Machine learning (ML) has been defined as a "field of study that gives computers the ability to learn without being explicitly programmed" (Samuel 1988). ML is a form of AI that allows a system to learn from data. ML employs data-learning algorithms to identify data and repetitively predict data-related results. Algorithms receive training data, which makes it possible to produce models with more accurate results.

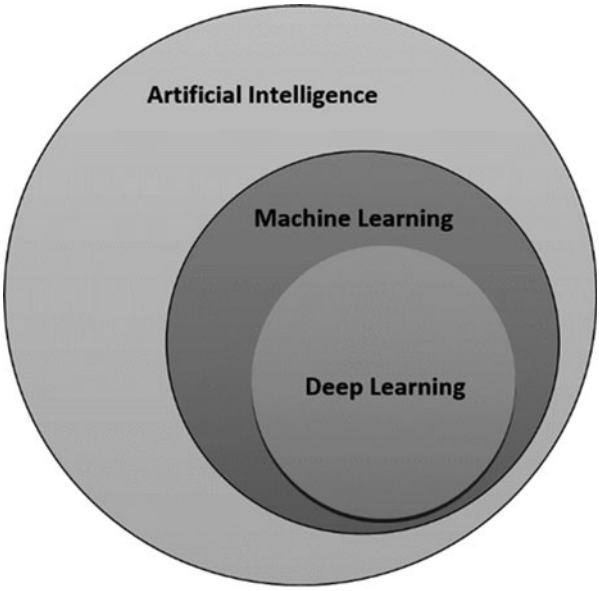

Fig. 12.1 Overview of artificial intelligence and its main subdivisions

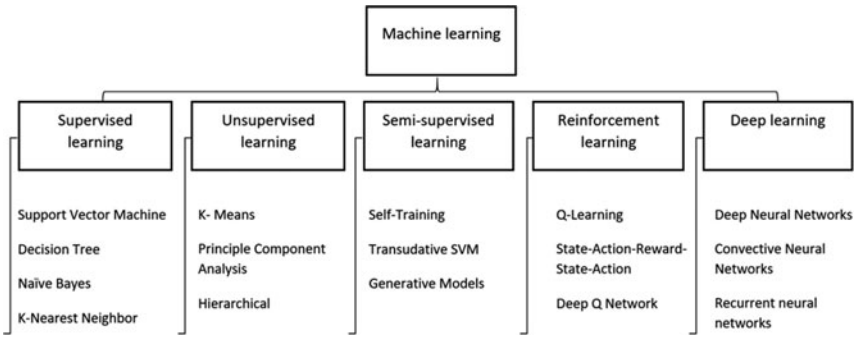

Fig. 12.2 The taxonomy of machine learning approaches

Once a system has been trained, it is expected to produce meaningful output when an input is given to the trained model (Franklin 2005). A prediction algorithm is created and once trained, providing the model with data returns a prediction based on educational data. The two main tasks for machine learning algorithms are prediction and classification (Ahmed and Hayri 2018; James et al. 2013). Prediction is used in the case of quantitative system output in models learned from data. In cases where the input data is qualitative, the methods used to determine or classify which class each data instance belongs to.

The intensive study of machine learning has led to many strategies and algorithms being proposed. Learning strategies used in ML are supervised, unsupervised, semi-supervised, reinforced, and deep learning (James et al. 2013). The taxonomy of machine learning approaches is shown in Fig. 12.2 (Dey 2016). Models created by supervised learning aim to train the relationship between target values through a group of input values and to produce the outputs closest to the target values. The best model obtained will give the closest output for the new input values. In unsupervised learning, the relationship between input values without target values is revealed. With the help of these relationships, close values are grouped, as in clustering algorithms. A new entry will belong to a set, depending on whichever one of the sets it links. Semi-supervised learning algorithm premise between the former two concepts, using a larger part of unlabeled data compared to the labeled data. In the reinforced learning algorithm, instead of a consultant, a criterion evaluates the obtained output as good or bad versus the given input and is used to give the target output. Deep learning is a more powerful method to solve data analytics and learning problems found in large datasets and will be discussed further in subsequent sections.

12.1.3 Deep Learning

Deep learning (DL) is a component of the machine learning family that is capable of performing feature extraction, classification, and transformation operations using large amounts of data; its structure and capabilities mimic the human brain to solve complex problems. Each DL algorithm can be called a machine learning algorithm as it performs learning from data. In contrast, not every machine learning algorithm is a DL algorithm, since DL is a specific kind of machine learning. The structure of DL methods is based on artificial neural networks (ANN) calculation with an additional deep network structure. The ability of DL to solve complex problems derives from the ability of ANN to solve nonlinear problems. In deep learning, increasing numbers of layers represent the depth of the model that provides a basis for solving complex problems (Patterson and Gibson 2017).

Historically, the elementary learning algorithm of the supervised multilayer deep-feed perceptron was introduced by Ivakhnenko and Lapa (1966). In this study, the best features of each layer were selected by statistical methods and transmitted to the next layer, where the applied learning algorithm was the least-squares method. The first DL architecture was introduced by Fukushima in 1979 as depicted in Fig. 12.3. A self-organizing network was developed with "teacherless learning" in the structure that is inspired from visual nervous systems. Fukushima's nets included multiple interconnected layers similar to modern neural nets (Fukushima 1980). The lack of learning in deep architectures is manifested in the backpropagation of errors in multiple layers. Although backpropagation algorithms have been proposed in previous years, the first successful deep neural network application was developed by LeCun et al. (1989). However, it was found that this method is unsuitable for critical time applications since training lasted approximately 3 days. Later authors

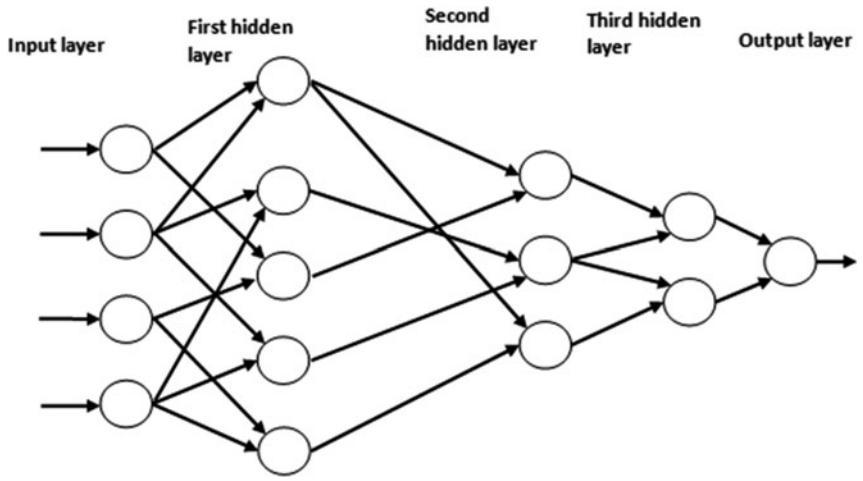

Fig. 12.3 The first deep network architecture

(LeCun et al. 1990) applied coiled backpropagation to classify handwriting numbers. In 1995, the wake-sleep algorithm was developed (Hinton et al. 1995). In this method, network training with six interconnected layers and hundreds of hidden layers was formed, with training over 2 days. In 1997, recurrent neural networks such as long short-term memory was proposed, which made important improvements (Hochreiter and Schmidhuber 1997).

Due to the cost of computation in the traditional ANN, from the 1990s to the 2000s, the application of vector machines has become a popular choice. Consequently, major advances were made owing to the faster processing of computers and the emergence of graphics processing units (GPUs). Computational speed has increased 1000-fold over 10 years. The neural network has begun to replace support vector machines (Schmidhuber 2015). GPUs have been used to increase training speed and have proven efficacy with a normalized method called "dropout" (Hinton et al. 2012) that was prepared later to reduce overfitting in fully connected layers (Krizhevsky et al. 2012). Large companies such as Google, Facebook, and Microsoft have realized this trend and utilize deep learning (Şeker et al. 2017).

12.1.4 Differences Between Machine Learning and Deep Learning

The presence of automatic feature extraction signifies the main difference between traditional machine learning and DL. To extract features, DL algorithms need a big dataset. The traditional machine learning model specifies the characteristics or (features) of each class before training and classifying (Fig. 12.4), while in deep learning these features are automatically extracted and learned (Vieira and Ribeiro 2018). Deep learning does not require an extra feature extraction stage because the network learns to extract features while training. In the multilayered perceptron structure, less than two hidden layers can be used, whereas a deep learning neural network makes use of many hidden layers. Although both networks have error-based

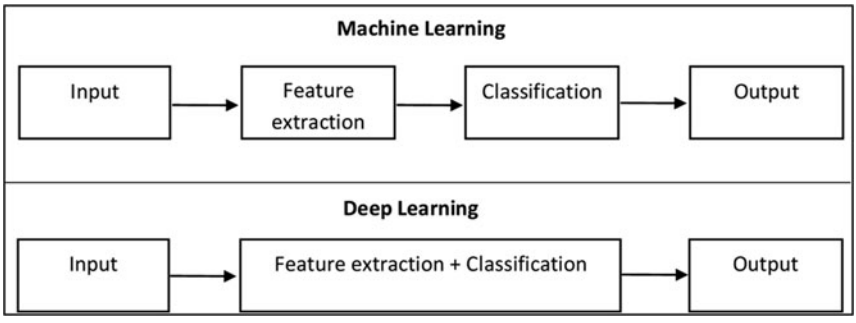

Fig. 12.4 Machine learning versus deep learning

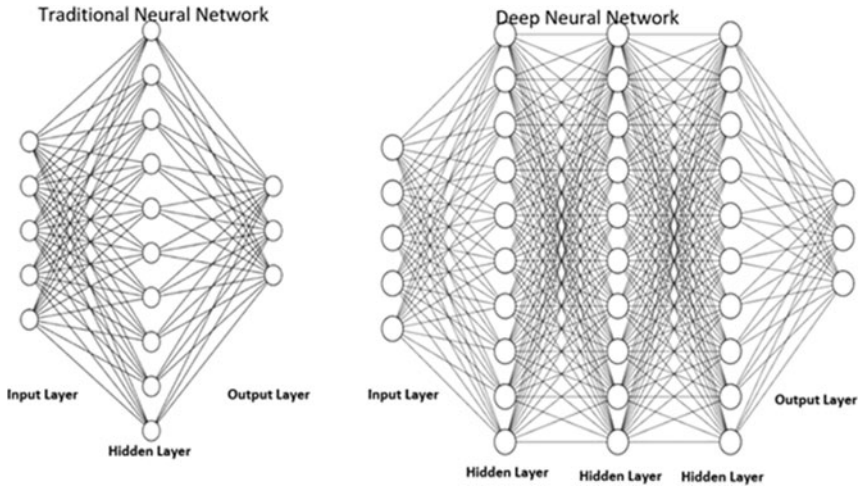

Fig. 12.5 Comparison between a simple neural network and deep learning neural network

Table 12.1 Comparing machine learning and deep learning

Comparison parameter	Machine learning	Deep learning
Data dependency	Excellent performance in small/medium dataset	Excellent performance in a large dataset
Hardware requirements	It can work on a relatively low-end machine	It requires a powerful machine, preferably GPU: it needs hardware capable of performing multiple matrix multiplications
Feature extraction	They need to know the characteristics that data represent	It does not need to know the best feature representing data
Training time	It may take from a few minutes to hours	It may take up to weeks. This is because the artificial neural network needs to calculate a significant amount of weight

learning, supervised learning is done in the multilayered perceptron structure, while DL performs potentially unrestrained learning (Goodfellow et al. 2016).

The main feature that distinguishes deep learning network structure from a simple artificial neural network is that it has multiple hidden layers and a more complex network structure as can be seen in Fig. 12.5.

In Table 12.1, machine learning and deep learning are compared in terms of data dependence, hardware dependencies, feature extraction, and training time. For deep learning algorithms to perform well compared to standard machine learning, data and powerful hardware may be required (Kin 2019).

12.2 Deep Learning Processes

The main process of DL involves the stages of definition, selection, and testing. Definition of the problem and determination of the suitability of the solution with deep learning leads to the definition of related datasets and being ready for analysis. Consequently, the appropriate deep learning architecture is chosen, followed by training of the system using the dataset and selected deep learning architecture. These steps enable the final process of testing the performance of the trained system with test data that was not used for the training.

12.3 Theories of Deep Learning Algorithms

Deep learning consists of three main algorithms: deep neural network (DNN), convolutional neural networks, and recurrent neural networks. The theories of each deep learning algorithm are illustrated in subsections.

12.3.1 Deep Neural Network

Artificial neural networks are an artificial intelligence technique developed by modelling the processing structure of the human brain. Biological nerve cell neurons form the nervous system. ANNs are also called neurons. The neural network architecture includes the number of neurons, the number of layers, and the types of interlayer connections. The human brain consists of a complex network connection of neurons. These neurons serve to transmit information from the brain to the body. According to scientific studies, the human brain may have an average of 100,000,000,000 neurons (Gurney 2014). Each of these neurons is connected to others, with an average of 6000 connections each. These networks of connections are responsible for our perception and learning of everything around us. Artificial neural network neurons consist of input, weights of inputs, bias, activation function, and output. Figure 12.6 illustrates the artificial neural network neuron and its connections.

By adding bias b value to the sum of the product of a neuron's output-input values $(x_1, x_2, \ldots, x_n)$ and their weights, $(w_1, w_2, \ldots, w_n)$ are obtained by passing $(z = \sum_{1}^{n} x_i * w_i + b)$ through the activation function α.

DNNs are a type of multilayer perceptron (MLP) artificial neural network with a large number of hidden layers (Patterson and Gibson 2017). Multilayer artificial neural networks are an example of DNN.

12.3.2 Multilayer Artificial Neural Networks

The human brain has a layered structure. Data from the senses is transferred from one layer to another and transformed into information. This data is processed by transferring from the bottom layer of the visual cortex to the top layer. The last layer determines which object is visible in the image. This layered structure in the human nervous system is modelled to create an artificial neural network, called a multilayer artificial neural network. The first layer on the left is called the input layer, and the neurons in the input layer are called input neurons. The middle layer is called the hidden layer, and the right layer is called the output layer (Schmidhuber 2015). Multilayer structure is shown in Fig. 12.7

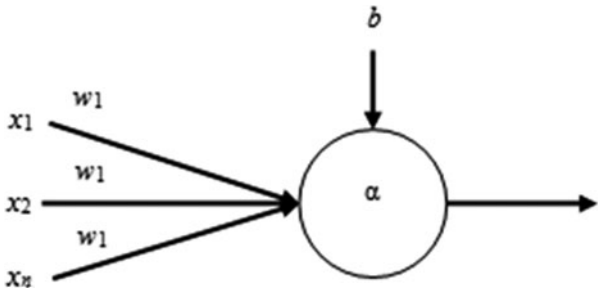

Fig. 12.6 Artificial neural network from the 1990s to the 2000s

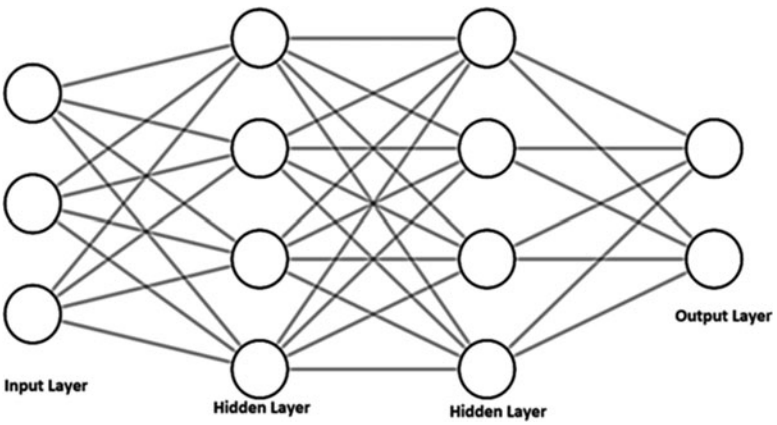

Fig. 12.7 Multilayer artificial neural network

12.4 Convolutional Neural Networks

In the last decade, convolutional neural networks (CNN) have shown significant development in research and applications. Convoluted neural networks can work with large amounts of data produced today. In general, CNNs show very high accuracy images and video classification applications. The success of CNN is seen in self-driving vehicles and online services offered by large companies such as Tesla or Google. The high level of data, new-generation CNN algorithms, and high-performance GPUs led to create a new trend in the industrial revolution (Hu et al. 2015).

Traditional CNN architecture includes five main layers, the input layer followed by the convolution layer, then the pooling layer, the fully connected layer, and finally the output layer. Researchers are working with CNN architectures such as "AlexNet," "ResNet," "Inception," and "VGG," which are created with different layouts of these five layers. In this section, the three main layers of CNN architecture will be examined in more detail. An example of CNN structure is shown in Fig. 12.8 (Hu et al. 2015).

12.4.1 Convolution Layer

The concept of convolution was first introduced by LeCun et al. (1990). Convolution is a customized linear process. These networks are simply networks that perform convolution instead of matrix multiplication in one layer (Goodfellow et al. 2016). The discrete-time convolution of CNNs is expressed by Eq. (12.1) (Goodfellow et al. 2016):

$$s_t = (x * w)_t = \sum_{i=-\infty}^{\infty} x_i * w_{t-i} \tag{12.1}$$

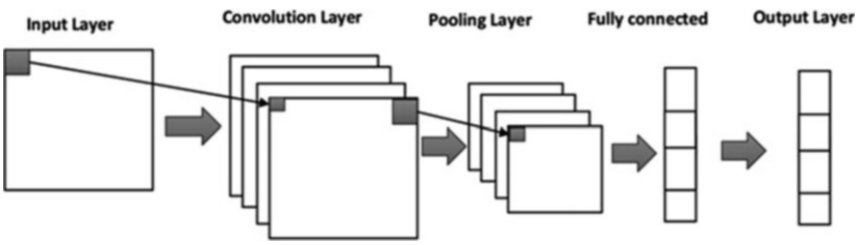

Fig. 12.8 Example of convoluted neural network structure

In Eq. (12.1), filter (kernel) w, input x, time t, and s are expressed as a result. When a two-dimensional input such as a picture is used as the input convolution process, Eq. (12.2) is expressed by Goodfellow et al. (2016):

$$s_{i,j} = (I * K)_{i,j} = \sum_m \sum_n I_{i,j} K_{i-m,j-n} \tag{12.2}$$

In Eq. (12.2), the terms i and j refer to the positions of the new matrix to be obtained as a result of the convolution process. In many cases, the center of the filter is positioned at the origin (Goodfellow et al. 2016).

12.4.2 Pooling Layer

In pooling operations, the output size is reduced by using functions, such as average or maximum value, to summarize the subregions. The pooling process subtracts a value by averaging or calculating the maximum of values within a specified area. The pooling process is implemented by the sliding window method. The sliding window creates value from the corresponding input field according to the pooling method determined each time and adds it to the output layer (Dumoulin and Visin 2016). Through pooling layers in a convolutional neural network, small portions of the aforementioned input are reduced to a single constant value according to the preferred method. Accordingly, pooling layer calculations are less costly than convolution layer calculations.

The output size (o) of the pooling layer, the relationship between the input size (i), the window (part) size (k), and the number of steps (s) on which operations will be performed are shown in Eq. (12.3) (Dumoulin and Visin 2016).

$$o = \left(\frac{i-k}{s}\right) + 1 \tag{12.3}$$

The relationship in Eq. (12.3) applies to all types of docking (Dumoulin and Visin 2016).

12.4.3 Fully Connected Layer

This layer works as an artificial neural network. The values generated as a result of convolution and pooling operations are processed by this layer as input, and the result is generated by the number of classes in the output layer.

12.4.4 Network Hyperparameters

To achieve the best results for convolutional networks as well as basic neural networks, hyperparameters should be ideally adjusted. Hyperparameter details include depth, number, and input size.

The depth is the number of filters that are applied; each filter looks for different attributes in the input. For example, when the convolution layer receives an image as input, different neurons in each filter will be active due to the corner or different colors present in that input. All neurons that look at a certain part of the input and look for different characteristics are called depth columns (Goodfellow et al. 2016).

The number of steps is the hyperparameter that specifies how many pixels the filter will shift over the input.

Padding is the process of filling the input with zeros. The reason for padding is to control the size of the output after convolution. The effect of the fill on the output size is determined using Eq. (12.4) for the input size (i), filter size (k), number of strides (unit strides), and any fill (p) value (Dumoulin and Visin 2016; Goodfellow et al. 2016).

$$o = (i - k) + 2p + 1 \tag{12.4}$$

Given the input size and output size are the same as the result of convolution, the fill value should be 1. This is called half padding and can be expressed mathematically. For any value i and ($k = 2n + 1$, $n \in N$), the result is calculated with ($o = i$), where the number of strides (s) $= 1$ and the padding p $= [k/2]$ (Dumoulin and Visin 2016; Goodfellow et al. 2016).

Although convolution generally decreases the size of the output relative to the input, it is sometimes necessary to reverse it. The appropriate fill value should be preferred to increase the output size. For any value i and k, the number of strides is 1, and the padding is calculated with Eq. (12.5), where p $= k - 1$ (Dumoulin and Visin 2016; Goodfellow et al. 2016).

$$o = i + (k + 1) \tag{12.5}$$

Generally, the result for any input size (i), filter size (k), padding value (p), and some strides (s) is calculated by Eq. (12.6) (Dumoulin and Visin 2016; Goodfellow et al. 2016):

$$o = \left[\frac{i + 2p - k}{s}\right] + 1 \tag{12.6}$$

In artificial neural networks, the pooling layer ensures the output does not change against minor deflection of the input. The most common type is maximum pooling, which breaks up the input and takes only the maximum value of each segment. Since the docking process is the continuous application of the input to different parts like

the convolution process, the expression defined in Eq. (12.6) can be used. Since the fill value is zero in the pooling process ($p = 0$), the result is calculated by Eq. (12.7) (Dumoulin and Visin 2016; Goodfellow et al. 2016):

$$o = \left[\frac{i-k}{s}\right] + 1 \tag{12.7}$$

Equation (12.7) can be used in any kind of pooling operation that applies to any i, k, and s value (Dumoulin and Visin 2016; Goodfellow et al. 2016).

12.5 Recurrent Neural Networks

Recurrent neural networks (RNN) represent a class of artificial neural networks with connections among units with a directed loop (Goodfellow et al. 2016). RNN is a feedforward type of neural network reinforced through the addition of edges extending along with adjacent time steps, which gives the concept of time to the normal neural network model. Similar to feedforward networks, RNN may not have loops between conventional edges. However, the repetitive edge connecting adjacent time steps can form loops, including length loops that are self-connecting from an edge. At time t, repetitive edges are retrieved from the current data point x_t and the hidden node values $h_{(t\ -\ 1)}$ from the previous state of the network (LeCun and Bengio 1995).

The output y_t is calculated by the values of the hidden node h_t at time t. The input $x_{(t\ -\ 1)}$ at time $t - 1$ can affect the output y_t and the other repetitive connections at time t; x input at time b can affect output at time t y and later through repetitive connections. In a simple RNN, all calculations required are shown for calculation at any time step forward as in Eqs. (12.8) and (12.9) (LeCun and Bengio 1995):

$$h_t = \sigma(w_{hx}x_t + w_{hh}h_{t-1} + b_h) \tag{12.8}$$

$$y_t = \text{softmax}\left(w_{yh}h_t + b_y\right) \tag{12.9}$$

Here, w_{hx} refers to the conventional weight matrix between the hidden layer and the input, while w_{hh} is the repetitive weights matrix between the hidden layer in the adjacent time steps and itself. The bias parameters b_h and b_y allow each node to learn the offset. In Fig. 12.9, a block diagram of a simple RNN structure is given.

In Sect. 12.7, long short-term memory is detailed with RNN.

12.6 Long Short-Term Memory

One of the common structures that use components of RNN architecture is long short-term memory (LSTM) (Goodfellow et al. 2016). The structure of LSTM networks consists of memory blocks with memory cells and gate units. There are three special doors in the LSTM memory block: entry, forget, and exit. The core structure of the LSTM is demonstrated in Fig. 12.10. The data input flow to the memory cell is controlled by the input port. The output port manages the output flow from the memory cell to the rest blocks. Forget gate determines the extent to which the former block outputs are effective in the current block. This gate is managed by a simple single-layer neural network. In this gate, the activation is determined in the Eq. (12.10) following Chen and Wang (2017).

$$f_t = \sigma\left(W[x_t, h_{t-1}, c_{t-1}] + b_f\right) \tag{12.10}$$

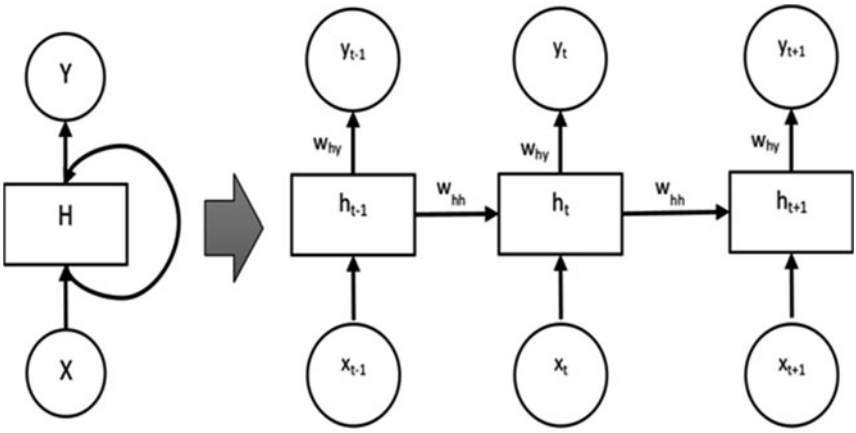

Fig. 12.9 Recurrent neural network structure

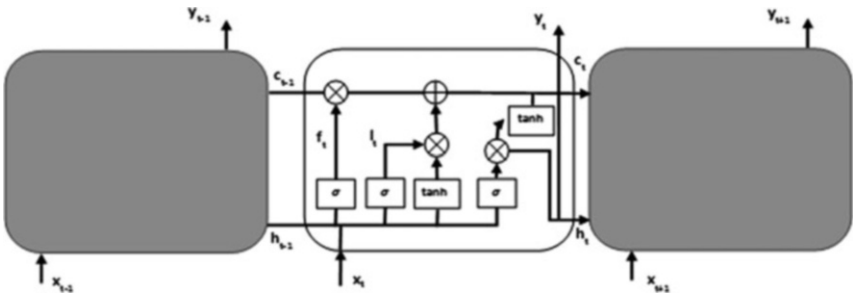

Fig. 12.10 The internal structure of long short-term memory (LSTM)

Here, x_t forms the former block output $h_{t\ -\ 1}$, the former LSTM block memory c_{t-1}, and the bias vector b_f. W is the weight vector of the inputs. The sigmoid activation function represents the output of the forget gate and is implemented by multiplying the previous block memory. Thus, the extent that which the earlier block memory will be effective for the current network is calculated. When the activation of the output vector includes values near zero, the prior memory is forgotten.

Another gate represents the section in which the new memory is formed by a simple neural network (NN) with the "tanh" activation function and the former block memory effect. The mathematical expressions of these operations are shown in Eqs. (12.11) and (12.12), following Chen and Wang (2017).

$$i_t = \sigma(W[x_t, h_{t-1}, c_{t-1}] + b_i) \tag{12.11}$$

$$c_t = f_t * c_{t-1} + i_t * \tanh\left(W[x_t, h_{t-1}, c_{t-1}] + b_c\right) \tag{12.12}$$

Finally, the exit door is the section where the output of the existing LSTM block is produced. These outputs are calculated as in Eqs. (12.13) and (12.14) (Chen and Wang 2017):

$$o_t = \sigma(W[x_t, h_{t-1}, c_{t-1}] + b_o) \tag{12.13}$$

$$h_t = \tanh\left(c_t\right) * o_t \tag{12.14}$$

As with other networks, deep learning structures have become widespread, and the design of LSTM networks to include many layers has revealed the deep structures of these networks.

12.7 A Comparison Between Deep Learning Algorithms

A comparison between DNNs, CNNs, and RNNs deep learning methods is presented in Table 12.2.

12.8 Advantages and Challenges of Deep Learning

The following subsections describe the main advantages of using DL over other ML techniques and the recent challenges that face researchers using DL.

Table 12.2 Comparison between DNNs, CNNs, and RNNs

Features	Deep neural networks	Convolutional neural networks	Recurrent neural networks
Definition	DNNs are a type of MLP with a large number of hidden layers	CNNs are a type of neural network with different special-purpose layers that have been designed to map image data to an output variable	RNNs are a type of neural network with feedback loops in the recurrent layer which act as memory and used to work with sequence prediction problems
Architecture	DNNs include different interconnected layers such as an input layer, one or more hidden layers, and an output layer	The architecture of CNNs is similar to feed-forward artificial neural networks with several different special-purpose layers such as convolution, pooling, and fully connected layers	The architecture of RNNs consists of different interconnected recurrent layers with feedback loops that act as internal memory to process arbitrary sequences of inputs
Input/output size	Both input and output size are fixed	CNN uses inputs with fixed size and generates outputs with a fixed size	RNN can handle arbitrary input/output sizes
Suitability of classification/ regression problems	DNNs are suitable for classification and regression prediction problems	CNNs are suitable for classification and regression prediction problems	RNNS are suitable for Classification problems and Regression prediction problems
Type of data	DNNs can be used on Tabular data or time-series data	CNNs can be used on spatial data or image data	RNNs can be used on temporal data or sequential data
Applications	Applications deal with image data, text data, and time-series data	Applications deal with image data and video data	Applications deal with Text data, Speech data, and Generative models. However, RNNs are not appropriate for tabular and image data
Complexity	Complexity depends on data size and number of hidden layers	Complexity depends on data size, filter size, number of layers, as well as setting the hyperparameters	Complexity depends on data size, number of layers, and amount of required memory

12.8.1 Advantages of DL

The main advantages of DL over regular machine learning are given according to Alom et al. (2019) and Pouyanfar et al. (2018).

- Similar to neural network-based approaches, DL can be utilized in many different applications and data types.
- DL can automatically extract features from the data; therefore, no pre-feature extraction process is required.

- DL is able to drive new feature sets to form a dataset with a limited series of features.
- DL can automatically adapt to overcome the natural variations in the training data.
- With the usage of GPUs, DL can perform a massive amount of computations that can be achieved in a parallel manner. Therefore, DL can be used to generate complex models from large volumes of training data.

Hence, the flexible architecture of DL can be adapted to new problems relatively easily. The extreme performance of DL over other solutions makes DL preferable for different applications such as speech recognition, computer vision, natural language processing, and games.

12.8.2 Challenges of DL

There are several challenges for DL including Alom et al. (2019) and Pouyanfar et al. (2018).

- Data availability and quality: DL performance increases with the amount of available training data. In most industrial applications, large amounts of training data are not often easily available. This becomes a big challenge for DL to work with this small amount of training data and provides high performance. Another challenge for DL is the quality of the training data. When the data is used for training, DL models contain high noise, which can lead DL to degrade and reduce its performance.
- Security: DL is often used to improve and strengthen cybersecurity applications. However, DL networks are vulnerable to malicious attacks by modifying the input to security DL models.
- Higher processing power: When working with large amounts of training data, DL algorithms perform intensive computations and require a huge amount of processing power. Providing powerful computation platforms while keeping the cost down becomes an important challenge for DL.
- Hyperparameter optimisation: DL performance depends on identifying the optimal hyperparameters which are the network parameters required to be initialized before the training process. Identifying the optimal values of DL networks, hyperparameter is the most important challenge for DL, and setting these parameters incorrectly can impact the performance of DL and cause overfitting problems.

12.9 Utilization of DL in Environmental Systems Applications

Natural phenomena affecting planet Earth represent one of the hottest global topics. These phenomena lead to an increase in natural disasters and threaten humans and other life on Earth. Hence, the prediction of changes in environmental systems could be interpreted in reality as protecting thousands of human lives as well as saving resources and money. The losses of facts and statistics regarding natural disasters can be found in the Insurance Information Institute (https://www.iii.org/ accessed 12 May 2021). This topic has attracted the attention of decision-making leadership and the scientific community. Several factors contribute to disasters. In this context, the application of deep learning in predicting different phenomena has been applied. The prediction of earthquakes, rainfall, and environmental protection is discussed in subsections.

12.9.1 Application of DL in Earthquake Prediction

Earthquakes cause great and sudden destruction; these natural disasters negatively affect the lives of thousands of people. Severe earthquakes cause many psychological and negative effects as well as loss of life and property. Every year, there are a large number of earthquakes in different locations with various magnitudes. Figure 12.11 shows the number of earthquakes across the world that occurred in the last decade for the period 2009–2019 according to the United States Geological Survey (https://earthquake.usgs.gov/earthquakes/map/?extent=-55.77657,-520.66406&extent=84.16085,-183.16406) Retrieved 2019.

Natural disasters such as earthquakes do not provide any obvious warning before occurrence; associated losses cannot be prevented. The prediction of earthquakes has always been an interesting subject, and the success of the prediction may save many

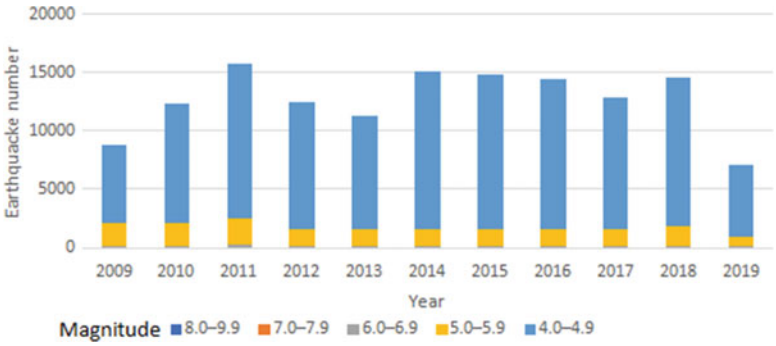

Fig. 12.11 The number of earthquakes worldwide for 2009–2019

thousands of human lives. There are earthquake studies based on mathematical analysis and machine learning algorithms like decision trees and support vector machines, ANNS, and precursors signal in the literature (Sobolev 2015). However, due to the unpredictable complex and, dynamic nature of earthquakes, these methods do not provide consistently accurate results (Sobolev 2015). Deep learning algorithms such as RNN and CNN can capture the complex nonlinear correlations among data with high performance and, therefore, receive huge attention from researchers on the subject of earthquake prediction.

12.9.2 Using RNN Deep Learning for Earthquake Prediction

The work presented by Wang et al. (2017) exploits the DL method of RNN for earthquake prediction. In earthquake prediction, regular machine learning methods are incapable of providing respectable results due to the unpredictable and the dynamic nature of earthquake data. Deep learning methods such as RNNs have the advantage of capturing the complex nonlinear relations in data and so are suitable for complex time-series prediction required in earthquake prediction. Due to crust movement in earthquakes, spatiotemporal correlations of earthquake history data are considered to increase the accuracy of predictions. LSTM variation of RNNs has a strong capability of learning and capturing the nonlinear correlation in earthquake data with long-term intervals.

To improve earthquake prediction, earthquakes have been modelled based on spatiotemporal correlations dividing the area of interest into different subregions.

The model was built based on the raw information of earthquakes such as events ($E = \{e_1, e_2, \ldots\}$), time (t), latitude (La), longitude (Lo), and magnitude (Ma) (Wang et al. 2017). The first step of building the earthquake model is selecting the area of interest in a rectangle shape with four vertices expressed as View, Vsw, Vne, and Vse. The whole area is designated M equal to m_h (horizontal edge) multiplied by m_v (vertical edge); this may be divided into multiple subregions (SR) using Eqs. (12.15) and (12.16).

$$\mathrm{SR_{ve}} = |\mathrm{La(Vnw)} - \mathrm{La(Vsw,)}|/m_h \tag{12.15}$$

$$\mathrm{SR_{he}} = |\mathrm{Lo(Vnw)} - \mathrm{Lo(Vne)}|/m_v \tag{12.16}$$

where $\mathrm{SR_{ve}}$ is the vertical edged subregion and $\mathrm{SR_{he}}$ is the horizontal edged subregion. Each earthquake event is allocated its corresponding subregion as in Eqs. (12.17) and (12.18):

$$i = \left\lfloor \frac{|\mathrm{Lo(e)} - \mathrm{Lo(Vne)}|}{\mathrm{SR_{he}}} \right\rfloor \tag{12.17}$$

$$j = \left\lfloor \frac{|\mathrm{La(e)} - \mathrm{La(Vsw)}|}{\mathrm{SR_{ve}}} \right\rfloor \tag{12.18}$$

Consequently, a temporal segmentation method may be applied to produce the events frequency of each subregion in each time interval Δt. This results in the multi-hot input vector with dimension Mx 1 (M is the total number of subregions) which is later combined with earthquake time series vector L to generate a two-dimensional vector called X and used as an input to the LSTM deep learning algorithm.

For earthquake prediction, LSTM deep learning algorithm is used for training the two-dimensional vector X. At each LSTM layer, h_t is calculated using the following equation:

$$h_t = o_t.\varnothing(c_t) \tag{12.19}$$

The dropout operation is applied to prevent overfitting issues. Then, the results pass through dense network layers to calculate $h_t^D = W_D W_P h_t^L + b$ which passed to softmax activation function and then calculate the loss function based on cross-entropy. The network is learned by minimizing the loss function using a gradient descent scheme.

Two case studies are used for evaluating the performance of the system by training the LSTM using a one-dimensional data vector and the second by training the LSTM using a two-dimensional data vector.

To train the system, the one-dimensional earthquake data is obtained from USGS (US Geological Survey) website for the period between 2006 and 2016 with a 1-month interval and magnitudes greater than 2.5. The results using one-dimensional data show 63.50% for the overall prediction accuracy.

In the second case study, the two-dimensional earthquake data (spatiotemporal) is obtained from USGS website for mainland China in the period 1966–2016 with a 1-month interval and magnitudes greater than 4.5.

The evaluation result for the second case study shows a prediction accuracy of 74.81%. Finally, to compare LSTM deep learning method with the regular machine learning method, the two-dimensional earthquake data are used to train MLP neural networks and obtained an accuracy of 66.99%, which is much lower than the results obtained by using the LSTM deep learning method.

12.9.3 Using CNN Deep Learning for Earthquake Prediction

The work presented by Perol et al. (2018) utilizes the CNN DL method for earthquake prediction. There are many human-induced non-natural causes of earthquakes. Injection of wastewater under the surface of the Earth has a major impact on inducing a large number of moderate and small size earthquakes which can later trigger large magnitude earthquakes. Many earthquake detection methods are designed to detect earthquakes with large magnitudes and not consider the small magnitude earthquakes covered by seismic noise. Detecting small size earthquakes is the key to unlocking their causes to reduce future risks.

In deep learning, CNN (ConvNetQuake) is used to detect and locate earthquakes based on seismogram data. CCN is trained on a big dataset of labeled raw seismic waveforms and learns a compact representation that can discriminate seismic noise from earthquake signals. A large number of raw seismic waveform data along with labels are used to train CNN to discriminate earthquakes from seismic noise. Unlike the regular detection methods, which detect earthquake waveforms based on similarity to other waveforms, the used method is considered a nonlinear local filter that is used to select features in the waveforms that are most relevant to classification. This helps to detect earthquake signals which were missed during training and increases the system performance.

In the modelling of earthquakes using CNN ConvNetQuake, the input of networks takes a three-channel window of waveform data with M number of classes, represented as a two-dimensional tensor $Z^0_{t,c}$ where c is the number of channels and t is 10 s sampling period. The input is fed into a feed-forward network consisting of eight convolutional layers connected to a fully connected Z layer which outputs class scores. Each convolution layer processes the data based on Eq. (12.20):

$$Z^i_{t,c} = \sigma\left(b^i_c + \sum_{\acute{c}=1}^{c_i}\sum_{\acute{t}=1}^{3} Z^{i-1}_{c,st+\acute{t}-1}.W^i_{c\acute{c}}\right) \; i = 1,2,3 \tag{12.20}$$

where σ is the activation function called nonlinear ReLU (rectified linear unit). The output and input channels are indexed with c and $\acute{c}$, respectively, the time dimension is indexed with t and $\acute{t}$, c_i is the number of channels in layer i, and W represents the weights of the network.

The output of the eighth layer is reshaped into a one-dimensional tensor called $\overline{Z}^8$ which contains 128 features. The $\overline{Z}^8$ features vector is followed by a fully connected layer to compute class scores following Eq. (12.21).

$$z_c = \sum_{\acute{c}=1}^{128} \overline{Z}^8_{\acute{c}}.W^9_{c\acute{c}} + b^9_c \tag{12.21}$$

This fully connected layer enables the network to learn and combine multiple parts of the signal to generate the final class score.

Finally, the softmax normalization function is applied to the class scores to generate the final prediction result. The L2-regularized cross-entropy loss function is used as the cost function optimiser for training the ConvNetQuake.

For building the earthquake detection model using ConvNetQuake, continuous ground velocity data records were used. This data was obtained from two local stations GS.OK027 and GS.OK029 in the state of Oklahoma. This data consists of 2918 windows of labeled earthquakes and 831,111 windows of seismic noise for the period 15 February 2014 and 16 November 2016. The training set contains 2709 events and 700,039 noise windows, and the test set contains 209 events and 131,072 windows of noise. The evaluation results of the earthquake detection model using ConvNetQuake deep learning show 94.8% precision and 100% recall which leads to a value of 97% of F-score.

ConvNetQuake earthquake detection method shows better and faster prediction results compared to autocorrelation and "Fingerprint and Similarity Thresholding" (FAST) earthquake detection methods.

12.9.4 Applications of DL in Climate and Weather Forecasting

Predicting changes in climate and weather is a very important issue. Such predictions aid the location of the best places to plant crops as well as prepare for emergency conditions including floods and drought. Machine learning technology can be used successfully to predict the behavior of the climate and the weather. The focus here will be on the application of deep learning approaches to predict rainfall.

12.9.4.1 Rainfall Prediction Using DL

With the gradual increase in temperature of the world associated with global warming, rainfall prediction is increasingly vital for the economy and daily life of many countries. An efficient method of predicting rainfall is a key topic for scientists. Input parameters/attributes which can be utilized to predict rainfall are shown in Table 12.3. Deep learning is one of the promising computation tools that can be used to predict rainfall by using more complex neural network architectures. Recurrent

Table 12.3 Input parameters/attributes for the classifier (Niu and Zhang 2015)

Parameters	Attributes
Temperature	Minimum and maximum values
Humidity	Average value
Pressure	Average, minimum, and maximum values
Evaporation	Minimum and maximum values
Wind	Average and maximum values
Sunshine	Total time

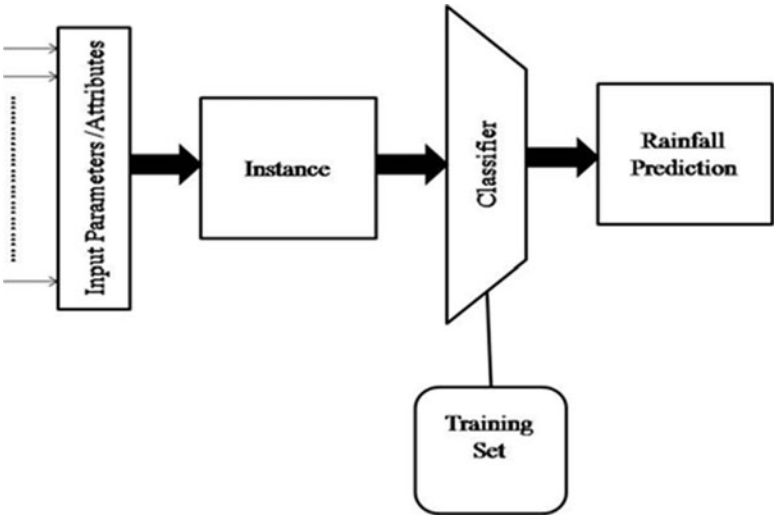

Fig. 12.12 The general structure of rainfall prediction model based on historical data (Niu and Zhang 2015)

neural networks model changes in rainfall through time (Patterson and Gibson 2017). Figure 12.12 shows the general structure of rainfall prediction.

Several methods have been used for rainfall forecasting. Two of those commonly used are empirical and dynamical methods. Regression, stochastic, artificial neural network, and fuzzy logic are examples of empirical methods, which rely on the analysis of available historical data of the weather with the correlation to different atmospheric variables. The second approach for prediction is represented by employing physical models, which are dependent on modeling equations of the climate system based on the atmospheric conditions (Zaw and Naing 2008).

The common forecasting processes of empirical methods to quantify the amount of rainfall are as follows:

(i) Gathering data
(ii) Reduction explanatory predictors
(iii) Building a model using one of the empirical methods
(iv) Checking through the validation procedure

However, RNN DL algorithm is applicable for rainfall prediction problems as it can model changes in data across time which is a property of rainfall data. Due to the fact that RNNs are generally used for classification problems and rainfall prediction problem is considered a regression problem, a regression output layer can be added to a RNN. Figure 12.13 shows the architecture of RNN used for regression problems. The general equation of deep RNNs is shown in Eq. (12.22) (LeCun and Bengio 1995).

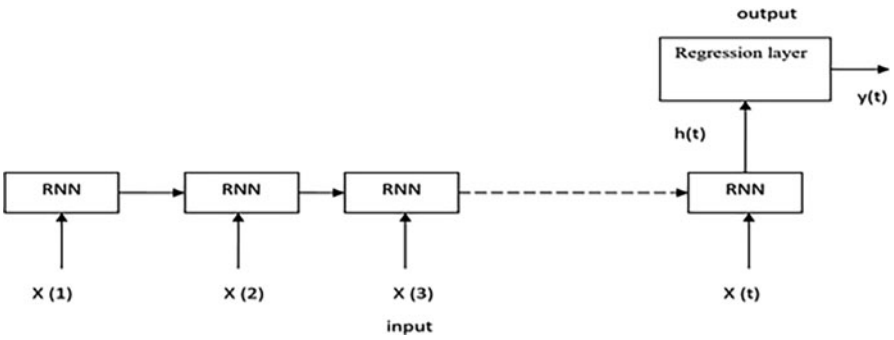

Fig. 12.13 RNN architecture for regression problems

$$y_t = W_{hy} \tanh\left(W_{hh}h_{t-1} + W_{xh}x_t\right) \tag{12.22}$$

where x_t is input and y_t is the output and W is the network weight.

12.9.5 Applications of DL in Environmental Protection and Sustainability

Environmental issues such as air pollution or water contamination are global problems, requiring special efforts from governments and individuals. Hence, using DL techniques, as part of information technology, in predicting conditions of the environment is a key research topic. One of the research trends is to rely on Google search data to expect the state of pro-environmental consumption, which can be achieved by using the consumption index. This index has been determined as an indication of pro-environmental consumption policy, calculated for each country by international organizations. It is worth mentioning that there are different indexes developed for specific purposes, including the Environmental Performance Index (EPI) and the Environmental Sustainability Index (ESI). The values of indexes range from 0 to 100. Calculation methods are of importance and can be achieved based on the principle of *proximity to target* to find how close the policies of countries are in environmental objectives recognized by international organizations (Lee et al. 2017). For forecasting the pro-environmental consumption index, a model is built using a RNN deep learning algorithm. RNN is one of the deep learning technologies that builds through the ANN model but can use prior relationships. In the operation of the RNN model, the data of a previous period (h_{t-1}) is incorporated recursively as input data, and the output (y_t) for time (t) will be calculated as shown in Eq. (12.23).

$$y_t = f\left(h_{t-1} \times W^h + x_t \times W^x\right) \tag{12.23}$$

The RNN model consists of a Gompertz of activation function, 100 Epoch repetitions, and the number of hidden layers and is 10 with 20 batch sizes and a 0.02 learning rate. The model was built using RNN for pro-environmental consumption forecasting was tested and verified using 84 different datasets and provides better results than traditional neural network methods (Lee et al. 2017).

Sustainability denotes the production of manufactured products through economic processes that minimize negative environmental impacts while conserving energy and natural resources (Lee et al. 2017). Hence, important points that should be applied to maintain sustainable manufacturing are (Dincer and Acar 2015) minimizing the reduction of natural resources and the possibility of fulfilling the present and future energy requirements, providing products with high efficiency, and avoiding or keeping toxic emissions including greenhouse gases emission to minimum levels. DL shows its extreme power in many areas and applications. However, sustainability and energy efficiency problems still require more investigation. DL is a powerful tool that will provide the framework to work towards environmental sustainability solutions in the future (Meng et al. 2018).

12.10 Conclusion

This chapter has focused on DL technology with environmental applications. DL can be considered a promising tool in the field of environmental challenges including both classifications and predictions. The chapter also discussed the main algorithms of DL with a brief comparison revealing the advantages and the challenges of each. There are several applications of DL in environmental systems; three of the most common applications have been exemplified, earthquake prediction, rainfall prediction, and environmental protection and sustainability. In environmental systems applications, the advantage of using DL is that it achieves better accuracy and reliability compared to regular ML techniques.

DL could be applied in earthquake prediction for both classification and regression problems, where it is used to predict the occurrence and magnitude of earthquakes. Rainfall prediction can be considered as a regression problem, and DL may be used to predict the amount of rain in particularly vulnerable regions. In environmental protection and sustainability applications, problems can be treated as classification and regression problems, and DL can be utilized to predict several issues such as the amount of air pollution and water contamination. Regarding sustainability applications, DL can be used to find proper solutions for production problems in manufacturing, which may ensure the efficient consumption of natural resources. Hence, DL is a powerful tool representing a key to unlocking complexity and validating future applications of environmental systems.

References

Ahmed RN, Hayri S (2018) A large-scale Arabic sentiment corpus construction using online news media. J Eng Appl Sci 13:7329–7340

Alom MZ, Taha TM, Yakopcic C et al (2019) A state-of-the-art survey on deep learning theory and architectures. Electronics 8(3):292

Chen J, Wang D (2017) Long short-term memory for speaker generalization in supervised speech separation. J Acoust Soc Am 141(6):4705–4714

Dey A (2016) Machine learning algorithms: a review. Int J Comput Sci Inf Technol 7(3): 1174–1179

Dincer I, Acar C (2015) A review of clean energy solutions for better sustainability. Int J Energy Res 39(5):585–606

Dumoulin V, Visin F (2016) A guide to convolution arithmetic for deep learning. arXiv. https://doi.org/10.48550/arXiv.1603.07285

Franklin J (2005) The elements of statistical learning: data mining, inference and prediction. Math Intell 27:83–85. https://doi.org/10.1007/BF02985802

Fukushima K (1980) Neocognitron: a self-organizing neural network model for a mechanism of pattern recognition unaffected by shift in position. Biol Cybern 36(4):193–202

Goodfellow I, Bengio Y, Courville A (2016) Deep learning. MIT press. https://doi.org/10.1007/s10710-017-9314-z

Gurney K (2014) An introduction to neural networks. CRC Press. https://doi.org/10.1117/3.633187

Hernández-Orallo J (2017) Evaluation in artificial intelligence: from task-oriented to ability-oriented measurement. Artif Intell Rev 48(3):397–447

Hinton GE, Dayan P, Frey BJ et al (1995) The "wake-sleep" algorithm for unsupervised neural networks. Science 268(5214):1158–1161

Hinton GE, Srivastava N, Krizhevsky A et al (2012) Improving neural networks by preventing co-adaptation of feature detectors. arXiv. https://doi.org/10.48550/arXiv.1207.0580

Hochreiter S, Schmidhuber J (1997) Long short-term memory. Neural Comput 9(8):1735–1780. https://doi.org/10.1162/neco.1997.9.8.1735

Hu W, Huang Y, Wei L et al (2015) Deep convolutional neural networks for hyperspectral image classification. J Sens 2:1–12. https://doi.org/10.1155/2015/258619

Ivakhnenko AG, Lapa VG (1966) Cybernetic predicting devices (No. TR-EE66-5). Purdue Univ Lafayette Ind School of Electrical Engineering

James G, Witten D, Hastie T et al (2013) An introduction to statistical learning. Springer Texts in Statistics. Springer

Kin ZB (2019) Classification of Turkish sign language alphabet by deep learning method. Master's thesis, Başkent University Institute of Science and Technology

Krizhevsky A, Sutskever I, Hinton GE (2012) Imagenet classification with deep convolutional neural networks. In: NIPS'12 Proceedings of the 25th International Conference on Neural Information Processing Systems – Vol 1. https://doi.org/10.5555/2999134.2999257

LeCun Y, Bengio Y (1995) Convolutional networks for images, speech, and time series. In: Arbib MA (ed) The handbook of brain theory and neural networks. MIT Press

LeCun Y, Boser B, Denker JS et al (1989) Backpropagation applied to handwritten zip code recognition. Neural Comput 1(4):541–551

LeCun Y, Boser BE, Denker JS et al (1990) Handwritten digit recognition with a back-propagation network. In: Touretzky D (ed) Advances in neural information processing systems (NIPS 1989). Morgan Kaufmann, Denver

Lee D, Kang S, Shin J (2017) Using deep learning techniques to forecast environmental consumption level. Sustainability 9(10):1894. https://doi.org/10.3390/su9101894www.mdpi.com/journal/sustainability

McCarthy JJ, Minsky ML, Rochester N (1959) Artificial intelligence. Research Laboratory of Electronics (RLE) at the Massachusetts Institute of Technology (MIT)

Meng Y, Yang Y, Chung H et al (2018) Enhancing sustainability and energy efficiency in smart factories: a review. Sustainability 10(12):4779

Niu J, Zhang W (2015) Comparative analysis of statistical models in rainfall prediction. In: 2015 IEEE international conference on information and automation. IEEE, pp 2187–2190

Patterson J, Gibson A (2017) Deep learning: a practitioner's approach. O'Reilly Media, Inc

Perol T, Gharbi M, Denolle M (2018) Convolutional neural network for earthquake detection and location. Sci Adv 4(2):e1700578. https://doi.org/10.1126/sciadv.1700578

Pouyanfar S, Sadiq S, Yan Y et al (2018) A survey on deep learning: algorithms, techniques, and applications. ACM Comput Surv 51(5):92

Samuel AL (1988) Some studies in machine learning using the game of checkers II – recent progress. IBM J Res Dev 1967:601–617. Reprinted In: Levy DL (ed) Computer games. Springer-Verlag

Schmidhuber J (2015) Deep learning in neural networks: an overview. Neural Netw 61:85–117. https://doi.org/10.1016/j.neunet.2014.09.003

Şeker A, Diri B, Balık HH (2017) A review of deep learning methods and applications. Gazi J Eng Sci 3(3):47–64

Sobolev GA (2015) Methodology, results, and problems of forecasting earthquakes. Her Russ Acad Sci 85(2):107–111

Vieira A, Ribeiro B (2018) Deep learning: an overview. In: Viero A, Ribeiro B (eds) An introduction to deep learning business applications for developers. Apress, Berkeley. https://doi.org/10.1007/978-1-4842-3453-2_2

Wang Q, Guo Y, Yu L et al (2017) Earthquake prediction based on spatio-temporal data mining: an LSTM network approach. IEEE Trans Emerg Top Comput 8(1):148–158

Zaw WT, Naing TT (2008) Empirical statistical modeling of rainfall prediction over Myanmar. World Acad Sci Eng Technol 2(10):500–504

Index

J. N. Furze et al. (eds.), *Earth Systems Protection and Sustainability*,
https://doi.org/10.1007/978-3-030-98584-4